

**THE SEARCH FOR $VH \rightarrow VWW$ STANDARD MODEL
HIGGS PRODUCTION IN THE TRILEPTON SIGNATURE
WITH 5.9fb^{-1} OF DATA FROM $p\bar{p}$ COLLISIONS
AT $\sqrt{S} = 1.96\text{ GEV}$**

by

Jason Michael Nett

A dissertation submitted in partial fulfillment of
the requirements for the degree of

Doctor of Philosophy

(Department of Physics)

at the

UNIVERSITY OF WISCONSIN–MADISON

2010

DISCARD THIS PAGE

TABLE OF CONTENTS

	Page
LIST OF TABLES	v
LIST OF FIGURES	vii
NOMENCLATURE	xii
ABSTRACT	xv
1 Introduction	1
2 The Higgs Mechanism and the Standard Model of Particle Physics	6
2.1 Intro. to the Standard Model of Particle Physics	6
2.2 Elementary Particles in the Standard Model	7
2.2.1 Fermions	7
2.2.2 Bosons	8
2.3 Electroweak Interactions in the Standard Model: Spontaneously Broken Local $SU(2)_L \times U(1)_Y$ Symmetry	9
2.3.1 Global $U(1)$ Symmetry	9
2.3.2 Local $U(1)$ Symmetry	11
2.3.3 Global $SU(2)$ Symmetry	12
2.3.4 Local $SU(2)$ Symmetry	14
2.3.5 Isospin, Weak Hypercharge, and $SU(2) \times U(1)$ Symmetry	16
2.4 The Higgs Mechanism and Fermion Masses	19
2.4.1 $SU(2) \times U(1)$ Symmetry For Massless Fermions	20
2.4.2 The Higgs Mechanism in Fermion Mass Generation	22
2.5 The Higgs Field, Quark Mixing, and the CKM Matrix	24
2.6 The Electroweak Lagrangian of the Standard Model	25
2.7 Higgs Boson Associated Production with a Vector Boson	29
2.8 Higgs Boson Decay ($H \rightarrow WW$)	32

	Page
3 The Tevatron	34
3.1 Beginning of the Beam: Cockcroft-Walton	34
3.2 LINAC: The Linear Accelerator	36
3.3 Booster	36
3.4 Main Injector	36
3.5 Anti-protons	36
3.6 The Tevatron	37
3.7 The Performance of the Tevatron in Run II	38
4 The CDF II Detector	40
4.1 CDF Coordinates	42
4.2 Trackers	43
4.2.1 The Silicon Detectors	43
4.2.2 Central Outer Tracker	45
4.3 Calorimeters	46
4.3.1 CDF Central Electromagnetic Calorimeter (CEM)	46
4.3.2 CDF Hadronic Calorimeters (CHA, WHA)	47
4.3.3 CDF Forward Calorimeters (PEM, PHA)	47
4.4 Muon Detectors	48
4.5 CDF Detector Summary for $VH \rightarrow VWW \rightarrow \text{Trileptons}$	49
5 Triggers, Datasets, and Event Selection	50
5.1 Level 1	50
5.2 Level 2	50
5.3 Level 3	51
5.4 Trigger Paths (“Datasets”) of the $H \rightarrow WW$ Group	51
5.4.1 ELECTRON_CENTRAL_18	52
5.4.2 MUON_CMUP18	52
5.4.3 MUON_CMX18	53
5.4.4 MET_PEM	53
5.4.5 MUON_CMP18_PHI_GAP	54
5.4.6 MUON_CMU18_ETA_GAP	54
6 High p_T Object Identification	56
6.1 Lepton Identification	56
6.1.1 Track Formation	58

Appendix

	Page
6.1.2 Electron ID	59
6.1.3 Muon ID	60
6.1.4 Unspecified Track ID	61
6.2 Jet ID	66
6.3 Missing Transverse Energy (E_T)	66
6.4 Fake Leptons	67
6.5 Lepton Efficiencies	71
6.6 Lepton Scale Factors	71
7 Computations with Artificial Neural Networks	74
8 Statistics of Confidence Level Limits In the Search for New Physics	77
8.1 Poisson Statistics and Physical Processes	77
8.2 Gaussian Statistics and Systematic Errors	78
8.3 Likelihood and Confidence Level Computation	79
9 The High Mass Higgs Boson Analysis in the Trilepton Signature	82
9.1 Motivation for Trileptons	83
9.2 Event Summary and Signatures of the WH and ZH Trilepton Analyses	87
9.2.1 Trilepton Signal Regions Defined	87
9.2.2 Backgrounds	97
9.3 Neural Net	99
9.3.1 Discriminating Variables	99
9.3.2 Neural Network Scores	107
9.4 Systematic Errors	111
9.5 Results	116
9.6 Conclusions	125

APPENDICES

Appendix A:	$U(1)$ Global Symmetry Breaking	129
Appendix B:	$U(1)$ Local Symmetry Breaking	134
Appendix C:	$SU(2)$ Global Symmetry Breaking	138
Appendix D:	$SU(2)$ Local Symmetry Breaking	141
Appendix E:	The Higgs Mechanism in the $SU(2) \times U(1)$ Local Spontaneous Symmetry Breaking	146
Appendix F:	The $SU(2)_L \times U(1)_Y$ Local Gauge Invariant Lagrangian and the [massless] Fermions	151

Appendix

	Page
Appendix G: The Higgs Mechanism and Fermion Mass Generation	163
Appendix H: The Higgs Sector in Standard Model Electroweak Physics	168
Appendix I: WH Production Amplitude	173
Appendix J: $H \rightarrow WW$ Lagrangian Density To Invariant Amplitude	182
Appendix K: $H \rightarrow WW$ Invariant Amplitude to Decay Rate (Γ)	185
Appendix L: WZ Cross Section Measurement in 5.9fb^{-1}	190
Appendix M: Monte Carlo Samples	194
Appendix N: Signal Summary for 19 Mass Points from $m_H = 110\text{ GeV}$ to $m_H = 200$ GeV	198
Appendix O: Basic Event Information for the Signal and Control Regions	200
Appendix P: Neural Net Input Variables for the Signal Regions	204
Appendix Q: Neural Net Input Variables for the Control Regions	231
Appendix R: Neural Net Scores	240
LIST OF REFERENCES	247

DISCARD THIS PAGE

LIST OF TABLES

Table	Page
2.1 Quarks of the Standard Model. The superscript indicates the particles' electric charges (the top charge refers to the "particles" while the bottom charge refers to the "anti-particles"). As fermions, all quarks have spin of $1/2$	7
2.2 Leptons of the Standard Model. The particles in the top row exist as both "matter" (electric charge of -1) and "anti-matter" (electric charge of $+1$). The bottom row consists of the associated "neutrinos" which have no electric charge. As fermions, all particles listed here have spin $1/2$	8
2.3 Weak isospin and hypercharge quantum numbers for the first generation of leptons. Left and right handed electrons are listed separately.[33]	16
2.4 Weak isospin and hypercharge quantum numbers for the first generation of quarks. Left and right handed quarks are listed separately.[33]	17
4.1 Basic Summary of CDF Muon Detectors [48]	48
6.1 Phoenix (PHX) electron definition	62
6.2 Base muon identification criteria for all categories	62
6.3 Cuts for CMUP muons beyond the base muon cuts	63
6.4 Cuts for CMP muons beyond the base muon cuts	63
6.5 Cuts for CMU muons beyond the base muon cuts.	63
6.6 Cuts for CMX muons beyond the base muon cuts	64
6.7 Cuts for BMU muons beyond the base muon cuts	64
6.8 Cuts for CMIOCES muons beyond the base muon cuts	65
6.9 Cuts for CMIOPEs muons beyond the base muon cuts	65

Appendix

Table	Page
6.10 Cuts for CrkTrk muons beyond the base muon cuts	65
6.11 Muon scale factors in Diboson_v17 data [19].	72
6.12 Muon scale factors in Diboson_v17 data [19].	72
6.13 Electron scale factors in Diboson_v17 data [19].	73
6.14 Electron scale factors in Diboson_v17 data [19].	73
9.1 Event count for the signal and background processes in the trilepton signal regions for 5.9fb^{-1} of collected data	95
9.2 Event count for the signal and background processes in the trilepton control regions for 5.9fb^{-1} of collected data	96
9.3 Systematic Uncertainties: Standard values for systematics used in other $H \rightarrow WW$ analyses are used wherever applicable.	115
9.4 Systematic errors used to account for jet energy scaling ambiguities	115
9.5 WH trilepton analysis limits for 5.9fb^{-1}	118
9.6 ZH (1 Jet) trilepton analysis limits for 5.9fb^{-1}	120
9.7 ZH (≥ 2) trilepton analysis limits for 5.9fb^{-1}	122
9.8 Trilepton combined analysis limits for 5.9fb^{-1}	124
9.9 HWW Limits	128

Appendix

Table	
M.1 Monte Carlo samples used in this analysis	195
M.2 Associated Higgs production with a W boson [20].	196
M.3 Associated Higgs production with a Z boson [20].	197
N.1 Signal Summary	199

DISCARD THIS PAGE

LIST OF FIGURES

Figure	Page
1.1 Experimental exclusion limits at 95% confidence level from the LEP collider at CERN [18].	2
1.2 Standard Model branching ratios for the Higgs boson at the Tevatron as computed by the HDECAY algorithm [24].	3
3.1 The Tevatron Accelerator Chain [11]	35
3.2 The Tevatron Run II luminosity performance [8]	39
4.1 The CDF II Detector	41
4.2 Diagram showing the types of objects various layers are constructed to detect.	42
4.3 Diagram showing a side view of the tracking, solenoid, and forward calorimeter systems. The horizontal axis is the \hat{z} -direction from the interaction vertex and the vertical axis is the radial direction from the beamline.	44
4.4 End view of L00 (left) and the full silicon system (right)[5],[6]	44
6.1 Fake rates for electrons. PHX and LBE have no track isolation requirement. TCE is include for comparison. [20]	69
6.2 Fake rates for muons. [20]	70
7.1 Neural Network “neurode”	75
7.2 Neural Network “network node”	76
7.3 “Neural Network”	76
9.1 WH trilepton signal topology	83
9.2 ZH trilepton signal topology	84

Figure	Page
9.3 Leptonic τ decays to an electron or muon	84
9.4 Trilepton WH signal region lepton p_T (for muons) or E_T (for electrons)	90
9.5 Trilepton ZH (1 Jet) signal region lepton p_T (for muons) or E_T (for electrons)	91
9.6 Trilepton ZH (≥ 2) Jet signal region lepton p_T (for muons) or E_T (for electrons)	93
9.7 Trilepton WH Control Region lepton p_T (for muons) or E_T (for electrons)	94
9.8 Trilepton ZH Control Region lepton p_T (for muons) or E_T (for electrons)	94
9.9 The histograms on the left have each processed normalized to an area of 1.0 to compare shapes, while the histograms on the right are properly weighted to 5.9 fb^{-1}	100
9.10 Number of jets for all jet bins in the Z -selected region	101
9.11 “ $V - A$ Angular Distribution: $W \rightarrow l\nu_l$ decay distribution shape for a W with spin +1 (left) and with spin -1 (right).	102
9.12 The histograms on the left have each processed normalized to an area of 1.0 to compare shapes, while the histograms on the right are properly weighted to 5.9 fb^{-1}	102
9.13 The histograms on the left have each processed normalized to an area of 1.0 to compare shapes, while the histograms on the right are properly weighted to 5.9 fb^{-1} . ZH events in the 1-jet region just use the single jet in the mass reconstruction while ZH events in the ≥ 2 jets region use the leading two jets by energy.	104
9.14 NeuroBayes neural network score for the signal regions of the trilepton analysis with 5.9 fb^{-1}	109
9.15 NeuroBayes neural network score for the control regions of the trilepton analysis with 5.9 fb^{-1}	110
9.16 Trilepton WH Signal Region Limits	117
9.17 Trilepton ZH (1 Jet) Signal Region Limits	119
9.18 Trilepton ZH (≥ 2 Jets) Signal Region Limits	121
9.19 Trilepton Combined Limits	123

Figure	Page
9.20 HWW Combined Limits (with Trileptons)	125
9.21 HWW Combined Limits (with Trileptons)	126
Appendix	
Figure	
I.1 Associated Production with a W boson	173
O.1 Trilepton WH signal region lepton p_T (for muons) or E_T (for electrons)	201
O.2 Trilepton ZH (1 Jet) signal region lepton p_T (for muons) or E_T (for electrons)	202
O.3 Trilepton ZH (≥ 2 Jet) signal region lepton p_T (for muons) or E_T (for electrons)	203
P.1 WH Analysis: m_T (Lep3, \cancel{E}_T), ΔR b/w Opp. Sign Close Lept.	205
P.2 WH Analysis: Lepton types, Dimass Opp. Sign Leptons (closer pair in ϕ).	206
P.3 WH Analysis: ΔR Opp. Sign Far Lept., 2 nd Lepton p_T	207
P.4 WH Analysis: $\Delta\phi(\text{Lep2}, \cancel{E}_T)$, Inv. Mass(Lep3, \cancel{E}_T , Jets)	208
P.5 WH Analysis: $m_T(\text{all lept.}, \cancel{E}_T, \text{Jets})$, H_T	209
P.6 WH Analysis: \cancel{E}_T , m_T Trilepton Mass	210
P.7 WH Analysis: NJet, Inv. Mass(Lep1, Lep2, \cancel{E}_T)	211
P.8 WH Analysis: m_T (all lept., \cancel{E}_T , jets)	212
P.9 ZH (1-jet) Analysis: \cancel{E}_T , $\Delta R(W\text{-lep, lead jet})$	213
P.10 ZH (1-jet) Analysis: Lead jet E_T , ΔR b/w Opp. Sign Close Lept.	214
P.11 ZH (1-jet) Analysis: $\Delta\phi(W\text{-lep, } \cancel{E}_T)$, $\Delta\phi(\text{lept. sum, } \cancel{E}_T)$	215
P.12 ZH (1-jet) Analysis: ZH Higgs Mass, ΔR Opp. Sign Far Lept	216
P.13 ZH (1-jet) Analysis: $m_T(\text{all lept.}, \cancel{E}_T, \text{Jets})$, Inv. Mass (all lept.)	217
P.14 ZH (1-jet) Analysis: Lepton Types, $\Delta\phi(\text{Lep2}, \cancel{E}_T)$	218

Figure	Page
P.15 ZH (1-jet) Analysis: H_T , Inv. Mass (W -lep., E_T)	219
P.16 ZH (1-jet) Analysis: m_T (W -lep., E_T), Inv. Mass(Lep3, E_T ,Jets)	220
P.17 ZH (1-jet) Analysis: m_T Trilepton Mass	221
P.18 ZH (≥ 2 -jet) Analysis: Inv. Mass ($1^{\text{st}} \& 2^{\text{nd}}$ jet), E_T	222
P.19 ZH (≥ 2 -jet) Analysis: ΔR (W -lep, 1^{st} jet), 1^{st} jet E_T	223
P.20 ZH (≥ 2 -jet) Analysis: $\Delta\phi$ (lept. sum, E_T), NJet	224
P.21 ZH (≥ 2 -jet) Analysis: $\Delta\phi$ (Lep2, E_T), Lepton Types	225
P.22 ZH (≥ 2 -jet) Analysis: ΔR b/w Opp. Sign Close Lept., Inv. Mass (W -lep., E_T) . . .	226
P.23 ZH (≥ 2 -jet) Analysis: ZH Higgs Mass, ΔR Opp. Sign Far Lept.	227
P.24 ZH (≥ 2 -jet) Analysis: m_T (Leptons, E_T ,Jets), Inv. Mass (all lept.)	228
P.25 ZH (≥ 2 -jet) Analysis: ΔR ($1^{\text{st}} \& 2^{\text{nd}}$ jet), Inv. Mass(Lep3, E_T ,Jets)	229
P.26 ZH (≥ 2 -jet) Analysis: $\Delta\phi$ (W -lep, E_T), H_T	230
Q.1 WH Analysis: m_T (Lep3, E_T), ΔR b/w Opp. Sign Close Lept., Lepton types, Dimass Opp. Sign Leptons (closer pair in ϕ)	232
Q.2 WH Analysis: ΔR Opp. Sign Far Lept., 2^{nd} Lepton p_T , $\Delta\phi$ (Lep2, E_T), Inv. Mass(Lep3, E_T ,Jets)	233
Q.3 WH Analysis: m_T (all lept., E_T ,Jets), H_T , E_T , m_T Trilepton Mass	234
Q.4 WH Analysis: NJet, Inv. Mass(Lep1,Lep2, E_T), m_T (all lept., E_T , jets)	235
Q.5 ZH Analysis: E_T , ΔR b/w Opp. Sign Close Lept., $\Delta\phi$ (W -lep, E_T), $\Delta\phi$ (lept. sum, E_T)	236
Q.6 ZH Analysis: ΔR Opp. Sign Far Leptons, m_T (all lept., E_T ,Jets), Inv. Mass (all lept.), Lepton Types	237
Q.7 ZH Analysis: $\Delta\phi$ (Lep2, E_T), H_T , Inv. Mass (W -lep., E_T), m_T (W -lep., E_T)	238
Q.8 ZH Analysis: Inv. Mass(Lep3, E_T ,Jets), m_T Trilepton Mass	239

Figure	Page
R.1 Trilepton WH NeuroBayes Neural Network output (linear scale)	241
R.2 Trilepton WH NeuroBayes Neural Network output (log scale)	242
R.3 Trilepton ZH (1 Jet) NeuroBayes Neural Network output (linear scale)	243
R.4 Trilepton ZH (1 Jet) NeuroBayes Neural Network output (log scale)	244
R.5 Trilepton ZH (≥ 2 Jets) NeuroBayes Neural Network output (linear scale)	245
R.6 Trilepton ZH (≥ 2 Jets) NeuroBayes Neural Network output (log scale)	246

DISCARD THIS PAGE

NOMENCLATURE

- Dilepton** The resulting signature of a $p\bar{p}$ collision that produces exactly two high p_T (for muons) or high E_T (for electrons) charged leptons (electrons or muons, taus are not directly observed) as reconstructed by the CDF collider detector
- Gluon (g)** The fundamental particle of the Standard Model that mediates the strong force of quantum chromodynamics
- Jet** In the signature of a $p\bar{p}$ collision, this is a collection of energy deposited in the electromagnetic and/or hadronic calorimeters of a collider detector. Jets are considered to be localized collections of many particles produced in the collision. The jet is made of hadrons produced in the fragmentation and hadronization process when bare quarks separate.
- Lepton** Spin-1/2 “electrons,” “muons,” “taus,” and their corresponding “neutrinos” in the Standard Model
- Neutrino** Neutrinos exist in the three known lepton flavors: electron, muon, and tau. They are neutrally charged and only interact weakly.
- Photon (γ)** The fundamental particle of the Standard Model that mediates the electromagnetic force of electroweak theory

- Quark Spin-1/2 fermions (“up,” “down,” “charm,” “strange,” “top,” “bottom”) of the Standard Model described by $SU(3)$ symmetries of quantum chromodynamics
- Standard Model The present physical theory describing quarks and leptons as the known fundamental particles of the universe and the forces (electromagnetism, weak, strong) by which they interact according to an $SU(3)_C \times SU(2)_L \times U(1)_Y$ gauge symmetry. The as-yet undiscovered Higgs boson, which is thought to be a consequence of electroweak symmetry breaking and generates non-zero masses for the other particles, is also a part of the Standard Model. The gravitational interaction is the one known force of the universe that is not covered by the Standard Model.
- Trilepton The resulting signature of a $p\bar{p}$ collision that produces exactly three high p_T (for muons) or high E_T (for electrons) leptons (electrons or muons, taus are not directly observed) as reconstructed by the CDF collider detector
- W -boson Electrically charged (± 1) massive weak vector boson
- Weak Vector Boson A spin-1 gauge boson that mediates the weak force in the Standard Model
- Z -boson Electrically neutral massive weak vector boson

THE SEARCH FOR $VH \rightarrow VWW$ STANDARD MODEL HIGGS PRODUCTION IN THE TRILEPTON SIGNATURE WITH 5.9fb^{-1} OF DATA FROM $p\bar{p}$ COLLISIONS AT $\sqrt{S} = 1.96 \text{ GEV}$

Jason Michael Nett

Under the supervision of Associate Professor Matthew Herndon

At the University of Wisconsin-Madison

We present here the search for Standard Model $VH \rightarrow VWW \rightarrow lll + E_T$ (missing energy due to neutrinos) production, where V is a W or Z weak vector boson, which uses up to 5.9 fb^{-1} of integrated luminosity. This analysis has recently added to the CDF high-mass Higgs group three new signal topologies characterized by a **tri**-lepton signature, which are chosen to isolate the $VH \rightarrow VWW$ associated production signals in the three-lepton signature. As such, we define three new regions for a WH analysis, a ZH 1-jet analysis, and a $ZH \geq 2$ -jet analysis with which we expect to contribute an additional $\sim 5.8\%$ (for $m_H = 165 \text{ GeV}$) acceptance to the current $H \rightarrow WW$ dilepton analysis.

The ZH trilepton regions are defined by events passing a Z -boson selection: events having at least one lepton pairing (among three possible pairings) with opposite sign, same flavor, and a dilepton invariant mass within $[76.0, 106.0] \text{ GeV}$ —a $\pm 15 \text{ GeV}$ window around the Z -boson mass. The WH trilepton region is then defined as the set of trilepton events that are complement to those chosen by the Z -boson selection.

These three new event topologies make a substantial contribution to the $H \rightarrow WW$ group result. As a measure of the sensitivity of this search, we compute the median expected limit on the at 95% confidence level (“C.L.”) on the production cross section (effectively the rate of production) for a Standard Model Higgs boson and report the result as a ratio to the theoretical production cross section. An observed limit ratio of one or less at a given mass would rule out the production of a Standard Model Higgs boson at that mass with 95% confidence. At $m_H = 165 \text{ GeV}$, the WH

analysis expected limits reach 7.2 times the standard model cross section; the ZH 1-jet analysis is set at 29 times the expected standard model cross section; the $ZH \geq 2$ -jet analysis is set at 9.9 times the expected standard model cross section; and the combined trilepton analysis is set at 4.9 times the expected standard model cross section.

We announce that the combination of this trilepton $VH \rightarrow VWW$ Higgs boson search and the previous CDF dilepton $H \rightarrow WW$ search achieves an expected median limit of 1.00 at 165 GeV/ c^2 . The expected median limit of 1.00 indicates we anticipate a 50% probability of ruling out the existence of a Standard Model Higgs boson with a mass of 165 GeV/ c^2 . This is the first time a single hadron collider experiment has achieved sensitivity to the production of a Standard Model Higgs boson. We do not see evidence for a significant signal of Higgs bosons in the data and place observed limits on the production of a Standard Model Higgs boson of 165 GeV/ c^2 at 1.08 times Standard Model production cross section.

Matthew Herndon

ABSTRACT

We present here the search for Standard Model $VH \rightarrow VWW \rightarrow lll + \cancel{E}_T$ (missing energy due to neutrinos) production, where V is a W or Z weak vector boson, which uses up to 5.9 fb^{-1} of integrated luminosity. This analysis has recently added to the CDF high-mass Higgs group three new signal topologies characterized by a **tri**-lepton signature, which are chosen to isolate the $VH \rightarrow VWW$ associated production signals in the three-lepton signature. As such, we define three new regions for a WH analysis, a ZH 1-jet analysis, and a $ZH \geq 2$ -jet analysis with which we expect to contribute an additional $\sim 5.8\%$ (for $m_H = 165 \text{ GeV}$) acceptance to the current $H \rightarrow WW$ dilepton analysis.

The ZH trilepton regions are defined by events passing a Z -boson selection: events having at least one lepton pairing (among three possible pairings) with opposite sign, same flavor, and a dilepton invariant mass within $[76.0, 106.0] \text{ GeV}$ —a $\pm 15 \text{ GeV}$ window around the Z -boson mass. The WH trilepton region is then defined as the set of trilepton events that are complement to those chosen by the Z -boson selection.

These three new event topologies make a substantial contribution to the $H \rightarrow WW$ group result. As a measure of the sensitivity of this search, we compute the median expected limit on the at 95% confidence level (“C.L.”) on the production cross section (effectively the rate of production) for a Standard Model Higgs boson and report the result as a ratio to the theoretical production cross section. An observed limit ratio of one or less at a given mass would rule out the production of a Standard Model Higgs boson at that mass with 95% confidence. At $m_H = 165 \text{ GeV}$, the WH analysis expected limits reach 7.2 times the standard model cross section; the ZH 1-jet analysis is set at 29 times the expected standard model cross section; the $ZH \geq 2$ -jet analysis is set at 9.9

times the expected standard model cross section; and the combined trilepton analysis is set at 4.9 times the expected standard model cross section.

We announce that the combination of this trilepton $VH \rightarrow VWW$ Higgs boson search and the previous CDF dilepton $H \rightarrow WW$ search achieves an expected median limit of 1.00 at 165 GeV/c². The expected median limit of 1.00 indicates we anticipate a 50% probability of ruling out the existence of a Standard Model Higgs boson with a mass of 165 GeV/c². This is the first time a single hadron collider experiment has achieved sensitivity to the production of a Standard Model Higgs boson. We do not see evidence for a significant signal of Higgs bosons in the data and place observed limits on the production of a Standard Model Higgs boson of 165 GeV/c² at 1.08 times Standard Model production cross section.

Chapter 1

Introduction

The Standard Model of particle physics describes types of matter that are presently considered to be fundamental (not existing as composite states of multiple other particles) as well as the forces (except for gravity) by which they interact. Those forces are themselves mediated by fundamental particles. That is, the electromagnetic force arises from the exchange of a “photon” (γ); the weak force arises from the exchange of a “weak vector boson” (W^+ , W^- , Z); and the strong force arises from the exchange of a “gluon” (g). The final piece of the Standard Model is the Higgs boson, which remains the sole particle whose existence or non-existence has yet to be confirmed experimentally. If the Higgs boson does exist as postulated in the Standard Model, it is a key consequence of our understanding of the origin of mass in the universe.

The Higgs boson was postulated in 1964 separately by Peter Higgs [35, 36]; by Francois Englert and Robert Brout [26]; and by Gerald Guralnik, C.R. Hagan, and T.W.B. Kibble[32] as a consequence of a mathematical mechanism that rectified an apparent contradiction in the fledgling quantum field theories being formulated at that time. That mathematical mechanism is grounded in broken symmetries of the $SU(2)_L \times U(1)$ group, from which the electroweak force of the Standard Model arises [30, 50, 47]. With Schrodinger equation-based quantum mechanics describing the physics of very small particles and special relativity describing the physics of high energy motion, physicists were naturally attempting to formulate a theory consistent with both realms—effectively, the physics of high energy fundamental particles. Before the Higgs mechanism was postulated, there was an inherent contradiction. Particles are known to have nonzero mass from experience and experiment, but introducing mass terms directly into the Lagrangian breaks certain

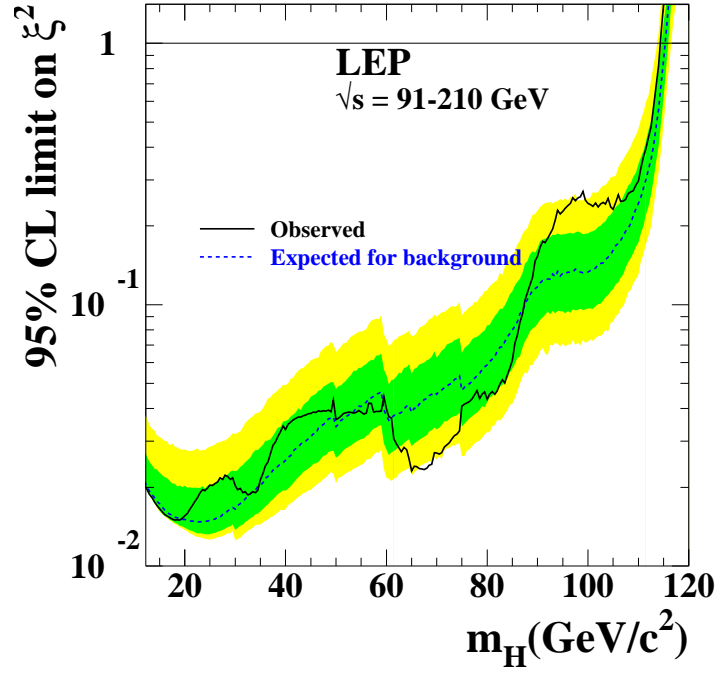


Figure 1.1 Experimental exclusion limits at 95% confidence level from the LEP collider at CERN [18].

symmetry requirements. The Higgs mechanism resolved the problem and lead to the formulation of a coherent quantum field theory that allows for massive fundamental particles.

The first experimental search to yield serious results for the Higgs boson was conducted by the Large Electron-Positron Collider (LEP) at the European Organization for Nuclear Research (CERN “*Organisation Européenne pour la Recherche Nucléaire*”) which operated from 1989 to 2000. The Higgs sector of the Standard Model does not directly postulate or predict the mass of the Higgs boson, so a wide range of possible masses must be explored. LEP experimentally ruled out the existence of a Standard Model Higgs boson for masses $m_H < 114\text{GeV}/c^2$. The LEP exclusion limits are shown in figure 1.1[18].

The Tevatron, a proton-antiproton ($p\bar{p}$) collider at the Fermi National Accelerator Laboratory, has carried the torch since LEP was dismantled in 2000 to construct the Large Hadron Collider (LHC) in its place. In $p\bar{p}$ interactions, the search for the Higgs boson is divided between a “low mass” region ($114 < m_H < 135\text{GeV}/c^2$) and a “high mass” region ($135 < m_H < 200\text{GeV}/c^2$). Observe in figure 1.2 that this low mass region corresponds to masses of the Higgs boson where it

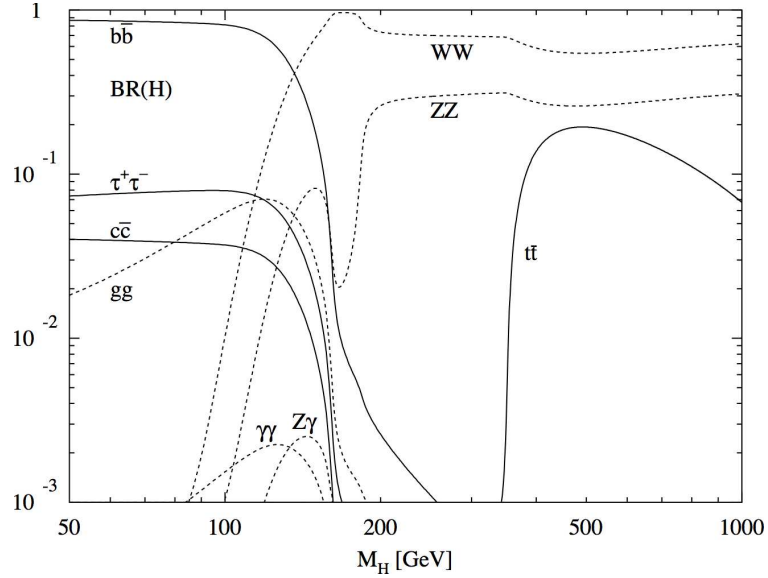


Figure 1.2 Standard Model branching ratios for the Higgs boson at the Tevatron as computed by the HDECAY algorithm [24].

decays primarily to b -quark pairs and the high mass region corresponds to masses where it decays primarily to weak vector boson (W^+ , W^- , Z) pairs. This thesis contributes a new search for the Standard Model Higgs boson in the high mass region ($H \rightarrow WW$), orthogonal to and augmenting the search that preceded it.

Until recently, the high mass Higgs search exclusively studied $H \rightarrow WW$ interactions that result in a two-lepton signature [20]. The reason is that the dominant production of a high mass Higgs boson is via gluon fusion, which is then best studied in the case where both Higgs- W -bosons decay leptonically. The cases of having one or both Higgs- W -bosons decay hadronically is severely limited by large backgrounds. This thesis presents for the first time a search for a high mass Higgs boson in the three-lepton signature, shifting focus to the associated production channels $WH \rightarrow WWW \rightarrow l\nu, l\nu, l\nu$ and $ZH \rightarrow ZWW \rightarrow ll, l\nu, \text{jet}$, where the jet is the result of a W -boson decaying hadronically.

This dissertation focuses on three new regions chosen specifically to isolate the $WH \rightarrow WWW$ and $ZH \rightarrow ZWW$ associated production processes because of their unique characteristics. The signal of WH associated production in the three lepton signature requires the W -boson to radiate a Standard Model Higgs boson that decays to two more W -bosons. Subsequently, all three W -bosons decay leptonically to produce a trilepton signature. Similarly, the ZH associated

production signal requires a Z -boson to radiate a standard model Higgs boson that decays to two W -bosons. The Z -boson then decays to two leptons and we need one of the Higgs- W -bosons to decay leptonically and the other hadronically to produce an exact three-lepton signature. While four-lepton events are rejected from this analysis, some portion of ZH events in the three-lepton signature are actually events with a $ZH \rightarrow lll$ topology where one of the four leptons failed to be identified.

The ZH search is then split into a 1-jet analysis and a ≥ 2 jet analysis, with the 0-jet bin reserved as the ZH control region (see definition 1.1), the WH control region being characterized by low missing energy as expounded in chapter 9. There are advantages to having a ZH signal region that requires at least two jets (presumably the two jets from the hadronically decaying Higgs- W -boson) such as fully reconstructing the mass of the Higgs boson and using the angular separation of the two jets (presumably the two highest energy jets). Correspondingly, the new regions we introduce for trileptons in $H \rightarrow WW$ are denoted *trilepton-NoZPeak* (for the WH -centered analysis) and *trilepton-InZPeak* (for the ZH -centered analyses) to be defined in section 9.2.

Definition 1.1 A *control region* is a set of selection criteria chosen to compliment and be mutually exclusive to the signal region in a manner that maximizes contribution from background processes and minimizes expected contribution from the signal processes (though not necessarily fully “maximized” and “minimized” in a mathematical sense), though still remains topologically similar to the region in which signal events are searched for. This region allows the experimentalist to verify that the expected background processes agree with collected data.

The three lepton + E_T signature with an unspecified number of jets is a relatively complex event topology that introduces a correspondingly large number of variables that describe the event. This is a fortuitous circumstance as it allows the formulation of many variables that powerfully discriminate the signals from backgrounds in both of these new *trilepton-NoZPeak* (WH analysis) and *trilepton-InZPeak* (ZH analysis) regions. Together, they represent a strong addition to the search for the Standard Model Higgs boson.

As a measure of the sensitivity of this search, we compute the median expected limits at 95% confidence level (“C.L.”) on the production cross section (effectively the rate of production) for a Standard Model Higgs boson and report the result as a ratio to the theoretical production cross section, $\sigma_{VH,measured}/\sigma_{VH,SM}$. An observed limit ratio of one or less at a given mass would rule out the production of a Standard Model Higgs boson at that mass with 95% confidence. At $m_H = 165$ GeV, the WH analysis expected limits reach 7.2 times the standard model cross section; the ZH 1-jet analysis is set at 29 times the expected standard model cross section; the $ZH \geq 2$ -jet analysis is set at 9.9 times the expected standard model cross section; and the combined trilepton analysis is set at 4.8 times the expected standard model cross section.

We will see in the Results section (section 9.5) that the expected median limit of 1.00 indicates we anticipate a greater than 50% change of ruling out the existence of a Standard Model Higgs boson of 165 GeV/ c^2 assuming the Higgs boson does not exist or has a different mass. We announce that the Collider Detector at Fermilab (CDF) has achieved Standard Model sensitivity with an expected median limit of 1.00. We do not see evidence for a significant signal of Higgs bosons in the data and place observed limits on the production of a Standard Model Higgs boson of 165 GeV at 1.08 times Standard Model.

Chapter 2

The Higgs Mechanism and the Standard Model of Particle Physics

2.1 Intro. to the Standard Model of Particle Physics

The “Standard Model” of particle physics is a collection of gauge “quantum field theories,” reformulations of Schrodinger-based quantum mechanics that are consistent with Einstein’s special theory of relativity. Of the four known forces in nature (gravity, electromagnetism, weak force, and strong force), the Standard Model incorporates and establishes a quantum theory for all but gravity. Although hypothesized models exist, there is not yet a quantum theory of gravity, which is instead described macroscopically by Einstein’s general theory of relativity.

The standard model is based on the gauge group formed from the product space of three special unitary gauge groups: $SU(3)_C \times SU(2)_L \times U(1)_Y$. The $SU(3)_C$ component represents the symmetry group describing the strong force interaction, with the C subscript referring to “color charge” of quantum chromodynamics. The rest of the gauge group is the “electroweak” portion of the Standard Model, represented by the $SU(2)_L \times U(1)_Y$ group. The “ L ” refers to the $SU(2)$ group’s containing particularly *left-handed* weak doublets and the “ Y ” (a conserved quantum number) refers to the $U(1)$ group’s *right-handed* weak hypercharge singlets.

The Standard Model also contains known particles that interact via these forces. The known particles are categorized as “fermions” (see section 2.2.1) and “bosons” (see section 2.2.2). The fermions of the Standard Model are then divided among “quarks” and “leptons,” which are the known fundamental constituents of matter. The forces by which they interact manifest from the exchange of gauge bosons that exist as a consequence of various symmetries in the Standard Model’s

$SU(3)_C \times SU(2)_L \times U(1)_Y$ gauge group. The existence of all the quarks, leptons, and gauge bosons described so far have been verified experimentally.

There does remain one last constituent of the Standard Model has not yet been experimentally verified: the Higgs boson. Unlike the other bosons that are related to the forces of nature, the Higgs boson is postulated as a consequence of a spontaneously broken symmetry in the electroweak sector ($SU(2)_L \times U(1)_Y$) which is hypothesized to be the property of the universe that results in fundamental particles and weak gauge bosons with non-zero mass. The rest of this chapter will describe the function of the Higgs boson in the Standard Model and the focus of this thesis is on a new contribution to the experimental search for the Higgs boson at the CDFII experiment.

2.2 Elementary Particles in the Standard Model

Particle physics is the study of the most fundamental known constituents of matter in the universe and the forces by which they interact. The “Standard Model” of particle physics is composed of all known fundamental particles, plus the postulated Higgs boson and the forces by which they interact.

We separate the known fundamental particles of the Standard Model into two categories: fermions and bosons.

2.2.1 Fermions

$u^{\pm\frac{2}{3}}$ “up”	$c^{\pm\frac{2}{3}}$ “charm”	$t^{\pm\frac{2}{3}}$ “top”
$d^{\mp\frac{1}{3}}$ “down”	$s^{\mp\frac{1}{3}}$ “strange”	$b^{\mp\frac{1}{3}}$ “bottom”

Table 2.1 Quarks of the Standard Model. The superscript indicates the particles’ electric charges (the top charge refers to the “particles” while the bottom charge refers to the “anti-particles”). As fermions, all quarks have spin of $1/2$.

Fundamental particles are known from experiment to have intrinsic angular momentum denoted colloquially as “spin.” In quantum mechanical systems, particles are capable of assuming only discrete spin states, just as they are also capable of only discrete energy states in a bound system.

$e^{\mp 1}$ “electron”	$\mu^{\mp 1}$ “muon”	$\tau^{\mp 1}$ “tau”
ν_e “electron neutrino”	ν_μ “muon neutrino”	ν_τ “tau neutrino”

Table 2.2 Leptons of the Standard Model. The particles in the top row exist as both “matter” (electric charge of -1) and “anti-matter” (electric charge of $+1$). The bottom row consists of the associated “neutrinos” which have no electric charge. As fermions, all particles listed here have spin $1/2$.

Fermions are defined as particles with half-integer spin magnitudes: $1/2, 3/2, 5/2, \dots$, where the spin is given in units of the Plank constant $\hbar = 6.582 \times 10^{-16}(\text{eV} \cdot \text{s})$ [46]. Physically, \hbar relates cycles (in radians because $\hbar = h/2\pi$) to energy as $E = \hbar\omega$. All the fundamental particles listed in tables 2.1 and 2.2 have spin magnitude $1/2$.

2.2.2 Bosons

Bosons are defined as particles with integer spin magnitudes: $0, 1, 2, \dots$. The three forces of nature described by the Standard Model manifest from an exchange of a boson among the quarks and leptons. These force-carrying bosons arise from symmetries in the Standard Model’s $SU(3)_C \times SU(2)_L \times U(1)_Y$ gauge group. They are:

- *photons* (γ): The gauge boson of the $SU(2)_L \times U(1)_Y$ group which manifests as the electromagnetic force.
- W^+, W^-, Z^0 : The gauge bosons of the $SU(2)_L \times U(1)_Y$ group which manifest as the weak force.
- *gluons* (g): The gauge bosons of the $SU(3)_C$ group which manifest as the strong force.

The Standard Model Higgs boson is unique in that it is not associated with a force of nature and that it arises as a consequence of a broken symmetry referred to as “electroweak symmetry breaking.” We will look at this electroweak symmetry breaking in section 2.3. Then in section 2.4, we will see how the fermion masses are consequences of the Higgs field. Section 2.5 will briefly discuss the role the Higgs boson plays in quark mixing and the CKM matrix. Finally, sections 2.7

and 2.8 will discuss phenomenological calculations of Higgs production and decay, respectively, involved in the experimental search covered by this thesis.

2.3 Electroweak Interactions in the Standard Model: Spontaneously Broken Local $SU(2)_L \times U(1)_Y$ Symmetry

The forces of nature appear to manifest from inherent symmetries. The logical foundation of a physical system is a postulated “lagrangian,” from which the interactions of nature can then be derived. When the fields in a lagrangian can be transformed by an arbitrary element of a particular algebraic “group” and the lagrangian (and therefore the consequential physics) is left unchanged, then we say the lagrangian is “symmetric” to transformations under that particular group.

Definition 2.1 A *group* is a set G along with any binary operation \star on G that satisfies the following three axioms[25]:

- Associativity: $(a \star b) \star c = a \star (b \star c)$, $\forall a, b, c \in G$
- Identity: $\exists e \in G$, denoted the *identity*, such that $\forall a \in G$ we have $a \star e = e \star a = e$.
- Inverse: $\forall a \in G$, $\exists a^{-1} \in G$, denoted the *inverse* of a , such that $a \star a^{-1} = a^{-1} \star a = e$.

For electroweak physics, we will be concerned with just two groups: $U(1)$ and $SU(2)$. Both of these groups are “unitary,” which is critical to establishing such symmetries in the lagrangian.

Definition 2.2 A *unitary matrix* is an $n \times n$ complex matrix M that satisfies $M^\dagger M = M M^\dagger = I_n$, where I_n is the n -dimensional identity matrix and \dagger denotes the Hermitian conjugate (complex conjugate and transpose).

2.3.1 Global $U(1)$ Symmetry

Definition 2.3 The *unitary group* $U(n)$ is a group of unitary $n \times n$ matrices with the binary operation of matrix multiplication. The $U(1)$ unitary group is then the group of complex numbers that equal 1 when multiplied by their complex conjugate, effectively becoming the group of rotations in the complex plane via Euler’s relation: $\cos x + i \sin x = e^{ix}$.

Let's begin by assuming a scalar, complex particle $\phi = \frac{1}{\sqrt{2}}(\phi_1 + i\phi_2)$ and the corresponding Klein-Gordon lagrangian:

$$\mathcal{L} = (\partial_\mu \phi)^\dagger (\partial^\mu \phi) - m_0^2 \phi^\dagger \phi - \frac{1}{4} \lambda (\phi^\dagger \phi)^2 \quad (2.1)$$

This lagrangian is invariant to a $U(1)$ “global” (not dependent on spacetime coordinate) transformation $\phi \rightarrow \phi' = e^{i\alpha} \phi$ because of the unitary nature of $U(1)$ [33]. Lagrangians have the structure of kinetic energy minus potential energy, so the potential described here is $V(\phi) = m_0^2 \phi^\dagger \phi + \frac{1}{4} \lambda (\phi^\dagger \phi)^2$. This potential is symmetric in the complex plane and has an extremum at the origin. If $m_0^2 > 0$, then the extremum is a minimum and we determine the particle spectrum by calculating perturbative oscillations about the minimum. The system describes a complex scalar particle of mass m_0 .

However, Higgs physics in the Standard Model is based on *broken* symmetry, so assume $m_0^2 < 0$. Now the extremum at the origin is unstable and we instead have a minima circle of radius v . To find the particle spectrum in this case, express the field ϕ in polar coordinates

$$\phi(x) = \underbrace{\frac{\rho(x)}{\sqrt{2}}}_{\text{Radial Perturbation}} \cdot \underbrace{e^{\frac{i}{v}\theta(x)}}_{\text{Angular Perturbation}} \quad (2.2)$$

$$\rho(x) \equiv v + h(x) \quad (2.3)$$

and expand about any arbitrary point in the minima manifold. Substituting this form back into the lagrangian yields

$$\mathcal{L} = \frac{1}{2}(\partial_\mu h)^2 + v(\partial_\mu h) + \frac{1}{2}v^2 + \left(\frac{1}{2v^2}h^2 + \frac{1}{v^2}hv + \frac{1}{2v^2}v^2 \right) (\partial_\mu \theta)^2 \quad (2.4)$$

$$- \frac{1}{2}m_0^2 h^2 - m_0^2 v h - \frac{1}{2}m_0^2 v^2 - \frac{1}{16}\lambda(h+v)^4 \quad (2.5)$$

$$= \frac{1}{2}(\partial_\mu h)^2 + \frac{1}{2}(\partial_\mu \theta)^2 - \frac{1}{2}m_0^2 h^2 + \dots \quad (2.6)$$

$$(2.7)$$

Hence, we find that the field perturbation in the radial direction h acquires a mass (note: the direction that climbs the potential) while the angular field perturbation θ (note: directed within

the minima manifold) does not acquire a mass. So field perturbations that climb the potential represent particle states that acquire mass, while not climbing away from the minima manifold of the potential keeps the particle massless. Also, given this parametrization of $\phi(x)$, the vacuum expectation value is

$$\langle 0 | \phi | 0 \rangle = \frac{v}{\sqrt{2}} \quad (2.8)$$

See appendix A for a detailed calculation of these results.

This is a situation where a symmetric field potential is spontaneously broken in nature and this breaking manifests in a physical system different from the situation of the origin being a stable extremum, in which case the symmetry would not spontaneously break in nature.

2.3.2 Local $U(1)$ Symmetry

The global $U(1)$ symmetry of section 2.3.1 is a special case of “local” (the transformation *does* depend on spacetime coordinate) $U(1)$ symmetry. Now, let the angle of rotation in the complex plane α depend on coordinate: $\phi \rightarrow \phi' = e^{i\alpha(x)}\phi$. The lagrangian (eqn. 2.1) of the previous section is not invariant to local $U(1)$ transformations.

To have a lagrangian that is invariant to $U(1)$ local transformations, we must replace the derivative with a “covariant derivative”

$$\partial_\mu \rightarrow D_\mu = \partial_\mu + iqA_\mu \quad (2.9)$$

Thus, to keep the lagrangian invariant, we are postulating the existence of a “gauge field” A_μ and must introduce kinetic terms $F^{\mu\nu} = \partial^\mu A^\nu - \partial^\nu A^\mu$ for it. So the new postulated $U(1)$ locally invariant lagrangian is

$$\mathcal{L} = [(\partial^\mu + iqA^\mu)\phi]^\dagger [(\partial_\mu + iqA_\mu)\phi] - \frac{1}{4}F_{\mu\nu}F^{\mu\nu} - \frac{1}{4}\lambda(\phi^\dagger\phi)^2 - m_0^2(\phi^\dagger\phi) \quad (2.10)$$

$$(2.11)$$

where the gauge field itself transforms as

$$A^\mu(x) \rightarrow A'^\mu(x) = A^\mu(x) + \frac{1}{q}\partial^\mu\alpha(x) \quad (2.12)$$

(see appendix B). If we then use the field parametrization as in the $U(1)$ global case (eqn. 2.2) we find that the field equation is

$$\square A^\nu - \partial^\nu (\partial_\mu A^\mu) = -v^2 q^2 \left(A^\nu - \frac{\partial^\nu \theta}{vq} \right) \quad (2.13)$$

where on the right hand side we see the angular field perturbation θ in a term that looks just like the form of the gauge field transformation. As such, define

$$A'^\nu = A^\nu - \frac{\partial^\nu \theta}{vq} \quad (2.14)$$

Then the field equation becomes

$$(\square + v^2 q^2) A'^\nu - \partial^\nu \partial_\mu A'^\mu = 0 \quad (2.15)$$

Thus, because of $U(1)$ local gauge symmetry, we have two physical consequences: first, we must postulate the existence of a gauge field A_μ ; second, the symmetry allows us to choose a particular $U(1)$ transformation that causes the gauge field A_μ to absorb the θ term and become massive. This technique will be critical in more complicated symmetry groups for computing the massive weak vector bosons and the massless photon. See appendix B for a detailed calculation of these results.

2.3.3 Global $SU(2)$ Symmetry

Definition 2.4 The *special unitary groups* $SU(n)$ are groups of $n \times n$ matrices with determinant 1 that have the binary operation matrix multiplication. The particular case of $n = 2$ is critical to electroweak physics.

Consider a doublet of complex scalar particles

$$\phi = \begin{bmatrix} \phi^+ \\ \phi^0 \end{bmatrix} = \begin{bmatrix} \frac{1}{\sqrt{2}}(\phi_1 + i\phi_2) \\ \frac{1}{\sqrt{2}}(\phi_3 + i\phi_4) \end{bmatrix} \quad (2.16)$$

where ϕ^+ destroys positively charged particles and creates negatively charged particles, and ϕ^0 destroys neutral particles and creates neutral antiparticles.

Postulate the form of the lagrangian as a direct generalization of section 2.3.1.

$$\mathcal{L} = (\partial_\mu \phi)^\dagger (\partial^\mu \phi) - m_0^2 \phi^\dagger \phi - \frac{\lambda}{4} (\phi^\dagger \phi)^2 \quad (2.17)$$

where $m_0^2 < 0$. This lagrangian is not only invariant to global $SU(2)$ transformations, but also to the global $U(1)$ transformations of section 2.3.1 (and appendix A). We treat the global $SU(2)$ case here, so α is not dependent on spacetime coordinate. The $SU(2)$ transformation takes a form similar to the $U(1)$ case:

$$\phi \rightarrow \phi' = e^{-\frac{i}{2} \vec{\alpha} \cdot \vec{\tau}} \phi \quad (2.18)$$

where the $\vec{\tau}$ are the Pauli spin matrices.

To determine the particle spectrum, we again want to find the minima manifold of the potential and compute oscillations from a point in it. The minimum is found at

$$\frac{\partial \mathcal{L}}{\partial (\phi^\dagger \phi)} = -m_0^2 - \frac{\lambda}{2} (\phi^\dagger \phi)_{\min} = 0 \quad (2.19)$$

$$(\phi^\dagger \phi)_{\min} = \frac{-2m_0^2}{\lambda} \equiv \frac{v^2}{2} \quad (2.20)$$

As before, we take the minimum to be the vacuum.

$$\langle 0 | \phi^\dagger \phi | 0 \rangle = \frac{v^2}{2} = \langle 0 | \phi_1^2 + \phi_2^2 + \phi_3^2 + \phi_4^2 | 0 \rangle \quad (2.21)$$

To obtain the particle spectrum we expand the fields ϕ about the choice of vacuum. Again, rather than a single point, we have a whole space of minima to choose from. Let,

$$\langle 0 | \phi | 0 \rangle = \begin{bmatrix} 0 \\ \frac{v}{\sqrt{2}} \end{bmatrix} \quad (2.22)$$

Oscillations about this vacuum choice are parametrized by

$$\phi = e^{-\frac{i}{2} (\vec{\theta}(x) \cdot \vec{\tau}) v} \begin{bmatrix} 0 \\ \frac{1}{\sqrt{2}} (v + H(x)) \end{bmatrix} \quad (2.23)$$

We now have three “angular” field oscillations $\vec{\theta}$ and one radial $H(x)$. Just as in the $U(1)$ case, the angular oscillations are massless particles while $H(x)$ is massive. The lagrangian becomes:

$$\mathcal{L} = \frac{1}{8v^2}(\partial^\mu \vec{\theta} \cdot \vec{\tau})(\partial_\mu \vec{\theta} \cdot \vec{\tau})(v + H)^2 + \frac{1}{2}(\partial^\mu H)(\partial_\mu H) - \frac{m_0^2}{2}v^2 \quad (2.24)$$

$$- \frac{m_0^2}{2}vH - \frac{m_0^2}{2}H^2 - \frac{\lambda}{4}(v + H)^4 \quad (2.25)$$

where we see mass terms for $H(x)$ and no mass terms for the $\vec{\theta}$ fields. We will again exploit the symmetry to gauge the $\vec{\theta}$ fields away. See appendix C for a detailed calculation of these results.

2.3.4 Local $SU(2)$ Symmetry

To generalize to local $SU(2)$ symmetry, we again must assume $\vec{\alpha}$ to be spacetime coordinate dependent.

$$\phi(x) \rightarrow \phi'(x) = e^{\frac{ig}{2}\vec{\tau} \cdot \vec{\alpha}(x)} \phi(x) \quad (2.26)$$

where the factor g is inserted to represent the coupling strength.

Just as in the local $U(1)$ case, our particles are not covariant under this transformation unless we replace the derivatives with suitable covariant derivatives.[15] Our $SU(2)$ covariant derivative is

$$D^\mu \equiv \partial^\mu + \frac{ig}{2}\vec{\tau} \cdot \vec{W}^\mu \quad (2.27)$$

where $\vec{W}^\mu \equiv (W_1^\mu, W_2^\mu, W_3^\mu)$, a slight precursor to the weak vector bosons. These three gauge fields transform as (see appendix D for this derivation)

$$\vec{W}'^\mu = \vec{W}^\mu - \partial^\mu \vec{\epsilon}(x) - g \left[\vec{\epsilon}(x) \times \vec{W}^\mu \right] \quad (2.28)$$

Now that we know how the gauge field and the covariant derivative transform with an $SU(2)$ gauge transformation, we can compute the consequences from our basic postulated lagrangian, which can now be repostulated in $SU(2)$ invariant form

$$\mathcal{L} = (D_\mu \phi)^\dagger (D^\mu \phi) - m_0^2 \phi^\dagger \phi - \frac{\lambda}{4} (\phi^\dagger \phi)^2 - \frac{1}{4} \vec{W}_{\mu\nu} \cdot \vec{W}^{\mu\nu} \quad (2.29)$$

where $\vec{W}_{\mu\nu} \equiv \partial_\mu \vec{W}_\nu - \partial_\nu \vec{W}_\mu - g \vec{W}_\mu \times \vec{W}_\nu$, where the last term is necessary because of the non-Abelian nature of the $SU(2)$ group.

Note that if $m_0^2 > 0$, then we just have a system of four scalar particles of mass m_0 . However, we are interested in the $m_0^2 < 0$ symmetry breaking case. Just as for the $U(1)$ case, we want to find the minima manifold.

$$\frac{\partial \mathcal{L}}{\partial(\phi^\dagger \phi)} = 0 \quad (2.30)$$

$$(\phi^\dagger \phi)_{\min} = -\frac{2m_0^2}{\lambda} = \frac{1}{2} (\phi_1^2 + \phi_2^2 + \phi_3^2 + \phi_4^2) \quad (2.31)$$

We must choose some particular point on the minima manifold upon which to expand and calculate the particle spectrum, so choose $\phi_1 = \phi_2 = \phi_4 = 0$ and then we are left with

$$\frac{1}{2}\phi_3^2 = \frac{-2m_0^2}{\lambda} \quad (2.32)$$

$$\phi_3 = 2\sqrt{\frac{-m_0^2}{\lambda}} \equiv v \quad (2.33)$$

Then our complex field doublet at this minimum becomes

$$\phi_{\min} = \frac{1}{\sqrt{2}} \begin{bmatrix} \phi_1 + i\phi_2 \\ \phi_3 + i\phi_4 \end{bmatrix} = \frac{1}{\sqrt{2}} \begin{bmatrix} 0 \\ v \end{bmatrix} \quad (2.34)$$

Again, completely analogous to the $U(1)$ case, we can parametrize perturbations about this minimum as

$$\phi(x) = \frac{\rho(x)}{\sqrt{2}} e^{\frac{i}{v} \vec{\tau} \cdot \vec{\theta}(x)} \quad , \text{ where} \quad (2.35)$$

$$\rho(x) = \begin{bmatrix} 0 \\ v + h(x) \end{bmatrix} \quad (2.36)$$

and analogous to the $U(1)$ case again, we can choose particular $SU(2)$ transformations to gauge away the $\vec{\theta}$ fields to be left with massive gauge bosons \vec{W} and $H(x)$. This is another example of the Higgs mechanism.

See appendix D for a detailed calculation of these results.

2.3.5 Isospin, Weak Hypercharge, and $SU(2) \times U(1)$ Symmetry

We have now discussed the two basic symmetries, invariance to $U(1)$ and $SU(2)$ transformations that are fundamental to understanding electroweak physics. Just as translational symmetry implied conservation of momentum and temporal symmetry implies conservation of energy in classical physics, for example, these symmetries also imply conserved quantities or “quantum numbers.” From $U(1)$ symmetry, we have conserved quantum number Y (“weak hypercharge”); and from $SU(2)$ symmetry, we have conserved quantum number t_3 (“weak isospin”). In this section, we explore the physics implied by symmetries under the product group $SU(2) \times U(1)$ and see that our choice of location on the minima manifold to expand on will leave the vacuum invariant to a transformation of the form ‘ $U(1) + 3^{\text{rd}}$ component of $SU(2)$.’ Y and t_3 will together define the electric charge of the fundamental particles according to

$$Q = t_3 + \frac{Y}{2} \quad (2.37)$$

Examples of values for the first generation of quarks and leptons are given in tables 2.3 and 2.4.

Leptons	Q	t_3	Y
ν_e	0	$\frac{1}{2}$	-1
e_L^-	-1	$-\frac{1}{2}$	-1
e_R^-	-1	0	-2

Table 2.3 Weak isospin and hypercharge quantum numbers for the first generation of leptons. Left and right handed electrons are listed separately.[33]

For a theory that is invariant to local transformations, we must introduce three $SU(2)$ gauge fields (see appendix D) and one $U(1)$ gauge field (see appendix B). Denote them here as $W_i^\mu(x)$ for $i = 1, 2, 3$ and $B^\mu(x)$, respectively. Also, the derivatives must be replaced with a covariant derivative for both $U(1)$ and $SU(2)$.

$$D^\mu \phi = \left(\partial^\mu + \underbrace{\frac{ig}{2} \vec{\tau} \cdot \vec{W}^\mu}_{SU(2)\text{piece}} + \underbrace{\frac{ig'Y}{2} B^\mu}_{U(1)\text{piece}} \right) \phi \quad (2.38)$$

Quarks	Q	t_3	Y
u_L	$\frac{2}{3}$	$\frac{1}{2}$	$\frac{1}{3}$
d_L	$-\frac{1}{3}$	$-\frac{1}{2}$	$\frac{1}{3}$
u_R	$\frac{2}{3}$	0	$\frac{4}{3}$
d_R	$-\frac{1}{3}$	0	$-\frac{2}{3}$

Table 2.4 Weak isospin and hypercharge quantum numbers for the first generation of quarks. Left and right handed quarks are listed separately.[33]

Kinetic terms for the new gauge fields must also be included.

$$\vec{F}^{\mu\nu} = \partial^\mu \vec{W}^\nu - \partial^\nu \vec{W}^\mu - g \vec{W}^\mu \times \vec{W}^\nu \quad (2.39)$$

$$G^{\mu\nu} = \partial^\mu B^\nu - \partial^\nu B^\mu \quad (2.40)$$

So the new full lagrangian is

$$\mathcal{L} = (D_\mu \phi)^\dagger (D^\mu \phi) + m_0^2 \phi^\dagger \phi - \frac{\lambda}{4} (\phi^\dagger \phi)^2 - \frac{1}{4} \vec{F}_{\mu\nu} \cdot \vec{F}^{\mu\nu} - \frac{1}{4} G_{\mu\nu} G^{\mu\nu} \quad (2.41)$$

$$(2.42)$$

For electroweak theory, we should be left with three massive gauge bosons (W^\pm, Z) and one massless gauge boson (photon). Being massless, the photon corresponds to some symmetry that is left unbroken. Weinberg suggested [15]

$$\langle 0 | \phi | 0 \rangle = \begin{bmatrix} 0 \\ \frac{\sqrt{2}m_0}{\sqrt{\lambda}} \end{bmatrix} \equiv \begin{bmatrix} 0 \\ \frac{v}{\sqrt{2}} \end{bmatrix} \quad (2.43)$$

This choice leaves the vacuum invariant to a transformation of $U(1)$ + third component of $SU(2)$.

That is,

$$(1 + \tau_3) \langle 0 | \phi | 0 \rangle = (1 + \tau_3) \begin{bmatrix} 0 \\ \frac{v}{\sqrt{2}} \end{bmatrix} = \begin{bmatrix} 2 & 0 \\ 0 & 0 \end{bmatrix} \begin{bmatrix} 0 \\ \frac{v}{\sqrt{2}} \end{bmatrix} = \begin{bmatrix} 0 \\ 0 \end{bmatrix} \quad (2.44)$$

where the $\vec{\tau}$ are the Pauli matrices. This is also why we eventually find the electric charge to be expressed in terms of weak hypercharge Y and third component of isospin t_3 [33]. We are about to

see that this interplay between the $U(1)$ symmetry (corresponding to Y) and the third component of $SU(2)$ symmetry (corresponding to t_3) manifests as a mixing of the W_3^μ and B^μ gauge fields to yield the photon field A^μ and the neutral weak vector boson Z .

To consider oscillations about the vacuum, parametrize the degrees of freedom by

$$\phi = e^{-\frac{i}{2v}\vec{\theta}(x)\cdot\vec{\tau}} \begin{bmatrix} 0 \\ \frac{1}{\sqrt{2}}(v + H(x)) \end{bmatrix} \quad (2.45)$$

However, recall that the three $\vec{\theta}$ field perturbations, which would become Goldstone bosons, disappear if we make the appropriate gauge transformation. So we effectively use

$$\phi = \begin{bmatrix} 0 \\ \frac{1}{\sqrt{2}}(v + H(x)) \end{bmatrix} \quad (2.46)$$

The consequences for the lagrangian are (details of how the following form of the lagrangian are calculated are in appendix H)

$$\mathcal{L} = \frac{1}{2}(\partial_\mu H)(\partial^\mu H) + \frac{m_0^2}{2}(v + H)^2 - \frac{\lambda}{16}(v + H)^4 - \frac{1}{4}\vec{F}_{\mu\nu} \cdot \vec{F}^{\mu\nu} - \frac{1}{4}G_{\mu\nu}G^{\mu\nu} \quad (2.47)$$

$$\mathcal{L} = \frac{1}{2}(\partial_\mu H)(\partial^\mu H) + \frac{m_0^2}{2}(v + H)^2 - \frac{\lambda}{16}(v + H)^4 \quad (2.48)$$

$$- \frac{1}{4}(\partial_\mu W_{1\nu} - \partial_\nu W_{1\mu})(\partial^\mu W_1^\nu - \partial^\nu W_1^\mu) + \frac{1}{8}g^2v^2W_{1\nu}W_1^\nu \quad (2.49)$$

$$- \frac{1}{4}(\partial_\mu W_{2\nu} - \partial_\nu W_{2\mu})(\partial^\mu W_2^\nu - \partial^\nu W_2^\mu) + \frac{1}{8}g^2v^2W_{2\nu}W_2^\nu \quad (2.50)$$

$$- \frac{1}{4}(\partial_\mu W_{3\nu} - \partial_\nu W_{3\mu})(\partial^\mu W_3^\nu - \partial^\nu W_3^\mu) - \frac{1}{4}G_{\mu\nu}G^{\mu\nu} \quad (2.51)$$

$$+ \frac{1}{8}v^2(gW_{3\mu} - g'YB_\mu)(gW_3^\mu - g'YB^\mu) + \text{Higgs interactions} \quad (2.52)$$

The second and third lines show that the W_1 and W_2 gauge fields are massive and have the same mass $m_W = \frac{gv}{2}$. These are the W^+, W^- vector gauge bosons in electroweak theory. The Higgs interaction terms are being ignored here because we are focusing on the generation of the Standard Model gauge bosons in this section. In appendix H, I go through the details of deriving the full version of this and discuss the interactions between the Higgs and gauge bosons that are produced.

The Higgs boson decaying to gauge bosons is precisely the kind of interaction that this dissertation explores experimentally.

The last two lines show that the gauge fields W_3 and B are mixed. The key clue is to notice in the last line it is the combination $(gW_3^\mu - g'Y B^\mu)$ that has a mass. Introduce the linear combinations

$$Z^\mu \equiv W_3^\mu \cos \theta_W - B^\mu \sin \theta_W \quad (2.53)$$

$$A^\mu \equiv W_3^\mu \sin \theta_W + B^\mu \cos \theta_W \quad (2.54)$$

where

$$\cos \theta_W = \frac{g}{\sqrt{g^2 + g'^2 Y^2}} \quad (2.55)$$

$$\sin \theta_W = \frac{g'Y}{\sqrt{g^2 + g'^2 Y^2}} \quad (2.56)$$

Using this, we can write the last two lines of the lagrangian in terms of A^μ and Z^μ , instead of B^μ and W_3^μ . They become:

$$-\frac{1}{4} (Z_{\mu\nu} Z^{\mu\nu} + \mathcal{F}_{\mu\nu} \mathcal{F}^{\mu\nu}) + \frac{1}{8} v^2 Z_\mu Z^\mu (g^2 + g'^2 Y^2) \quad (2.57)$$

for $\mathcal{F}_{\mu\nu} \equiv \partial_\mu A_\nu - \partial_\nu A_\mu$ and $Z_{\mu\nu} \equiv \partial_\mu Z_\nu - \partial_\nu Z_\mu$.

Hence, we have unmixed the two fields. They become the Z boson and the photon.

$$m_Z = \frac{1}{2} v^2 \sqrt{g^2 + g'^2 Y^2} = \frac{m_W}{\cos \theta_W} \quad (2.58)$$

$$m_A = 0 \quad (2.59)$$

where $Y = 1$ and $t_3 = -1/2$ breaks both $SU(2)$ and $U(1)_Y$ symmetries, but leaves the $U(1)_{em}$ symmetry unbroken ($Q = t_3 + Y/2 = -1/2 + 1/2 = 0$).[33]

See appendix E for a detailed calculation of these results.

2.4 The Higgs Mechanism and Fermion Masses

Section 2.3 explored $SU(2) \times U(1)$ spontaneous symmetry breaking and the Higgs mechanism for scalar particles, with Klein-Gordon lagrangians. However, leptons and quarks are fermions. We

will first explore spontaneous $SU(2)_L \times U(1)_Y$ symmetry breaking for a massless fermion doublet, then focus on how the Higgs mechanism generates the fermion masses. We will also see that the same covariant derivatives used for scalar particles will be applicable here and produce the gauge bosons.

For more extensive computational details pertinent to this section, please refer to the appendices F and G.

2.4.1 $SU(2) \times U(1)$ Symmetry For Massless Fermions

We know now from section 2.3 what our postulated lagrangian should look like in order to be both $U(1)$ and $SU(2)$ invariant, which necessarily involved the weak vector bosons and the photon. Let's look at $SU(2) \times U(1)$ gauge invariance for the first generation of quarks; the calculation is identical for the higher generations. The calculation for the lepton generations is also very similar and so not repeated in this dissertation.

The Higgs mechanism is *not* included here so the quarks will still be massless; that will be dealt with in section 2.4.2. Instead, we will deal with fermions that appear as a left-handed doublet and right-handed singlets for both particles.

Suppose we have the (fermion) quark doublet

$$q = \begin{bmatrix} u \\ d \end{bmatrix} \quad (2.60)$$

and recall that

$$\psi_L = \left(\frac{1 - \gamma_5}{2} \right) \psi \quad (2.61)$$

$$\psi_R = \left(\frac{1 + \gamma_5}{2} \right) \psi \quad (2.62)$$

are relations distinguishing the left and right handed components.

As always, we must postulate a lagrangian. In the sections exploring $U(1)$ and $SU(2)$ symmetries, we used generalizations of the Klein-Gordon equation's lagrangian for scalar particles. Now we want to look at spin-1/2 fermions, so we must use the Dirac lagrangian in our gauge invariant form.

Recall the Dirac lagrangian

$$\mathcal{L} = i\bar{\psi}\gamma_\mu\partial^\mu\psi - m\bar{\psi}\psi \quad (2.63)$$

Now we want a massless version for a fermion doublet:

$$\mathcal{L} = \bar{q}i\not{D}q \quad (2.64)$$

$$\mathcal{L} = \bar{q}_Li\not{D}_Lq_L + \bar{u}_Ri\not{D}_Ru_R + \bar{d}_Ri\not{D}_Rd_R \quad (2.65)$$

where the covariant derivative for the doublet \not{D}_L is $SU(2) \times U(1)$ invariant, and \not{D}_R is only $U(1)$ invariant for the singlet:

$$D_L^\rho = \partial^\rho + \frac{ig}{2}\vec{\tau} \cdot \vec{W}^\rho + \frac{ig'Y}{2}B^\rho \quad (2.66)$$

$$D_R^\rho = \partial^\rho + \frac{ig'Y}{2}B^\rho \quad (2.67)$$

After exhaustive computation reminiscent of previous sections (and found in appendix F) we arrive at

$$\mathcal{L} = i\bar{u}\gamma_\rho\left(\frac{1+\gamma_5}{2}\right)(\partial^\rho u) + i\bar{d}\gamma_\rho\left(\frac{1+\gamma_5}{2}\right)(\partial^\rho d) \quad (2.68)$$

$$+ i\bar{u}\gamma_\rho\left(\frac{1-\gamma_5}{2}\right)(\partial^\rho u) + i\bar{d}\gamma_\rho\left(\frac{1-\gamma_5}{2}\right)(\partial^\rho d) \quad (2.69)$$

$$+ \frac{1}{\sqrt{2}}g\bar{u}\gamma_\rho W^\rho\left(\frac{1-\gamma_5}{2}\right)d + \frac{1}{\sqrt{2}}g\bar{d}\gamma_\rho W^{\rho\dagger}\left(\frac{1-\gamma_5}{2}\right)u \quad (2.70)$$

$$+ \frac{g}{2\cos\theta_W}Z^\rho\left[\bar{u}\gamma_\rho\left(\frac{1+\gamma_5}{2}\right)u\left(\frac{4}{3}\sin^2\theta_W\right) - \bar{d}\gamma_\rho\left(\frac{1+\gamma_5}{2}\right)d\left(\frac{2}{3}\sin^2\theta_W\right)\right] \quad (2.71)$$

$$+ \bar{u}\gamma_\rho\left(\frac{1-\gamma_5}{2}\right)u\left(-1 + \frac{4}{3}\sin^2\theta_W\right) - \bar{d}\gamma_\rho\left(\frac{1-\gamma_5}{2}\right)d\left(-1 + \frac{2}{3}\sin^2\theta_W\right) \quad (2.72)$$

$$- \frac{2e_0}{3}\bar{u}\gamma_\rho u A^\rho + \frac{e_0}{3}\bar{d}\gamma_\rho d A^\rho \quad (2.73)$$

where the electric charge is defined as $e_0 = g \sin \theta_W$. This form illustrates the interactions among the quarks in the fermion doublet and the gauge bosons.

2.4.2 The Higgs Mechanism in Fermion Mass Generation

The kinetic part of a free Dirac fermion does not mix the left and right components of the field:

$$\bar{\psi}\gamma_\mu\partial^\mu\psi = \bar{\psi}_R\gamma_\mu\partial^\mu\psi_R + \bar{\psi}_L\gamma_\mu\partial^\mu\psi_L \quad (2.74)$$

Because of this, we can gauge the left and right handed components differently. Weak interactions are parity violating in the Standard Model and the $SU(2)_L$ covariant derivative acts only on the left-handed term. However, a Dirac mass term has the form

$$-m(\bar{\psi}_L\psi_R + \bar{\psi}_R\psi_L) \quad (2.75)$$

when we write the left and right handed components separately. So the components are coupled, meaning any such mass term breaks $SU(2)_L$ gauge invariance.

In a theory with spontaneous symmetry breaking, there is a way of giving mass to fermions without explicitly introducing gauge invariance breaking mass terms in the lagrangian. Consider the electron $SU(2)_L$ doublet

$$l = \begin{bmatrix} \nu \\ e \end{bmatrix}_L \quad (2.76)$$

the Higgs doublet

$$\phi = \begin{bmatrix} \phi^+ \\ \phi^0 \end{bmatrix} \quad (2.77)$$

$$\phi^+ = \frac{1}{\sqrt{2}}(\phi_1 - i\phi_2) \quad (2.78)$$

$$\phi^0 = \frac{1}{\sqrt{2}}(\phi_3 - i\phi_4) \quad (2.79)$$

and the right handed electron singlet in a Yukawa model.

$$\mathcal{L}_e = -g_e \bar{l}_L \phi e_R - g_e \bar{e}_R \phi^\dagger l_L \quad (2.80)$$

Recall from section 2.3.5 that the vacuum expectation value of the Higgs doublet assumes the value

$$\langle 0 | \phi | 0 \rangle = \begin{bmatrix} 0 \\ \frac{v}{\sqrt{2}} \end{bmatrix} \quad (2.81)$$

The consequence for a fermion doublet in this lagrangian is

$$\mathcal{L}_e = -g_e \bar{l}_L \phi e_R - g_e \bar{e}_R \phi^\dagger l_L \quad (2.82)$$

$$= -\frac{g_e v}{\sqrt{2}} [\bar{e}_L e_R + \bar{e}_R e_L] \quad (2.83)$$

This is exactly a Dirac mass with $m_e = \frac{g_e v}{\sqrt{2}}$. That was precisely the vacuum. Now let's see that if we consider also oscillations about the vacuum we generate a coupling between the electron and the Higgs field. In the last line, use $v + H$ instead of just v .

$$\langle 0 | \mathcal{L}_e | 0 \rangle = -\frac{g_e v}{\sqrt{2}} [\bar{e}_L(v + H)e_R + \bar{e}_R(v + H)e_L] \quad (2.84)$$

$$= -\frac{g_e v}{\sqrt{2}} \left[\underbrace{v \bar{e} e}_{\text{Dirac electron mass}} + \underbrace{\bar{e} H e}_{\text{electron-Higgs coupling}} \right] \quad (2.85)$$

Notice for the coupling term

$$\left(\frac{-g_e}{\sqrt{2}} \right) \bar{e} H e = \left(-\frac{m_e}{v} \right) \bar{e} H e = \left(-\frac{g m_e}{2m_W} \right) \bar{e} H e \quad (2.86)$$

So in addition to interactions of the form $f \bar{f} \rightarrow (\gamma \text{ or } Z^0) \rightarrow W^+ W^-$ we also have the possibility $f \bar{f} \rightarrow H \rightarrow W^+ W^-$ —precisely the interaction this dissertation conducts an experimental search for. The presence of the fermion mass in the coupling to the Higgs is significant.

Summarily, to give the electron-neutrino $SU(2)$ doublet mass (as well as the other lepton and quark doublets), we are adding more terms to the lagrangian derived at the end of section F of the form:

$$\mathcal{L}_{f,\text{Higgs}} = \sum_{l=e,\mu,\tau} \left[-\frac{g_l}{\sqrt{2}} \left[v \bar{l} + \bar{l} H l \right] - \frac{g_{\nu_l}}{\sqrt{2}} \left[v \bar{\nu}_l \nu_l + \bar{\nu}_l H \nu_l \right] \right] \quad (2.87)$$

for the three lepton generations and similar terms for the three quark doublets. Because of the Higgs mechanism, we now have sensible masses for Standard Model particles; however, it should be noted that this does not quite give the final form of the quark mass terms. A similar treatment for all three generations of quarks yields a results that includes “quark mixing,” the ability of quarks to change flavor via charged weak interactions in which the Higgs boson plays a central role. This treatment is outlined in section 2.5. (See appendix G for more details).

2.5 The Higgs Field, Quark Mixing, and the CKM Matrix

Generating the masses of quarks and leptons is not the only function the Higgs boson serves in the Standard Model. It also plays a central role in “quark mixing,” the ability of quarks to change flavor via weak charge changing interactions.

Consider three doublets of left-handed quark fields:

$$q_{L1} = \begin{bmatrix} u_{L1} \\ d_{L1} \end{bmatrix}; \quad q_{L2} = \begin{bmatrix} u_{L2} \\ d_{L2} \end{bmatrix}; \quad q_{L3} = \begin{bmatrix} u_{L3} \\ d_{L3} \end{bmatrix} \quad (2.88)$$

and the six corresponding right-handed singlets: $u_{R1}, d_{R1}, u_{R2}, d_{R2}, u_{R3}, d_{R3}$. The lagrangian is then similar to the case for leptons already considered. The difference is that there are three quark families and each $SU(2)_L$ scalar (such as $\bar{q}_{Li}\phi_c$) can be paired with any of the three u_{Rj} , for $i, j \in \{1, 2, 3\}$. So allowing “mixing” of the families results in nine pairings. The nine couplings form the 3×3 CKM matrix.

We begin with the lagrangian

$$\mathcal{L} = \sum_{\{i,j\}=1,2,3} \left[a_{ij} \bar{q}_{Li} \phi_c u_{Rj} + a_{ij}^\dagger \bar{u}_{Rj} \phi_c^\dagger q_{Li} + b_{ij} \bar{q}_{Li} \phi_c d_{Rj} + b_{ij}^\dagger \bar{d}_{Rj} \phi_c^\dagger q_{Li} \right] \quad (2.89)$$

So far, a_{ij} and b_{ij} may be any complex value and are included as values to gauge the coupling strength. After much working over, the lagrangian becomes[15]

$$\mathcal{L} = \sum_k \left[m_{a,k} \left(\bar{u}_{Lk} u_{Rk} \left(1 + \frac{H}{v} \right) + \bar{u}_{Rk} u_{Lk} \left(1 + \frac{H}{v} \right) \right) \right. \quad (2.90)$$

$$\left. + m_{b,k} \left(\bar{d}_{Lk} d_{Rk} \left(1 + \frac{H}{v} \right) + \bar{d}_{Rk} d_{Lk} \left(1 + \frac{H}{v} \right) \right) \right] \quad (2.91)$$

where v appears again from the parametrization of the potential minimum in the Higgs mechanism, and $m_{a,k} = a_{kk}v/\sqrt{2}$, $m_{b,k} = b_{kk}v/\sqrt{2}$ are the quark masses. Notice also that quark couplings to the Higgs boson are another consequence.

It is important to note that the mass and Higgs interaction terms are not the only places that quark field appear in the Standard Model lagrangian. There were certain variable transformations performed to get this result— whose details are not pertinent to this disseratation—that must be

propagated in the terms of line 2.70, above. Beginning with that line for all three generations of quarks:

$$\sum_{k=1,2,3} \frac{1}{\sqrt{2}} g \bar{u}_k \gamma_\rho W^\rho \left(\frac{1 - \gamma_5}{2} \right) d_k + \frac{1}{\sqrt{2}} g \bar{d}_k \gamma_\rho W^{\rho\dagger} \left(\frac{1 - \gamma_5}{2} \right) u_k \quad (2.92)$$

We now perform a change of variables on the u and d quarks with unitary matrices S and T :

$$u_k = U_{ki} u_i \quad (2.93)$$

$$d_k = S_{kj} d_j \quad (2.94)$$

to get the following:

$$= \frac{g}{\sqrt{2}} \sum_{i,j,k} \left[(U_{ki} u_i)^\dagger \gamma_0 W (S_{kj} d_j) \left(\frac{1 - \gamma_5}{2} \right) + (S_{kj} d_j)^\dagger \gamma_0 W^\dagger (U_{ki} u_i) \left(\frac{1 - \gamma_5}{2} \right) \right] \quad (2.95)$$

$$= \frac{g}{\sqrt{2}} \sum_{i,j,k} \left[u_i^\dagger U_{ik}^* \gamma_0 W S_{kj} d_j \left(\frac{1 - \gamma_5}{2} \right) + d_j^\dagger S_{jk}^* \gamma_0 W^\dagger U_{ki} u_i \left(\frac{1 - \gamma_5}{2} \right) \right] \quad (2.96)$$

$$= \frac{g}{\sqrt{2}} \sum_{i,j,k} \left[\bar{u}_i W d_j (U_{ik}^* S_{kj}) \left(\frac{1 - \gamma_5}{2} \right) + \bar{d}_j W^\dagger u_i (S_{jk}^* U_{ki}) \left(\frac{1 - \gamma_5}{2} \right) \right] \quad (2.97)$$

$$(2.98)$$

That is, the charge changing weak interactions link the three u_i quarks with a unitary rotation of the triplet of d_i quarks, with this rotation given by the unitary matrix $V \equiv U^\dagger S$,

$$V = \begin{bmatrix} V_{ud} & V_{us} & V_{ub} \\ V_{cd} & V_{cs} & V_{cb} \\ V_{td} & V_{ts} & V_{tb} \end{bmatrix} \quad (2.99)$$

2.6 The Electroweak Lagrangian of the Standard Model

The basic structure of the electroweak sector of the Standard Model (i.e. quantum chromodynamics, or the “strong force”, is excluded) has now been outlined piecewise, so let’s bring them together and comprehensively illustrate the components.

The electroweak Standard Model lagrangian is:

$$\mathcal{L}_{\text{SM}} = \underbrace{\sum_{l=e,\mu,\tau} \bar{l}_L i \not{D}_L l_L}_{\text{left-handed lepton doublets, section 2.4.1}} + \underbrace{\sum_{q=1,2,3} \bar{q}_L i \not{D}_L q_L}_{\text{left-handed quark doublets, same as section 2.4.1}} \quad (2.100)$$

$$+ \underbrace{\sum_{l=e,\mu,\tau} \bar{l}_R i \not{D}_R l_R + \sum_{q=u,d,s,c,t,b} \bar{q}_R i \not{D}_R q_R}_{\text{all leptons \& quark right-handed singlets, section 2.4.1}} \quad (2.101)$$

$$- \underbrace{\frac{1}{4} \vec{F}_{\mu\nu} \cdot \vec{F}^{\mu\nu} - \frac{1}{4} G_{\mu\nu} G^{\mu\nu}}_{W^\pm, Z, \gamma \text{ kinetic \& self-interaction terms, section 2.3.5}} \quad (2.102)$$

$$+ \underbrace{(D_{L,\mu} \phi)^\dagger (D_{L,\mu} \phi) + m_H^2 \phi^\dagger \phi - \frac{\lambda}{4} (\phi^\dagger \phi)^2}_{\text{Higgs Sector: } W^\pm, Z, \gamma \text{ Higgs masses and couplings, section 2.3.5}} \quad (2.103)$$

$$- \underbrace{\sum_{l=e,\mu,\tau} g_l \left(\bar{l}_L \phi l_R + \bar{l}_R \phi^\dagger l_L \right)}_{\text{Lepton masses \& Higgs couplings, section 2.4.2}} \quad (2.104)$$

$$- \underbrace{\sum_{\{i,j\}=1,2,3} \left[a_{ij} \bar{q}_{Li} \phi_c u_{Rj} + a_{ij}^\dagger \bar{u}_{Rj} \phi_c^\dagger q_{Li} + b_{ij} \bar{q}_{Li} \phi d_{Rj} + b_{ij}^\dagger \bar{d}_{Rj} \phi^\dagger q_{Li} \right]}_{\text{Quark masses, mixing, Higgs couplings, section 2.5}} \quad (2.105)$$

where we have the following terms summarily defined:

$$D_L^\rho = \partial^\rho + \frac{ig}{2} \vec{\tau} \cdot \vec{W}^\rho + \frac{ig'Y}{2} B^\rho \quad (2.106)$$

$$D_R^\rho = \partial^\rho + \frac{ig'Y}{2} B^\rho \quad (2.107)$$

$$l_L = \begin{bmatrix} l \\ \nu_l \end{bmatrix} \quad (2.108)$$

$$l_R = l_R(\text{right-handed lepton singlet}) \quad (2.109)$$

$$q_L = \begin{bmatrix} u_L \\ d_L \end{bmatrix} \quad (2.110)$$

$$q_R = q_R(\text{right-handed quark singlet}) \quad (2.111)$$

$$(2.112)$$

$$\phi = \begin{bmatrix} \phi^+ \\ \phi^0 \end{bmatrix} \quad (2.113)$$

$$\phi^+ = 1/\sqrt{2}(\phi_1 - i\phi_2) \quad (2.114)$$

$$\phi^0 = 1/\sqrt{2}(\phi_3 - i\phi_4) \quad (2.115)$$

$$\langle 0|\phi|0\rangle = \begin{bmatrix} 0 \\ \frac{v}{\sqrt{2}} \end{bmatrix} \quad (2.116)$$

$$\phi_c = i\tau_2\phi = \begin{bmatrix} \phi_0^\dagger \\ -\phi^- \end{bmatrix} \quad (2.117)$$

$$\phi^- = 1/\sqrt{2}(\phi_2 + i\phi_1) \quad (2.118)$$

Thus, from this postulate is derived all known physics except for the gravitational force from general relativity and the strong force from quantum chromodynamics. It accounts for the masses and interactions of all known fundamental particles, the Higgs boson, and the electroweak force. To reiterate, the Higgs boson is the only particle in this lagrangian that has not been experimentally discovered, it's presence in this model is required for the other particles to have nonzero masses (except the photon), and is crucial to our understanding of how heavy quarks are capable of decaying to lighter ones. If neither the Standard Model Higgs boson nor any of its analogous supersymmetric counterparts (not addressed in this dissertation) were to not exist, this lagrangian could no longer be postulated as a true theory of science and the state of physics would face a massive rewriting.

Assuming the Standard Model Higgs boson does exist, let's observe why it is searched for in decays to W -boson pairs. The Higgs sector of the lagrangian above (lines 2.102 and 2.103) is detailed in appendix H, where the lagrangian terms can be solved into a form that better reveals

the details of the physics implied.

$$\mathcal{L}_{\text{Higgs}} = \underbrace{\frac{1}{2}(\partial_\mu H)(\partial^\mu H) + \frac{1}{2}m_0^2(v + H)^2 - \frac{\lambda}{16}(v + H)^4}_{\text{Higgs kinetic, mass, and self-interaction terms}} \quad (2.119)$$

$$- \underbrace{\frac{1}{4}(\partial_\mu W_{1\nu} - \partial_\nu W_{1\mu})(\partial^\mu W_1^\nu - \partial^\nu W_1^\mu) - \frac{1}{4}(\partial_\mu W_{2\nu} - \partial_\nu W_{2\mu})(\partial^\mu W_2^\nu - \partial^\nu W_2^\mu)}_{W^\pm \text{ kinetic terms}} \quad (2.120)$$

$$- \frac{1}{4}(\partial_\mu W_{3\nu} - \partial_\nu W_{3\mu})(\partial^\mu W_3^\nu - \partial^\nu W_3^\mu) - \frac{1}{4}G_{\mu\nu}G^{\mu\nu} \quad (2.121)$$

$$+ \underbrace{\frac{1}{8}v^2(gW_{3\mu} - g'YB_\mu)(gW_3^\mu - g'YB^\mu)}_{\text{Terms that become the } Z\text{-boson and photon}} \quad (2.122)$$

$$+ \frac{g^2v^2}{4}W_\mu^\dagger W^\mu + \frac{g^2v}{2}W_\mu^\dagger W^\mu H + \frac{g^2}{4}W_\mu^\dagger W^\mu H^2 + \frac{g^2v}{4}|W_3|^2H + \frac{g^2}{8}|W_3|^2H^2 \quad (2.123)$$

$$- \underbrace{\frac{gg'Yv}{2}W_{3\mu}B^\mu H - \frac{gg'Y}{2}W_{3\mu}B^\mu H^2 + \frac{g'^2Y^2v}{4}|B|^2H + \frac{g'^2Y^2}{8}|B|^2H^2}_{W^\pm \text{ mass, trilinear, quadrilinear couplings with the Higgs}} \quad (2.124)$$

$$\underbrace{\frac{1}{2}g(\vec{W}_\mu \times \vec{W}_\nu) \cdot (\partial^\mu \vec{W}^\mu - \partial^\nu \vec{W}^\nu) - \frac{1}{4}g^2[|W_\mu|^2|W_\nu|^2 - |\vec{W}_\mu \cdot \vec{W}_\nu|^2]}_{\text{Quadrilinear couplings among the gauge bosons}} \quad (2.125)$$

In this, notice in particular the two terms describing the W -boson mass and the term describing trilinear interaction between the W and Higgs: $\frac{g^2v^2}{4}W_\mu^\dagger W^\mu + \frac{g^2v}{2}W_\mu^\dagger W^\mu H$. The coefficients reveal that the mass of the W -boson and its coupling to the Higgs boson are intertwined. The vacuum expectation value is proportional to v and the Higgs field is a perturbation H from the minimum manifold (discussed earlier) that is defined as the vacuum. To get the interaction term between the W and Higgs from the W mass term, a factor of the vacuum expectation value v is replaced with the Higgs field H . Thus, a highly valued W -boson mass (described by $\frac{g^2v^2}{4}$) implies a strong coupling to the Higgs field (described by $\frac{g^2v}{2}$), especially for highly valued Higgs masses. When the Higgs mass is assumed to be ≥ 160 GeV, it can decay to two real W -bosons ($m_W \approx 80$ GeV) and that becomes the dominant decay mode. The decay rate for this high mass Higgs boson is described in section 2.8 and computed in detail in appendix J.

The Higgs mass itself is not postulated or predicted by the Standard Model, but there are several pieces of information available to constrain a mass range in which it should exist (if it exists at all). The Higgs mass term indicates $m_H = v\sqrt{2\lambda} = \sqrt{2}m_0$ [16, 44]. The Higgs boson's mass depends on the magnitudes of the coupling factor λ as well as v . On the low end, The Higgs boson mass must be greater than about 114 GeV because of experimental exclusion from LEP [18]. On the high end, the measurement of the top quark mass ($m_t \approx 173$ GeV) constrains the Higgs' mass because the quark masses depend on the value of v (see section 2.5).

The most recent constraints on the Higgs' mass to date, which account for Tevatron results as well as the older constraints from LEP, are summarized in [27]. With 90% confidence level, the mass of the Higgs boson is $115 \leq m_H \leq 148$ GeV.

2.7 Higgs Boson Associated Production with a Vector Boson

There are four major ways to produce a Standard Model Higgs boson in the mass range relevant to the high mass search: gluon fusion, vector boson fusion, associated production with a W -boson, and associated production with a Z -boson. In the $H \rightarrow WW$ trilepton channel, only the two associated production processes contribute a non-negligible amount of signal.

The Tevatron consists of a proton beam and an anti-proton beam that collide within the heart of the CDF detector. Protons are composite particles of two up quarks and one down quark while anti-protons are composed of one up quark and two down quarks, so the specific interactions involved are:

- $u^{+\frac{2}{3}} + \bar{d}^{+\frac{1}{3}} \rightarrow W^+ \rightarrow HW^+$
- $\bar{u}^{-\frac{2}{3}} + d^{-\frac{1}{3}} \rightarrow W^- \rightarrow HW^-$
- $\bar{q} + q \rightarrow Z \rightarrow HZ$

To calculate the cross section for one of these interactions, we begin with the fundamental postulate of experimentally verified physics (except, of course, for the Higgs boson itself): the Standard Model Lagrangian. The relevant terms for the first interaction listed above, for example,

are:

$$\mathcal{L} = \underbrace{\frac{1}{2} (\partial_\mu H) (\partial^\mu H) + \frac{1}{2} \mu^2 H^2 + \frac{g^2 v^2}{4} W_\mu^\dagger W^\mu + \frac{g^2 v}{2} W_\mu^\dagger W^\mu H}_{\text{Higgs Sector}} \quad (2.126)$$

$$- \underbrace{\frac{1}{4} \sum_{i=1,2} (\partial_\mu W_{i\nu} - \partial_\nu W_{i\mu}) (\partial^\mu W_i^\nu - \partial^\nu W_i^\mu)}_{\text{W boson kinetic terms}} \quad (2.127)$$

$$+ \underbrace{i \bar{u} \gamma_\rho \left(\frac{1 - \gamma_5}{2} \right) \partial^\rho u + i \bar{d} \gamma_\rho \left(\frac{1 - \gamma_5}{2} \right) \partial^\rho d + \frac{g V_{ud}}{\sqrt{2}} \bar{d} \gamma_\rho W^{\dagger\rho} \left(\frac{1 - \gamma_5}{2} \right) u}_{\text{Quark Doublet}} \quad (2.128)$$

We see in the first line the ‘‘Higgs Sector’’ which contains the kinetic term for the Higgs boson, the self-energy of the Higgs boson and W boson, and the term allowing interactions between the W -boson and the Higgs boson. The second line contains the W -boson kinetic terms and the third line yields the left-handed quark doublet (the $\left(\frac{1 - \gamma_5}{2}\right)$ factor ensures left-handedness) and their interaction with the W -boson. Following the computations of appendix I, we arrive at the invariant amplitude.

$$i\mathcal{M} = \left[-i \frac{\alpha m_W V_{ud}}{\sqrt{2} \sin^2 \theta_W} \right] \epsilon_\mu^{s*}(k') \left[\frac{-g^{\mu\rho} + \frac{q^\mu q^\rho}{m_W^2}}{q^2 - m_W^2 + i\varepsilon} \right] \bar{d}^{r_1}(p') \gamma_\rho \left(\frac{1 - \gamma_5}{2} \right) u^{r_2}(p) \quad (2.129)$$

The next step in finding the differential cross section is to compute $|\mathcal{M}|^2$, for which we first need \mathcal{M}^* .

$$\mathcal{M}^* = - \frac{\alpha m_W V_{ud}}{\sqrt{2} \sin^2 \theta_W} \left[\epsilon_\mu^{s*}(k') \left[\frac{-g^{\mu\rho} + \frac{q^\mu q^\rho}{m_W^2}}{q^2 - m_W^2 + i\varepsilon} \right] \bar{d}^{r_1}(p') \gamma_\rho \left(\frac{1 - \gamma_5}{2} \right) u^{r_2}(p) \right]^* \quad (2.130)$$

$$= - \frac{\alpha m_W V_{ud}}{\sqrt{2} \sin^2 \theta_W} \bar{u} \gamma_\rho \left(\frac{1 - \gamma_5}{2} \right) d \left[\frac{-g^{\mu\rho} + \frac{q^\mu q^\rho}{m_W^2}}{q^2 - m_W^2 + i\varepsilon} \right] \epsilon_\mu^s(k') \quad (2.131)$$

The beam at the Tevatron is unpolarized, so average over spins r_1, r_2 of the quarks. The polarization of the end states is not measured, so the cross section is a sum of the possible polarization states of the W . As such, we want to compute

$$\frac{1}{2} \sum_{r_1} \frac{1}{2} \sum_{r_2} \sum_s |\mathcal{M}|^2 \quad (2.132)$$

To do this, we use the spin sums (see eqns. (3.66), (3.67) of Peskin and Schroeder [45])

$$\sum_s u^s(p) \bar{u}^s(p) = \gamma \cdot p + m \quad (2.133)$$

$$\sum_s v^s(p) \bar{v}^s(p) = \gamma \cdot p - m \quad (2.134)$$

$$\sum_s \epsilon_\sigma^s(k') \epsilon_\mu^{s*}(k') = -g_{\sigma\mu} + \frac{k'_\sigma k'_\mu}{m_W^2} \quad (2.135)$$

to get

$$\frac{1}{4} \sum_{r_1, r_2, s} |\mathcal{M}|^2 = \frac{1}{4} \left(\frac{\alpha m_W V_{ud}}{\sqrt{2} \sin^2 \theta_W} \right)^2 \sum_{r_1, r_2, s} \left[\epsilon_\mu^{s*}(k') \left[\frac{-g^{\mu\rho} + \frac{q^\mu q^\rho}{m_W^2}}{q^2 - m_W^2 + i\varepsilon} \right] \bar{d}^{r_1}(p') \gamma_\rho \right. \quad (2.136)$$

$$\left. \left(\frac{1 - \gamma_5}{2} \right) u^{r_2}(p) \bar{u}^{r_2}(p) \gamma_\nu \left(\frac{1 - \gamma_5}{2} \right) d^{r_1}(p') \left[\frac{-g^{\sigma\nu} + \frac{q^\sigma q^\nu}{m_W^2}}{q^2 - m_W^2 + i\varepsilon} \right] \epsilon_\mu^s(k') \right] \quad (2.137)$$

$$= \frac{1}{4} \left(\frac{\alpha m_W V_{ud}}{\sqrt{2} \sin^2 \theta_W} \right)^2 \left[\left(-g_{\sigma\mu} + \frac{k'_\sigma k'_\mu}{m_W^2} \right) \left(\frac{-g^{\mu\rho} + \frac{q^\mu q^\rho}{m_W^2}}{q^2 - m_W^2 + i\varepsilon} \right) \left(\frac{-g^{\sigma\nu} + \frac{q^\sigma q^\nu}{m_W^2}}{q^2 - m_W^2 + i\varepsilon} \right) \right] \quad (2.138)$$

$$\text{Tr} \left[\gamma_\rho \left(\frac{1 - \gamma_5}{2} \right) (\not{p} + m_u) \gamma_\nu \left(\frac{1 - \gamma_5}{2} \right) (\not{p}' - m_d) \right] \quad (2.139)$$

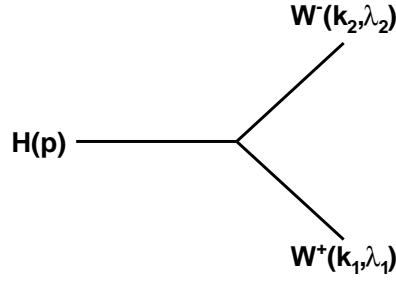
It remains to evaluate the trace and simplify the terms, then use the invariant amplitude squared to compute the cross section with general form [45]

$$d\sigma = \frac{1}{2E_A \cdot 2E_B |v_A - v_B|} \left[\frac{d^3 k}{2E_k (2\pi)^3} \frac{d^3 k'}{2E'_k (2\pi)^3} \right] \frac{1}{4} \sum_{r_1, r_2, s} |\mathcal{M}|^2 (2\pi)^4 \delta^4(k + k' - p - p') \quad (2.140)$$

where $|v_A - v_B| \cong 2c$ is the relative velocity difference in the lab frame.

Finally, the cross section for Higgs boson associated production with a W boson is (in terms of the Mandelstam variables) [17]

$$\boxed{\sigma(u\bar{d} \rightarrow WH) = \frac{\pi \alpha^2 |V_{ud}|^2}{36 \sin^4 \theta_W} \frac{2k}{\sqrt{s}} \frac{k^2 + 3m_W^3}{(s - m_W^2)^2}} \quad (2.141)$$



Similarly, the cross section for associated production with a Z boson is[17]

$$\sigma(q\bar{q} \rightarrow ZH) = \frac{2\pi\alpha^2(l^2 + r^2)}{144 \sin^4 \theta_W \cos^4 \theta_W} \frac{2k}{\sqrt{s}} \frac{k^2 + 3m_Z^3}{(s - m_Z^2)^2} \quad (2.142)$$

where $l \equiv 2(t_3 - Q \sin^2 \theta_W)$, $r \equiv -2Q \sin^2 \theta_W$, Q is the electric charge, and t_3 is the weak isospin quantum number.

2.8 Higgs Boson Decay ($H \rightarrow WW$)

Now that we have a physical model with a Higgs boson and have computed the cross sections of its production channels pertinent to our experimental search, let's see how it decays.

Consider the decay in figure 2.8. The lagrangian density for a Standard Model Higgs boson decaying to two W -bosons comes from the Higgs sector of the Standard Model lagrangian.

$$\mathcal{L} = \underbrace{\frac{1}{2} (\partial_\mu H) (\partial^\mu H) + \frac{1}{2} \mu^2 H^2 + \frac{g^2 v^2}{4} W_\mu^\dagger W^\mu + \frac{g^2 v}{2} W_\mu^\dagger W^\mu H}_{\text{Higgs Sector}} \quad (2.143)$$

$$\underbrace{-\frac{1}{4} \sum_{i=1,2} (\partial_\mu W_{i\nu} - \partial_\nu W_{i\mu}) (\partial^\mu W_i^\mu - \partial^\nu W_i^\mu)}_{\text{W boson kinetic terms}} \quad (2.144)$$

$$(2.145)$$

The decay rate derived from this lagrangian is (see appendix J for details):

$$\Gamma = \frac{G_F m_H^3}{8\sqrt{2}\pi} \left(1 - \frac{4m_W^2}{m_H^2} + \frac{12m_W^4}{m_H^4} \right) \sqrt{1 - \frac{4m_W^2}{m_H^2}} \quad (2.146)$$

$$(2.147)$$

This solution assumes a Higgs mass of $m_H \geq 2m_W$ (where $m_W \approx 80$ GeV), the region of most interest to this analysis. Assuming $m_H < 2m_W$ leads to a different solution and is applicable to the low mass Higgs search.

Chapter 3

The Tevatron

This contribution to the search for the Standard Model Higgs boson is conducted at the Fermi National Accelerator Laboratory with the “Tevatron,” a roughly four mile circular track around which protons and antiprotons are accelerated and collided with a center of mass energy of 1.96 TeV. These collisions occur at the “Collider Detector at Fermilab” experiment (CDF) where the data is recorded for future analysis. The collection, manipulation, and collision of protons and antiprotons is a formidable task. This chapter outlines the process that leads to the colliding beams of the Tevatron while the CDF collider experiment is detailed in chapter 4

Figure 3.1 illustrates the stages of producing the colliding beams, beginning with the Cockcroft-Walton site and ending with the Tevatron collisions in the CDF and D0 experiments.

3.1 Beginning of the Beam: Cockcroft-Walton

The beams begin simply as hydrogen gas. The gas is injected into an electric field that is strong enough to strip the electrons from the hydrogen nuclei, leaving positively charged hydrogen ions (H^+). In the electric field, these ions are then directed towards a cesium anode where they acquire two electrons, become *negatively* charged H^- ions now. With a newly acquired negative net charge, these H^- ions are repelled from the anode and accelerated to 750 KeV by a Cockcroft-Walton accelerator—a type of Van de Graaf accelerator—towards a linear accelerator.

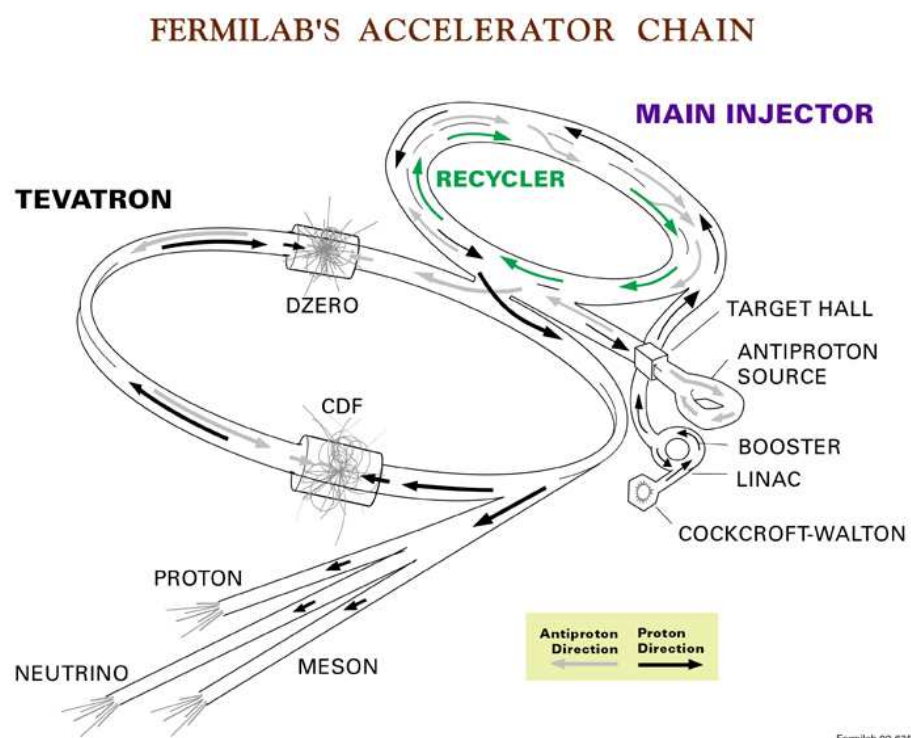


Figure 3.1 The Tevatron Accelerator Chain [11]

3.2 LINAC: The Linear Accelerator

The 750 KeV hydrogen ions enter a linear accelerator that operates with a succession of drift tubes generating an electric field oscillating with a radio frequency. H^- ions arriving at the linac in phase with the field oscillation are accelerated to 400 MeV over a distance of 130 meters, while those arriving out of phase with the linac's field are lost. This creates a beam of discrete bunches of ions rather than a steady stream. At the end of the linac, the bunched beam of ions impinges on a carbon barrier that strips the electrons from the hydrogen nuclei which are now just protons that pass.

3.3 Booster

Observe in figure 3.1 that the linac tangentially intersects the circular “booster.” Sequentially, this is the first synchrotron—a circular accelerator with carefully synchronized electric and magnetic field to direct the beam of ions—that the protons encounter on their path to the colliders. The booster accelerates the protons from 400 MeV to 8 GeV.

3.4 Main Injector

After being ramped to an energy of 8 GeV in the Booster, the protons are redirected towards the “main injector”—another larger synchrotron that accelerates the proton bunches to 150 GeV for injection into the Tevatron. The main injector also plays a central role in the production of the antiprotons. Some protons from the main injector are used to produce antiprotons, which are accumulated separately. They are then also directed into the main injector which will inject the antiprotons into the Tevatron. [3]

3.5 Anti-protons

Protons in the main injector are accelerated to 150 GeV if they are to be injected into the Tevatron, but are accelerated to 120 GeV if they are to be used for antiproton production. These 120 GeV protons are directed to impact a nickel-based target every 1.5 seconds causing a variety

of interactions. For every one million protons that hit the nickel target, only ~ 20 antiprotons are produced with enough energy to enter the “accumulator.”

After passing the nickel target, the products pass through a “lithium lens” that focuses them into a beam that passes through a magnet. This magnet then filters the antiprotons by redirecting them on a unique path that leads them to the “debuncher.” Because of the radio-frequency used to accelerate the 120 GeV protons in the main injector, the antiprotons are still in a beam of discrete bunches. These antiprotons also have a large spread in energy, so the debuncher is tuned in a way that decelerates higher energy antiprotons and accelerates lower energy antiprotons.

After the debuncher is finished with the antiprotons, they are successively stored in the “accumulator” at 8 GeV over many hours (or even up to a few days) while waiting to be transferred to the Tevatron for a fresh beam. When the Tevatron is ready for new colliding beams, the antiprotons are transferred from the accumulator to the “recycler” (also an 8 GeV ring) before moving on to the main injector and the Tevatron. [2]

3.6 The Tevatron

The first version of the tevatron became operational in 1983. It was the world’s first superconducting synchrotron, containing about 1000 superconducting magnets. Because superconducting wires provide no resistance to the flow of charge, stronger magnetic fields are achievable and operational costs are reduced because electricity is not lost to dissipation.

The collider physics program at the Tevatron is separated between a *Run I* (1992-1996, 1.8 TeV) and *Run II* (2001-present, 1.96 TeV). As the Tevatron approaches the last years of *Run II* operation, the CDF and D0 experiments are quickly closing in on achieving Standard Model sensitivity for the Higgs boson search. [10]

The Tevatron receives the proton and antiproton beams from the main injector, both at 150 GeV. Both beams are injected in 36 discrete bunches, though not in equal densities since antiprotons are far more difficult to collect than protons. Each bunch contains on the order of 10^{11} protons or 10^{10} antiprotons.

Once all 36 bunches of each beam have been injected into the Tevatron, the beam is ramped from the 150 GeV to its colliding energy of 980 GeV. They are then focused, or “squeezed,” and collimators are used to absorb extraneous particles orbiting the beam. This is sometimes denoted the “beam halo.”

The instantaneous luminosity for the collisions is given by:

$$L_{\text{inst.}} = \frac{36f N_p N_{\bar{p}}}{4\sigma_x \sigma_y} \quad (3.1)$$

where the 36 denotes the number of bunches in each beam, f is the frequency of the revolutions, N_p is the number of protons in the bunch, $N_{\bar{p}}$ is the number of antiprotons in a bunch, and σ_x, σ_y are Gaussian profiles of a transverse cross section of the beams. Integrated (over time) luminosities are typically given in units of inverse barns, which can then be easily multiplied by the cross section for a particular process (units in barns) to obtain the expected number of occurrences for that physical interaction. [4]

3.7 The Performance of the Tevatron in Run II

As of March 30, 2010, the Tevatron is no longer the world’s most powerful particle collider. The LHC produced collisions at 7 TeV. However, the Tevatron continues to produce impressive results. During the same calendar month, the Tevatron broke two of its own records: it delivered 272.7 pb^{-1} of integrated luminosity and saw an initial instantaneous luminosity record of $371 \times 10^{30} \text{ cm}^{-2} \text{ s}^{-1}$. It has also been consistently seeing initial instantaneous luminosities of $\sim 350 \times 10^{30} \text{ cm}^{-2} \text{ s}^{-1}$. Further, figure 3.1 illustrates consistent and accelerating progress in data delivery.

As such, the Tevatron will still retain a leading role in particle physics research for at least the next few years as of this writing (spring 2010).

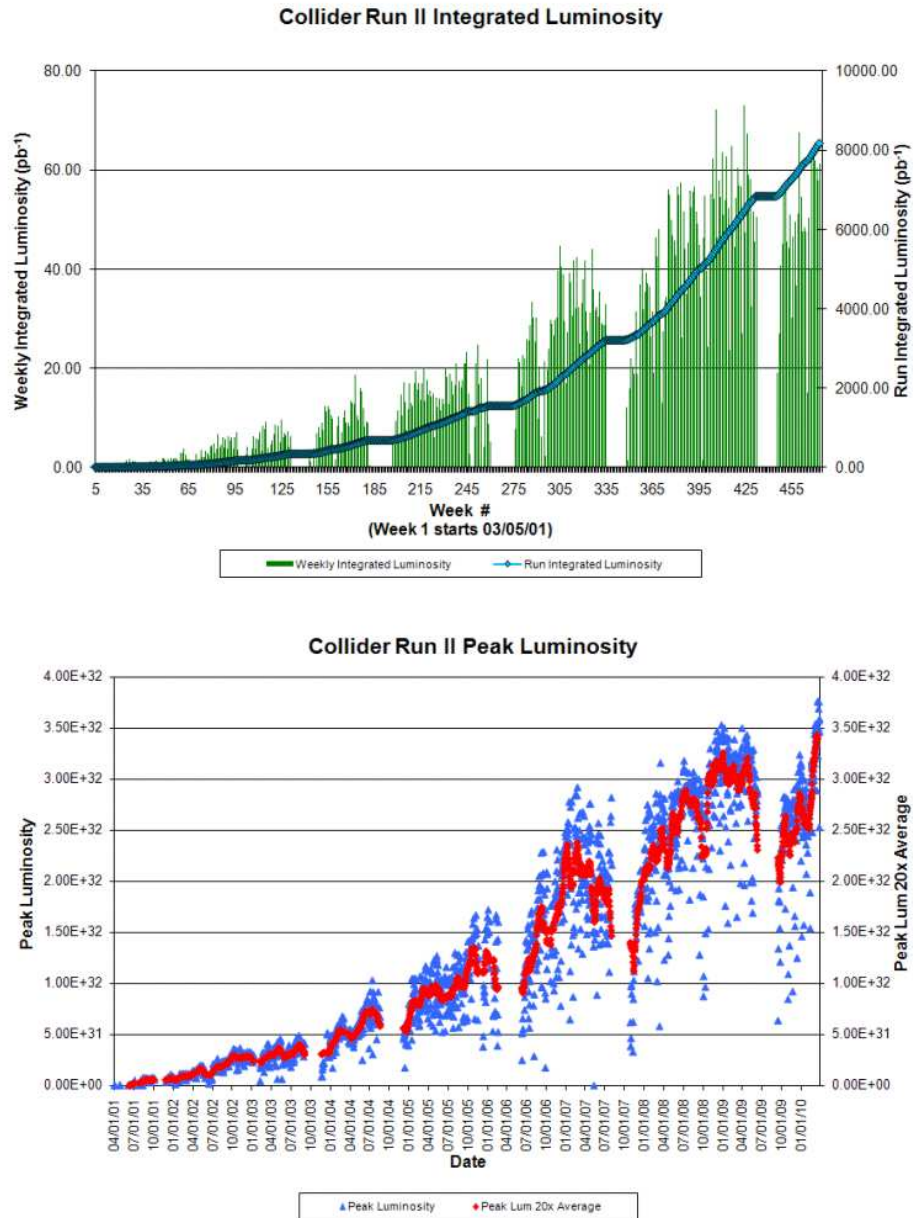


Figure 3.2 The Tevatron Run II luminosity performance [8]

Chapter 4

The CDF II Detector

The CDF experiment resides at the B0 site of the Tevatron and is one of two experimental detectors that collide the proton-antiproton beams to record the consequences of the collisions. The present incarnation of the CDF detector (“Run II”) has been operational since 2001. It was originally designed with several specific purposes in mind: [23]

- Study the properties of the top quark
- Obtain more precise measurements of important quantities in electroweak physics
- Test perturbative Quantum Chromodynamics
- Constrain the CKM matrix with measurements of B decays
- Directly search for new physics

Since the Higgs boson has not been experimentally verified, the study presented in this dissertation falls into the “search for new physics” category. Although, it is certainly related to electroweak measurements as well.

An overview of the experimental apparatus can be seen in figure 4.1. It contains a variety of different detection systems designed to collectively distinguish a variety of objects that may result from the $p\bar{p}$ collisions. Closest to the beamline is the silicon detector, which records the tracks of charged particles like leptons and charged hadrons. The silicon is encased in the “Central Outer Tracker” (COT), which also provides tracking information (see section 4.2). The next layer outward is the electromagnetic calorimeter, which is designed to absorb and measure the energy

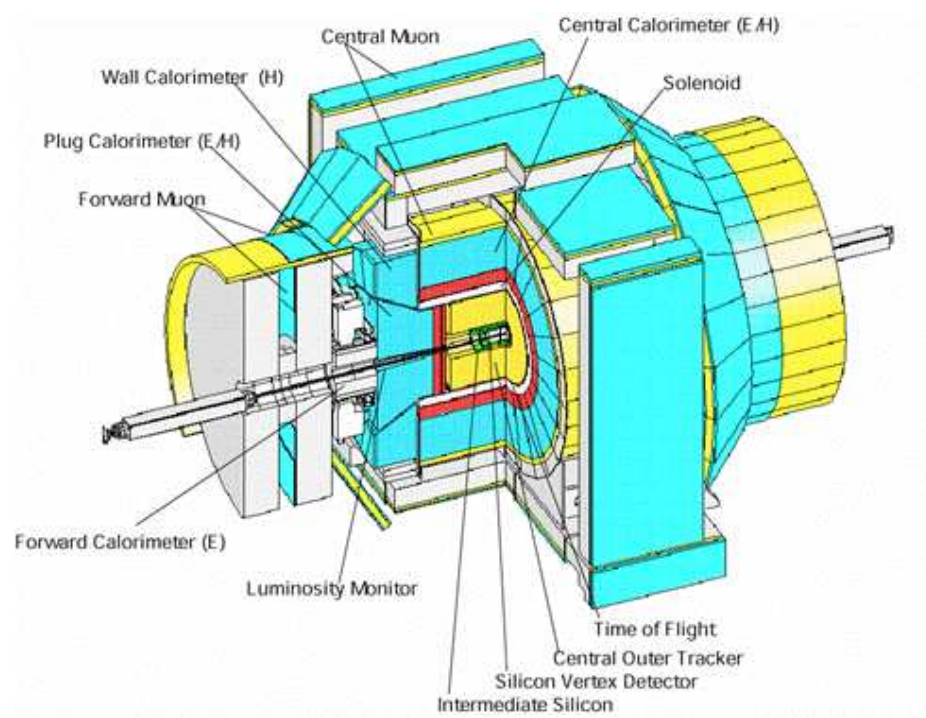


Figure 4.1 The CDF II Detector

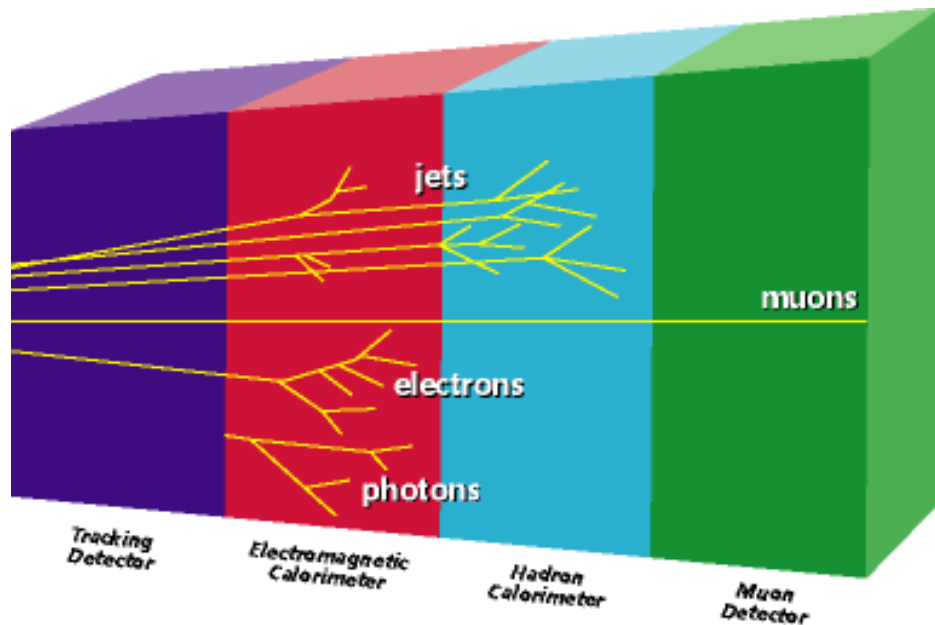


Figure 4.2 Diagram showing the types of objects various layers are constructed to detect.

of photons and electrons as indicated by figure 4.2. Hadrons tend to be more massive and are measured in the subsequent “hadronic calorimeter” (see section 4.3). Though charged, muons tend to punch through the calorimeter system and are then detected by one of several muon detection systems (see section 4.4).

The various systems are used interactively to detect any particular kind of object. Electrons, for example, are tracked through the silicon and COT, then these tracks are matched to energy deposits in the electromagnetic calorimeter. Muons are also tracked through the silicon and COT, then matched to signals left in the muon system. Jets are collections of particles that deposit energy in both the electromagnetic and hadronic calorimeter systems. All together, the CDF detector is designed to record the presence of any kind of electron, muon, photon, or jet produced in $p\bar{p}$ collisions.

4.1 CDF Coordinates

Tracking the paths of various detector quantities requires a common coordinate system and CDF places the origin at the center of the experiment, on the beamline, where collisions are most

likely to occur. The positive x coordinate points radially away from the center of the Tevatron, y points vertically upward, and z is directed tangent to the path of the proton beam.

The azimuthal angle is denoted ϕ and given by

$$\phi = \arctan\left(\frac{y}{x}\right) \quad (4.1)$$

The polar angle is denoted θ and given by

$$\theta = \arctan\left(\frac{y}{z}\right) \quad (4.2)$$

The angle θ , however, is not often used. Instead, we use “pseudorapidity,” where “rapidity” is defined as

$$\text{rapidity} = \frac{1}{2} \ln \frac{E + p_z}{E - p_z} \quad (4.3)$$

and in its massless approximation ($p \gg m$) becomes pseudorapidity:

$$\eta = -\ln \tan\left(\frac{\theta}{2}\right) \quad (4.4)$$

4.2 Trackers

The CDF II tracking system is composed of three major components: a silicon microstrip system that provides precise tracking of charged particles close to the beamline; the “Central Outer Tracker” (COT) that envelops the silicon system; and finally a solenoid magnet generating a 1.4 T field along the \hat{z} direction. The two tracking systems trace the paths of charged particles while the solenoid’s field causes those paths to follow a helical pattern. Positive and negative charges can then be distinguished by the direction the helical path curves, while the particle’s momentum can be calculated by the magnitude of the curvature.

4.2.1 The Silicon Detectors

The CDF II silicon detector is composed of three components: L00, SVXII, and ISL. Layer zero-zero (L00) is a single sided, radiation tolerant silicon strip detector, which is closest to the

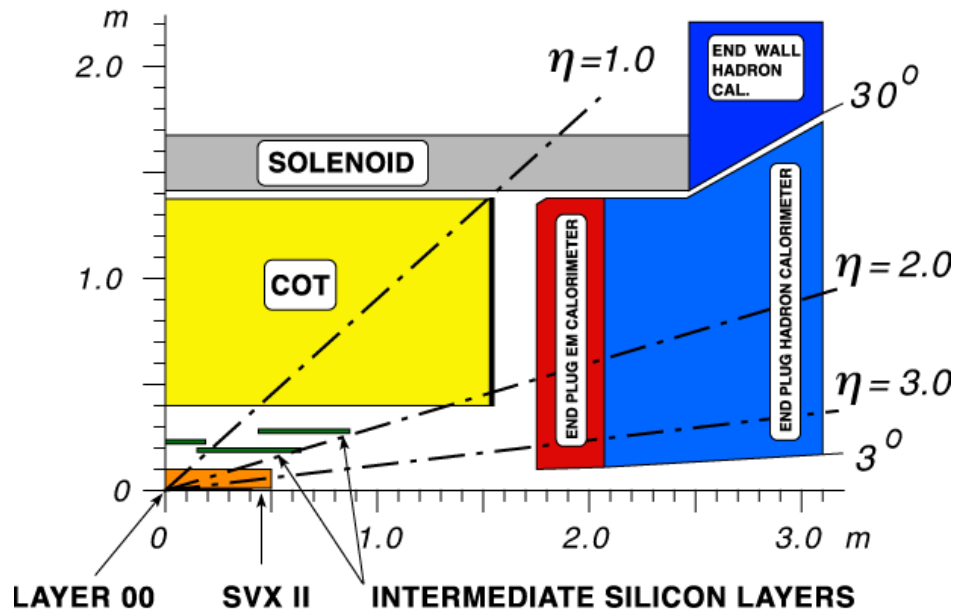


Figure 4.3 Diagram showing a side view of the tracking, solenoid, and forward calorimeter systems. The horizontal axis is the \hat{z} -direction from the interaction vertex and the vertical axis is the radial direction from the beamline.

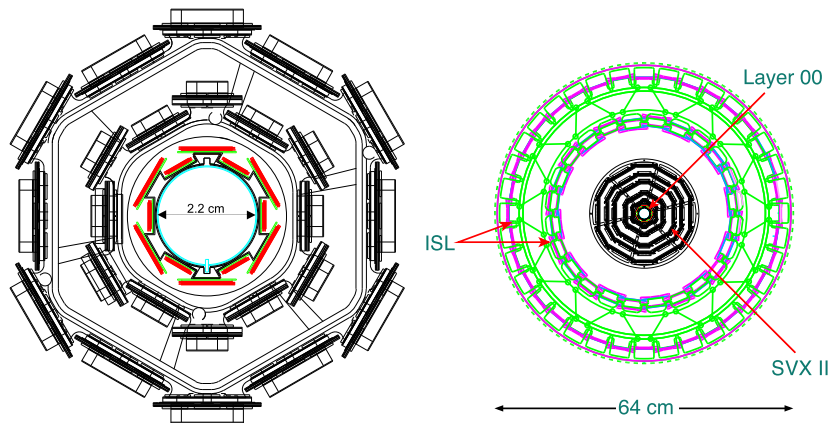


Figure 4.4 End view of L00 (left) and the full silicon system (right)[5],[6]

beamline. It is 87 cm long, centered on $z = 0$, and has a radius of just 1.1 cm (see figure 4.4). L00 is constructed in six segments in both z and ϕ . Each ϕ segment contains 128 channels of narrow, inner sensors and 256 channels of wider, outer sensors. Each z segment is composed of two long sensors. In total, L00 contains 13,824 channels. [5]

The SVX II silicon detector encapsulates L00. It is composed of three barrels, positioned end-to-end to achieve a length of 81 cm and full coverage in ϕ . Each barrel contains five layers of silicon microstrip detectors ranging from 2.4 cm to 10.6 cm from the beamline. In all, the SVX contains 405,504 detection channels and covers $|\eta| < 2.0$. [6],[23]

The “intermediate silicon layers” (ISL) are the outermost section of the silicon detector system, between the SVX and the COT (see figure 4.3). The ISL are an important complement to the SVX and COT (see section 4.2.2) in that they provide extra tracking information in $1.0 < |\eta| < 2.0$, where COT coverage is partial. In this forward region, there are two silicon layers placed at 20 cm and 28 cm from the beamline. There is also an additional ISL layer in the central region at 22 cm from the beamline. [7],[23]

4.2.2 Central Outer Tracker

The CDF Central Outer Tracker (COT) complements the silicon tracking system to provide additional tracking information. It covers the comparatively larger range of 40 cm to 130 cm from the beamline and is approximately three meters long. Instead of the wafers of silicon, the COT operates as a 96-layered drift chamber. The 96 layers are partitioned into 8 “superlayers” alternating between axial and stereo. “Axial” layers provide hit coordinates in the transverse plane (radial and azimuthal angle) while “stereo” layers supply the z coordinate, together yielding hit information in three dimensions.

The COT is filled with an equal mixture of argon and ethane in an electric field. When a charged particle enters the COT apparatus, it ionizes the gas by creating e^+e^- pairs. Electrons then drift under the influence of the electric field toward anode wires and signals are induced from the flow of charge. [9],[22]

Use of these tracking systems—in conjunction with the calorimeters and muon systems—is critical to the detection of leptons emanating from the $p\bar{p}$ collisions. This dissertation is devoted to the rare events that contain three recognized leptons, so a clear understanding of how physical leptons produced in $p\bar{p}$ interactions translate into detected leptons used for analysis is critical. This dissertation devotes chapter 6 to a detailed understanding of how the CDF subsystems are collectively used to identify leptons from charged tracks and other detector information.

4.3 Calorimeters

The calorimeter systems are located outside the solenoid and record the energies of particles resulting from $p\bar{p}$ interactions. They are composed of scintillators with layers of heavy metal to induce electromagnetic or hadronic showers.

Electromagnetic showers are induced for high energy photons and electrons via a combination of bremsstrahlung and pair production. When impinging on the heavy metal layer, a high energy electron will radiate high energy photons, which then converts to $e\bar{e}$ pairs, which go on to emit more photons, etc. This cycle continues until the individual photons and electrons no longer have enough energy to pair-produce and the ionization loss prevents further radiation. The physical depth achieved by this “shower” is then an indicator of how much energy the original electron or photon possessed. [43]

Hadronic showers occur when a high energy hadron experiences an inelastic nuclear collision with the heavy metal layer, producing secondary hadrons that go on to have their own collisions. This cycle continues until the individual hadrons no longer have enough energy to break up nuclei. Hadrons tend to be much more massive than electrons and a relatively large amount of energy is released from nuclear interactions, so the depth that a hadronic shower penetrates is larger and such calorimeters must be physically larger than the electromagnetic calorimeters.[43]

4.3.1 CDF Central Electromagnetic Calorimeter (CEM)

CDF’s central electromagnetic calorimeter (CEM) is composed of 48 wedges that each cover 15° in azimuth and 0.11 in pseudorapidity (η). Each 15° wedge has alternating lead and scintillator

layers. The energy resolution (in GeV) of the EM calorimeter is

$$\frac{\delta E}{E} = 13.5\%/\sqrt{E_T} + 1.7\% \quad (4.5)$$

[23]

4.3.2 CDF Hadronic Calorimeters (CHA,WHA)

The central hadronic calorimeter (CHA) and the endwall hadronic calorimeter (WHA) wedges are composed of alternating layers of iron and scintillator. Both the CHA and WHA are an array of 48 wedges, with the CHA covering $|\eta| < 0.9$ and the WHA covering $0.7 < |\eta| < 1.3$. The energy resolution of the CHA and WHA detectors are

$$\frac{\delta E}{E_T} = \frac{50\%}{\sqrt{E_T}} \quad (4.6)$$

and

$$\frac{\delta E}{E_T} = \frac{75\%}{\sqrt{E_T}} \quad (4.7)$$

repsectively.

4.3.3 CDF Forward Calorimeters (PEM, PHA)

The forward calorimeters are also divided between a “plug electromagnetic calorimeter” (PEM) and a “plug hadronic calorimeter” (PHA), covering $1.1 < |\eta| < 3.6$ and $1.2 < |\eta| < 3.6$, respectively. The design and function is similar to the central calorimeters. The energy resolution of the PEM is

$$\frac{\delta E}{E} = 16\%/\sqrt{E_T} + 1\% \quad (4.8)$$

and the energy resolution of the PHA is

$$\frac{\delta E}{E} = 80\%/\sqrt{E_T} + 5\% \quad (4.9)$$

[23]

4.4 Muon Detectors

The first thing to know about muon detectors is that there is no such thing as a muon detector, just a charged particle detector located behind so much material that only muons tend to reach it. Given that, the CDF muon detectors are located outside the calorimeter system from the beam-line. This way, any high energy photons will have already been absorbed by the EM calorimeter and any high energy hadrons will have already been absorbed by the hadronic calorimeter—aside from the occasional “punch through” hadron. The three muon detectors used for this analysis are the “Central MUon chambers” (CMU), “Central Muon uPgrade” (CMP), and the “Central Muon eXtension” (CMX). Not used is the “Intermediate MUon” (IMU) system in the forward region of the detector ($|\eta| > 1.0$), which contains the “Barrel MUon” chamber (BMU) and BSU/TSU scintillators (see table 4.1 for a summary).

The CMP and CMX muon detectors contain two systems: a stack of four single-cell drift chambers that provide a short track called a “stub” and a scintillation counter. The CMU has only a drift chamber. These muons detectors are used in tandem with the silicon and COT trackers to establish muon tracks from which the transverse momentum p_T is gauged by the track curvature. Since this analysis focuses on a signal with a leptonic signature, the detection of muon (along with electrons) is critical to finding, excluding, or setting limits on a signal. Also, we shall see in chapter 9 that distinguishing muons from electrons will be a useful tool in using a neural net (see chapter 7) to distinguish signal from particular backgrounds.

Chambers/Counters	$\Delta\eta$	$\Delta\phi$	$T_{\text{max drift}}$	# channels
CMU	[0.0, 0.6]	360°	800 ns	2304
CMP/CSP	[0.0, 0.6]	360°	1500 ns	1076/274
CMX/CSX	[0.6, 1.0]	360°	1600 ns	2208/324
BMU/BSU,TSU	[1.0/(1.0,1.3),1.5/(1.5,1.5)]	$270^\circ/270^\circ, 360^\circ$	800 ns	1728/432,144

Table 4.1 Basic Summary of CDF Muon Detectors [48]

4.5 CDF Detector Summary for $VH \rightarrow VWW \rightarrow \text{Trileptons}$

This chapter explored the basic structure and design of the CDF II detector. At the broadest level, the CDF detector is composed of trackers, calorimeters, and the muon detectors (very similar to the trackers). The trackers trace the paths of the charged particles while the calorimeters absorb and record their energies.

This analysis searches for a $VH \rightarrow VWW \rightarrow \text{Trilepton} + \cancel{E}_T$ signature, so understanding how physical leptons (electrons and muons) translate into detector quantities is critical for matching the Standard Model physics of chapter 2 to experimental observation.

The Tevatron generates collisions very quickly and most will produce interactions that are not of interest to the experimentalist. Therefore, collider detectors have “trigger systems” that can quickly use tracker and calorimeter information to make decisions in real time about whether or not a particular event ($p\bar{p}$ interaction) has generated products that are interesting for some reason. Because the $VH \rightarrow VWW$ signature of interest to this analysis contains leptons and \cancel{E}_T , triggers that are programmed to record specifically these events are of particular interest. We shall subsequently explore the idea of triggers and the particular triggers used in this analysis in chapter 5. Once the triggers have recorded datasets that *may* have the signature of interest, offline algorithms perform more computationally intensive calculations to more accurately decide if a collection of detector quantities does constitute a reconstructed lepton. Such reconstructed lepton identification will be explored in more detail in chapter 6. Although jet identification will be useful for distinguishing signal from backgrounds (ZH tends to have ~ 2 jets while its background tend to have 0 jets, for example), jet-based triggers will not be an item of interest to this analysis.

Chapter 5

Triggers, Datasets, and Event Selection

The Tevatron $p\bar{p}$ collisions happens every 396 ns; or equivalently, with a frequency of 2.5 MHz. The CDF detector cannot—and would not want to—record the products of every single collision that occurs. Instead, it has a three level “trigger” system that can decide whether or not to record an event using basic detector information. Ultimately, CDF is capable of recording at a rate only up to 100 Hz, so the trigger system is designed to filter the events to those of interest for current analyses. This is done with hardware systems at level 1 and 2, then a computer farm at level 3. Each particular “trigger” refers to a collection of decisions at all three levels.

5.1 Level 1

The level 1 trigger has $\sim 4 \mu\text{s}$ to make a decision and a maximum accept rate of $\sim 25 \text{ kHz}$. This hardware system is composed of three parallel processing streams. One stream finds calorimeter based objects (L1CAL), one looks for primitive muon signals (MUON PRIM-L1MUON), and the last finds tracks in the COT with the “eXtremely Fast Tracker” (XFT). Up to 64 level 1 triggers can be formed from the objects in these streams using simple boolean logic (AND & OR operators).

5.2 Level 2

After a level 1 acceptance, the information of an event proceeds to level 2 for a more detailed decision. The level 2 trigger has a maximum accept rate of $\sim 800 \text{ kHz}$. There are four buffers for processing an event coming from level 1, when a particular one of these buffers is busy processing an event it is not available for further use. When all four buffers are in use, further events coming

from level 1 are lost. The time that level 2 is busy processing and incapable of accepting more events from level 1 is denoted as “deadtime.”

Level 2 is capable of using silicon, shower max, and calorimeter information in addition to the level 1 information to perform further reconstruction of an event. Once the event data is loaded into the level 2 processors, a decision can be made about whether the event satisfies any of the level 2 triggers.

5.3 Level 3

The level 3 trigger has a maximum accept rate of ~ 100 Hz. It is divided between an event builder that stores raw detector data and a linux PC farm that makes a decision on whether to store an event using higher level event objects. Level 3 is designed to make a decision on an event using data that approximates full reconstruction.

5.4 Trigger Paths (“Datasets”) of the $H \rightarrow WW$ Group

“Trigger” tends to be a bit of an overloaded term; it may refer colloquially to a variety of objects. Any particular criteria within any of the three levels are often denoted as triggers, collections of criteria within one of the three levels are denoted as “LX triggers” ($X = 1, 2, 3$), as well as sets of criteria from all three levels. For the purposes of this dissertation, “trigger bits” will refer to particular criteria that exist within any one of the three “trigger levels” just discussed. There will be “LX triggers” ($X = 1, 2, 3$) for collective decision at a particular level. “Trigger paths” will be the broadest categories of collections of trigger bits that are chosen by analyses interested in data with particular features. For instance, the $H \rightarrow WW$ group is interested in leptonic decays from the weak vector bosons, so it chooses to use data from “trigger paths” that record high p_T lepton events during online operations.

The following are the triggers paths, or “datasets,” used for the CDF high mass Higgs boson group and this analysis. Trigger design may evolve over time, so note that these trigger paths refer

to their incarnations in trigger table PHYSICS_5_04_v-3. This trigger table can be referenced for a more detailed breakdown of the trigger bits within each trigger level. [13]

5.4.1 ELECTRON_CENTRAL_18

The ELECTRON_CENTRAL_18 trigger path is designed to select data with high p_T electrons absorbed by the central calorimeter.

- Level 1 (L1_CEM8_PT8_v-5): This trigger requires a cluster of energy in the central EM calorimeter with at least 8 GeV, the ratio of $E_{\text{Had}}/E_{\text{EM}} < 0.125$ to distinguish the EM energy deposit from charged hadrons that may deposit some of its energy in the EM calorimeter, and an XFT track with $p_T > 8.34$.
- Level 2 (L2_CEM18_PT8_v-1): Additional requirements of an EM cluster with at least 18 GeV and $|\eta| < 1.317$ are imposed here.
- Level 3 (L3_ELECTRON_CENTRAL_18_v-6):
 - $L_{shr} < 0.4$, a variable that compares lateral shower profile in towers next to the seed tower to some expected profile.
 - Δz between the COT track and the central EM calorimeter shower to match within 8 cm.
 - a central track with p_T at least 9 GeV
 - $E_T > 18.0$ GeV

5.4.2 MUON_CMUP18

The MUON_CMUP18 trigger path is designed to identify high p_T muons with tracks in both the CMU and CMP muon detectors.

- Level 1 (L1_CMUP6_PT4_v-2): This trigger requires an XFT track with $p_T > 4.09$ GeV and fiducial to a CMU stub with $pt > 6$ GeV, and a CMP stub.

- Level 2 (L2_CMUP6_PT15_3DMATCH_v-1): This trigger tightens the XFT criteria by requiring a four layer track with $p_T > 14.77$ GeV.
- Level 3 (L3_MUON_CMUP_18_v-3): This trigger raises the p_T cut to 18 GeV and continues the requirement of matching the track to stubs in the CMU and CMP.

5.4.3 MUON_CMX18

The MUON_CMX18 trigger path is designed to identify high p_T muons with tracks that lead to the CMX muon detector.

- Level 1 (L1_CMX6_PT8_CSX_v-2): This trigger requires an XFT track with $p_T > 8.34$ GeV and fiducial to a CMX stub with $p_T > 6$ GeV, as well as a hit in the CSX scintillator.
- Level 2 (L2_CMX6_PT15_3DMATCH_HTDC_v-1): This trigger tightens the XFT criteria by requiring a four layer track with $p_T > 14.77$ GeV.
- Level 3 (L3_MUON_CMX18_v-2): This trigger raises the p_T cut to 18 GeV and continues the requirement of matching the track to a CMX stub.

5.4.4 MET_PEM

The leptonic decays studied by the $H \rightarrow WW$ group, and especially the associated production leptonic decay of $WH \rightarrow WWW \rightarrow l\nu l\nu l\nu$, also tend to exhibit high values of missing transverse energy (E_T). So we are also interested in the dataset pertaining to the MET_PEM trigger path that is designed to accept events with energy clusters in the plug electromagnetic calorimeter in association with E_T . Note that this online version of E_T —denoted here as E_T^{raw} —simply uses the sum of transverse energies over the calorimeter towers and does not employ the muon or jet corrections described later in chapter 6. This trigger also allows for electron acceptance beyond what is covered by the COT.

- Level 1 (L1_EM8_&_MET15_v-11): At this level, the trigger requires either a central or plug EM cluster with $E_T > 8$ GeV, with $E_{\text{Had}}/E_{\text{EM}} < 0.125$ for a central cluster and $E_{\text{Had}}/E_{\text{EM}} <$

0.0625 for a plug cluster. The L1_MET15 trigger bit is also employed for a $\cancel{E}_T^{\text{raw}} > 15$ GeV cut.

- Level 2 (L2_PEM20_MET15_v-1): This trigger continues to require a $\cancel{E}_T^{\text{raw}} > 15$ GeV cut, requires a plug EM object with $E_T > 20$ GeV, and $1.1 < |\eta| < 3.6$.
- Level 3 (L3_PEM20_MET15_v-8): This level imposes a plug calorimeter requirement of 3 towers with $E_T > 20$ GeV, $E_{\text{Had}}/E_{\text{EM}} < 0.125$ for the plug cluster, and a $\cancel{E}_T^{\text{raw}} > 15$ GeV cut again.

5.4.5 MUON_CMP18_PHI_GAP

The MUON_CMP18_PHI_GAP trigger path is designed to account for gaps in ϕ coverage between the calorimeter wedges which have the CMU muon chambers attached to the out edge. This puts a 2.25 degree gap in the CMU ϕ coverage every 15 degrees. The basic idea of this trigger is to require tracks that point towards a gap to be coincidence with a CMP stub and a CSP hit. Previous incarnations of this trigger had problems keeping the rate under reasonable levels at high instantaneous luminosities, so it does employ a dynamic prescale up to a factor of 60. [21]

- Level 1 (L1_CMP3_PT15_3D_PHIGAP_DPS_v-2): This trigger requires an XFT track with $p_T > 14.77$ GeV.
- Level 2 (L2_CMP3_PT15_3D_PHIGAP_CSP_v-1): This level goes on to require a CSP hit.
- Level 3 (L3_MUON_CMP18_v-1): At level 3, this trigger requires
 - cmpDx=20
 - $p_T > 18$ GeV
 - CMP stub

5.4.6 MUON_CMU18_ETA_GAP

This trigger path has been working properly only since period 21 data-taking [19] and covers gaps in CMU rapidity coverage.

- Level 1 (L1_CMU6_PT4_&_TRK10_DPS_v-1)
- Level 2 (L2_CMU6_PT15_3DMATCH_ETAGAP_v-1)
- Level 3 (L3_MUON_CMU18_v-1)

Chapter 6

High p_T Object Identification

Datasets from any given trigger path begin as little more than collections of detector signals: hits in the silicon and COT, showers in the calorimeters with some measured energy, etc. Translating these signals into objects the experimentalist is looking for (leptons, jets, photons, etc.) is a formidable and detailed task. This chapter will first discuss the details of lepton identification (section 6.1), jet identification (section 6.2), and how missing energy is computed (section 6.3). Then other important details related to the shortcomings of object identification like “fake leptons” (section 6.4), as well as efficiencies and scale factors related to lepton ID (sections 6.5 and 6.6) will be discussed.

6.1 Lepton Identification

This analysis is mostly interested in the identification of electrons and muons, as well as missing energy (E_T). To determine what pattern of detector information should be called “electrons” and “muons,” hits in the silicon and COT detectors must undergo essentially a high brow game of connect-the-dots to form “tracks.” Such tracks must then be fiducial to energy deposits in the EM calorimeter to be identified as electrons, or fiducial to short tracks (“stubs”) in one of the muons detectors to be identified as muons.

This analysis, along with the rest of the $H \rightarrow WW$ group, constructs from the trigger paths listed in section 5.4 these lepton categories:

- Electrons: Likelihood-based electrons, tight central electrons (TCE), phoenix electrons (see section 6.1.2)

- Muons: CMUP, CMP, CMU, CMX, CMXMsKs, BMU, CMIOCES, CMIOPEs (see section 6.1.3)
- Lepton of unspecified flavor: CrkTrk (“crack track”)

All of these categories will require some collection of several cuts on detector quantities such as [19]:

- E_{HAD}/E_{EM} – the ratio of the hadronic calorimeter energy to the electromagnetic calorimeter energy associated with the candidate
- E/P – the ratio of the EM cluster transverse energy to the COT track transverse momentum
- L_{shr} – the lateral shower profile in the transverse plane to the electron direction

$$L_{shr} = 0.14 \frac{\sum_i (M_i - P_i)}{\sqrt{(0.14\sqrt{E_{EM}})^2 + \sum_i (\Delta P_i)^2}} \quad (6.1)$$

where i is the sum over adjacent towers, M_i is the measured energy, and P_i is the predicted energy in the i^{th} tower [49].

- $CalIso$ – The energy E_T in a cone of radius $\Delta R = \sqrt{(\Delta\eta)^2 + (\Delta\phi)^2} \leq 0.4$ around the electron cluster excluding the electron cluster divided by the energy in the electron cluster:

$$CalIso = \frac{E_T^{cone} - E_T^{electron}}{E_T^{electron}}$$

- $TrkIso$ – the same variable as above $CalIso$ but measured using tracks instead of calorimeter
- $Q \times \Delta x_{CES}$ – The distance in the r - ϕ plane between the extrapolated, COT beam constrained track and the best matching CES cluster, times the charge Q of the track.
- Δz_{CES} – The distance in the r - z plane between the extrapolated, COT beam constrained track and the best matching CES cluster.

- $NCotHitsAx$ – number of COT hits on axial layers belonging to track associated to the candidate electron
- $NCotHitsSt$ – number of COT hits on stereo layers belonging to track associated to the candidate electron
- $\chi^2_{COT} - \chi^2$ associated with the COT hits belonging to track
- $NSvxHits$ – number of SVX hits belonging to track associated to the candidate electron
- Track p_T – Transverse momentum measured from the charged particle's track
- Track z_0 – Position along the longitudinal direction of the beamline.
- Axial and Stereo Superlayer – The number of axial and stereo superlayers in the COT having at least 5 hits associated to the track in question.
- CES ΔX – The difference in the $r - \phi$ plane between the best CES match and the COT beam-constrained track extrapolation to the CES.
- PEM 3x3 Fit – A χ^2 fit to electron test beam data of nine Plug EM towers.
- PES 5x9 U/V – The ratio of the central five tower energy to the total nine tower energy.
- χ^2 – This chi squared compares the fitted track to the actual hits in the trackers.
- Curvature Significance – The measured track curvature divided by the curvature error.

Section 6.1.1 will briefly discuss track formation from hits in the trackers, then sections 6.1.2, 6.1.3, and 6.1.4 will discuss how such tracks are combined with other detector information to be counted as lepton objects.

6.1.1 Track Formation

Recall from section 4.2 that the silicon and COT trackers are surrounded by a 1.4 T field along the \hat{z} direction. This field causes charged particles to follow the path of a helix with its axis parallel

to the magnetic field, so the connect-the-dots game is a matter of constructing an algorithm that will recognize a collection of silicon and COT hits that follow the path of a helix that leads near the $p\bar{p}$ interaction on one end and to either a calorimeter energy deposit or muon stub on the other end.

The COT forms segments with hits in the axial layers, then links these segments together into tracks. To form these tracks, the algorithm begins with segments in the outermost superlayers, then uses the curvature of the segment and the beamline location to search for possible other segments that could form a helix to the primary vertex. Stereo segments are then also linked to form a three dimensional track [34].

Once a COT track is formed, the silicon tracking uses this track as a “seed,” essentially a starting point, and then uses an “outside-in” tracking algorithm. This will start with the outermost layer and work inwards searching for hits that form the best possible helix back to the primary vertex [51].

Forward electrons may need a different strategy if their pseudorapidity is too large to make suitable COT seed tracks for the silicon. In this case, seed tracks are formed from “CdfEmObject” objects—energy deposits in the Plug EM calorimeter—which then drives the outside-in silicon pattern recognition [31].

6.1.2 Electron ID

Central electrons ($|\eta| < 1.0$) with high p_T are expected to traverse the silicon and COT detectors, leaving behind a track. Then they enter the EM calorimeter where they will cause an electromagnetic shower and deposit their energy. Until recently, these electrons had to pass a set of criteria called “tight central electron.” These criteria were a set of hard cuts, so if an object that looked very electron-like still failed even one cut it would not pass selection. This category has since been replaced by the “likelihood-based electron” (LBE) category that creates a single function out of mostly the same set of criteria, but then imposed just a single cut on the end value of that function. LBE criteria are [19]

- having a track fiducial to the CEM

- Track $z_0 < 60$ cm
- the electron candidate object is not a photon conversion
- $E_{HAD}/E_{EM} < 0.125$, which satisfies trigger requirements and cuts out charged hadronic objects.
- $CalIso < 0.3$, calorimeter isolation requirement to cut out fakeable objects
- $p_T(track) > 10$ GeV ($p_T(track) > 5$ GeV if $E_T < 20$ GeV)
- Likelihood cut: $\mathcal{L} > 0.90$

Given these, the values used in the likelihood function are: E_{HAD}/E_{EM} , E/P , L_{shr} , $CalIso$, $TrkIso$, $Q \times \Delta x_{CES}$, Δz_{CES} , $NCotHitsAx$, $NCotHitsSt$, $\chi_{COT}^2 - \chi^2$, and $NSvxHits$. Finally, the likelihood function itself is:

$$\mathcal{L}(\vec{x}) = \frac{L_{sig}}{L_{sig} + L_{bckg}} = \frac{\prod_{i=1}^N P_i^{sig}(x_i)}{\prod_{i=1}^N P_i^{sig}(x_i) + \prod_{i=1}^N P_i^{bckg}(x_i)} \quad (6.2)$$

Electrons in the pseudorapidity region $1.2 < |\eta| < 2.0$ would not be found by the LBE category because they are not fiducial to the CEM. They are instead found by the “phoenix” tracking algorithm which the more traditional path of making a collection of cuts (see table 6.1).

6.1.3 Muon ID

The muon categories are denoted by which muon detector a track is found in. Muons are “minimum ionizing particles,” meaning that they deposit only a small fraction of their energy in the calorimeters and can traverse through the entire CDF detector. All muon object candidates must pass a basic set of cuts (see table 6.2), then have a that is fiducial to one of the muon detectors.

- CMUP: CMUP muons are required to have stubs in both the CMP and CMU detectors, covering a pseudorapidity range of $|\eta| < 0.68$.
- CMU: High p_T tracks with a CMU stub, but not a CMP stub

- **CMP:** High p_T tracks with a CMP stub, but not a CMU stub
- **CMX:** High p_T tracks with a CMX stub, covering a pseudorapidity range of $0.6 < |\eta| < 1.0$.
- **BMU:** High p_T track with a BMU stub, covering a pseudorapidity range of $1.0 < |\eta| < 1.5$
- **CMIOCES:** A minimum ionizing track that does not register as CMUP, CMU, CMP, or CMX, but is fiducial to the central calorimeter
- **CMIOPEs:** A minimum ionizing track that does not register as BMU, but is fiducial to the plug calorimeter.
- **CMXMsKs:** A high p_T track that points to either the miniskirt or keystone detectors.

Two categories of muons used do not actually use muons stubs. CMIOCES and CMIOPEs muons are tracks that do not have muon stubs, but rather rely on a muon's minimum ionizing nature in a calorimeter. A track whose curvature implies high p_T , but does not deposit energy in either the EM or hadronic calorimeters strongly tends to be a muon since muons are the only particles produced that have this signature and do not tend to decay before traversing the entire CDF detector. See tables 6.3, 6.4, 6.5, 6.6, 6.7, 6.8, and 6.9 for specific cuts on each muon category. ¹

6.1.4 Unspecified Track ID

The last category of leptons considered in this analysis are tracks that are considered sufficiently lepton-like, but their flavor cannot be specified. This “CrkTrk” category is defined to cover tracks that specifically point to cracks in calorimeter acceptance

¹Based on the CDF $H \rightarrow WW$ group's Diboson_v17 framework

Forward Electrons (PHX)	
Region	Plug EM Cal.
η_{PES}	$1.2 < \eta < 2.0$
$E_{\text{HAD}}/E_{\text{EM}}$	< 0.05
PEM 3x3 Fit	true
χ^2_{PES}	10
PES 5x9 U	≥ 0.65
PES 5x9 V	≥ 0.65
Isolation/ E_T	≤ 0.1
$\Delta R(\text{PES}, \text{PEM})$	≤ 3.0
Track Matched	true
# of Silicon Hits	≥ 3
Track $ z_0 $	$\leq 60 \text{ cm}$

Table 6.1 Phoenix (PHX) electron definition

Muon Base Cuts	
p_T	$> 10 \text{ GeV}$
E_{EM}	$2 + \max(0, (p - 100) \cdot 0.0115)$
E_{HAD}	$6 + \max(0, (p - 100) \cdot 0.028)$
Isolation/ p_T	≤ 0.1
# Axial SL	≥ 3
# Stereo SL	≥ 2
Track $ z_0 $	$\leq 60 \text{ cm}$
Track $ d_0 $	$0.2 \text{ cm} (< 0.02 \text{ cm with silicon})$
$\chi^2/\text{deg. of freedom}$	$< 4.0 (< 3.0 \text{ if Run \#} > 186598)$

Table 6.2 Base muon identification criteria for all categories

CMUP Muons	
CMU Fiducial	$x_{\text{fid}} < 0, z_{\text{fid}} < 0 \text{ cm}$
CMP Fiducial	$x_{\text{fid}} < 0, z_{\text{fid}} < -3 \text{ cm}$
ΔX_{CMU}	7 cm
ΔX_{CMP}	$\max(6, 150/p_T) \text{ cm}$
CMU Stub	true
CMP Stub	true

Table 6.3 Cuts for CMUP muons beyond the base muon cuts

CMP Muons	
CMU Fiducial	$x_{\text{fid}} < 0, z_{\text{fid}} < 0 \text{ cm}$
CMP Fiducial	$x_{\text{fid}} < 0, z_{\text{fid}} < -3 \text{ cm}$
ΔX_{CMP}	$\max(6, 150/p_T) \text{ cm}$
Run Numbers	≥ 229764
CMP Stub	true

Table 6.4 Cuts for CMP muons beyond the base muon cuts

CMU Muons	
CMU Fiducial	$x_{\text{fid}} < 0, z_{\text{fid}} < 0 \text{ cm}$
CMP Fiducial	$x_{\text{fid}} < 0, z_{\text{fid}} < -3 \text{ cm}$
CMX Fiducial	$x_{\text{fid}} < 0, z_{\text{fid}} < -3 \text{ cm}$
ΔX_{CMU}	7 cm
CMU Stub	true

Table 6.5 Cuts for CMU muons beyond the base muon cuts.

CMX Muons	
CMX Fiducial	$x_{\text{fid}} < 0, z_{\text{fid}} < -3 \text{ cm}$
Fiducial to CMX Arches	true
Fiducial to CMX Miniskirt	false
Fiducial to CMX Keystone	false
ΔX_{CMX}	$\max(6, 125/p_T) \text{ cm}$
COT Exit Radius	$> 140 \text{ cm}$
CMX Stub	true

Table 6.6 Cuts for CMX muons beyond the base muon cuts

BMU Muons	
BMU Fiducial	true
BMU Stub	true
PES Fiducial	true
NSvxHits	≥ 3
Cal. Energy	$> 0.1 \text{ GeV}$
COT Hit Fraction	> 0.6
Curvature Significance	> 12
Run Number	≥ 162312

Table 6.7 Cuts for BMU muons beyond the base muon cuts

CMIOCES Muons	
Not CMUP or CMX	
Cal. Energy	$> 0.1 \text{ GeV}$
NCotStSeg	≥ 3
Fiduciality	CES
$\chi^2/\text{deg. of freedom}$	< 3.0

Table 6.8 Cuts for CMIOCES muons beyond the base muon cuts

CMIOPEs Muons	
Not BMU	
Cal. Energy	$> 0.1 \text{ GeV}$
Fiduciality	PES
COT Hit Fraction	> 0.6
Curvature Significance	> 12

Table 6.9 Cuts for CMIOPEs muons beyond the base muon cuts

CrkTrk Muons	
Not CMUP or CMX	
# Axial SL	≥ 3
# Stereo SL	≥ 3
Cal. Isolation	≤ 0.1 using CDF Muon or ≤ 0.1 using EM cluster
Fiduciality	Not CES or PES fiducial
Cal. Energy	$> 0.1 \text{ GeV}$
Fiduciality	PES
$\chi^2/\text{deg. of freedom}$	< 3.0

Table 6.10 Cuts for CrkTrk muons beyond the base muon cuts

6.2 Jet ID

Quarks are known to exist only in groups of two (“mesons”) or three (“hadrons”). The $p\bar{p}$ interactions have high enough energy to tear the quarks of the proton and antiproton out of their hadronic configurations. When this happens, they will subsequently recombine or even create pairs out of the vacuum. This typically results in a spray of particles with a common general direction which are denoted “jets” in particle physics. As such, jets tend to deposit energy in both the EM and hadronic calorimeters associated with multiple tracks.

In the analysis, jets are defined as calorimeter cluster within $\Delta R < 0.4$ and at least $E_T > 15$ GeV. The number of jets in a particular event will be an important variable for discriminating the WH and ZH signals from their backgrounds.

6.3 Missing Transverse Energy (\cancel{E}_T)

The $p\bar{p}$ beam is defined as the \hat{z} -direction in CDF coordinates. Hence, since the beginning state of the $p\bar{p}$ interaction has no momentum or energy directed in the plane transverse to the beamline, the energies of products after the $p\bar{p}$ interaction should sum to zero. Particles that do not interact with the detector do not have their energies included in the vector sum, so the result is “missing transverse energy” (\cancel{E}_T).

Neutrinos are the only known particles that will not interact with the detector and are inherent to the leptonic decays of W weak vector bosons. Therefore, \cancel{E}_T is an important quantity in the signatures of $WH \rightarrow WWW$ and $ZH \rightarrow ZWW$ signals of the $H \rightarrow WW$ group.

There are, however, some caveats that must be accounted for first. The raw missing transverse energy is just the sum over the calorimeter towers.

$$\vec{\cancel{E}}_T^{\text{raw}} = - \sum_i \vec{E}_T^i \quad (6.3)$$

where \vec{E}_T^i is the energy magnitude deposited in the i^{th} calorimeter tower with a unit vector pointing from the primary vertex to the center of the calorimeter tower artificially attached to make it a vector quantity, then the transverse component is taken. As discussed earlier, muons are minimum

ionizing particles, so they do not deposit much of their energy in the calorimeters. This also counts as missing energy in \vec{E}_T^{raw} so the \vec{E}_T is corrected by having the muon's energy added back, minus the small amount of energy the muon did deposit. The same goes for CrkTrk leptons which do not deposit energy in the calorimeters by definition. Lastly, jets undergo some energy corrections in reconstruction which then affects the vector energy sum.

6.4 Fake Leptons

Some small, but significant, portion of jets will produce a signature that passes one of the lepton definitions. These objects are denoted “fake leptons” or just “fakes.” Note that these are distinct from “photon converted leptons,” which are photons that interact with the detector apparatus to become an electron-positron pair and then register as an electron.

Modeling of fakes has been unreliable, so this background is instead estimated from “jet samples” of data. Four such jet samples are used, based on trigger paths requiring a leading jet E_T of at least 20 GeV, 50 GeV, 70 GeV, and 100 GeV. In these data samples, the number of jet-like objects that pass a very loose selection of lepton cuts are counted. These loose lepton selections are called “denominator objects,” and various denominator objects are defined for the different lepton categories. These are considered to be the collection of jet-objects that have any non-negligible chance at all of passing a full lepton definition. The “fake rate” is then the ratio of these denominator objects that actually do pass a full lepton definition to the full set that pass just a denominator definition. Note that the actual number of isolated, fully recognized leptons (i.e. “real” leptons) must be subtracted in the numerator and number of isolated lepton-objects passing the denominator definition must be subtracted from the denominator. Hence, for a generic lepton category i , the fake rate is [19]

$$f_i = \frac{N_I(\text{full leptons}) - \sum_{j \in \{\text{EWK}\}} N_{ij}(\text{full leptons})}{N_I(\text{denom. objects}) - \sum_{j \in \{\text{EWK}\}} N_{ij}(\text{denom. objects})} \quad (6.4)$$

The four data samples provide four independent estimates of the fake probability, the average of which are use as the fake probability in this analysis. The systematic uncertainty on the rate

beyond the statistical error is estimated by adding a parameter α as $\sqrt{\text{stat.} + \alpha}$ large enough so that all four samples agree to within one standard deviation.

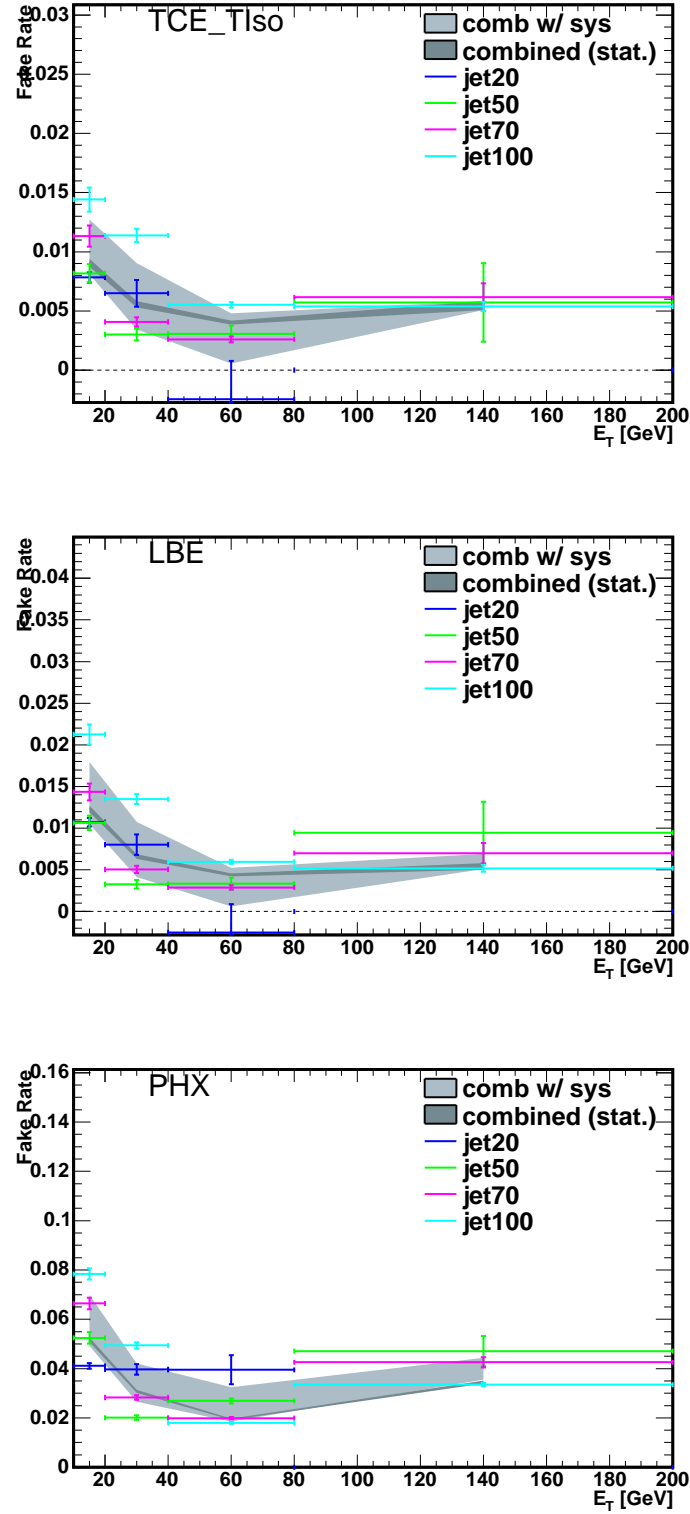


Figure 6.1 Fake rates for electrons. PHX and LBE have no track isolation requirement. TCE is include for comparison. [20]

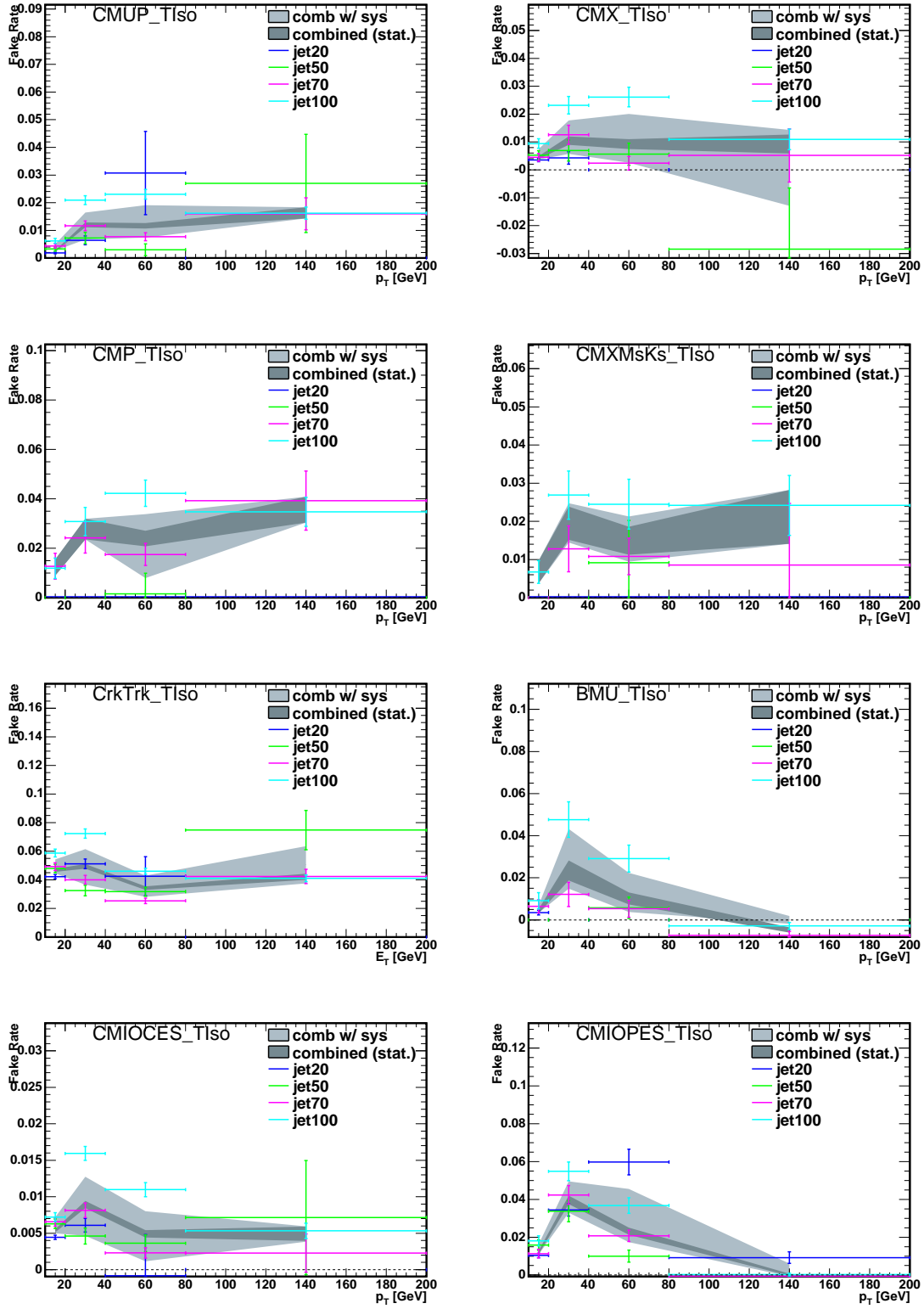


Figure 6.2 Fake rates for muons. [20]

6.5 Lepton Efficiencies

Monte carlo simulated backgrounds and signals must be appropriately calibrated to the data to be accurate. Lepton efficiencies are measured with Drell-Yan ($Z \rightarrow ll$) events in MC and data because of the relatively large sample size, then compared. Such corrections are then applied to all MC processes.

Lepton efficiency is defined as

$$\epsilon_{\text{ID}} = \frac{N_{TT}}{N_{TL}} \quad (6.5)$$

where N_{TT} is the count of tight-tight lepton pairs and N_{TL} is the count of tight-loose pairs ($\{N_{TT}\} \subset \{N_{TL}\}$) [42].

6.6 Lepton Scale Factors

The “lepton scale factor” is the ratio of lepton identification efficiencies in data to the monte carlo. This factor is used later in determining how to weight each event in an MC process. It is recalculated for different periods in data taking.

$$s = \frac{\epsilon_{\text{ID}}^{\text{data}}}{\epsilon_{\text{ID}}^{\text{MC}}} \quad (6.6)$$

Lepton Category	Period 0	Period 1-4	Period 5-7	Period 8-10
CMUP	0.973 ± 0.012	0.938 ± 0.009	0.932 ± 0.013	0.955 ± 0.009
CMU	0.000 ± 1.000	0.000 ± 0.500	0.000 ± 0.577	0.000 ± 0.577
CMP	0.000 ± 1.000	0.000 ± 0.500	0.000 ± 0.577	0.965 ± 0.032
CMX	1.027 ± 0.016	1.020 ± 0.017	1.026 ± 0.019	1.007 ± 0.014
CMXMsKs	0.000 ± 1.000	0.000 ± 0.500	0.000 ± 0.577	0.930 ± 0.036
BMU	1.127 ± 0.032	1.107 ± 0.025	1.076 ± 0.032	1.099 ± 0.021
CMIOCES	1.049 ± 0.019	1.060 ± 0.015	1.085 ± 0.018	1.086 ± 0.014
CMIOPEs	1.000 ± 0.000	1.005 ± 0.020	1.029 ± 0.025	0.980 ± 0.018
CrkTrk μ	0.958 ± 0.015	0.978 ± 0.012	0.976 ± 0.015	0.973 ± 0.012

Table 6.11 Muon scale factors in Diboson_v17 data [19].

Lepton Category	Period 11-12	Period 13	Period 14-25
CMUP	0.924 ± 0.011	0.937 ± 0.011	0.884 ± 0.004
CMU	0.000 ± 0.707	0.000 ± 1.000	0.000 ± 1.000
CMP	0.893 ± 0.022	0.987 ± 0.022	0.876 ± 0.009
CMX	0.981 ± 0.018	0.986 ± 0.020	0.978 ± 0.008
CMXMsKs	0.935 ± 0.032	0.890 ± 0.033	0.912 ± 0.012
BMU	1.064 ± 0.028	1.142 ± 0.037	1.100 ± 0.013
CMIOCES	1.204 ± 0.019	1.186 ± 0.022	1.196 ± 0.011
CMIOPEs	0.955 ± 0.023	0.998 ± 0.037	0.970 ± 0.010
CrkTrk μ	0.990 ± 0.020	0.952 ± 0.021	0.959 ± 0.008

Table 6.12 Muon scale factors in Diboson_v17 data [19].

Lepton Category	Period 0	Period 1-4	Period 5-7	Period 8-10
LBE($\mathcal{L} > 0.9$)	1.012 ± 0.004	1.001 ± 0.003	0.996 ± 0.004	0.992 ± 0.003
PHXTrk	0.998 ± 0.005	1.007 ± 0.004	1.018 ± 0.005	1.001 ± 0.004
PHXPEM	0.951 ± 0.006	0.953 ± 0.005	0.944 ± 0.006	0.931 ± 0.004
PEM	0.943 ± 0.011	0.916 ± 0.010	0.911 ± 0.015	0.875 ± 0.010
CrkTrk e	0.950 ± 0.016	0.989 ± 0.016	0.957 ± 0.019	0.948 ± 0.014
PESTrk	0.913 ± 0.013	0.949 ± 0.013	0.974 ± 0.017	0.947 ± 0.012

Table 6.13 Electron scale factors in Diboson_v17 data [19].

Lepton Category	Period 11-12	Period 13	Period 14-25
LBE($\mathcal{L} > 0.9$)	0.993 ± 0.004	0.994 ± 0.005	0.991 ± 0.001
PHXTrk	0.999 ± 0.004	1.004 ± 0.057	1.026 ± 0.002
PHXPEM	0.939 ± 0.005	0.936 ± 0.007	0.911 ± 0.002
PEM	0.870 ± 0.013	0.871 ± 0.013	0.829 ± 0.005
CrkTrk e	1.002 ± 0.021	0.966 ± 0.021	0.964 ± 0.007
PESTrk	0.966 ± 0.015	0.922 ± 0.021	0.907 ± 0.006

Table 6.14 Electron scale factors in Diboson_v17 data [19].

Chapter 7

Computations with Artificial Neural Networks

This analysis uses the NeuroBayes artificial neural network to discriminate the Higgs boson signal from its backgrounds. After all analysis cuts are made and we have a final event count for the monte carlo signals and backgrounds, as well as the experimental data, variables showing separation in the distributions of signals and backgrounds can be used as a collection of input variables for a neural network. This neural network then uses the N_{in} input variables to compute a single one-dimensional distribution—denoted the “neural network score” in this dissertation—for each signal and background. In the end, the distributions in the neural network score should show much better separation between signals and backgrounds than any one of the input variables since the information of distribution separation of all the input variables is included in the final neural net score.

The neural network itself is an information processing system that is characteristically nonlinear, nonalgorithmic, and parallel. The NeuroBayes version of a neural net begins with a set of N_{in} inputs $\{x\}$ of any value and a single output $z_{\text{net}} \in (-1, 1)$. The output z_{net} is computed from some function of the N_{in} input variables, as well as weights and thresholds that may be associated with the variables [29]:

$$z_{\text{net}} = F_{\text{net}}(\{x\}, \{w\}, \{T\}) \quad (7.1)$$

The most basic structure of a neural net is called a “neurode” (see figure 7.1), which has some N input variables, their weights, and some single threshold value. From these, the neurode outputs a single value a .

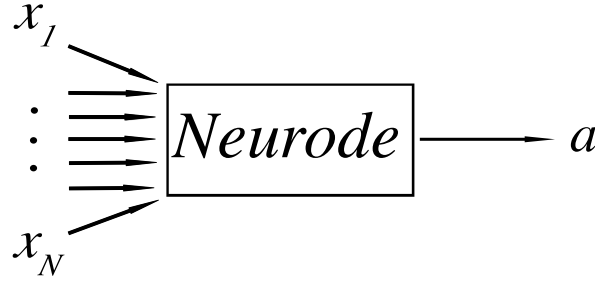


Figure 7.1 Neural Network “neurode”

Next, suppose we group together N_2 neurodes, each taking as input a set of N_1 variables. This structure is denoted a “network node” (see figure 7.2). With N_2 neurodes composing it, the network node has then a set $\{a_i\}$, $i \in \{1, \dots, N_2\}$ of outputs values—one output value for each neurode.

Finally, consider a network node with N_{in} input variables and N_1 output values. Then use these N_1 values as the input variables for another network node, which will output some N_2 values. Such a succession of network nodes using the output of the previous network node as the input for the next is called a “neural network” (see figure 7.3). The first network node is called the “first hidden layer,” the i^{th} network node is the “ i^{th} hidden layer,” until the last network node—the “output layer”—is reached and outputs the single score value z_{net} .

Having a neural network and having it do something useful are two distinct tasks. The tricky part is finding a network that yields $z_{\text{net}} \simeq -1$ for backgrounds and $z_{\text{net}} \simeq +1$ for signals. This requires a properly “trained” neural network. To do this, an “error function” [29]—sometimes called “quadratic loss function”—(χ_{net}^2) is defined on the N_{in} input variables so that small values for signals and a comparatively larger values for backgrounds are returned. NeuroBayes uses [28]:

$$\chi_{\text{net}}^2 = \sum_j w_j \frac{1}{2} \sum_i (T_{ji} - z_{ji})^2 \quad (7.2)$$

where j runs over the outputs of a network node, i runs over the event list, and T_{ji} is the target value for the node.

By doing this, we have established an N_{in} -dimensional space whose minimum characterizes a signal-like signature and whose maximum characterizes a background-like signature. “Training”

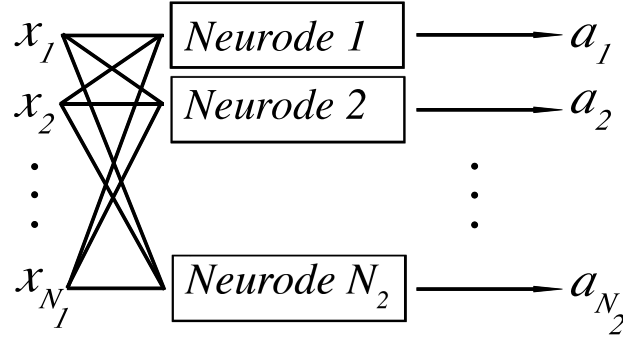


Figure 7.2 Neural Network “network node”

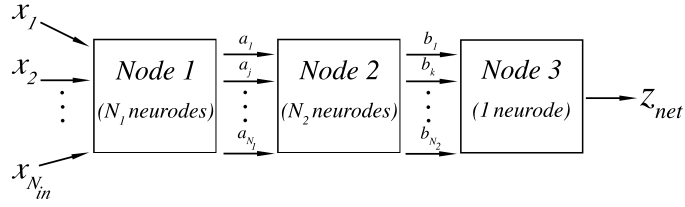


Figure 7.3 “Neural Network”

the neural net is synonymous with locating the minima of χ_{net}^2 as closely as possible ($\frac{d\chi_{\text{net}}^2}{dz} = 0$). Note that one of the great dangers of training a neural net is having a quadratic loss function get stuck in a *local* minima inadvertently. Though, the technical details of how the minimization is performed are designed with this in mind. Once this is done, the trained error function is used in the neural network to yield $z_{\text{net}} \simeq -1$ for background-like events and $z_{\text{net}} \simeq +1$ for signal-like events.

The usage and results of the neural network method in this particular analysis is expounded in section 9.3, where the inputs variables and neural network scores for the ‘ $VH \rightarrow VWW \rightarrow$ trilepton’ analysis is examined in detail.¹

¹Special thanks to Janis Finkelman for creating these neural network structure diagrams

Chapter 8

Statistics of Confidence Level Limits In the Search for New Physics

8.1 Poisson Statistics and Physical Processes

It is not presumptive to state that this analysis does not constitute a discovery of the Higgs boson. Rather, this analysis sets and updates an experimental limit excluding the Higgs boson of a particular mass range with a certain confidence level. As such, this chapter explains the method of how such a statistical exclusion is computed in general, while the experimental exclusion set for this analysis in particular is given in chapter 9.5.

Let's begin by explicitly identifying some basic assumptions inherent to particle interactions. These assumptions provide the logical foundation upon which the rest of the statistical aspects of the analysis are based:

1. The probability for a particular outcome of interest occurring more than once in a single event is negligible. This analysis searches for a higgs boson in the trilepton signature. The cross sections of Higgs production mechanisms explored—as well as all of the backgrounds—is so small that we can assume that none of the processes occur more than once in a single event.
2. Each $p\bar{p}$ interaction is an independent event.
3. The occurrence of any particular outcome of interest (both backgrounds and signals) is independent of other occurrences. In other words, a process occurring or not occurring in one event does not affect the probability that it will occur in another event.

This set of assumptions implies the processes studied will follow a Poisson distribution [39].

Definition 8.1 The *Poisson distribution* is the continuous distribution attained from the discrete binomial distribution when taking the limit of an infinite number of events ($n \rightarrow \infty$). Let n be the number of events, p be the probability of an occurrence of interest happening, k is the number of events in which the occurrence of interest is observed, and $\lambda \equiv np$ remain constant (this becomes the expected value). Then the *Poisson distribution* is [40]:

$$\lim_{n \rightarrow \infty} \binom{n}{k} p^k (1-p)^{n-k} = \frac{e^{-\lambda} \lambda^k}{k!}, \quad \forall k \in \{0 \cup \mathbb{Z}\}. \quad (8.1)$$

8.2 Gaussian Statistics and Systematic Errors

In any kind of experimental measurement, infinite precision is impossible. Knowing what we know always must include knowing what we don't know. Systematic errors of measurement must be set in order to not overstate the significance of a measurement.

Collider physics experiments inherently contain a plethora of systematic uncertainties. There are uncertainties of the beam intensity, acceptances, theoretical cross sections of the processes, etc. (see section 9.4 for the full list of systematic uncertainties inherent to this analysis). In statistics, these are sometimes called “nuisance parameters,” but this analysis will use the term “systematic uncertainty.”

Suppose, for the sake of argument, a particular quantity is to be measured and the measurement is performed many times on the exact same quantity, with the measurement performed in the same manner each time. Because infinite precision of measurement is impossible, there must be some distribution formed about the measurable value. The “Gaussian distribution” (or “Normal distribution” to statisticians) describes data that is clustered about some mean, so systematic errors in particle physics are assumed to have a Gaussian-like distribution.

Definition 8.2 [41] A random variable is *normally distributed*—or follows a *Gaussian distribution*—with mean μ and variance σ^2 if

$$f(y) = \frac{1}{\sigma\sqrt{2\pi}} e^{-\frac{1}{2}\left(\frac{y-\mu}{\sigma}\right)^2} \quad (8.2)$$

8.3 Likelihood and Confidence Level Computation

Without any a priori expectations about the outcome of the analysis, it either must compute the significance of a signal observed or set an exclusion if one is not observed. In either case, the data is compared to two hypotheses: one model using background processes only and one that includes both the background and signal estimate. Confidence level computations in this analysis are performed by a program called `MCLimit`—written specifically for CDF analyses [38].

The benchmark for excluding a signal is set at 95% confidence level. This means that a 95% confidence level exclusion should be obtained no more than 5% of the time if a real signal is present. If the discovery of a signal is possible, then data surplus over background must be distinguished as being a signal rather than an upward statistical fluctuation of the background hypothesis. Therefore, the probability of an upward fluctuation of the background must be computed. A signal is “observed” if the probability of an upward fluctuation of the background is no more than the integrated probability of the 5σ tails of the Gaussian distribution.

Let’s proceed by defining a “likelihood” and “likelihood ratio,” then move on to their use in computing “confidence levels.” The starting point is the neural net score described in chapter 7. With the background and signal distributions separated as much as possible, a stronger confidence level can be computed in the end. The neural net score is divided into some number of bins; each bin will have its own Poisson probability term in the likelihood.

Definition 8.3 The *likelihood* function \mathbb{L} is a product of Poisson probabilities for each bin of the neural net score, in this analysis. Further, there is a separate product of Gaussian distributions for each systematic error.

$$\mathbb{L} = \left(\prod_i \frac{\mu_i^{n_i} e^{-\mu_i}}{n_i!} \right) \cdot \prod_c e^{-\frac{S_c^2}{2}} \quad (8.3)$$

where μ_i is the total expectation in the i -th bin and n_i is the number of data events in the i -th bin. μ_i is given by

$$\mu_i = \sum_k \alpha_k \left[\prod_c (1 + f_k^c S_c) \right] (N_k^{Exp})_i \quad (8.4)$$

Here f_k^c is the fractional uncertainty associated with the systematic S_c and process k .

Now, μ_i is the total expectation of the i -th bin, but the expectation can differ depending on which hypothesis we use: the background-only hypothesis or the background-plus-signal hypothesis. Both shall be employed in the likelihood ratio.

Definition 8.4 A *test statistic* is a value X which discriminates signal-like outcomes from background-like outcomes. For the purposes of this analysis, the likelihood ratio is chosen to be the test statistic [37].

Definition 8.5 Ignoring systematic errors for now, the *likelihood ratio* is the ratio of the likelihood function for the background-plus-signal hypothesis to the likelihood function for the background-only hypothesis.

$$X = \prod_{i=1}^n \frac{\frac{e^{-(s_i+b_i)}(s_i+b_i)^{d_i}}{d_i!}}{\frac{e^{-b_i}b_i^{d_i}}{d_i!}} \quad (8.5)$$

where s_i is the signal expectation in the i -th bin of the neural net score, b_i is the background expectation, and d_i is the number of events observed in data.

To include the systematic errors, let X_i be the i^{th} term in the product of expression 8.5 such that $X = \prod_{i=1}^n X_i$. Then replace the errorless test statistic X_i with X'_i [37]:

$$X'_i = \frac{\int_0^\infty ds' \int_0^\infty db' e^{-\left(\frac{(s'-s_i)^2}{2\sigma_{s_i}^2} + \frac{(b'-b_i)^2}{2\sigma_{b_i}^2}\right)} \frac{1}{2\pi\sigma_{s_i}\sigma_{b_i}} \cdot X_i}{\int_0^\infty ds' \int_0^\infty db' e^{-\left(\frac{(s'-s_i)^2}{2\sigma_{s_i}^2} + \frac{(b'-b_i)^2}{2\sigma_{b_i}^2}\right)} \frac{1}{2\pi\sigma_{s_i}\sigma_{b_i}}} \quad (8.6)$$

So the Poisson distributed physics is being obscured by a collection of systematic errors with a Gaussian form.

Definition 8.6 The *confidence level* for exclusion of the signal-plus-background hypothesis is the probability of the test statistic X being less than or equal to the test statistic of the observed data

$X_{\text{obs.}}$

$$CL_{s+b} = P_{s+b}(X \leq X_{\text{obs.}}) \quad (8.7)$$

$$P_{s+b}(X \leq X_{\text{obs.}}) = \sum_{X(\{d'_i\}) \leq X(\{d_i\})} \prod_{i=1}^n \frac{e^{-(s_i+b_i)} (s_i+b_i)^{d'_i}}{d'_i!} \quad (8.8)$$

where $X(\{d_i\})$ is computed for the observed candidates for each channel $\{d_i\}$ and the sum is over final outcomes $\{d'_i\}$ with test statistic value less than or equal to the observed one [37].

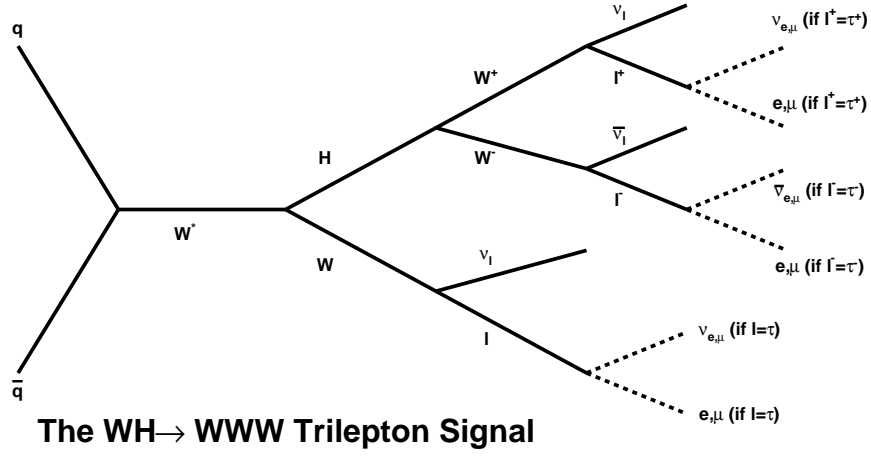
An exclusion of at least 95% confidence level is achieved if $CL_{s+b} \leq 0.05$. The confidence level reported by this analysis will be normalized to the Standard Model background hypothesis $CL/CL_{\sigma_{\text{SM}}}$. Hence, $CL/CL_{\sigma_{\text{SM}}} = 1$ means that the background-plus-signal hypothesis has been excluded at 95% confidence level. This is then compared to the same confidence level normalized to Standard Model computed with pseudoexperiments assuming the background hypothesis and normalized to the amount of data available to date. When an insufficient amount of data has been collected to distinguish the $s + b$ hypothesis from the b hypothesis, $CL/CL_{\sigma_{\text{SM}}} > 1$. As more data is collected, this value decreases. When these pseudoexperiments assuming the background hypothesis achieve $CL/CL_{\sigma_{\text{SM}}} = 1$, we say we have “achieved Standard Model sensitivity” at the 95% confidence level.

Chapter 9

The High Mass Higgs Boson Analysis in the Trilepton Signature

Chapter 2 explored the physics of the Higgs boson and why it is central to the understanding of the origin of mass in all known matter. Chapters 3 and 4 introduced the experimental apparatus of the Tevatron that provides the $p\bar{p}$ interactions and the CDF detector that records the outcomes of such collisions. Chapter 5 explained how triggers are used by the CDF detector to select particular kinds of data that may be of interest so that time is not wasted by running computations on data that is already known to not contain any interesting information. Once these particular categories of data are filtered down, the raw experimental data is processed to a more usable form. For the case of this analysis, chapter 6 explained the identification procedures for high energy objects like leptons and jets, as well as missing energy (implying neutrino production). With such objects identified, the data is in an experimentally usable form and efforts to distinguish any possible signal can begin. Chapter 7 explained what neural networks are and how they can be useful for separating background-like data from signal-like data. Finally, chapter 8 described the statistical tools that will be used to determine the strength of a signal, if any; or the confidence with which we can say there is no signal if none is detected.

This chapter will explain the details of the analysis itself, bringing together the tools developed in the earlier chapters. Before this analysis, CDF’s high mass Higgs boson group—or “ $H \rightarrow WW$ group”—exclusively studied $p\bar{p}$ collisions that produced exactly two leptons. We now supplement those two-lepton analyses with the full three-lepton region, minus the portions used as control regions.

Figure 9.1 WH trilepton signal topology

9.1 Motivation for Trileptons

The production cross sections for WH and ZH may be small relative to the gluon fusion cross section of the current $H \rightarrow WW$ analysis, but until now the trilepton signature has been completely unexplored, the uniqueness of the trilepton signature keeps background low, and every little bit counts as we push observed and expected limits toward Standard Model sensitivity.

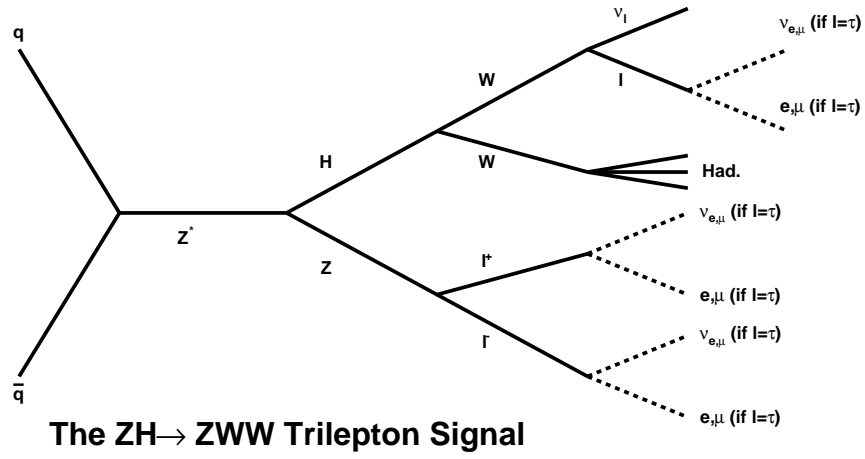
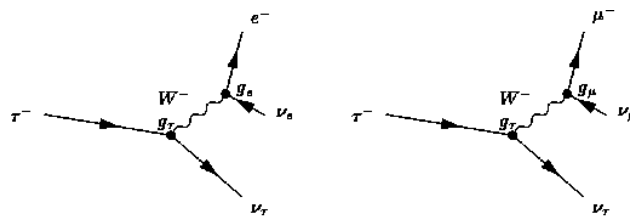
Leptons decaying from a W -boson are physically detectable from an experimental point of view if the W decays to an electron or a muon. W decays to a tau are also acceptable provided that the tau goes on to decay weakly to an electron or muon (see figure 9.1). Given a W -boson, the probability of getting an electron or muon via any of these decays is [17, 24]: ¹

$$P(W \rightarrow l\nu_l) = P(W \rightarrow e\nu_e) + P(W \rightarrow \mu\nu_\mu) \quad (9.1)$$

$$+ P(W \rightarrow \tau\nu_\tau) [P(\tau \rightarrow e\nu_e, \nu_\tau) + P(\tau \rightarrow \mu\nu_\mu, \nu_\tau)] \quad (9.2)$$

$$= 0.2528 \quad (9.3)$$

¹Basic decay values are from PDG Particle Physics Booklet (July 2006), Institute of Physics

Figure 9.2 ZH trilepton signal topologyFigure 9.3 Leptonic τ decays to an electron or muon

Similarly, given a Z -boson, the probability of having a decay to an electron or muon pair is

$$P(Z \rightarrow l\bar{l}) = P(Z \rightarrow e\bar{e}) + P(Z \rightarrow \mu\bar{\mu}) \quad (9.4)$$

$$+ P(Z \rightarrow \tau\bar{\tau}) [P(\tau \rightarrow e\nu_e, \nu_\tau) + P(\tau \rightarrow \mu\nu_\mu, \nu_\tau)]^2 \quad (9.5)$$

$$= 0.07147 \quad (9.6)$$

The relevant cross sections for a $m_H = 165$ GeV Higgs boson are (from tables M.2, M.3 in appendix M [20])

- $\sigma_{\text{gg}H165} = 0.4607$ pb
- $\sigma_{\text{WH}165} = 0.0510$ pb
- $\sigma_{\text{ZH}165} = 0.0331$ pb

The dominant mode for the current $H \rightarrow WW$ group analysis is gluon fusion in the two-lepton bin. The expected yield is found by multiplying the cross section by the proportion (“branching ratio”) of $gg \rightarrow H$ that have the Higgs decay to two W -bosons, then multiply by branching ratio of each W -boson decaying leptonically:

$$\sigma_{\text{gg}H165} \cdot \mathcal{BR}(H \rightarrow WW) \cdot P(W \rightarrow l)^2 = 0.02653 \text{pb}$$

By comparison, the expected yield for WH associated production in the three-lepton bin is:

$$\sigma_{\text{WH}165} \cdot \mathcal{BR}(H \rightarrow WW) \cdot P(W \rightarrow l)^3 = 7.425 \times 10^{-4} \text{pb}$$

or 2.8% the yield of the dilepton analysis (for $m_H = 165$ GeV).

ZH associated production may have a smaller cross section than WH , but given one such event there is a higher probability of producing three leptons. In this case, the Z decays to two leptons so we need only one of the two Higgs- W -bosons to decay leptonically and there are two

ways for this to happen:

$$P(W \rightarrow l, W \rightarrow l) = P(W \rightarrow l)^2 = 0.06391$$

$$P(W \rightarrow l, W \rightarrow \text{had.}) = P(W \rightarrow l) [1 - P(W \rightarrow l)] = 0.1889$$

$$P(W \rightarrow \text{had.}, W \rightarrow l) = P(W \rightarrow l) [1 - P(W \rightarrow l)] = 0.1889$$

$$P(W \rightarrow \text{had.}, W \rightarrow \text{had.}) = [1 - P(W \rightarrow l)]^2 = 0.5583$$

² So the expected ZH yield is

$$\sigma_{ZH165} \cdot \mathcal{BR}(H \rightarrow WW) \cdot P(Z \rightarrow ll) \cdot 2 \cdot P(W \rightarrow l, W \rightarrow \text{had.}) = 8.054 \times 10^{-4} \text{pb}$$

or 3.0% of the current $H \rightarrow WW$ dilepton analysis (for $m_H = 165$ GeV). Experimentally, this is also augmented by ZH events producing four leptons, with one failing to be reconstructed for some reason. Given the prevalence of the ZZ background seen in subsequent sections, this is not unlikely. Thus, based on cross sections and branching ratios alone we pursued this trilepton analysis expecting to contribute another $\sim 5.7\%$ acceptance compared to the gluon fusion process dominating the current $H \rightarrow WW$ dilepton analysis. In the end, this analysis provides a somewhat stronger contribution because of low backgrounds and good discrimination between signal and background provided by a neural network treatment.

Incidentally, one of the future improvements to this analysis is to accept events with single hadronic τ leptons. Noting that the above prediction assumes that vector boson decays to τ 's result in a detectable lepton only if that τ decays to an electron or muon, if we repeat the prediction assuming we may accept one hadronically decaying tau into the trilepton analysis, then the 5.7% becomes 6.9% (for $m_H = 165$ GeV). Another improvement waiting to be made is to include $H \rightarrow ZZ$ decays for all production mechanisms.

²Observe that $0.06391+0.1889+0.1889+0.5583=1.0$

9.2 Event Summary and Signatures of the WH and ZH Trilepton Analyses

With the usefulness of studying trilepton events in the high mass Higgs boson search motivated, let's precisely define the regions to be searched and identify which backgrounds are expected in them.

9.2.1 Trilepton Signal Regions Defined

Before this trilepton search, the $H \rightarrow WW$ group analysis was constrained only to the study of events with exactly two leptons, which focuses primarily on the gluon fusion Higgs boson signal because of its large cross section relative to associated production. This trilepton analysis, however, focuses entirely on the two associated production channels because there are three vector bosons that allow for decays to more than two leptons, whereas the gluon fusion and vector boson fusion signals do not contribute a real third lepton. Monte Carlo signal simulation does indicate that gluon fusion and vector-boson fusion have negligible contribution to the three-lepton bin. Thus, we are left with two signals to study: a $p\bar{p} \rightarrow WH \rightarrow WWW \rightarrow l\nu, l\nu, l\nu$ signal and a $p\bar{p} \rightarrow ZH \rightarrow ZWW \rightarrow ll, l\nu, \text{jet(s)}$ signal. Among these two signals, three new trilepton signal regions are defined, ameliorating the effort to discriminate each from background based on their unique characteristics.

Consider the three leptons as ordered by their transverse momentum p_T (or transverse energy E_T for electrons) such that the highest p_T lepton is the “1st lepton” and the lowest p_T lepton is the “3rd lepton.” First, we filter trilepton events into an *In-Z-Peak* category if any of the three possible dilepton pairings (that is, pairing the 1st lepton with the 2nd lepton; the 1st lepton with the 3rd lepton; or the 2nd lepton with the 3rd lepton) has an invariant mass value that falls within a ± 15 GeV window around the Z -boson mass at 91 GeV, have opposite signs, and have same flavor. This *In-Z-Peak* region is chosen to isolate the ZH signal process from the WH process. The rest of the trileptons events are directed toward the *No-Z-Peak* region, which focuses on the WH signal process. Once this distinction is made, the events in the ZH region (those with an identified Z -peak) are divided among a 0-jet category, 1-jet category, and a ≥ 2 jet category. The 0-jet category

will be the control region (defined below) for the ZH analysis, while the other two will be distinct signal regions. These regions are new to the $H \rightarrow WW$ analysis group.

Additionally, the WH analysis has a missing transverse energy cut of $E_T > 20$ GeV. This cut drastically reduces the $Z\gamma$ background (see section 9.2.2) contribution and also provides a WH control region in $10.0 < E_T < 20.0$ GeV. Because the $WH \rightarrow WWW \rightarrow l\nu l\nu l\nu$ event topology has three $W \rightarrow l\nu$ decays, the missing energy is relatively large and a negligible amount of signal is lost from having the E_T cut as high as 10.0 GeV.

The E_T distribution for the $ZH \rightarrow ZWW$ trilepton events is somewhat lower than that of the WH analysis because it produces fewer neutrinos ($WWW \rightarrow l\nu, l\nu, l\nu$ has three neutrinos while $ZWW \rightarrow ll, l\nu, jet$ has only one), so defining a control region by a similar E_T cut is less appropriate. The ZH analyses also have somewhat larger backgrounds than the WH region and is topologically similar to the most significant background, WZ . However, for a $ZH \rightarrow ZWW$ event to produce a three-lepton signature we either have one of the W -leptons decaying hadronically or—less frequently—we have a $ZH \rightarrow ZWW \rightarrow lll$ physics event that loses one of its leptons to an area of the detector that is incapable of reconstructing a track (detector holes or too far forward in pseudorapidity, for example) but is still recorded by the calorimeter system. Therefore, ZH trilepton events inherently have a higher number of jets than the backgrounds and very little signal in the $N_{Jet} = 0$ bin. This characteristic of the ZH trilepton signal allows us to create a control region for the ZH analysis in the $N_{Jet} = 0$ bin with very little signal loss, and so $N_{Jet} = 0$ events are not included in the ZH analysis.

The WH and ZH signals have particular characteristics that guide the definitions of the control regions defined for each, and also serve to distinguish the signals from their backgrounds within the defined control regions. The first and most obvious characteristic is the three-lepton signature. Next, the WH signal has three $W \rightarrow l\nu_l$ decays and so at least three neutrinos carrying away energy. This lends towards a signature with high E_T . The E_T of the ZH signal is not quite as high as the WH signal because there are fewer neutrinos produced, but still higher than the backgrounds. Augmenting this, the Higgs boson's scalar nature means that the two W -bosons it decays to have opposite spins, meaning the lepton's they decay to tend to be very close in ΔR

separation. The ZH signal has one of the two Higgs- W -bosons decaying hadronically, so it tends to have a two-jet signature, whereas its backgrounds all tend toward a zero-jet signature (except for $t\bar{t}$, but the rate is so low there's negligible effect). Because of these characteristics, all the analyses select on three-lepton events, a E_T cut, and the ZH analysis focuses on events with two jets or more, though there is still some contribution from the one-jet ZH events.

Summarily, the signal regions are defined as:

1. WH Analysis (“BaseWHTrilep”):

- Z -Peak is removed ($m_{ll} \notin [76.0, 106.0]$ GeV)
- $E_T > 20.0$ GeV
- Any number of jets

2. ZH , NJet=1 Analysis (“BaseZH1Jets”):

- Z -Peak is selected ($m_{ll} \in [76.0, 106.0]$ GeV)
- $E_T > 10.0$ GeV
- Number of jets = 1

3. ZH , NJet ≥ 2 Analysis (“BaseZH2orMoreJets”): Z -Peak is selected

- Z -Peak is selected ($m_{ll} \in [76.0, 106.0]$ GeV)
- $E_T > 10.0$ GeV
- Number of jets ≥ 2

where all regions require the 1st lepton to have at least 20 GeV and the other two leptons to have at least 10 GeV. The event count for all backgrounds and the signals at $m_H = 165$ GeV in the analysis regions are found in table 9.1. See section 9.2.2 for a more detailed description of the backgrounds.

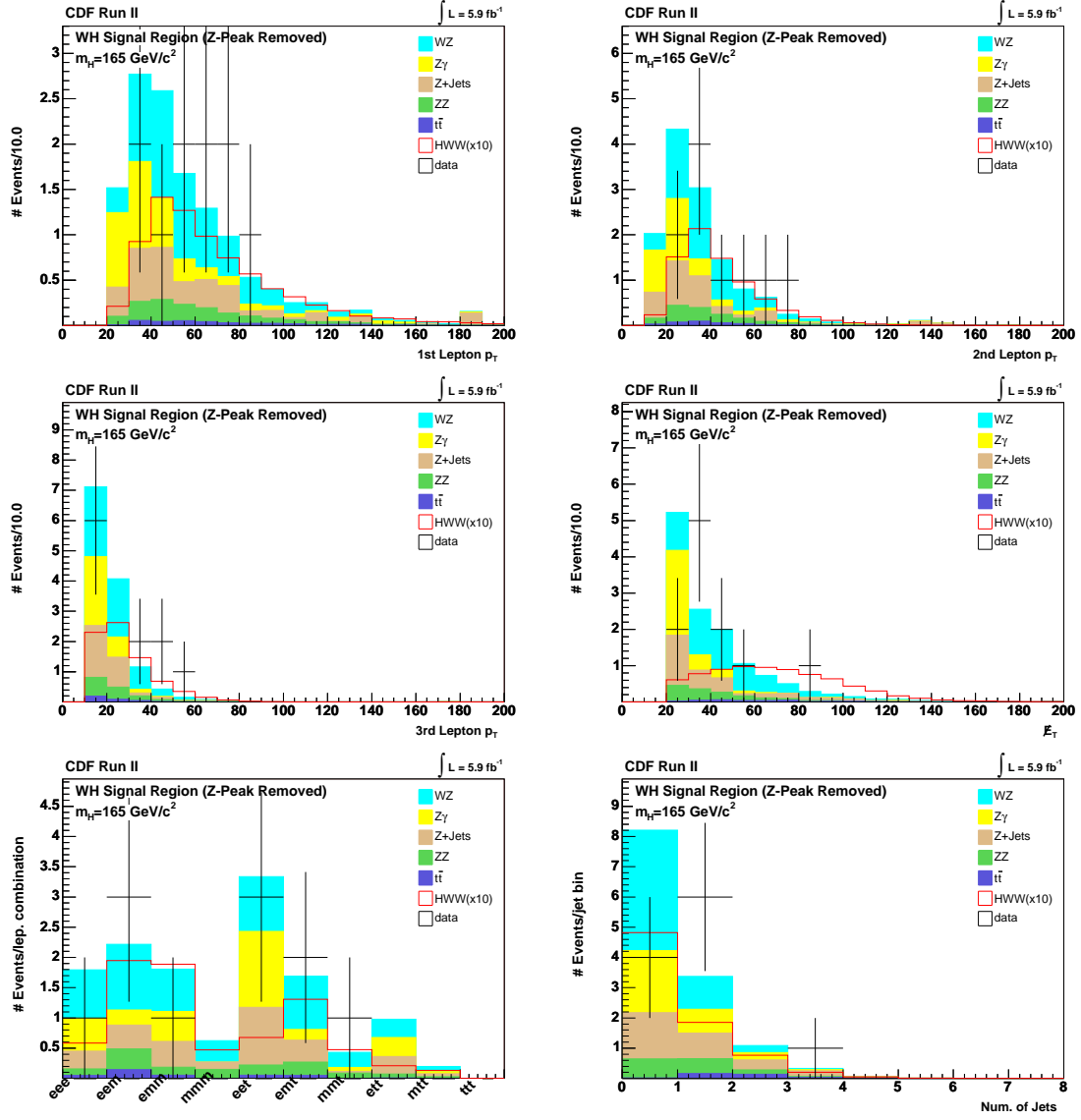


Figure 9.4 Tripleton WH signal region lepton p_T (for muons) or E_T (for electrons)

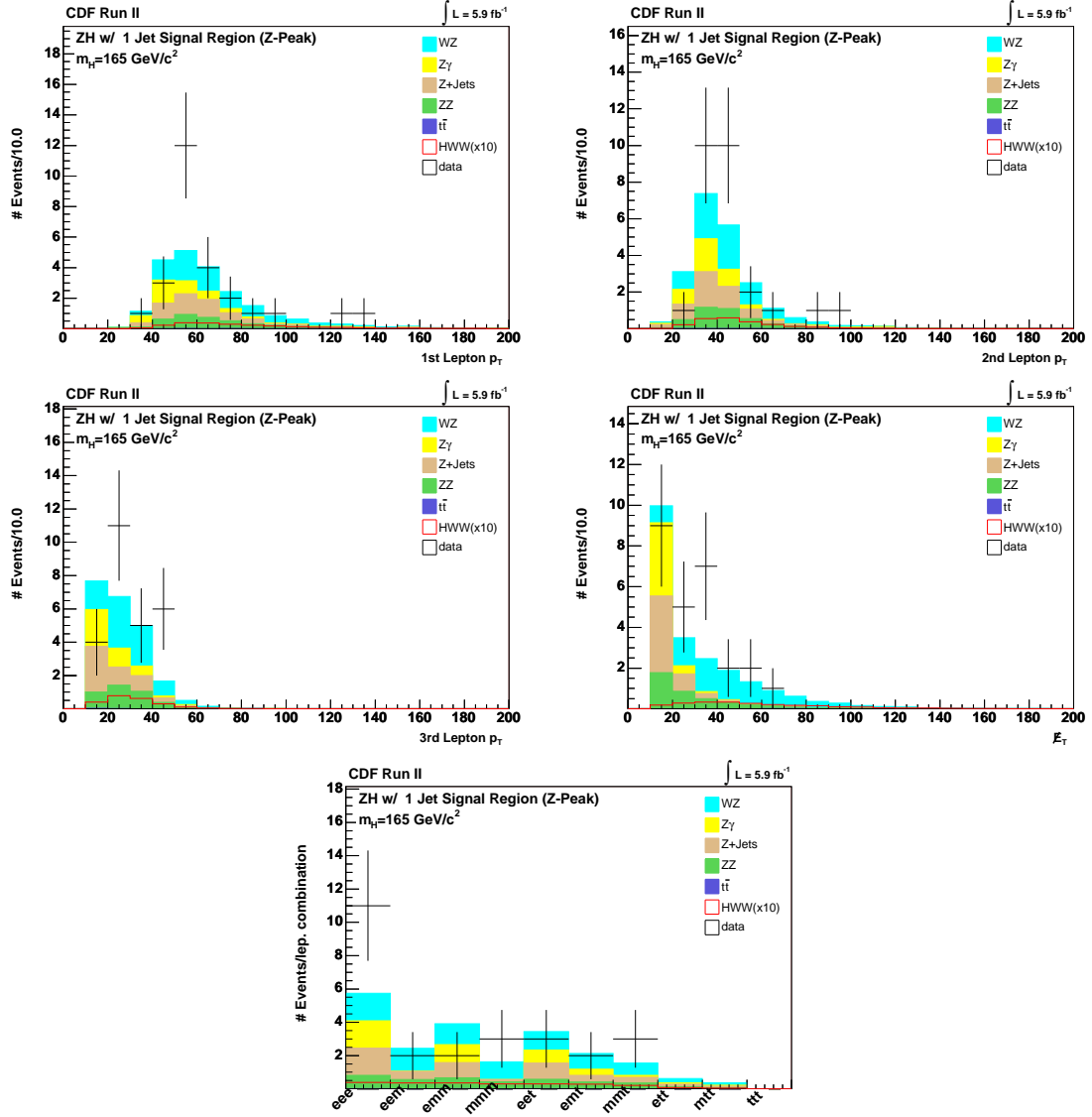


Figure 9.5 Tripleton ZH (1 Jet) signal region lepton p_T (for muons) or E_T (for electrons)

Once signal regions are defined, “control regions” are also required. These control regions are selected specifically in areas where very little signal is expected so that background models can be objectively tested against the data. If background modeling is inaccurate, then there is a serious risk of having false-positive signals. Two control regions are defined for this analysis, one for the WH signal and one for the ZH signal:

1. WH Control Region:

- Z -Peak is removed ($m_{ll} \notin [76.0, 106.0]$ GeV)
- $10.0 < \cancel{E}_T < 20.0$ GeV
- Any number of jets

2. ZH Control Region:

- Z -Peak is selected ($m_{ll} \in [76.0, 106.0]$ GeV)
- $\cancel{E}_T > 10.0$ GeV
- Number of jets = 0

The event count for the control regions is in table 9.2.1.

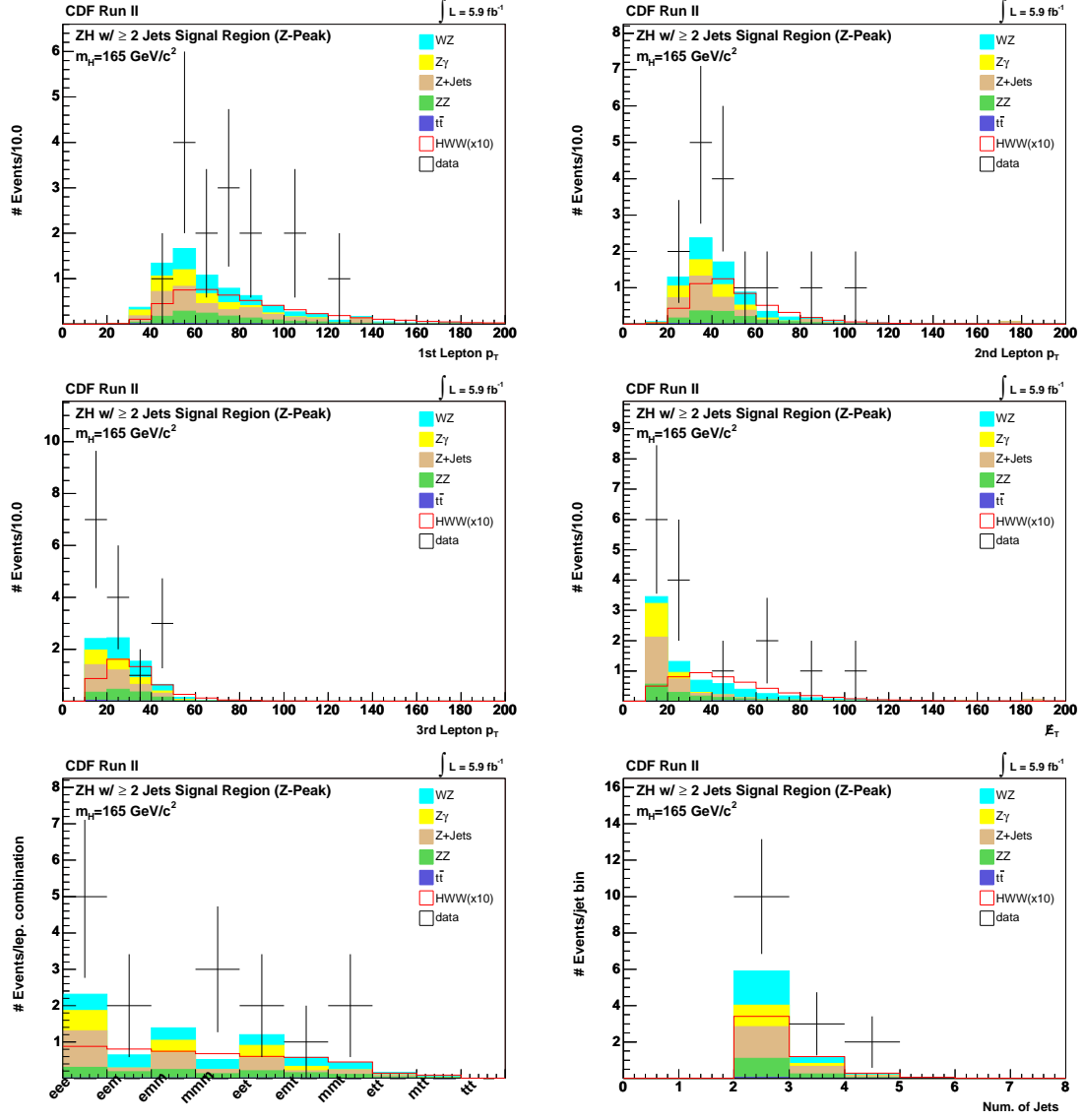


Figure 9.6 Trilepton ZH (≥ 2) Jet signal region lepton p_T (for muons) or E_T (for electrons)

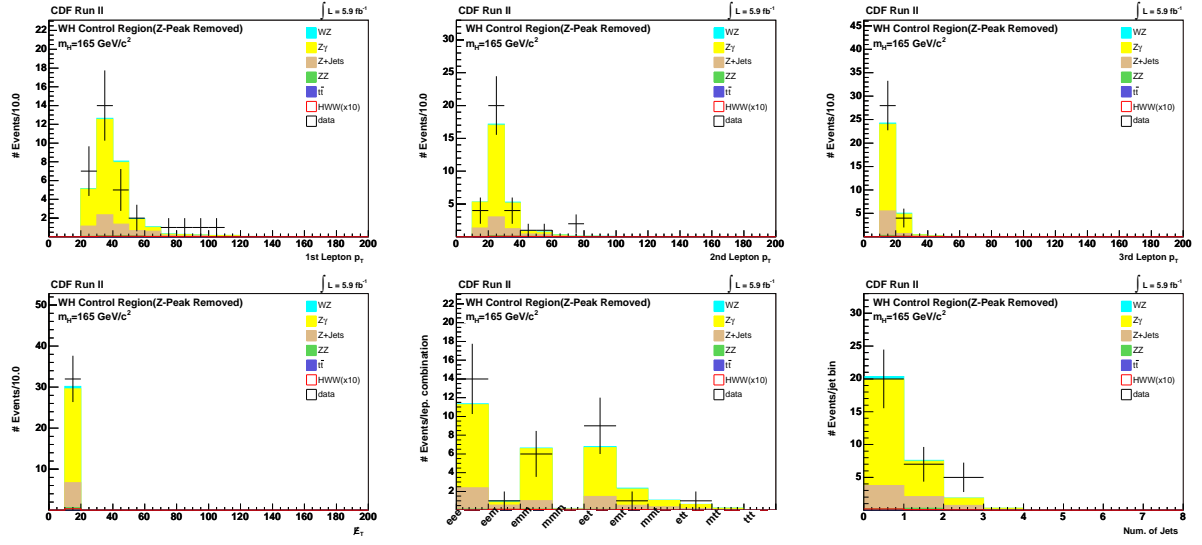


Figure 9.7 Trilepton WH Control Region lepton p_T (for muons) or E_T (for electrons)

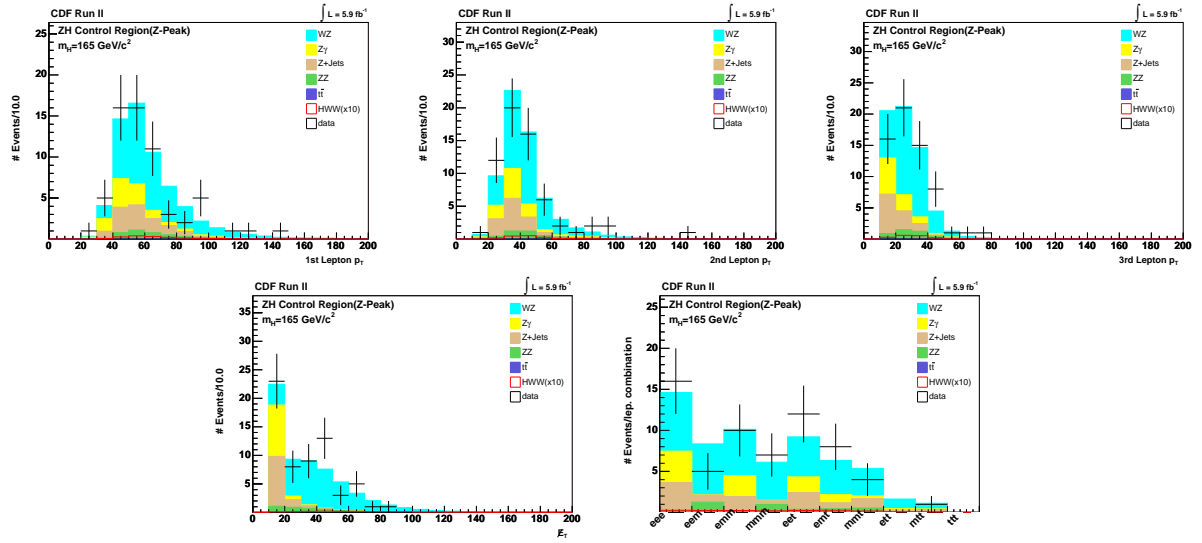


Figure 9.8 Trilepton ZH Control Region lepton p_T (for muons) or E_T (for electrons)

CDF Run II			$\int \mathcal{L} = 5.9 \text{ fb}^{-1}$		
$(m_H = 165 \text{ GeV}/c^2)$	WH		ZH (NJet= 1)		ZH (NJet\geq 2)
WZ	5.35	± 0.75	8.53	± 1.37	2.28 ± 0.52
ZZ	1.30	± 0.18	3.97	± 0.57	1.32 ± 0.25
$Z\gamma$	3.13	± 0.62	4.14	± 0.86	1.36 ± 0.37
Fakes (WW, Z +Jets)	2.92	± 0.72	5.13	± 1.32	2.27 ± 0.58
$t\bar{t}$	0.37	± 0.12	0.07	± 0.02	0.08 ± 0.03
Total Background	13.1	± 1.46	21.8	± 2.69	7.30 ± 1.19
WH	0.61	± 0.08	0.03	± 0.004	0.008 ± 0.002
ZH	0.16	± 0.02	0.20	± 0.03	0.49 ± 0.07
Total Signal	0.77	± 0.10	0.23	± 0.03	0.50 ± 0.07
Data	11		26		15

High Mass

Table 9.1 Event count for the signal and background processes in the trilepton signal regions for 5.9fb^{-1} of collected data

CDF Run II	$\int \mathcal{L} = 5.9 \text{ fb}^{-1}$				
$(m_H = 165 \text{ GeV}/c^2)$	WH Control Region			ZH Control Region	
WZ	0.60	\pm	0.08	37.8	\pm 7.32
ZZ	0.60	\pm	0.08	4.23	\pm 0.01
$Z\gamma$	22.9	\pm	4.56	9.92	\pm 2.10
Fakes ($WW, Z+\text{Jets}$)	6.07	\pm	1.51	10.9	\pm 3.27
$t\bar{t}$	0.02	\pm	0.005	0.002	\pm 0.0004
Total Background	30.2	\pm	4.84	62.9	\pm 9.59
WH	0.03	\pm	0.004	0.10	\pm 0.02
ZH	0.01	\pm	0.002	0.07	\pm 0.01
Total Signal	0.04	\pm	0.005	0.17	\pm 0.03
Data	32			63	

High Mass

Table 9.2 Event count for the signal and background processes in the trilepton control regions for 5.9fb^{-1} of collected data

9.2.2 Backgrounds

Both regions of this tripleton analysis have five background categories considered: WZ , ZZ , $Z\gamma$ (replacing Drell-Yan), Fakes (data-based, mostly Z +jets), and $t\bar{t}$. Each is summarized in table 9.1 along with the predicted signal for a $m_H = 165$ GeV standard model Higgs boson and the data.

- *Heavy Dibosons (WZ , ZZ):* The WZ and ZZ diboson contributions provide three physical leptons, with WZ being the dominant background in all tripleton signal regions. Both samples are Pythia-based, where the W is allowed to decay inclusively and the Z is forced to decay leptonically (electron, muon, or tau pairs)[20]. Incidentally, as a side project to this analysis I have also made the first measurement of the WZ diboson cross section since its discovery was first published in 2007 (see appendix L for a brief description of the results).
- *$Z\gamma$:* The $Z\gamma$ background in the tripleton analyses replaces the Drell Yan contribution of the dilepton analyses and is created by the Bauer generator. The third lepton from a Drell Yan process is acquired when either an initial or final state radiated photon undergoes a “conversion” (the photon interacts with detector apparatus to become an $e\bar{e}$ pair) and showers in the calorimeter for the third lepton signature. As such, the $Z\gamma$ is the restriction of Drell Yan to those events which do radiate a photon for the purpose of working with a larger statistical sample.
- *Fakes(Z +Jets):* In the dilepton analysis, the Fakes category is measured from single high p_T lepton data (rather than MC) and assumed to have a predominantly Z +jets event topology, where the two leptons are from the Z -boson (see section 6.4 for a detailed description).
- *$t\bar{t}$:* The $t\bar{t}$ process is the smallest background, but arguably the most complex. This process decays to a pair of b -jets accompanied by a W bosons. For the case of tripletons, we consider the situation of the two W ’s decaying leptonically. The third lepton signature is then due to one of the b -jets, which is supposed to produce a lepton candidate with higher probability than a light jet, but this rate is not precisely known.

Because of this, we cannot ignore the possible contribution of $t\bar{t}$ in our Fakes background category where the lepton decayed from the b -jet is the fake lepton (denominator object). However, any $t\bar{t}$ that might be included in the high p_T lepton data of the Fakes background is then scaled down by a fake rate determined for a sample of jets assumed to be mostly light—hence, the $t\bar{t}$ contribution to the Fakes background is scaled down further than it should be since its jets are only the heavy b -jets.

The standard MC $t\bar{t}$ ntuple used by the $H \rightarrow WW$ group requires reconstructed leptons to pass a matching criteria to either a generator-level lepton or photon (for the case of photon conversion). For our purposes in the trilepton analysis, we are interested in a third lepton whose signature is the result of those b -jets, so we have our own MC $t\bar{t}$ sample that allows matching to b -jets as well as leptons and photons. The MC $t\bar{t}$ sample accounts for such events that result in three fully identified leptons, as opposed to the 2 leptons+1 fake lepton signature of the Fakes background.

Lastly, there is inevitably some overlap between the $t\bar{t}$ that occurs implicitly in the Fakes data-based background and the MC sample. By measuring the difference between the 3-lepton bin of the default $t\bar{t}$ sample (lepton match only to generator-level leptons or photons) with another $t\bar{t}$ sample allowing matching to b -jets as well, we take half the percentage difference to be the systematic error accounting for overlap.

Although three trilepton signal regions have been defined to separately focus on the WH and ZH associated production channels, all signal regions do contain both signals and are summarized for all generated masses in table N.1 (appendix N).

9.3 Neural Net

Chapter 7 described the concept and structure of neural networks. Many distributions that show separation between background and signal curves are used by the neural network to generate a single distribution with better separation than any one particular input. This $H \rightarrow WW$ trilepton analysis exploits several physical characteristics of the signals to generate a useful result. Let's discuss a few of the most important ones.

9.3.1 Discriminating Variables

One of the clearest and simplest distributions used is the missing transverse energy (E_T) of an event (see section 6.3). The WH trilepton signal involves at least three decays producing neutrinos—more if tau leptonic decays are involved. The ZH trilepton signal also produces at least one neutrino so E_T is useful for that signal as well. Figure 9.9 illustrates the separation of the WH and ZH signals from their backgrounds in E_T —the signal distributions clearly have higher valued E_T than the backgrounds.

Another simple distribution used is the number of jets reconstructed per event. The ZH trilepton signal occurs when the Z decays to two leptons, the Higgs decays to two W -bosons, and one of these W -bosons decays leptonically (producing the third lepton) while the other W decays to two quarks that produce two hadronic jets. As such, the ZH signal tends to have two jets while its backgrounds tend to have zero jets (except for $t\bar{t}$ which does tend toward two jets, but can be discriminated in other variables and has nearly negligible contribution anyways). See figure 9.10 for the NJet distribution of the ZH signal. NJet turned out to be such a good discriminator for the ZH signal that the 0-jet bin was partitioned off to be a control region for the analysis. Further, and much more recently, the rest of the ZH signal region was partitioned into two separate analyses: a 1-jet bin analysis and a ≥ 2 -jet bin analysis. As a discriminating variable, NJet is still used in the ≥ 2 -jet bin analysis, but is not as powerful a discriminator as it once was. The advantage to splitting the ZH signal region into two separate analyses is in having a region that guarantees the presence of at least two jets from the hadronic Higgs- W decay. This way, such variables as the

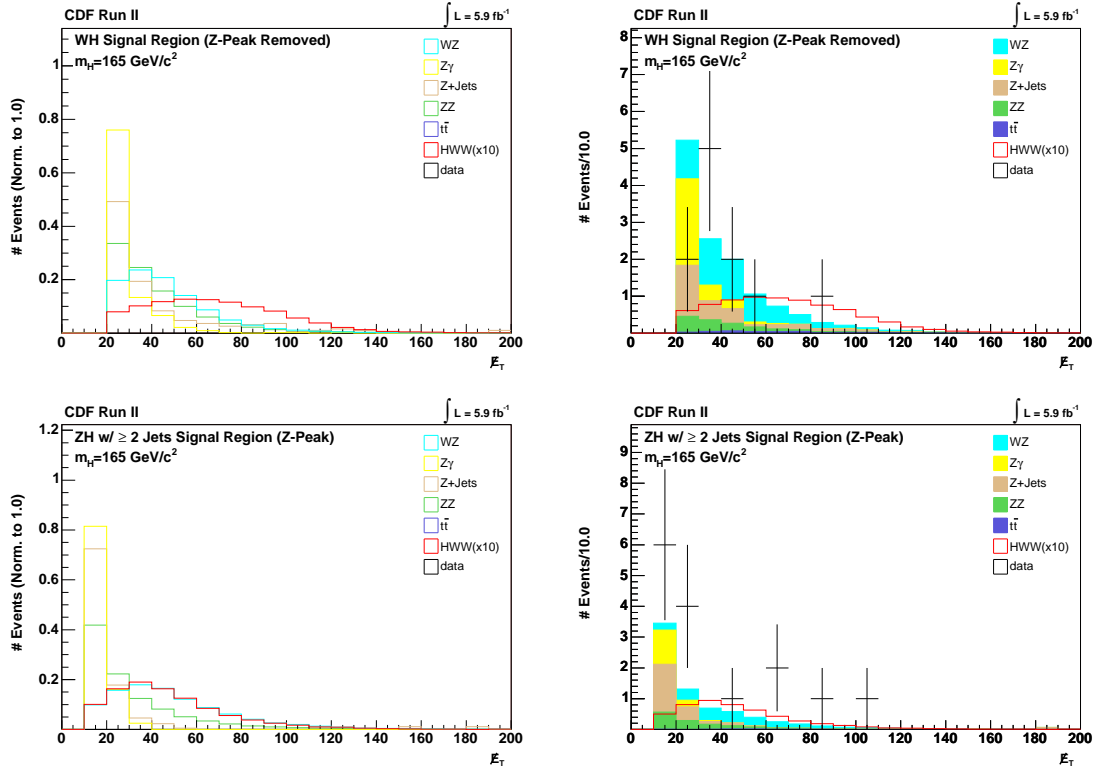


Figure 9.9 The histograms on the left have each processed normalized to an area of 1.0 to compare shapes, while the histograms on the right are properly weighted to 5.9 fb^{-1} .

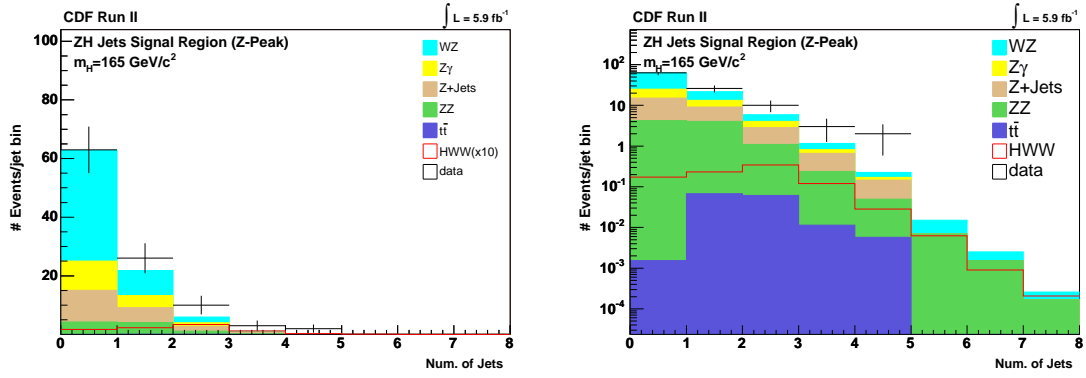


Figure 9.10 Number of jets for all jet bins in the Z -selected region

invariant mass of the two jets, the ΔR between the two jets, and the reconstructed transverse ZH higgs mass (leading lepton, E_T , and leading two jets) can be exploited in the discrimination.

The Higgs boson itself has another important physical property to exploit: the scalar nature of the SM Higgs boson. In the WH signal topology, the Higgs boson decays to a pair of W -bosons which go on to decay to leptons. The quasi-angular distance value commonly used to measure the distance between two high p_T objects in collider physics— $\Delta R = \sqrt{\Delta\phi^2 + \Delta\eta^2}$, where ϕ is the azimuthal angle around the beamline and η is the pseudorapidity—shows that the two leptons ultimately descending from the Higgs boson in WH decays tend to be close in proximity. The reason for this is because the scalar Higgs boson decays to two roughly back-to-back W spin ± 1 vector bosons. These W -bosons are known to decay to leptons according to the $V - A$ angular distribution pattern, where the zero angle is defined as the direction of the W 's momentum:

$$\frac{d\Gamma_{\pm}}{d(\cos\theta)} \propto (1 \mp \cos\theta)^2 \quad (9.7)$$

Figure 9.11 shows the general shape of the distribution, where the spin $+1$ vector boson decays its lepton backward along its path of motion and the spin -1 vector boson decays its lepton forward along its path of motion. Hence, the two leptons decaying from the scalar Higgs tend to be close in ΔR . Figure 9.12 illustrates this distribution by plotting the ΔR value of the closest of the three possible pairings of the three leptons in an event (requiring opposite charges).

While there are many more useful discriminating variables briefly summarized below, one more deserves particular attention for illustrating the application of neural networks to separate signal from background. All of these “discriminating variables” exploit physical characteristics of a signal that distinguish it from its backgrounds. When searching for a particle of a particular

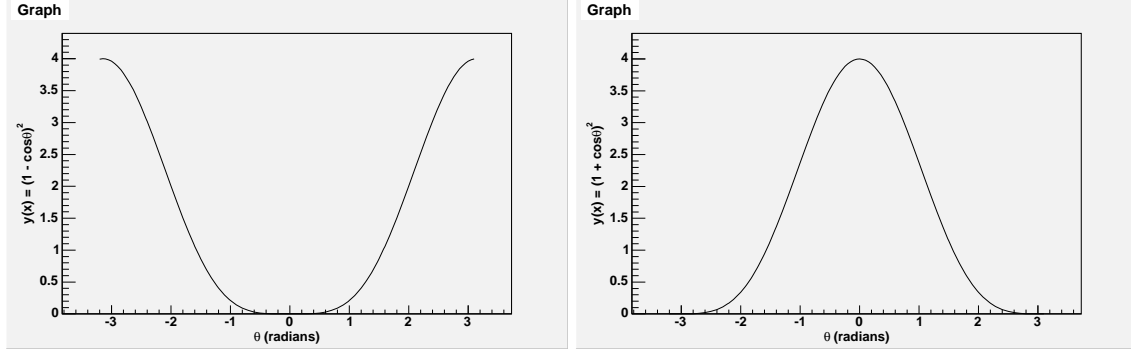


Figure 9.11 “ $V - A$ Angular Distribution: $W \rightarrow l\nu_l$ decay distribution shape for a W with spin $+1$ (left) and with spin -1 (right).

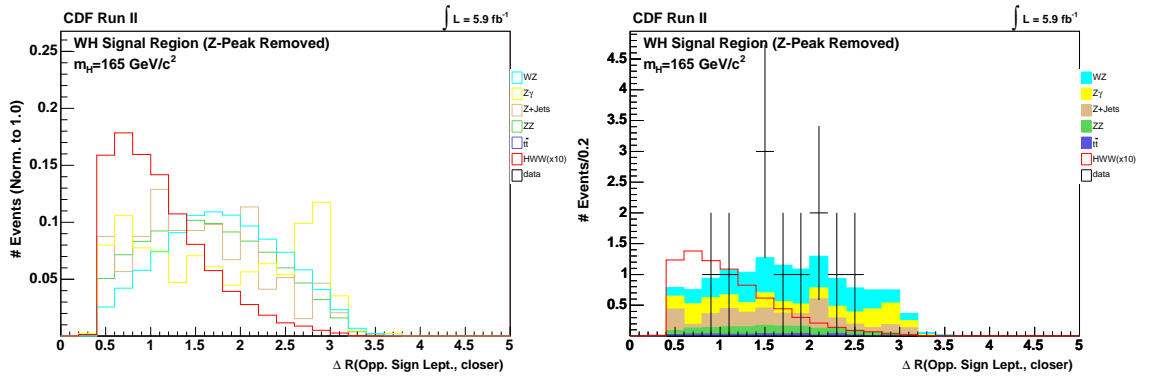


Figure 9.12 The histograms on the left have each processed normalized to an area of 1.0 to compare shapes, while the histograms on the right are properly weighted to 5.9 fb^{-1} .

mass, reconstructing the mass value itself is useful. While this cannot be done in the WH analysis because we cannot know the energies of multiple particular neutrinos (only overall “missing energy”), the Higgs boson of the ZH signal contains one lepton, one neutrino, and two jets. Figure 9.13 show the “transverse mass” of a $m_H = 165$ GeV Higgs signal compared to its backgrounds.

Definition 9.1 *Transverse Mass*: While momenta are vector values, energy is a scalar in physics. However, a common practice in collider physics is to artificially attach a unit vector to the scalar energy value pointing from the primary interaction vertex to the center of the calorimeter in which an energy value is recorded. This construction allows the energy value to be used as a vector, so with all four Minkowski-space components having spatial directions we can speak of energy and mass projected with direction as well. In this case, the *transverse mass* is the mass reconstructed from Minkowski-space vectors in the plane transverse to the beamline:

$$m^2 = E^2 - p_x^2 - p_y^2 - p_z^2 \quad (9.8)$$

$$m_T \equiv m^2 + p_x^2 + p_y^2 = E^2 - p_z^2 \quad (9.9)$$

Each of the three signal regions considered in this analysis has its own set of discriminating variables, though many of these variables are used in more than one region. The following is a list of all discriminating variables used in any of the signal regions. See appendix P for tables of which particular discriminating variables are used for each signal region, ordering them by their significance in discriminating signal from background.

- E_T : The missing transverse energy of the signal is high because of the neutrinos decaying from W -bosons.
- NJet: The ZH signal tends to have two jets while the background tends to have zero jets (except for $t\bar{t}$).
- ΔR b/w Opp. Sign Close Leptons: With three leptons there are three possible pairings of leptons. Events with all three leptons having the same sign are rejected from this analysis, so every event has two possible pairings of opposite-signed leptons. Of those two pairings, this variable is the ΔR value of the pairing with lower ΔR value.

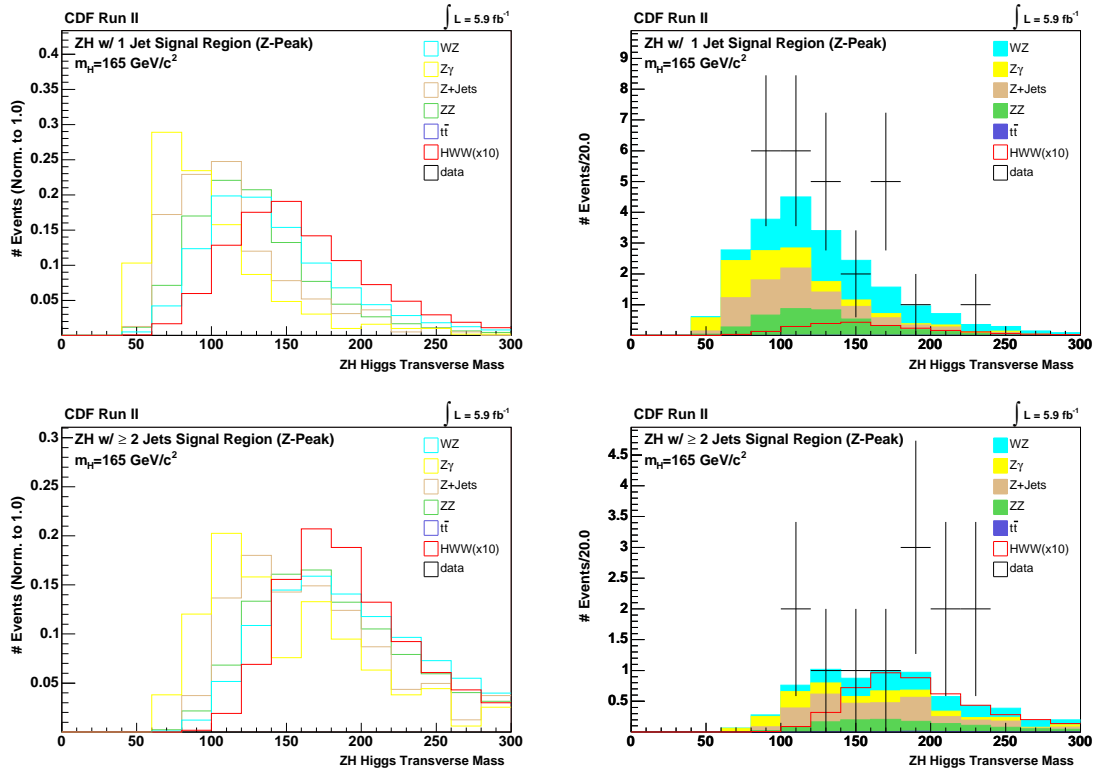


Figure 9.13 The histograms on the left have each processed normalized to an area of 1.0 to compare shapes, while the histograms on the right are properly weighted to 5.9 fb^{-1} . ZH events in the 1-jet region just use the single jet in the mass reconstruction while ZH events in the ≥ 2 jets region use the leading two jets by energy.

- H_T : Sum of the transverse energies of all three leptons, the \cancel{E}_T , and all jets. Basically, this is a sum of all transverse energy produced in the event.
- Invariant mass of opposite-signed leptons closest in ϕ : This is a partial reconstruction of the WH Higgs boson mass with the energy of the neutrinos left out. Since there are two neutrinos inherent to this decay, we cannot know how much energy each individually had. Also, if such neutrinos have momentum vectors with magnitudes in opposite directions, those values would cancel out, so using the sum of these two leptons with the \cancel{E}_T would be inappropriate.
- $\Delta\phi(\text{Lep2}, \cancel{E}_T)$: The magnitude of the difference in ϕ between the 2nd lepton by p_T and the \cancel{E}_T .
- $\text{Inv. Mass}(\text{Lep3}, \cancel{E}_T, \text{Jets})$: Invariant mass of the vector sum of the 3rd lepton, \cancel{E}_T , and Jets.
- $m_T(\text{Leptons}, \cancel{E}_T, \text{Jets})$: Transverse mass of the vector sum of all three leptons, \cancel{E}_T , and all jets.
- p_T of the 2nd lepton by p_T : The signals tend to produce pairs of leptons with similar momenta, so the second lepton by p_T trends higher for signals than backgrounds.
- ΔR Opp. Sign Far Leptons: With three leptons there are three possible pairings of leptons. Events with all three leptons having the same sign are rejected from this analysis, so every event has two possible pairings of opposite-signed leptons. Of those two pairings, this variable is the ΔR value of the pairing with higher ΔR value.
- m_T Trilepton Mass: Transverse mass of the vector sum of the three leptons.
- $m_T(\text{Lep3}, \cancel{E}_T)$: Transverse mass of the vector sum of the 3rd lepton and the \cancel{E}_T .
- $\text{Inv. Mass}(\text{Lep1}, \text{Lep2}, \cancel{E}_T)$: Invariant mass of the vector sum of the 1st lepton, 2nd lepton, and \cancel{E}_T .

- Lead Jet E_T : Transverse energy of the leading jet. The ZH analysis tends to have high energy jets since they come from a W that comes from the Higgs boson.
- $\Delta R(W\text{-Lep}, \text{Lead Jet})$: The *InZPeak* region is defined by having one lepton paring (opposite signed, same flavor) near the Z boson mass. Denote the one other lepton not in this pairing as the W -lepton. This variable is then the ΔR between the W -lepton and the leading jet, both descending from the Higgs.
- $\text{Dimass}(W\text{-Lep}, E_T)$: The ZH analysis regions are defined by having one lepton paring (opposite signed, same flavor) near the Z -boson mass. Denote the one other lepton not in this pairing as the W -lepton. This variable is then the invariant mass of the vector sum of the W -lepton and the E_T .
- $m_T(W\text{-Lep}, E_T)$: Transverse mass of the vector sum of the W -lepton and the E_T .
- $\Delta\phi(\text{Leptons}, E_T)$: $\Delta\phi$ between the vector sum of the three leptons and the E_T .
- The invariant mass of the vector sum of the three leptons.
- m_T Jets: Transverse mass of the vector sum of all jets.
- $\Delta\phi(Z\text{-Leptons}, W\text{-Lepton})$: ΔR between the vector sum of the two leptons identified as the Z -leptons, and the other lepton.
- Lepton Type Combination: Identified lepton flavor combination, eee , $ee\mu$, $e\mu\mu$, etc.
- Invariant mass of the leading two jets.
- ΔR between the leading two jets.
- ZH Higgs mass: Invariant mass of the leading two jets and the W -lepton.

Further, the control regions are important for more than just testing event count of the backgrounds against the data. They are also used to test the distribution shapes of various basic kinematic values as well as the discriminating variables themselves. This Higgs trilepton analysis is

especially plagued by low statistical samples to work with. The sample size of the control regions are still quite low, but are at least more numerous than the signal regions. There are far too many control region histograms to list here, so see appendix Q for a comprehensive list.

9.3.2 Neural Network Scores

With the collections of discriminating variables defined for each signal region, the neural network scores (z_{net}) can be computed. Recall that the discriminating variables are used to push background-like events towards the value -1 while pushing signal-like events towards the value $+1$. The histograms draw a stacked plot of the MC background prediction, draw over that the MC signal prediction, then the data events are also plotted.

Ostensibly, if the data events follow the background prediction alone, then there is no evidence for a signal. If the data events follow the background plus the signal—there is a pileup of events near $z_{\text{net}} = +1$ significantly over the background prediction—then there is evidence of a signal. In this Higgs boson analysis, however, the signal production is predicted to be too low to reliably distinguish the background-only hypothesis from the background-plus-signal hypothesis with a neural network treatment alone. This is why we go on to use these neural network scores in the calculation of statistical confidence levels. The hope is that with enough data this analysis can be combined with the other analyses of the $H \rightarrow WW$ group to see a signal or set a reliable exclusion of one.

See the histograms in figure 9.14 for the neural network scores pertinent to each signal region, assuming a SM Higgs boson mass of $m_H = 165$ GeV. The control regions are used to test for proper training in the neural network as well. The events of the WH low E_T control region are input to the neural network trained on the WH signal region. If the neural network is trained and functioning properly, the control region processes are expected to output a very background-like neural network score. Similarly, the ZH NJet=0 control region is used as input for both the neural networks trained on the ZH NJet=1 signal region and the ZH NJet ≥ 2 signal region. The neural network scores for these control regions are illustrated in figure 9.15 (again for a SM Higgs boson mass of $m_H = 165$ GeV) and confirm the background-like nature of the control regions and the

data found in the control regions. See appendix R for a comprehensive list of neural network scores in the signal regions for SM Higgs boson masses ranging from $m_H = 110$ GeV to $m_H = 200$ GeV.

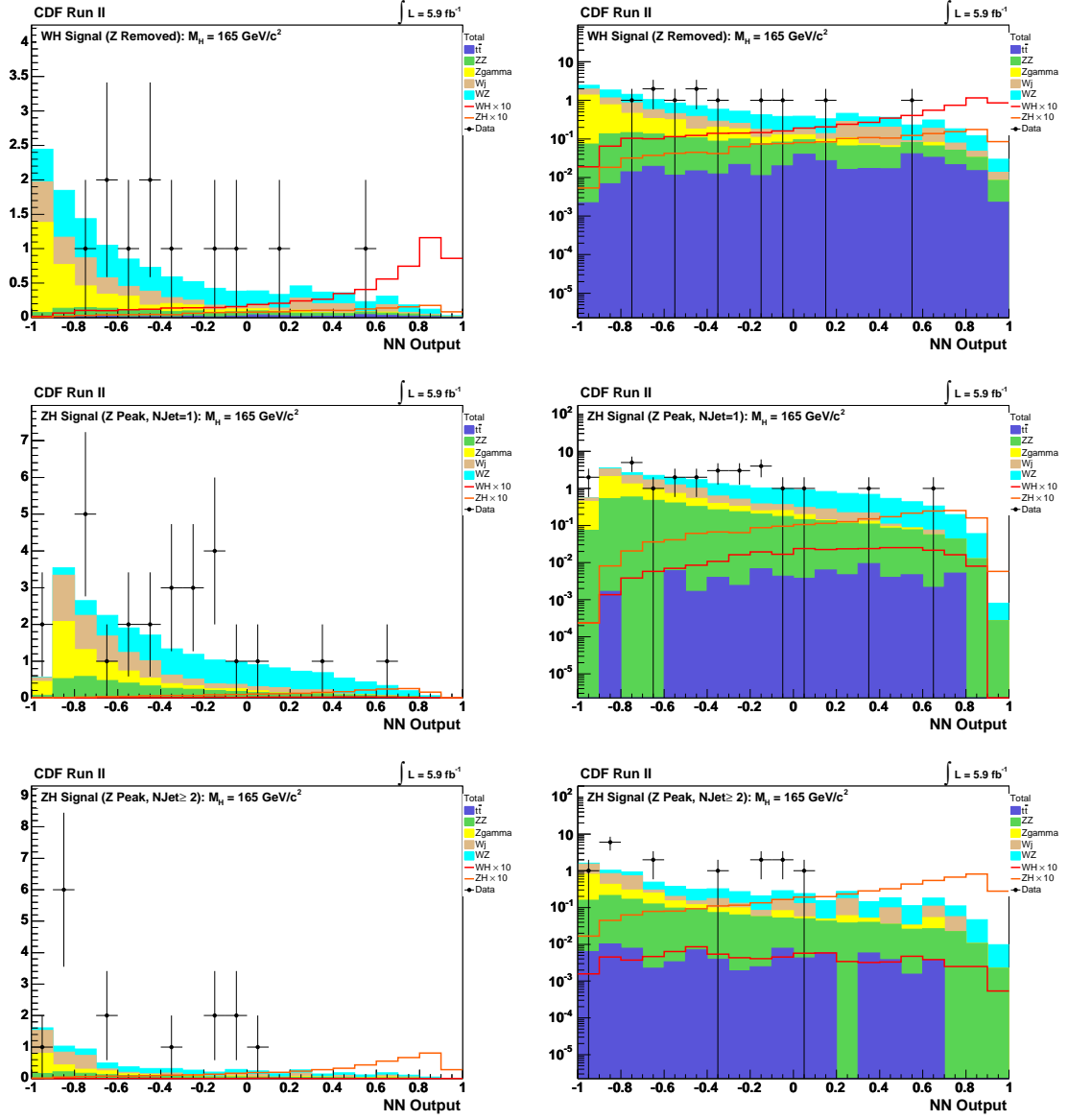


Figure 9.14 NeuroBayes neural network score for the signal regions of the tripleton analysis with 5.9 fb^{-1}

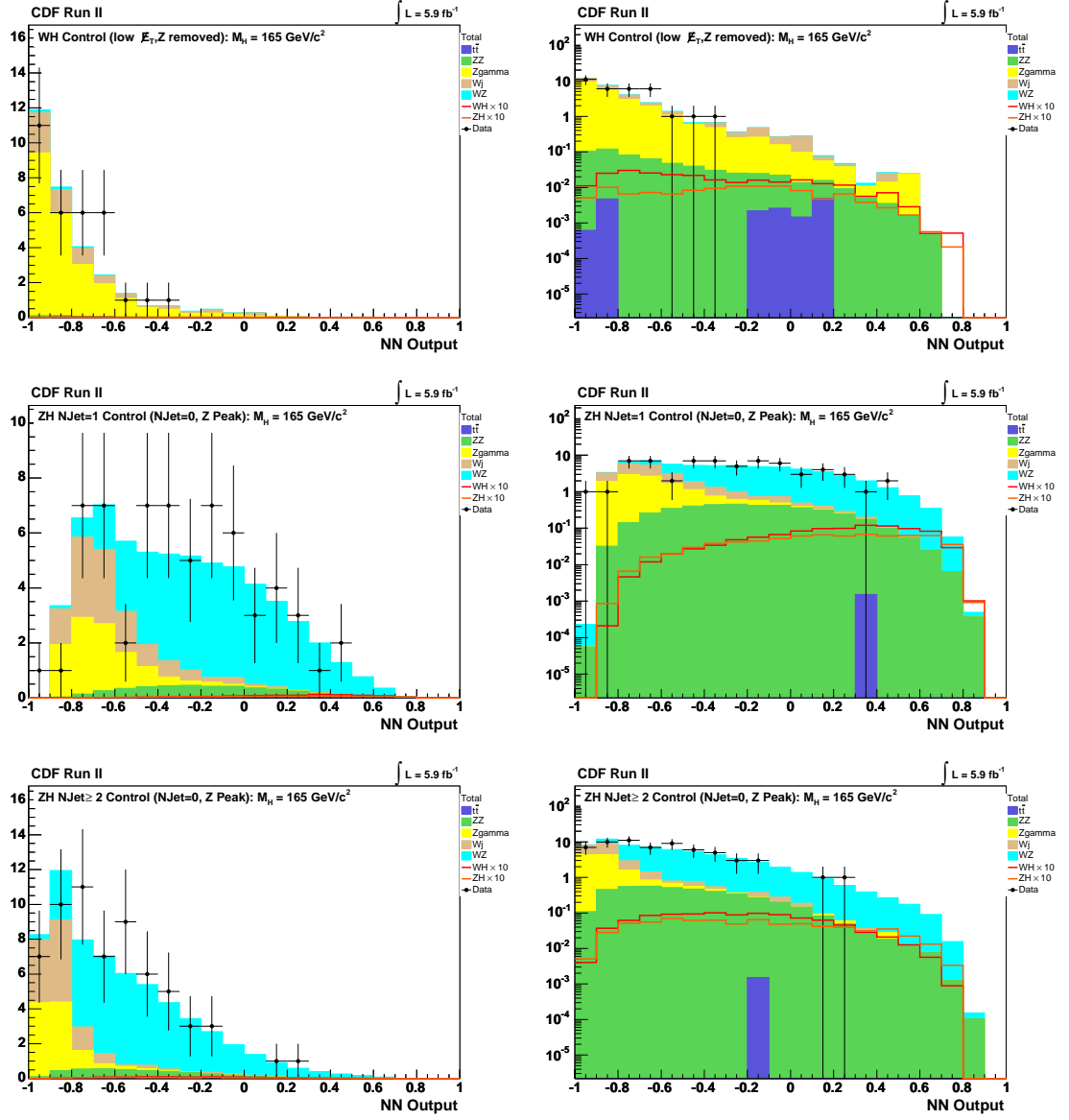


Figure 9.15 NeuroBayes neural network score for the control regions of the trilepton analysis with 5.9 fb⁻¹

9.4 Systematic Errors

We explored the idea of systematic uncertainty and their Gaussian pattern in section 8.2. The following is a list of the systematic uncertainties assumed in this analysis along with their values in table 9.3.

- *WH, ZH Higher Order Diagrams*: Higgs processes generated with PYTHIA at (leading order + phenomenological model of parton showering), accounts for variations from MC@NLO modelling[14, 1].
- *Diboson Acceptance*: This systematic refers to the uncertainty on the acceptance of events from diboson processes (WZ and ZZ). Since the production processes are very similar, we assume these uncertainties are correlated.
- *$t\bar{t}$ Acceptance*: This systematic refers to the uncertainty on the acceptance of events from $t\bar{t}$, which is uncorrelated from other acceptance uncertainties. At leading order, $t\bar{t}$ has two W -bosons that decay leptonically to provide two leptons, with the third lepton faked from one of the two b -jets for the event to be in the signal region.
- *Higgs Acceptance*: Uncertainty on the acceptance of the Higgs boson.
- *PDF Model*: This uncertainty is calculated in the usual manner by looking at the maximum and minimum difference using the CTEQ6m eigenvectors and weighting the acceptance. These uncertainties range from 1.9 to 4.1%.
- *Lepton ID*: The estimated errors in lepton identification efficiencies are fluctuated up and down by 1σ . The difference in the acceptance of these two fluctuations divided by the nominal acceptance is taken to be the uncertainty due to variations in the lepton identification efficiency. All lepton efficiencies are varied in the same direction simultaneously.
- *Trigger Efficiency*: The trigger efficiencies are varied up and down by their 1σ uncertainties to determine the % change in the acceptance, which is taken to be the systematic quoted here. The trigger efficiencies are varied in a correlated way.

- *Light Jet Fake Rate (for “Fakes” background)*: Fake probabilities, or the probability that a jet-like object will be falsely identified as a lepton, are calculated using the jet-triggered data samples. These fake probabilities are calculated as a function of both lepton type and E_T (or p_T). These probabilities are then applied to the Z +jets (fakeable object) sample from data. The fake probabilities are varied up and down to get an estimate of the uncertainty on the yield. This systematic only applies to the fakes (or Z +jets) sample.
- *b -Jet Fake Rate*: Although $t\bar{t}$ is a small contribution to the background for these high m_H standard model Higgs boson in the trilepton case, we do have to account for the peculiar situation that our 3rd lepton is faked from a b -jet and the rate at which a b -jet fakes a lepton—as opposed to a light jet—is not well known. Further, as a background with two real leptons and one faked, we cannot ignore the possible coverage of $t\bar{t}$ in the data-based Fakes category. We know that the fake rates used in the Fakes category are based on jet samples populated mostly with light jets and presume that b -jets in particular are more likely than light jets to produce a signature that could fake a lepton. Hence, whatever $t\bar{t}$ contribution that exists in the Fakes category is scaled down by the light jet dominated fake rate, meaning it is scaled down too far. To make up for the difference we use an MC $t\bar{t}$ sample that allows reconstructed leptons to match to generator-level leptons, photons, or b -jets (typically, for these reconstructed MC leptons to be considered fully “found” they must pass a matching criterion to a generator-level lepton or photon only). Now, of course, we have the problem of possible double-counting of $t\bar{t}$ between the MC and what implicit $t\bar{t}$ contribution populates the Fakes category. To account for the double-counting possibility, we assign a systematic error defined to be one half the percentage difference between the MC $t\bar{t}$ sample that allows leptons to match to generator-level leptons, photons, and b -jets; and the MC $t\bar{t}$ sample that allows such matching to generator-level leptons and photons only. The systematic errors adopted are:
 - WH Analysis: 0.273
 - ZH 1-jet Analysis: 0.420

– $ZH \geq 2$ -jet Analysis: 0.222

The reason ZH 1-jet has a much higher systematic is because the ‘ $t\bar{t}$ with b-match’ sample has proportionately more events in that region than a $t\bar{t}$ sample that does not match leptons to b ’s. One of the two b -jets gets identified as a lepton rather than a jet.

- *Luminosity*: The standard 5.9% uncertainty is taken on the luminosity. The exception to this is the Z +jets sample, which we do not assign a luminosity uncertainty since it is derived from the data itself.
- *MC Run Dependence*: The $Z\gamma$ stntuples used cover only periods 0 – 11, so we assign the customary MC run dependence systematics for such samples. This is determined by comparing a WW sample with partial run dependence (periods 0 – 7) with a fully run-dependent WW sample.
- *Jet Energy Scaling*: Jet energy scaling is modeled inclusively to all jet bins, so removing the zero-jet bin as a control region for the ZH analysis and dividing the signal region into two analyses by jet bin introduces a slight mismodeling for the signal region. To account for this, we re-run the analysis with different MC samples that have the jet energy scaling increased and decreased by one standard deviation.

If the jet energy scale is shifted down, then the jets of an event have lower energy, so the event counts fewer jets on average because fewer jets have enough energy to be considered above the energy threshold to be counted as such. Similarly, if the jet energy scale is shifted up, then the jets of an event have higher energy, so events count more jets on average because more jets have enough energy to be considered above the threshold energy to be counted.

Since the ZH analysis signal region is divided into two analyses: $N_{\text{Jet}} = 1$ and $N_{\text{Jet}} \geq 2$, the events from samples with jet energy scaled down have fewer jets on average so more events are shifted to lower jet bins. Likewise, events with the jet energy scaled up will count more jets on average and shift events toward higher jet bins. These shifts change the weighted

count for the backgrounds for some given integrated luminosity. As such, we must assign a systematic error for each background corresponding to the error of the jet energy scaling.

We then take the average of the percent difference between each and the original samples. Different values are found in each of the regions and for each process.

We explored the possibility of having a jet energy scaling **shape** systematic as well. That is, even if the total count of a particular process does not change appreciably, we must account for the possibility that the distribution of the process in the neural net output (the templates that serve as the inputs for calculating statistical limits) changes. The subsequent limits could be altered if a process is shifted towards or away from the signal region of the templates. To check, we used the shape systematic error for the limit calculation at the $m_H = 165$ GeV mass point and compared the results to default values. We found no difference in the limit values and so find no need for a shape systematic error.

- *Z γ Conversion*: This process is generated by the “Baur” generator and is known to have some mismodeling in the rate. As such, a systematic is included to cover the possibility of rate measurement ambiguity.

Systematic Uncertainty	WZ	ZZ	$Z\gamma$	$t\bar{t}$	Fakes	WH	ZH
Diboson Acceptance	0.100	0.100					
$t\bar{t}$ Higher Order Diagrams				0.100			
Higgs Higher Order Diagrams						0.100	0.100
PDF Model	0.027	0.027	0.027	0.021		0.012	0.009
Lepton ID Efficiencies	0.020	0.020	0.020	0.020		0.020	0.020
Trigger Efficiencies	0.021	0.021	0.021	0.020		0.021	0.021
Light Jet Fake Rates					$\sim 0.25^d$		
b -Jet Fake Rate ^c				b			
Luminosity	0.059	0.059	0.059	0.059		0.059	0.059
MC Run Dependence			0.050 ^c				
Jet Energy Scale	a	a	a	a	a	a	a
$Z\gamma$ Conversion			0.10				
σ_{Diboson}	0.060	0.060					
$\sigma_{t\bar{t}}$				0.100			
σ_{VH}						0.050	0.050
$\sigma_{Z\gamma}$			0.010 ^c				

Table 9.3 Systematic Uncertainties: Standard values for systematics used in other $H \rightarrow WW$ analyses are used wherever applicable.

^a JES systematic errors are measured individually to each process and in each region. See table 9.4.

^b WH : 0.273, $ZH(1 \text{ Jet})$: 0.420, $ZH(\geq 2 \text{ Jets})$: 0.222

^c New to trilepton analysis, not in dilepton analysis.

^d WH : 0.248, $ZH(1 \text{ Jet})$: 0.258, $ZH(\geq 2 \text{ Jets})$: 0.253

	WZ	ZZ	$Z\gamma$	$t\bar{t}$	WH	ZH
WH	0	0	0.027	0	0	0
ZH 1 jet	0.076	0.024	0.053	0.094	0.059	0.080
$ZH \geq 2 \text{ jets}$	0.178	0.131	0.182	0.036	0.154	0.049

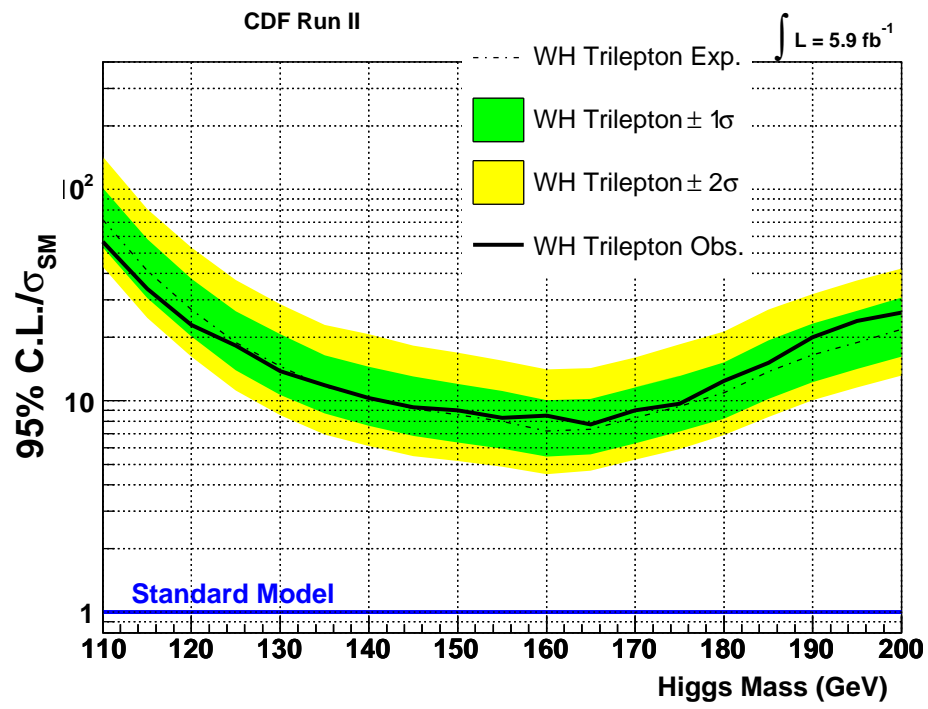
Table 9.4 Systematic errors used to account for jet energy scaling ambiguities

9.5 Results

Chapter 8 described the method of using confidence levels to set experimental limits on the Standard Model Higgs boson cross section for 19 mass hypotheses ranging from $m_H = 110$ GeV to $m_H = 200$ GeV. Let's look at the three individual analyses first, then the combined trilepton analysis.

The limit calculations presented were computed with HWWLimit version of MCLimit, both developed within the CDF experiment. Expected limits for the three trilepton analyses and combined trileptons were calculated in each case with 10,000 pseudoexperiments assuming the Standard Model background hypothesis. The expected limit line (dotted line) going under the value 1.0 indicates Higgs boson masses at which CDF is now sensitive to excluding the existence of a SM Higgs boson at 95% confidence level, assuming it does not exist. The observed line (solid line) indicates the Higgs boson masses at which CDF has indeed experimentally excluded the existence of the SM Higgs boson at 95% confidence level. If the Higgs boson did exist at these masses, then we would expect to see the observed line recording a higher value than the expected line. The observed line increasing outside of the yellow bands indicates a 2 standard deviation signal. If the observed line were 3 standard deviations above the expected line, then we would have “evidence” of a signal. If the observed line were 5 standard deviations above the expected line, then we would have “discovered” a signal.

As it is, figures 9.16, 9.17, and 9.18 illustrate the limits set by the individual trilepton analyses. Figure 9.19 is the limit set by the combination of the three trilepton analyses. This shows that the $H \rightarrow WW$ trilepton analysis alone reaches an expected limit of 4.9 and an observed limit of 5.1. This indicates the trilepton analysis will constitute a stronger contribution than some of the other previously-existing $H \rightarrow WW$ analyses (such as the dilepton same-sign analysis and the low- m_{ll} analysis).

Figure 9.16 Trilepton WH Signal Region Limits

Limits	110	115	120	125	130	135	140	145	150	155
$+2\sigma/\sigma_{\text{SM}}$	140	82	54	37	29	24	20	18	17	15
$+1\sigma/\sigma_{\text{SM}}$	102	59	38	27	21	17	15	13	12	11
Median $/\sigma_{\text{SM}}$	72	42	27	19	15	12	10	9.3	8.6	7.9
$-1\sigma/\sigma_{\text{SM}}$	53	31	20	14	11	8.8	7.7	6.8	6.4	6.0
$-2\sigma/\sigma_{\text{SM}}$	43	25	16	11	8.7	7.1	6.2	5.5	5.2	5.0
Observed $/\sigma_{\text{SM}}$	57	34	23	17	14	12	11	9.8	9.6	8.5
Limits	160	165	170	175	180	185	190	195	200	
$+2\sigma/\sigma_{\text{SM}}$	14	14	17	19	22	27	32	37	42	
$+1\sigma/\sigma_{\text{SM}}$	10	12	13	15	15	19	23	27	30	
Median $/\sigma_{\text{SM}}$	7.3	7.4	8.5	9.4	11	14	17	19	21	
$-1\sigma/\sigma_{\text{SM}}$	5.5	5.7	6.4	7.1	8.4	10	12	14	16	
$-2\sigma/\sigma_{\text{SM}}$	4.6	4.7	5.3	6.0	6.9	8.5	10	12	13	
Observed $/\sigma_{\text{SM}}$	8.1	8.0	9.1	10	13	15	19	24	26	

Table 9.5 WH trilepton analysis limits for 5.9fb^{-1} .

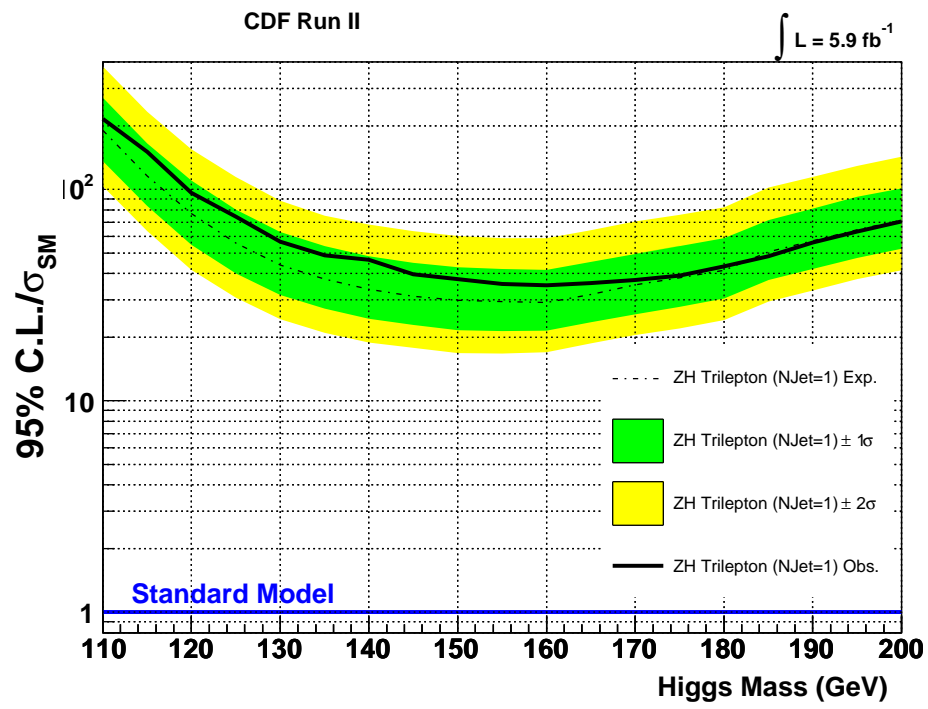


Figure 9.17 Trilepton ZH (1 Jet) Signal Region Limits

Limits	110	115	120	125	130	135	140	145	150	155
$+2\sigma/\sigma_{\text{SM}}$	380	230	160	110	90	76	68	64	61	60
$+1\sigma/\sigma_{\text{SM}}$	270	160	110	81	63	54	48	45	43	42
Median $/\sigma_{\text{SM}}$	190	115	77	56	44	37	34	31	30	29
$-1\sigma/\sigma_{\text{SM}}$	140	82	55	40	31	27	24	23	22	21
$-2\sigma/\sigma_{\text{SM}}$	100	63	42	30	24	21	18	17	17	16
Observed $/\sigma_{\text{SM}}$	220	150	97	75	57	49	47	40	38	36
Limits	160	165	170	175	180	185	190	195	200	
$+2\sigma/\sigma_{\text{SM}}$	59	64	70	75	85	102	115	130	140	
$+1\sigma/\sigma_{\text{SM}}$	42	46	50	54	60	73	82	92	100	
Median $/\sigma_{\text{SM}}$	29	32	35	38	41	51	58	64	71	
$-1\sigma/\sigma_{\text{SM}}$	21	24	25	28	30	37	42	47	52	
$-2\sigma/\sigma_{\text{SM}}$	17	18	20	22	24	29	33	37	41	
Observed $/\sigma_{\text{SM}}$	35	36	38	39	44	49	57	64	71	

Table 9.6 ZH (1 Jet) trilepton analysis limits for 5.9fb^{-1} .

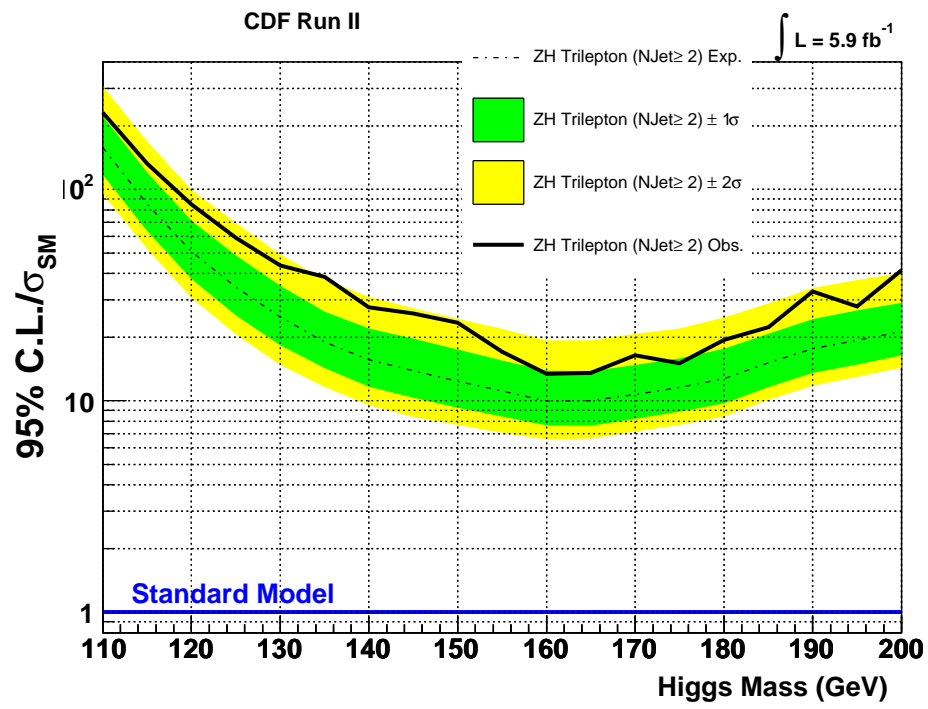


Figure 9.18 Trilepton ZH (≥ 2 Jets) Signal Region Limits

Limits	110	115	120	125	130	135	140	145	150	155
$+2\sigma/\sigma_{\text{SM}}$	320	170	100	70	51	39	32	29	25	23
$+1\sigma/\sigma_{\text{SM}}$	230	120	73	51	36	28	23	20	18	16
Median $/\sigma_{\text{SM}}$	160	88	52	35	26	20	16	14	13	11
$-1\sigma/\sigma_{\text{SM}}$	120	66	39	26	19	15	12	11	9.5	8.6
$-2\sigma/\sigma_{\text{SM}}$	99	54	32	21	15	12	9.9	8.7	7.8	7.2
Observed $/\sigma_{\text{SM}}$	220	130	84	58	43	38	27	26	23	17
Limits	160	165	170	175	180	185	190	195	200	
$+2\sigma/\sigma_{\text{SM}}$	20	19	21	23	25	30	35	38	41	
$+1\sigma/\sigma_{\text{SM}}$	14	14	15	16	18	21	25	27	30	
Median $/\sigma_{\text{SM}}$	10	10	11	12	13	15	18	20	21	
$-1\sigma/\sigma_{\text{SM}}$	7.8	7.8	8.4	9.0	10	12	14	15	17	
$-2\sigma/\sigma_{\text{SM}}$	6.8	6.8	7.4	7.9	8.7	10	12	13	15	
Observed $/\sigma_{\text{SM}}$	13	13	16	14	19	22	32	27	41	

Table 9.7 ZH (≥ 2) trilepton analysis limits for 5.9fb^{-1} .

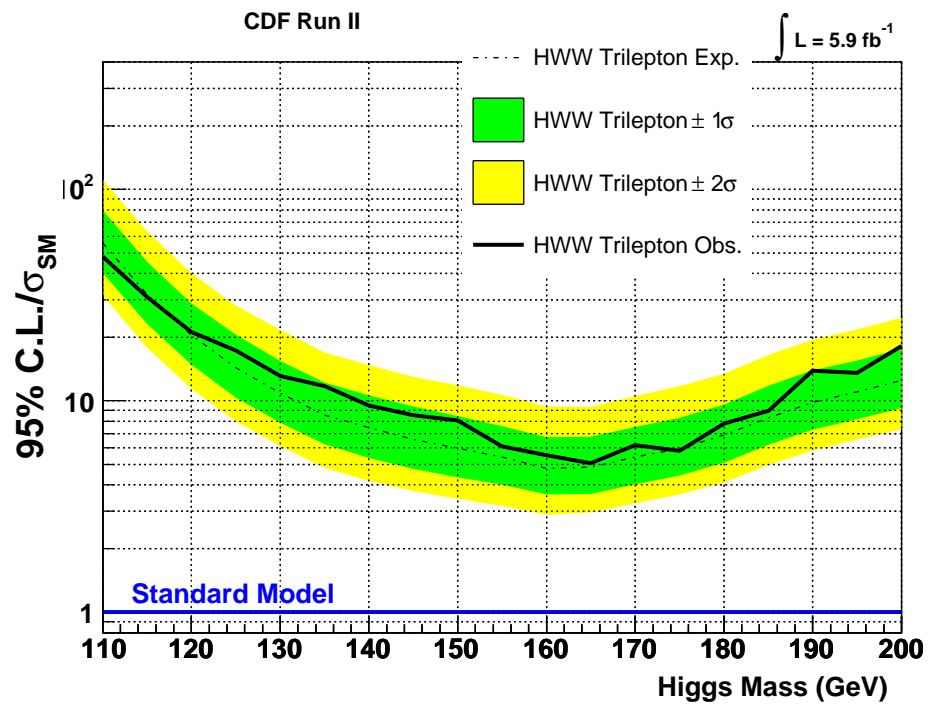


Figure 9.19 Trilepton Combined Limits

Limits	110	115	120	125	130	135	140	145	150	155
$+2\sigma/\sigma_{\text{SM}}$	110	64	42	29	22	18	15	13	12	11
$+1\sigma/\sigma_{\text{SM}}$	80	46	29	20	16	12	11	9.6	8.6	7.6
Median $/\sigma_{\text{SM}}$	56	32	21	14	11	8.7	7.5	6.7	6.1	5.4
$-1\sigma/\sigma_{\text{SM}}$	41	24	15	10	7.9	6.4	5.5	4.9	4.5	4.0
$-2\sigma/\sigma_{\text{SM}}$	32	18	12	8.1	6.2	5.0	4.2	3.8	3.5	3.2
Observed $/\sigma_{\text{SM}}$	47	30	21	16	13	12	9.4	8.7	8.3	6.1
Limits	160	165	170	175	180	185	190	195	200	
$+2\sigma/\sigma_{\text{SM}}$	9.7	9.7	11	12	14	17	20	22	25	
$+1\sigma/\sigma_{\text{SM}}$	6.9	6.9	7.8	8.7	9.8	12	14	16	18	
Median $/\sigma_{\text{SM}}$	4.9	4.9	5.6	6.1	6.9	8.5	10	11	12	
$-1\sigma/\sigma_{\text{SM}}$	3.7	3.7	4.1	4.5	5.1	6.3	7.4	8.3	9.2	
$-2\sigma/\sigma_{\text{SM}}$	3.0	3.0	3.3	3.7	4.1	5.0	6.0	6.7	7.4	
Observed $/\sigma_{\text{SM}}$	5.1	5.1	6.1	6.0	8.1	8.7	13	13	17	

Table 9.8 Trilepton combined analysis limits for 5.9fb^{-1} .

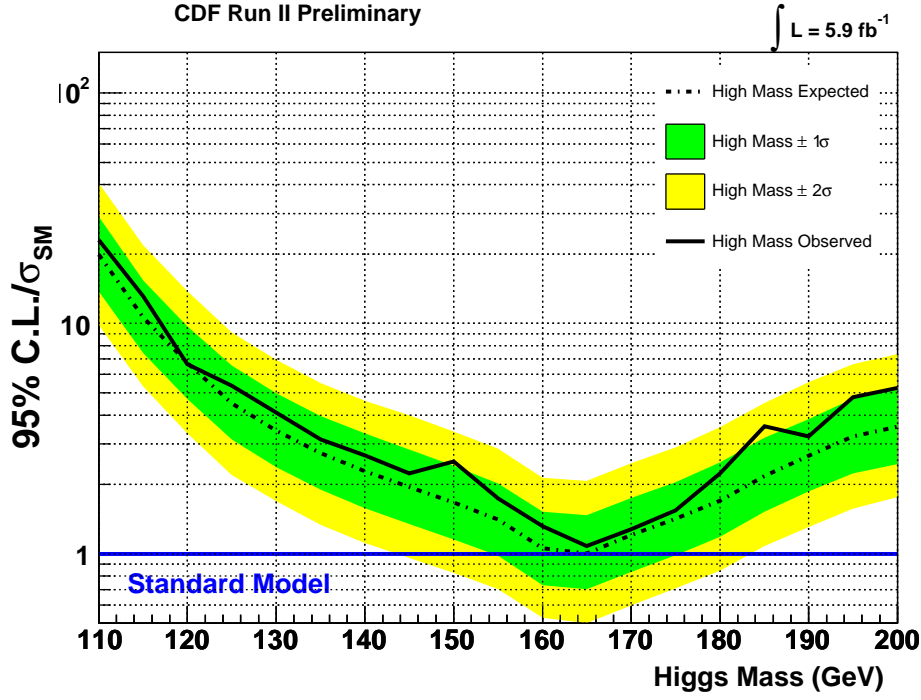


Figure 9.20 HWW Combined Limits (with Trileptons)

9.6 Conclusions

This dissertation describes a new analysis of the CDF high mass Standard Model Higgs boson group that was first incorporated into the group result in January 2010 with 4.8fb^{-1} . That original version of this trilepton analysis consisted of just two signal regions: one WH analysis region and one ZH analysis region using both the 1-jet events and the ≥ 2 jet events.

That analysis was combined with the CDF dilepton $H \rightarrow WW$ analysis improving the overall sensitivity of the CDF $H \rightarrow WW$ search by $\sim 8\%$. Since that initial combination, in collaboration with Dr. Geum-bong Yu of Duke University, the ZH analysis has been improved by subdividing it into two regions as presented here. The ZH (≥ 2 -jets) analysis has been improved by $\sim 10\%$, providing a $\sim 4\%$ improvement to the combined trilepton result. The expected sensitivity of the final combined CDF trilepton and dilepton analysis with 5.9fb^{-1} for a Higgs boson of 165 GeV is 1.00 and the observed limit is 1.08 times the Standard Model cross section.

With the trilepton contribution to the CDF $H \rightarrow WW$ group, we can now announce a CDF-only sensitivity to the Standard Model Higgs boson at $m_H = 165$ GeV for the first time. Previously, the Higgs had been excluded for $m_H \in [163, 166]$ GeV with a combined CDF and D0 result (Public

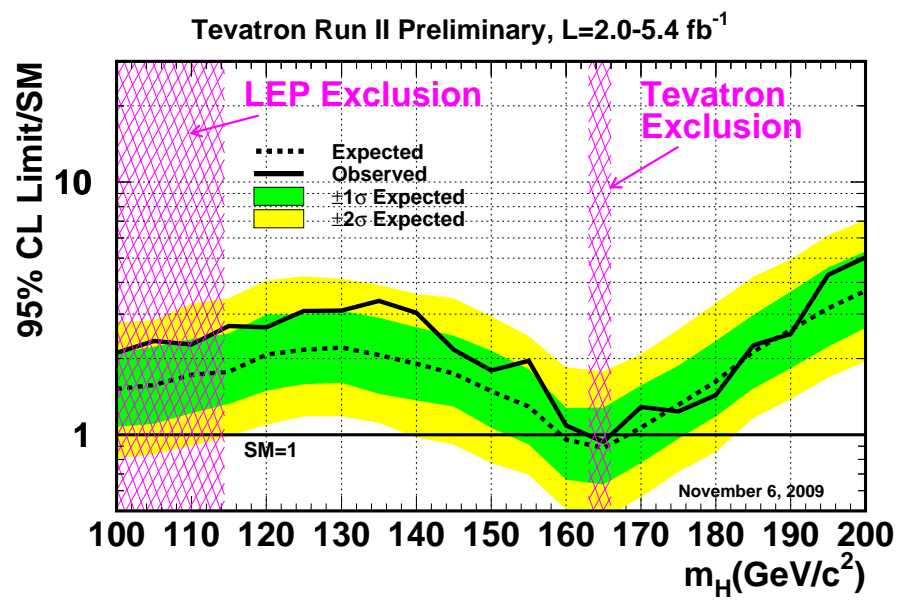


Figure 9.21 HWW Combined Limits (with Trileptons)

release page: [12]), which can be seen in figure 9.21. A new CDF+D0 combined limit has not yet been calculated, but it will be interesting to see how this exclusion window expands with the addition of new data and this trilepton analysis.

The field of particle physics has been excited about determining whether or not the Higgs mechanism is responsible for electroweak symmetry breaking and mass generation for decades, but arguably never more so than now because of the state of experimental technology and data-taking. Knowing where the Higgs boson is requires knowing where it isn't, and we have now achieved an important milestone in this search.

Limits	110	115	120	125	130	135	140	145	150	155
$+2\sigma/\sigma_{\text{SM}}$	41	22	14	9.1	7.0	5.5	4.6	4.0	3.4	2.9
$+1\sigma/\sigma_{\text{SM}}$	29	15	9.7	6.6	5.0	4.0	3.3	2.8	2.4	2.0
Median $/\sigma_{\text{SM}}$	20	11	6.7	4.5	3.4	2.7	2.3	1.95	1.67	1.40
$-1\sigma/\sigma_{\text{SM}}$	14	7.4	4.7	3.1	2.4	1.90	1.58	1.35	1.15	0.98
$-2\sigma/\sigma_{\text{SM}}$	9.9	5.3	3.3	2.2	1.7	1.3	1.1	0.96	0.83	0.70
Observed $/\sigma_{\text{SM}}$	23	13	6.7	5.4	4.1	3.1	2.7	2.2	2.5	1.74
Limits	160	165	170	175	180	185	190	195	200	
$+2\sigma/\sigma_{\text{SM}}$	2.1	2.1	2.5	2.9	3.6	4.5	5.6	6.7	7.4	
$+1\sigma/\sigma_{\text{SM}}$	1.53	1.47	1.75	2.1	2.5	3.2	3.8	4.7	5.2	
Median $/\sigma_{\text{SM}}$	1.05	1.00	1.20	1.42	1.70	2.2	2.7	3.2	3.6	
$-1\sigma/\sigma_{\text{SM}}$	0.73	0.70	0.83	0.99	1.18	1.53	1.86	2.2	2.45	
$-2\sigma/\sigma_{\text{SM}}$	0.53	0.50	0.60	0.71	0.85	1.08	1.30	1.57	1.76	
Observed $/\sigma_{\text{SM}}$	1.32	1.08	1.28	1.54	2.2	3.6	3.3	4.8	5.2	

Table 9.9 HWW Limits

DISCARD THIS PAGE

Appendix A: $U(1)$ Global Symmetry Breaking

The Standard Model and its component quantum field theories are based on symmetries of particular groups. Equally important is the concept that symmetries of nature may be spontaneously broken with physical consequences. In this and the subsequent few sections of the appendix, we shall explore the concept of spontaneously broken symmetries because the idea is central to the function of the Higgs boson in the Standard Model.

In this section, we shall explore the concept of spontaneously broken $U(1)$ symmetry for a complex scalar particle. An arbitrary complex field has real and imaginary components, by definition.[15]

$$\phi = \frac{1}{\sqrt{2}}(\phi_1 - i\phi_2) \quad (\text{A.1})$$

Its complex conjugate is then:

$$\phi^\dagger = \frac{1}{\sqrt{2}}(\phi_1 + i\phi_2) \quad (\text{A.2})$$

We postulate the lagrangian for this particle:

$$\mathcal{L} = (\partial_\mu \phi)^\dagger (\partial^\mu \phi) - m_0^2 \phi^\dagger \phi - \frac{1}{4} \lambda (\phi^\dagger \phi)^2 \quad (\text{A.3})$$

The first term has the typical form of kinetic energy, the second term is the potential energy or “rest mass,” and the last term governs the possibility of an interaction. If $m_0^2 > 0$, then the lagrangian describes a complex scalar particle with mass m_0 .

Denote the last two terms as $V(\phi) = m_0^2 \phi^\dagger \phi + \frac{1}{4} \lambda (\phi^\dagger \phi)^2$, the potential. The task of determining the particle spectrum of the ϕ field reduces to finding the minima of $V(\phi)$ and calculating perturbative oscillations from it.

Recall that the $U(1)$ symmetry group is the group of angular rotations in the complex plane. We say the lagrangian exhibits a $U(1)$ global symmetry, or is “invariant” under $U(1)$ transformations, because if we rotate the field ϕ in the complex plane by some arbitrary angle α in a manner not dependent on spacetime location

$$\phi \rightarrow \phi' = e^{i\alpha} \phi \quad (\text{A.4})$$

then the lagranian does not change

$$\mathcal{L} = (\partial_\mu \phi')^\dagger (\partial^\mu \phi') - m_0^2 \phi'^\dagger \phi' - \frac{1}{4} \lambda (\phi'^\dagger \phi')^2 \quad (\text{A.5})$$

$$= (\partial_\mu \phi e^{i\alpha})^\dagger (\partial^\mu \phi e^{i\alpha}) - m_0^2 \phi^\dagger e^{-i\alpha} \phi e^{i\alpha} - \frac{1}{4} \lambda (\phi^\dagger e^{-i\alpha} \phi e^{i\alpha})^2 \quad (\text{A.6})$$

$$= (\partial_\mu \phi)^\dagger (\partial^\mu \phi) - m_0^2 \phi^\dagger \phi - \frac{1}{4} \lambda (\phi^\dagger \phi)^2 \quad (\text{A.7})$$

$$(\text{A.8})$$

Consequently, the physics implied by the lagrangian also does not change. It is important that the rotation is not dependent on spacetime coordinates because if it was, then the partial derivatives would act on the rotation, extra terms would arise, and the lagrangian would therefore not be invariant under the transformation.

Symmetries in physics imply conservation of some property. Invariance to spatial location implies conservation of momentum; Invariance to temporal location implies conservation of energy; etc. In this case, invariance to rotations in the complex plane implies conservation by charge, which can be derived by studying the lagrangian under an infinitesimal $U(1)$ transformation $\phi \rightarrow \phi' = (1 + i\alpha)\phi$ [33]. However, this is not the task at hand.

If we assume $m_0^2 > 0$, then the potential simply has a unique and stable extremum at the origin. The quantum theoretical prescription for calculating the particle state spectrum is to determine small harmonic oscillations about this minimum. The symmetry about the origin is stable and would remain unbroken.

If, however, $m_0^2 < 0$, then the potential still exhibits the same cylindrical symmetry, but the extremum at the origin is now a maximum and there is a minima ring that assumes the lowest value of the potential. The potential at the origin is unstable, and so it is natural for the symmetry to “break” by having such a state fall to one corresponding to the minima ring.

Determining the particle spectrum now requires choosing some point on the minima circle to perform the perturbative expansion. The minima manifold is found at

$$\frac{dV}{d(\phi^\dagger\phi)} = m_0^2 + \frac{\lambda}{4} 2\phi^\dagger\phi = 0 \quad (\text{A.9})$$

$$\phi^\dagger\phi = -\frac{2m_0^2}{\lambda} \quad (\text{A.10})$$

$$v \equiv \sqrt{\phi_1^2 + \phi_2^2} = \sqrt{\frac{-4m_0^2}{\lambda}} \quad (\text{A.11})$$

The new parameter v is then the radius of the circle.

One way to proceed is to expand about the point $\phi_1 = v, \phi_2 = 0$. Let

$$\phi(x) = \frac{1}{\sqrt{2}} (v + \eta(x) + i\xi(x)) \quad (\text{A.12})$$

Then $\eta(x)$ is a field perturbation in the \Re direction and the perturbation $\xi(x)$ in the purely \Im direction. We find the consequent particle spectrum by putting this expression of $\phi(x)$ back into the lagrangian.

$$\mathcal{L} = (\partial_\mu\phi)^\dagger (\partial^\mu\phi) - m_0^2\phi^\dagger\phi - \frac{1}{4}\lambda (\phi^\dagger\phi)^2 \quad (\text{A.13})$$

$$= \frac{1}{2} (v + \partial_\mu\eta - i\partial_\mu\xi) (v + \partial^\mu\eta + i\partial^\mu\xi) - \frac{m_0^2}{2} (v + \eta - i\xi) (v + \eta + i\xi) \quad (\text{A.14})$$

$$- \frac{1}{16}\lambda [(v + \eta - i\xi) (v + \eta + i\xi)]^2 \quad (\text{A.15})$$

$$= \frac{1}{2}(\partial_\mu\xi)^2 + \frac{1}{2}(\partial_\mu\eta)^2 + m_0^2\eta^2 + (\text{cubic and quartic terms}) \quad (\text{A.16})$$

$$(\text{A.17})$$

From the $m_0^2\eta^2$ term, we see the η -field perturbation is associated with a particle of mass $m_\eta = \sqrt{-2m_0^2}$. There is no mass term for the ξ -field. In attempting to generate a massive gauge boson, spontaneously broken gauge theory has provided its own massless particle.

Pictorially, notice that the η -perturbation (the one that does result in a massive particle) climbs up the potential well while the ξ -perturbation (the massless one) is directed tangent to the circular minima manifold. Perturbing up the potential well implies the existence of an associated massive particle state.

This suggests a possibly more appropriate choice of how to parameterize the field perturbations. Remember that the choice to expand about $\phi_1 = v, \phi_2 = 0$ was arbitrary. Let's parameterize the perturbations in polar, rather than cartesian, coordinates. That way, we need not specify where on the minima manifold we expand around; the argument applies equivalently to all choices. One field perturbation will be in the radial direction, the other in the angular.

$$\phi(x) = \underbrace{\frac{\rho(x)}{\sqrt{2}}}_{\text{Radial Perturbation}} \cdot \underbrace{e^{\frac{i}{v}\theta(x)}}_{\text{Angular Perturbation}} \quad (\text{A.18})$$

Since the minima manifold has a radius v , $\rho(x) = v + h(x)$ (spoiler alert: the letter “ h ” is chosen for this perturbation off the potential minimum because this is a precursor to the Higgs boson).

Just as before, we put $\phi(x)$ back into the lagrangian and see what the particle spectrum looks like.

$$\mathcal{L} = (\partial_\mu \phi)^\dagger (\partial^\mu \phi) - m_0^2 \phi^\dagger \phi - \frac{1}{4} \lambda (\phi^\dagger \phi)^2 \quad (\text{A.19})$$

$$= \frac{1}{\sqrt{2}} e^{-\frac{i}{v}\theta(x)} \left[\partial_\mu \rho(x) - \frac{i}{v} \rho(x) \partial_\mu \theta(x) \right] \frac{1}{\sqrt{2}} e^{\frac{i}{v}\theta(x)} \left[\partial^\mu \rho(x) + \frac{i}{v} \rho(x) \partial^\mu \theta(x) \right] \quad (\text{A.20})$$

$$- \frac{1}{2} m_0^2 \rho^2(x) - \frac{1}{16} \lambda \rho^4(x) \quad (\text{A.21})$$

$$= \frac{1}{2} \left[(\partial_\mu \rho)(\partial^\mu \rho) + \frac{1}{v^2} \rho^2 (\partial_\mu \theta)(\partial^\mu \theta) \right] - \frac{1}{2} m_0^2 \rho^2 - \frac{1}{16} \lambda \rho^4 \quad (\text{A.22})$$

$$= \frac{1}{2} (\partial_\mu h + v)(\partial^\mu h + v) + \frac{1}{2v^2} (h + v)^2 (\partial_\mu \theta)^2 - \frac{1}{2} m_0^2 (h^2 + 2vh + v^2) - \frac{1}{16} \lambda (h + v)^4 \quad (\text{A.23})$$

$$= \frac{1}{2} (\partial_\mu h)^2 + v(\partial_\mu h) + \frac{1}{2} v^2 + \left(\frac{1}{2v^2} h^2 + \frac{1}{v^2} hv + \frac{1}{2v^2} v^2 \right) (\partial_\mu \theta)^2 \quad (\text{A.24})$$

$$- \frac{1}{2} m_0^2 h^2 - m_0^2 v h - \frac{1}{2} m_0^2 v^2 - \frac{1}{16} \lambda (h + v)^4 \quad (\text{A.25})$$

$$= \frac{1}{2} (\partial_\mu h)^2 + \frac{1}{2} (\partial_\mu \theta)^2 - \frac{1}{2} m_0^2 h^2 + \dots \quad (\text{A.26})$$

$$(\text{A.27})$$

Hence, choosing any arbitrary location on the minima manifold and calculating the particle spectrum via field perturbations, we have kinetic terms for both $h(x)$ and $\theta(x)$, but a mass term only

for $h(x)$. Also, given this parametrization of $\phi(x)$, the vacuum expectation value is

$$\langle 0 | \phi | 0 \rangle = \frac{v}{\sqrt{2}} \quad (\text{A.28})$$

This is a situation where a symmetric field potential is spontaneously broken in nature and this breaking manifests in a physics different from the situation of the origin being a stable extremum, in which case the symmetry would not spontaneously break in nature.

Appendix B: $U(1)$ Local Symmetry Breaking

The situation of global $U(1)$ symmetry explored in section A is a special case of the topic of this section, local $U(1)$ symmetry. This scenario is also referred to as the “abelian [commutative] Higgs model.”[15] It is not the fully Standard Model version, but still a critical step toward understanding the Higgs sector of the Standard Model. For that reason, the detailed treatment presented in these sections A through D are included in this thesis.

Recall the postulated globally gauge invariant lagrangian from section A.

$$\mathcal{L} = (\partial_\mu \phi)^\dagger (\partial^\mu \phi) - m_0^2 \phi^\dagger \phi - \frac{1}{4} \lambda (\phi^\dagger \phi)^2 \quad (\text{B.1})$$

To make this lagrangian invariant to local gauge transformations, we must replace the derivatives with “covariant derivatives” to keep the lagrangian invariant under transformation. The covariant derivative is not derived—we postulate the desired covariant derivative and consider its form to be justified by the fact that it works

$$\partial_\mu \rightarrow D_\mu = \partial_\mu + iqA_\mu \quad (\text{B.2})$$

and include a kinetic term for the “gauge field” A_μ that must be included to keep the lagrangian invariant under a local $U(1)$ transformation.

$$\mathcal{L} = [(\partial^\mu + iqA^\mu)\phi]^\dagger [(\partial_\mu + iqA_\mu)\phi] - \frac{1}{4} F_{\mu\nu} F^{\mu\nu} - \frac{1}{4} \lambda (\phi^\dagger \phi)^2 - m_0^2 (\phi^\dagger \phi) \quad (\text{B.3})$$

$$(\text{B.4})$$

where $F^{\mu\nu} = \partial^\mu A^\nu - \partial^\nu A^\mu$. Notice this part is the form of the Maxwell lagrangian and A^μ is analogous to the photon. We shall return to this point shortly.

This lagrangian is then invariant to a *local* $U(1)$ field transformation

$$\phi(x) \rightarrow \phi'(x) = e^{-i\alpha(x)} \phi(x) \quad (\text{B.5})$$

or, in infinitesimal form

$$\phi(x) \rightarrow \phi'(x) = (1 - i\alpha(x))\phi(x) \quad (\text{B.6})$$

We still do not know now the gauge field itself transforms. The point of this covariant derivative is to have $D^\mu \phi$ transform the same way ϕ does. So assume

$$D'^\mu \phi' = (1 - i\alpha(x))D^\mu \phi \quad (\text{B.7})$$

to be true and derive the transformation law for A_μ from it.

$$(\partial^\mu + iqA'^\mu)\phi' = (1 - i\alpha(x))(\partial^\mu + iqA^\mu)\phi \quad (\text{B.8})$$

Since this is an infinitesimal transformation, the transformation of A^μ should have a general form $A^\mu \rightarrow A'^\mu = A^\mu + \delta A^\mu$. Note that both $\alpha(x)$ and δA^μ are infinitesimals, so any terms infinitesimal to the 2nd order or higher drop.

$$(\partial^\mu + iqA^\mu + iq\delta A^\mu)(1 - i\alpha(x))\phi = (1 - i\alpha(x))(\partial^\mu + iqA^\mu)\phi \quad (\text{B.9})$$

$$(-i\partial^\mu \alpha(x) + iq\delta A^\mu)\phi = (-i\alpha(x)\partial^\mu)\phi \quad (\text{B.10})$$

$$iq\delta A^\mu \phi = (i\partial^\mu \alpha(x) - i\alpha(x)\partial^\mu)\phi \quad (\text{B.11})$$

$$q\delta A^\mu \phi = \partial^\mu(\alpha\phi) - \alpha(\partial^\mu \phi) \quad (\text{B.12})$$

$$q\delta A^\mu \phi = (\partial^\mu \alpha)\phi \quad (\text{B.13})$$

$$\delta A^\mu = \frac{1}{q}\partial^\mu \alpha \quad (\text{B.14})$$

Hence, the gauge field transforms as

$$A^\mu(x) \rightarrow A'^\mu(x) = A^\mu(x) + \frac{1}{q}\partial^\mu \alpha(x) \quad (\text{B.15})$$

Now we'll see how the gauge field A^μ absorbs the massless boson θ that was present in the treatment of the global $U(1)$ case in section A.

Recalling the Maxwell term in the lagrangian, let's study the field equation for A^μ

$$\square A^\nu - \partial^\nu(\partial_\mu A^\mu) = j_{\text{em}}^\nu = iq(\phi^\dagger(\partial^\nu \phi) - (\partial^\nu \phi)^\dagger \phi) - 2q^2 A^\nu \phi^\dagger \phi \quad (\text{B.16})$$

Now recall the $U(1)$ field parametrization for spontaneous symmetry breaking

$$\phi(x) = \underbrace{\frac{v + h(x)}{\sqrt{2}}}_{\text{Radial Perturbation}} \cdot \underbrace{e^{-\frac{i}{v}\theta(x)}}_{\text{Angular Perturbation}} \quad (\text{B.17})$$

The current becomes

$$j_{\text{em}}^\nu = iq \left[\frac{1}{\sqrt{2}}(v+h)e^{\frac{i}{v}\theta(x)} \left(\frac{1}{\sqrt{2}}(v+(\partial^\nu h))e^{-\frac{i}{v}\theta(x)} \right) + \frac{1}{\sqrt{2}}(v+h) \left(\frac{-i}{v}(\partial^\nu \theta) \right) e^{-\frac{i}{v}\theta(x)} \right] \quad (\text{B.18})$$

$$- \left(\frac{1}{\sqrt{2}}(v+(\partial^\nu h))e^{\frac{i}{v}\theta(x)} \frac{1}{\sqrt{2}}(v+h) \frac{i}{v}(\partial^\nu \theta)e^{\frac{i}{v}\theta(x)} \right) \frac{1}{\sqrt{2}}(v+h)e^{-\frac{i}{v}\theta(x)} \right] \quad (\text{B.19})$$

$$- 2q^2 A^\nu \cdot \frac{1}{2}(v+h)^2 \quad (\text{B.20})$$

$$j_{\text{em}}^\nu = -\frac{iq}{2} \left[(v+h)(v+\partial^\nu h) + (v+h)^2 \left(\frac{-i}{v} \partial^\nu \theta \right) \right] \quad (\text{B.21})$$

$$- (v+\partial^\nu h)(v+h) - (v+h)^2 \left(\frac{i}{v} \partial^\nu \theta \right) \right] \quad (\text{B.22})$$

$$- q^2 A^\nu (v+h)^2 \quad (\text{B.23})$$

$$(\text{B.24})$$

$$j_{\text{em}}^\nu = -\frac{iq}{2} \left[\frac{2i}{v}(v+h)^2 \partial^\nu \theta \right] - q^2 A^\nu (v+h)^2 \quad (\text{B.25})$$

$$j_{\text{em}}^\nu = \frac{q}{v}(v+h)^2 \partial^\nu \theta - q^2 A^\nu (v+h)^2 \quad (\text{B.26})$$

$$j_{\text{em}}^\nu = -v^2 q^2 \left(A^\nu - \frac{\partial^\nu \theta}{vq} \right) + \text{higher order terms} \quad (\text{B.27})$$

Using only the linear term for the current, put it back into the field equation for A^ν

$$\square A^\nu - \partial^\nu (\partial_\mu A^\mu) = j_{\text{em}}^\nu \quad (\text{B.28})$$

$$\square A^\nu - \partial^\nu (\partial_\mu A^\mu) = -v^2 q^2 \left(A^\nu - \frac{\partial^\nu \theta}{vq} \right) \quad (\text{B.29})$$

Now recall that a gauge transformation on A^μ has the form $A^\mu(x) \rightarrow A'^\mu(x) + \frac{1}{q} \partial^\mu \alpha(x)$, and notice that the right hand side already has this form. As such, define

$$A'^\nu = A^\nu - \frac{\partial^\nu \theta}{vq} \quad (\text{B.30})$$

Then the field equation becomes

$$\square A'^\nu - \partial^\nu \partial_\mu A'^\mu = -v^2 q^2 A'^\nu \quad (\text{B.31})$$

$$\boxed{(\square + v^2 q^2) A'^\nu - \partial^\nu \partial_\mu A'^\mu = 0} \quad (\text{B.32})$$

Finally, we see that the field equation becomes a free massive vector field for a particle with mass vq . In particular, notice how the appropriate choice of gauge allowed the massless gauge field A^ν to absorb the θ (“Goldstone” boson) field term and become massive as a result.

Summarily, generalizing from global to local $U(1)$ symmetry breaking required us to introduce a “gauge field” A^ν in order to keep the lagrangian invariant, or symmetric, under $U(1)$ transformations. After deriving the manner in which A^ν itself transforms, we were able to choose a particular “gauge,” or $U(1)$ transformation, that allows it to absorb the θ field (perturbations along the angular direction of the circular minima manifold of the previous section). In the end, we no longer had a θ field at all, but rather the gauge field A^ν that became massive after absorbing the θ field. What has just happened here is important for understanding how the Higgs boson is related to the photon and weak vector boson in the Standard Model theory.

Appendix C: $SU(2)$ Global Symmetry Breaking

The “special unitary group” $SU(2)$ transformations we will be considering in this section are similar to the $U(1)$ case of sections A and B, except that the rotation angle α now becomes rank-2 matrices $\vec{\alpha} \cdot \vec{\tau}$.

To recap, global $U(1)$ symmetry breaking lead to two fields: a massive field $h(x)$ and a massless field $\theta(x)$. Extending to local $U(1)$ symmetry required us to introduce a gauge boson A^ν and we exploited the gauge symmetry to have A^ν absorb the $\theta(x)$ field and become massive. Now, we will see that by generalizing the same arguments to global $SU(2)$ symmetry we will end up with another massive $H(x)$ field and three $\theta(x)$ fields instead of one.

Consider an $SU(2)$ doublet of complex bosons

$$\phi = \begin{bmatrix} \phi^+ \\ \phi^0 \end{bmatrix} = \begin{bmatrix} \frac{1}{\sqrt{2}}(\phi_1 + i\phi_2) \\ \frac{1}{\sqrt{2}}(\phi_3 + i\phi_4) \end{bmatrix} \quad (\text{C.1})$$

where ϕ^+ destroys positively charged particles and creates negatively charged particle, and ϕ^0 destroys neutral particles and creates neutral antiparticles.

Postulate the form of the lagrangian as a direct generalization of the previous two sections

$$\mathcal{L} = (\partial_\mu \phi)^\dagger (\partial^\mu \phi) - m_0^2 \phi^\dagger \phi - \frac{\lambda}{4} (\phi^\dagger \phi)^2 \quad (\text{C.2})$$

where $m_0^2 < 0$. This lagrangian is not only invariant to $SU(2)$ transformations, but also to the global $U(1)$ transformations of section A. We treat the global $SU(2)$ case here, so α is not dependent on spacetime coordinate.

$$\phi \rightarrow \phi' = e^{-\frac{i}{2} \vec{\alpha} \cdot \vec{\tau}} \phi \quad \text{for } SU(2) \quad (\text{C.3})$$

$$\phi \rightarrow \phi' = e^{-i\alpha} \phi \quad \text{for } U(1) \quad (\text{C.4})$$

The minimum occurs at

$$\frac{\partial \mathcal{L}}{\partial (\phi^\dagger \phi)} = -m_0^2 - \frac{\lambda}{2} (\phi^\dagger \phi)_{\min} = 0 \quad (\text{C.5})$$

$$(\phi^\dagger \phi)_{\min} = \frac{-2m_0^2}{\lambda} \equiv \frac{v^2}{2} \quad (\text{C.6})$$

As before, we take the minimum to be the vacuum.

$$\langle 0 | \phi^\dagger \phi | 0 \rangle = \frac{v^2}{2} = \langle 0 | \phi_1^2 + \phi_2^2 + \phi_3^2 + \phi_4^2 | 0 \rangle \quad (\text{C.7})$$

To obtain the particle spectrum we expand the fields ϕ about the choice of vacuum. Again, rather than a single point, we have a whole space of minima to choose from. Let,

$$\langle 0 | \phi | 0 \rangle = \begin{bmatrix} 0 \\ \frac{v}{\sqrt{2}} \end{bmatrix} \quad (\text{C.8})$$

Oscillations about this vacuum choice are parametrized by

$$\phi = e^{-\frac{i}{2}(\vec{\theta}(x) \cdot \vec{\tau})v} \begin{bmatrix} 0 \\ \frac{1}{\sqrt{2}}(v + H(x)) \end{bmatrix} \quad (\text{C.9})$$

We have here three fields $\vec{\theta}$ for possible “angular” oscillations associated with the $SU(2)$ symmetry, and one radial field oscillation $H(x)$. We shall see now that only the $H(x)$ field has nonzero mass, indicating that each $\vec{\theta}$ field oscillates in a direction within the minima manifold, i.e. does not climb the potential just as in the global $U(1)$ case. To do this, put ϕ back into the lagrangian and look for mass terms.

$$\partial^\mu \phi = \begin{bmatrix} 0 \\ -\frac{i}{2v}((\partial^\mu \vec{\theta}) \cdot \vec{\tau})e^{-\frac{i}{2v}\vec{\theta} \cdot \vec{\tau}}\frac{1}{\sqrt{2}}(v + H) + e^{-\frac{i}{2v}\vec{\theta} \cdot \vec{\tau}}\frac{1}{\sqrt{2}}\partial^\mu H \end{bmatrix} \quad (\text{C.10})$$

$$= e^{-\frac{i}{2v}\vec{\theta} \cdot \vec{\tau}} \begin{bmatrix} 0 \\ \frac{-i}{2\sqrt{2}v}((\partial^\mu \vec{\theta}) \cdot \vec{\tau})(v + H) + \frac{1}{\sqrt{2}}\partial^\mu H \end{bmatrix} \quad (\text{C.11})$$

Similarly,

$$(\partial^\mu \phi)^\dagger = \begin{bmatrix} 0 & \frac{i}{2\sqrt{2}v}((\partial^\mu \vec{\theta}) \cdot \vec{\tau})(v + H) + \frac{1}{\sqrt{2}}\partial^\mu H \end{bmatrix} \quad (\text{C.12})$$

Putting these terms into the lagrangian, we get:

$$\mathcal{L} = \frac{1}{8v^2}(\partial^\mu \vec{\theta} \cdot \vec{\tau})(\partial_\mu \vec{\theta} \cdot \vec{\tau})(v + H)^2 + \frac{1}{2}(\partial^\mu H)(\partial_\mu H) \quad (\text{C.13})$$

$$- \frac{m_0^2}{2}v^2 - \frac{m_0^2}{2}vH - \frac{m_0^2}{2}H^2 - \frac{\lambda}{4}(v + H)^4 \quad (\text{C.14})$$

Mass terms with different fields multiplied govern the interaction between the fields. Notice now since $\vec{\theta}(x)$ only appear in an exponent in the field ϕ , it only has derivative terms in the lagrangian. Thus, the particles associated with the $\vec{\theta}$ fields are massless. Only the $H(x)$ has a mass term.

Appendix D: $SU(2)$ Local Symmetry Breaking

Let's now generalize the $SU(2)$ global invariance of the previous section to local invariance in the same manner we did for $U(1)$ transformations in section B.

Local $SU(2)$ gauge transformations have the form

$$\phi(x) \rightarrow \phi'(x) = e^{\frac{ig}{2}\vec{\tau}\cdot\vec{\alpha}(x)}\phi(x) \quad (\text{D.1})$$

where the factor g is inserted to represent the coupling strength.

Just as in the case of electromagnetic interactions, no lagrangian for a free particle can be Lorentz invariant under this local gauge transformation. To make it Lorentz invariant, the derivative must be replaced by a covariant derivative. This way, $D^\mu\phi$ transforms the same way ϕ does, whereas $\partial^\mu\phi$ does not. Just as in the $U(1)$ case, this will necessarily involve the introduction of new gauge fields.

In the $SU(2)$ case,

$$\partial^\mu\phi'(x) = e^{\frac{ig}{2}\vec{\tau}\cdot\vec{\alpha}(x)}(\partial^\mu\phi(x)) + \frac{ig}{2}\vec{\tau}\cdot(\partial^\mu\vec{\alpha}(x))e^{\frac{ig}{2}\vec{\tau}\cdot\vec{\alpha}(x)}\phi(x) \quad (\text{D.2})$$

where it is the second term that breaks the covariance.

The covariant derivative D^μ must act like:

$$D'^\mu\phi'(x) = e^{\frac{ig}{2}\vec{\tau}\cdot\vec{\alpha}(x)}\phi(x)D^\mu\phi(x) \quad (\text{D.3})$$

The form of D^μ is just postulated, then justified by the fact that it works.

$$D^\mu \equiv \partial^\mu + \frac{ig}{2}\vec{\tau}\cdot\vec{W}^\mu \quad (\text{D.4})$$

where $\vec{W}^\mu \equiv (W_1^\mu, W_2^\mu, W_3^\mu)$, a slight precursor to the weak vector bosons.

The \vec{W}^μ are the $SU(2)$ gauge fields, analogous to the $U(1)$ gauge field A^μ , and the $\vec{\tau}$ are the Pauli spin matrices.

$$\vec{\tau} \cdot \vec{W}^\mu = \begin{bmatrix} 0 & 1 \\ 1 & 0 \end{bmatrix} W_1^\mu + \begin{bmatrix} 0 & -i \\ i & 0 \end{bmatrix} W_2^\mu + \begin{bmatrix} 1 & 0 \\ 0 & -1 \end{bmatrix} W_3^\mu \quad (\text{D.5})$$

$$= \begin{bmatrix} 0 & W_1^\mu \\ W_1^\mu & 0 \end{bmatrix} + \begin{bmatrix} 0 & -iW_2^\mu \\ iW_2^\mu & 0 \end{bmatrix} + \begin{bmatrix} W_3^\mu & 0 \\ 0 & -W_3^\mu \end{bmatrix} \quad (\text{D.6})$$

$$= \begin{bmatrix} W_3^\mu & W_1^\mu - iW_2^\mu \\ W_1^\mu + iW_2^\mu & -W_3^\mu \end{bmatrix} \quad (\text{D.7})$$

Remember that the three gauge fields \vec{W}^μ are spacetime dependent.

Let's examine the $SU(2)$ transformation in infinitesimal form

$$\phi' = \left(1 + \frac{ig}{2} \vec{\tau} \cdot \vec{\epsilon}(x) \right) \phi \quad (\text{D.8})$$

$$\partial\phi' = \left(1 + \frac{ig}{2} \vec{\tau} \cdot \vec{\epsilon}(x) \right) \partial^\mu \phi + \frac{ig}{2} \vec{\tau} \cdot (\partial^\mu \vec{\epsilon}) \phi \quad (\text{D.9})$$

We again see the noncovariant term. Let's use the covariant derivative instead.

$$D'^\mu \phi' = \left(1 + \frac{ig}{2} \vec{\tau} \cdot \vec{\epsilon}(x) \right) D^\mu \phi \quad (\text{D.10})$$

$$\left(\partial^\mu + \frac{ig}{2} \vec{\tau} \cdot \vec{W}'^\mu \right) \left[1 + \frac{ig}{2} \vec{\tau} \cdot \vec{\epsilon}(x) \right] \phi = \left[1 + \frac{ig}{2} \vec{\tau} \cdot \vec{\epsilon}(x) \right] \left(\partial^\mu + \frac{ig}{2} \vec{\tau} \cdot \vec{W}^\mu \right) \phi \quad (\text{D.11})$$

So far, we do not know how the gauge fields W^μ transform (notice that both \vec{W}'^μ and \vec{W}^μ appear). We proceed by assuming that the previous equality does, in fact, hold; and determine the transformation law for \vec{W}^μ from it.

The previous equality involves an infinitesimal transformation, so the transformation of \vec{W}^μ must look something like

$$\vec{W}^\mu \rightarrow \vec{W}'^\mu = \vec{W}^\mu + \delta\vec{W}^\mu \quad (\text{D.12})$$

Let's start the algebra.

$$\left[\partial^\mu + \frac{ig}{2} \vec{\tau} \cdot \vec{W}'^\mu \right] \left[1 + \frac{ig}{2} \vec{\tau} \cdot \vec{\epsilon}(x) \right] \phi = \left[1 + \frac{ig}{2} \vec{\tau} \cdot \vec{\epsilon}(x) \right] \left[\partial^\mu + \frac{ig}{2} \vec{\tau} \cdot \vec{W}^\mu \right] \phi \quad (\text{D.13})$$

$$\left[\partial^\mu + \frac{ig}{2} \vec{\tau} \cdot \vec{W}^\mu + \frac{ig}{2} \vec{\tau} \cdot \delta \vec{W}^\mu \right] \left[1 + \frac{ig}{2} \vec{\tau} \cdot \vec{\epsilon}(x) \right] \phi = \left[1 + \frac{ig}{2} \vec{\tau} \cdot \vec{\epsilon}(x) \right] \left[\partial^\mu + \frac{ig}{2} \vec{\tau} \cdot \vec{W}^\mu \right] \phi \quad (\text{D.14})$$

$$\left[\frac{ig}{2} \vec{\tau} \cdot \partial^\mu \vec{\epsilon} - \frac{1}{4} g^2 (\vec{\tau} \cdot \vec{W}^\mu) (\vec{\tau} \cdot \vec{\epsilon}) \frac{ig}{2} \vec{\tau} \cdot \delta \vec{W}^\mu \right] \phi = \left[\frac{ig}{2} (\vec{\tau} \cdot \vec{\epsilon}) \partial^\mu - \frac{g^2}{4} (\vec{\tau} \cdot \vec{\epsilon}) (\vec{\tau} \cdot \vec{W}^\mu) \right] \phi \quad (\text{D.15})$$

$$\frac{ig}{2} \vec{\tau} \cdot \partial^\mu (\vec{\epsilon} \phi) - \frac{1}{4} g^2 (\vec{\tau} \cdot \vec{W}^\mu) (\vec{\tau} \cdot \vec{\epsilon}) \phi + \frac{ig}{2} \vec{\tau} \cdot (\delta \vec{W}^\mu) \phi = \frac{ig}{2} \vec{\tau} \cdot (\vec{\epsilon} \partial^\mu \phi) - \frac{g^2}{4} (\vec{\tau} \cdot \vec{\epsilon}) (\vec{\tau} \cdot \vec{W}^\mu) \phi \quad (\text{D.16})$$

$$\frac{ig}{2} \vec{\tau} \cdot (\delta \vec{W}^\mu) \phi = \frac{ig}{2} \vec{\tau} \cdot [\vec{\epsilon} (\partial^\mu \phi) - \partial^\mu (\vec{\epsilon} \phi)] + \frac{g^2}{4} [(\vec{\tau} \cdot \vec{W}^\mu) (\vec{\tau} \cdot \vec{\epsilon}) - (\vec{\tau} \cdot \vec{\epsilon}) (\vec{\tau} \cdot \vec{W}^\mu)] \phi \quad (\text{D.17})$$

$$\frac{ig}{2} \vec{\tau} \cdot (\delta \vec{W}^\mu) \phi = \frac{ig}{2} \vec{\tau} \cdot [-(\partial^\mu \vec{\epsilon}) \phi] + \frac{g^2}{4} [(\vec{\tau} \cdot \vec{W}^\mu) (\vec{\tau} \cdot \vec{\epsilon}) - (\vec{\tau} \cdot \vec{\epsilon}) (\vec{\tau} \cdot \vec{W}^\mu)] \phi \quad (\text{D.18})$$

$$ig \frac{\vec{\tau} \cdot (\delta \vec{W}^\mu)}{2} = -ig \frac{\vec{\tau} \cdot (\partial^\mu \vec{\epsilon}(x))}{2} + (ig)^2 \left[\left(\frac{\vec{\tau} \cdot \vec{\epsilon}}{2} \right) \left(\frac{\vec{\tau} \cdot \vec{W}^\mu}{2} \right) - \left(\frac{\vec{\tau} \cdot \vec{W}^\mu}{2} \right) \left(\frac{\vec{\tau} \cdot \vec{\epsilon}}{2} \right) \right] \quad (\text{D.19})$$

$$\vec{\tau} \cdot (\delta \vec{W}^\mu) = -\vec{\tau} \cdot (\partial^\mu \vec{\epsilon}) - \frac{g}{2} [(\vec{\tau} \cdot \vec{\epsilon}) (\vec{\tau} \cdot \vec{W}^\mu) - (\vec{\tau} \cdot \vec{W}^\mu) (\vec{\tau} \cdot \vec{\epsilon})] \quad (\text{D.20})$$

$$(\text{D.21})$$

Let's take a closer look at the terms inside the brackets alone.

$$[(\vec{\tau} \cdot \vec{\epsilon}) (\vec{\tau} \cdot \vec{W}^\mu) - (\vec{\tau} \cdot \vec{W}^\mu) (\vec{\tau} \cdot \vec{\epsilon})] = (\vec{\epsilon} \cdot \vec{W}^\mu + i \vec{\tau} \cdot \vec{\epsilon} \times \vec{W}^\mu) \quad (\text{D.22})$$

$$- (\vec{W}^\mu \cdot \vec{\epsilon} + i \vec{\tau} \cdot \vec{W}^\mu \times \vec{\epsilon}) \quad (\text{D.23})$$

$$= i \vec{\tau} \cdot (\vec{\epsilon} \times \vec{W}^\mu - \vec{W}^\mu \times \vec{\epsilon}) \quad (\text{D.24})$$

$$= i \vec{\tau} \cdot (\vec{\epsilon} \times \vec{W}^\mu - \vec{\epsilon} \times \vec{W}^\mu) \quad (\text{D.25})$$

$$= 2i \vec{\tau} \cdot (\vec{\epsilon} \times \vec{W}^\mu) \quad (\text{D.26})$$

Let's put this back into equation D.20.

$$\vec{\tau} \cdot (\delta \vec{W}^\mu) = -\delta^\mu \vec{\epsilon}(x) - g \left[\vec{\epsilon}(x) \times \vec{W}^\mu \right] \quad (\text{D.27})$$

$$(\text{D.28})$$

This means the infinitesimal piece is

$$\delta \vec{W}^\mu = -\partial^\mu \vec{\epsilon}(x) - g \left[\vec{\epsilon}(x) \times \vec{W}^\mu \right] \quad (\text{D.29})$$

$$(\text{D.30})$$

Generalizing from global to local transformations introduces the extra $\partial^\mu \vec{\epsilon}(x)$ term. Hence, the gauge fields for a local $SU(2)$ gauge (phase) transform as

$$\vec{W}'^\mu = \vec{W}^\mu - \partial^\mu \vec{\epsilon}(x) - g \left[\vec{\epsilon}(x) \times \vec{W}^\mu \right] \quad (\text{D.31})$$

$$(\text{D.32})$$

Now that we know how the gauge field and the covariant derivative transform with an $SU(2)$ gauge transformation, we can compute the consequences from our basic postulated lagrangian from equation C.2, which can now be repostulated in $SU(2)$ invariant form

$$\mathcal{L} = (D_\mu \phi)^\dagger (D^\mu \phi) - m_0^2 \phi^\dagger \phi - \frac{\lambda}{4} (\phi^\dagger \phi)^2 - \frac{1}{4} \vec{W}_{\mu\nu} \cdot \vec{W}^{\mu\nu} \quad (\text{D.33})$$

where $\vec{W}_{\mu\nu} \equiv \partial_\mu \vec{W}_\nu - \partial_\nu \vec{W}_\mu - g \vec{W}_\mu \times \vec{W}_\nu$, where the last term is necessary because of the non-Abelian nature of the $SU(2)$ group.

Note that if $m_0^2 > 0$, then we just have a system of four scalar particles of mass m_0 . However, we are interested in the $m_0^2 < 0$ case. Just as for the $U(1)$ case, we want to find the minima of the potential and find an entire minima manifold.

$$\frac{\partial \mathcal{L}}{\partial (\phi^\dagger \phi)} = 0 \quad (\text{D.34})$$

$$(\phi^\dagger \phi)_{\min} = -\frac{2m_0^2}{\lambda} = \frac{1}{2} (\phi_1^2 + \phi_2^2 + \phi_3^2 + \phi_4^2) \quad (\text{D.35})$$

We must choose some particular point on the minima manifold upon which to expand and calculate the particle spectrum, so choose $\phi_1 = \phi_2 = \phi_4 = 0$ and then we are left with

$$\frac{1}{2}\phi_3^2 = \frac{-2m_0^2}{\lambda} \quad (\text{D.36})$$

$$\phi_3 = 2\sqrt{\frac{-m_0^2}{\lambda}} \equiv v \quad (\text{D.37})$$

Then our complex field doublet at this minimum becomes

$$\phi_{\min} = \frac{1}{\sqrt{2}} \begin{bmatrix} \phi_1 + i\phi_2 \\ \phi_3 + i\phi_4 \end{bmatrix} = \frac{1}{\sqrt{2}} \begin{bmatrix} 0 \\ v \end{bmatrix} \quad (\text{D.38})$$

Again, completely analogous to the $U(1)$ case, we can parametrize perturbations about this minimum as

$$\phi(x) = \frac{\rho(x)}{\sqrt{2}} e^{\frac{i}{v} \vec{\tau} \cdot \vec{\theta}(x)} \quad , \text{ where} \quad (\text{D.39})$$

$$\rho(x) = \begin{bmatrix} 0 \\ v + h(x) \end{bmatrix} \quad (\text{D.40})$$

This can be seen more intuitively when looked at in infinitesimal form.

Nevertheless, we now have an $SU(2)$ gauge invariant lagrangian with covariant derivatives and we know how the introduced gauge fields \vec{W}^μ change with an $SU(2)$ transformation. As such, the massless $\vec{\theta}(x)$ fields can be gauged away and we are left with massive \vec{W}^μ and h fields, another example of the Higgs mechanism.

For Standard Model physics, we will be combining this effect for both the $U(1)$ and $SU(2)$ cases to get the massive weak vector bosons and the photon—the higgs will be a necessary consequence. More details will be worked out in sections E, F, and H.

Appendix E: The Higgs Mechanism in the $SU(2) \times U(1)$ Local Spontaneous Symmetry Breaking

Recall that we had a scalar $SU(2)$ doublet

$$\phi = \begin{bmatrix} \phi^+ \\ \phi^0 \end{bmatrix} \quad (\text{E.1})$$

whose lagrangian is

$$\mathcal{L} = (\partial_\mu \phi)^\dagger (\partial^\mu \phi) - m_0^2 \phi^\dagger \phi - \frac{\lambda}{4} (\phi^\dagger \phi)^2 \quad (\text{E.2})$$

This lagrangian is invariant to $U(1)$ global transformations

$$\phi \rightarrow \phi' = e^{-i\alpha} \phi \quad (\text{E.3})$$

and global $SU(2)$ transformations

$$\phi \rightarrow \phi' = e^{-\frac{i}{2} \vec{\alpha} \cdot \vec{\tau}} \phi \quad (\text{E.4})$$

For a theory that is invariant to local transformations we must introduce three $SU(2)$ gauge fields (see section D) and one $U(1)$ gauge field (see section B). Denote them here as $W_i^\mu(x)$ for $i = 1, 2, 3$ and $B^\mu(x)$, respectively. Also, the derivatives must be replaced with a covariant derivative for both $U(1)$ and $SU(2)$.

$$D^\mu \phi = \left(\partial^\mu + \underbrace{\frac{ig}{2} \vec{\tau} \cdot \vec{W}^\mu}_{SU(2)\text{piece}} + \underbrace{\frac{ig'}{2} B^\mu}_{U(1)\text{piece}} \right) \phi \quad (\text{E.5})$$

Kinetic terms for the new gauge fields must also be included.

$$\vec{F}^{\mu\nu} = \partial^\mu \vec{W}^\nu - \partial^\nu \vec{W}^\mu - g \vec{W}^\mu \times \vec{W}^\nu \quad (\text{E.6})$$

$$G^{\mu\nu} = \partial^\mu B^\nu - \partial^\nu B^\mu \quad (\text{E.7})$$

So the new full lagrangian is

$$\mathcal{L} = (D_\mu \phi)^\dagger (D^\mu \phi) + m_0^2 \phi^\dagger \phi - \frac{\lambda}{4} (\phi^\dagger \phi)^2 - \frac{1}{4} \vec{F}_{\mu\nu} \cdot \vec{F}^{\mu\nu} - \frac{1}{4} G_{\mu\nu} G^{\mu\nu} \quad (\text{E.8})$$

$$(\text{E.9})$$

We already looked at spontaneous symmetry breaking for the $U(1)$ and $SU(2)$ cases individually, now we want to do so for the product group $SU(2) \times U(1)$ in such a way that we are left with three massive gauge bosons (W^\pm, Z) and one massless gauge boson (the photon γ). Being massless, the photon corresponds to some symmetry that is left unbroken. Weinberg suggested [15]

$$\langle 0 | \phi | 0 \rangle = \begin{bmatrix} 0 \\ \frac{\sqrt{2}m_0}{\sqrt{\lambda}} \end{bmatrix} \equiv \begin{bmatrix} 0 \\ \frac{v}{\sqrt{2}} \end{bmatrix} \quad (\text{E.10})$$

This choice leaves the vacuum invariant to a transformation of $U(1)$ + third component of $SU(2)$. That is,

$$(1 + \tau_3) \langle 0 | \phi | 0 \rangle = (1 + \tau_3) \begin{bmatrix} 0 \\ \frac{v}{\sqrt{2}} \end{bmatrix} = \begin{bmatrix} 2 & 0 \\ 0 & 0 \end{bmatrix} \begin{bmatrix} 0 \\ \frac{v}{\sqrt{2}} \end{bmatrix} = \begin{bmatrix} 0 \\ 0 \end{bmatrix} \quad (\text{E.11})$$

where the $\vec{\tau}$ are the Pauli matrices. This is also why we eventually find the electric charge to be expressed in terms of weak hypercharge Y and third component of isospin t_3 : $Q = \frac{Y}{2} + t_3$ [33]. We are about to see that this interplay between the $U(1)$ symmetry (corresponding to Y) and the third component of $SU(2)$ symmetry (corresponding to t_3) manifests as a mixing of the W_3^μ and B^μ gauge fields to yield the photon field A^μ and the neutral weak vector boson Z .

To consider oscillations about the vacuum, parametrize the degrees of freedom by

$$\phi = e^{-\frac{i}{2v}\vec{\theta}(x)\cdot\vec{\tau}} \begin{bmatrix} 0 \\ \frac{1}{\sqrt{2}}(v + H(x)) \end{bmatrix} \quad (\text{E.12})$$

However, recall that the three $\vec{\theta}$ field perturbations, which would become Goldstone bosons, disappear if we make the appropriate gauge transformation. So we effectively use

$$\phi = \begin{bmatrix} 0 \\ \frac{1}{\sqrt{2}}(v + H(x)) \end{bmatrix} \quad (\text{E.13})$$

The consequences for the lagrangian are (details of how the following form of the lagrangian are calculated are in section H)

$$\mathcal{L} = \frac{1}{2}(\partial_\mu H)(\partial^\mu H) + \frac{m_0^2}{2}(v + H)^2 - \frac{\lambda}{16}(v + H)^4 - \frac{1}{4}\vec{F}_{\mu\nu} \cdot \vec{F}^{\mu\nu} - \frac{1}{4}G_{\mu\nu}G^{\mu\nu} \quad (\text{E.14})$$

$$\mathcal{L} = \frac{1}{2}(\partial_\mu H)(\partial^\mu H) + \frac{m_0^2}{2}(v + H)^2 - \frac{\lambda}{16}(v + H)^4 \quad (\text{E.15})$$

$$- \frac{1}{4}(\partial_\mu W_{1\nu} - \partial_\nu W_{1\mu})(\partial^\mu W_1^\nu - \partial^\nu W_1^\mu) + \frac{1}{8}g^2 v^2 W_{1\nu} W_1^\nu \quad (\text{E.16})$$

$$- \frac{1}{4}(\partial_\mu W_{2\nu} - \partial_\nu W_{2\mu})(\partial^\mu W_2^\nu - \partial^\nu W_2^\mu) + \frac{1}{8}g^2 v^2 W_{2\nu} W_2^\nu \quad (\text{E.17})$$

$$- \frac{1}{4}(\partial_\mu W_{3\nu} - \partial_\nu W_{3\mu})(\partial^\mu W_3^\nu - \partial^\nu W_3^\mu) - \frac{1}{4}G_{\mu\nu} G^{\mu\nu} \quad (\text{E.18})$$

$$+ \frac{1}{8}v^2(gW_{3\mu} - g'B_\mu)(gW_3^\mu - g'B^\mu) + \text{Higgs interactions} \quad (\text{E.19})$$

The second and third lines show that the W_1 and W_2 gauge fields are massive and have the same mass $m_W = \frac{gv}{2}$. These are the W^+, W^- vector gauge bosons in electroweak theory. The Higgs interaction terms are being ignored here because we are focusing on the generation of the Standard Model gauge bosons in this section. In section H, I will go through the details of deriving the full version of this and discuss the interactions between the Higgs and gauge bosons that are produced. The Higgs boson decaying to gauge bosons is precisely the kind of interaction that this dissertation explores experimentally.

The last two lines show that the gauge fields W_3 and B are mixed. The key clue is to notice in the last line it is the combination $(gW_3^\mu - g'B^\mu)$ that has a mass. Introduce the linear combinations

$$Z^\mu \equiv W_3^\mu \cos \theta_W - B^\mu \sin \theta_W \quad (\text{E.20})$$

$$A^\mu \equiv W_3^\mu \sin \theta_W + B^\mu \cos \theta_W \quad (\text{E.21})$$

where

$$\cos \theta_W = \frac{g}{\sqrt{g^2 + g'^2}} \quad (\text{E.22})$$

$$\sin \theta_W = \frac{g'}{\sqrt{g^2 + g'^2}} \quad (\text{E.23})$$

Or, if we invert them

$$B^\mu = A^\mu \cos \theta_W - Z^\mu \sin \theta_W \quad (\text{E.24})$$

$$W_3^\mu = A^\mu \sin \theta_W + Z^\mu \cos \theta_W \quad (\text{E.25})$$

Using this, we can write the last two lines of the lagrangian in terms of A^μ and Z^μ , instead of B^μ and W_3^μ .

$$-\frac{1}{4}(\partial_\mu W_{3\nu} - \partial_\nu W_{3\mu})(\partial^\mu W_3^\nu - \partial^\nu W_3^\mu) - \frac{1}{4}G_{\mu\nu}G^{\mu\nu} + \frac{v^2}{8}(gW_{3\mu} - g'B_\mu)(gW_3^\mu - g'B^\mu) \quad (\text{E.26})$$

$$= -\frac{1}{4}(\partial_\mu(Z_\nu \cos \theta_W + A_\nu \sin \theta_W) - \partial_\nu(Z_\mu \cos \theta_W + A_\mu \sin \theta_W)) \quad (\text{E.27})$$

$$\cdot (\partial^\mu(Z^\nu \cos \theta_W + A^\nu \sin \theta_W) - \partial^\nu(Z^\mu \cos \theta_W + A^\mu \sin \theta_W)) \quad (\text{E.28})$$

$$- \frac{1}{4}(\partial_\mu(A_\nu \cos \theta_W - Z_\nu \sin \theta_W) - \partial_\nu(A_\mu \cos \theta_W - Z_\mu \sin \theta_W)) \quad (\text{E.29})$$

$$\cdot (\partial^\mu(A^\nu \cos \theta_W - Z^\nu \sin \theta_W) - \partial^\nu(A^\mu \cos \theta_W - Z^\mu \sin \theta_W)) \quad (\text{E.30})$$

$$+ \frac{1}{8}v^2(g(Z_\mu \cos \theta_W + A_\mu \sin \theta_W) - g'(A_\mu \cos \theta_W - Z_\mu \sin \theta_W)) \quad (\text{E.31})$$

$$\cdot (g(Z^\mu \cos \theta_W + A^\mu \sin \theta_W) - g'(A^\mu \cos \theta_W - Z^\mu \sin \theta_W)) \quad (\text{E.32})$$

$$= -\frac{1}{4}((\partial_\mu Z_\nu - \partial_\nu Z_\mu) \cos \theta_W + (\partial_\mu A_\nu - \partial_\nu A_\mu) \sin \theta_W) \quad (\text{E.33})$$

$$\cdot ((\partial^\mu Z^\nu - \partial^\nu Z^\mu) \cos \theta_W + (\partial^\mu A^\nu - \partial^\nu A^\mu) \sin \theta_W) \quad (\text{E.34})$$

$$- \frac{1}{4}((\partial_\mu A_\nu - \partial_\nu A_\mu) \cos \theta_W - (\partial_\mu Z_\nu - \partial_\nu Z_\mu) \sin \theta_W) \quad (\text{E.35})$$

$$\cdot ((\partial^\mu A^\nu - \partial^\nu A^\mu) \cos \theta_W - (\partial^\mu Z^\nu - \partial^\nu Z^\mu) \sin \theta_W) \quad (\text{E.36})$$

$$+ \frac{1}{8}v^2(Z_\mu(g \cos \theta_W + g' \sin \theta_W) + A_\mu(g \sin \theta_W - g' \cos \theta_W)) \quad (\text{E.37})$$

$$\cdot (Z^\mu(g \cos \theta_W + g' \sin \theta_W) + A^\mu(g \sin \theta_W - g' \cos \theta_W)) \quad (\text{E.38})$$

Define $\mathcal{F}_{\mu\nu} \equiv \partial_\mu A_\nu - \partial_\nu A_\mu$ and $Z_{\mu\nu} \equiv \partial_\mu Z_\nu - \partial_\nu Z_\mu$.

$$= -\frac{1}{4}(Z_{\mu\nu} \cos \theta_W + \mathcal{F}_{\mu\nu} \sin \theta_W)(Z^{\mu\nu} \cos \theta_W + \mathcal{F}^{\mu\nu} \sin \theta_W) \quad (\text{E.39})$$

$$- \frac{1}{4}(\mathcal{F}_{\mu\nu} \cos \theta_W - Z_{\mu\nu} \sin \theta_W)(\mathcal{F}^{\mu\nu} \cos \theta_W - Z^{\mu\nu} \sin \theta_W) \quad (\text{E.40})$$

$$\frac{1}{8}v^2 \left(Z_\mu \frac{g^2 + g'^2}{\sqrt{g^2 + g'^2}} + A_\mu \frac{gg' - g'g}{\sqrt{g^2 + g'^2}} \right) \cdot \left(Z^\mu \frac{g^2 + g'^2}{\sqrt{g^2 + g'^2}} + A^\mu \frac{gg' - g'g}{\sqrt{g^2 + g'^2}} \right) \quad (\text{E.41})$$

$$= -\frac{1}{4}(Z_{\mu\nu}Z^{\mu\nu} + \mathcal{F}_{\mu\nu}\mathcal{F}^{\mu\nu}) + \frac{1}{8}v^2 Z_\mu Z^\mu (g^2 + g'^2) \quad (\text{E.42})$$

Hence, we have unmixed the two fields. They become the Z boson and the photon.

$$m_Z = \frac{1}{2}v^2\sqrt{g^2 + g'^2} = \frac{m_W}{\cos\theta_W} \quad (\text{E.43})$$

$$m_A = 0 \quad (\text{E.44})$$

Now that we have our lagrangian in a usable form, we can finally start calculating the characteristics of Standard Model particles.

Appendix F: The $SU(2)_L \times U(1)_Y$ Local Gauge Invariant Lagrangian and the [massless] Fermions

We know now from section E what our postulated lagrangian should look like in order to be both $U(1)$ and $SU(2)$ invariant, which necessarily involved the weak vector bosons and the photon. Let's look at $SU(2) \times U(1)$ gauge invariance for the first generation of quarks; the calculation is identical for the higher generations. The calculation for the lepton generations is also very similar and so not repeated in this dissertation.

The Higgs mechanism is *not* included here so the quarks will still be massless; that will be dealt with in section G. Instead, we will deal with fermions that appear as a left-handed doublet and right-handed singlets for both particles. In the end, we will have computed the lagrangian that tells us how these fermions interact with each other, the weak vector gauge bosons, and the photon. The mass terms will, in the absence of the Higgs mechanism, be also absent for this section.

Suppose we have the (fermion) quark doublet

$$q = \begin{bmatrix} u \\ d \end{bmatrix} \quad (\text{F.1})$$

and recall that

$$\psi_L = \left(\frac{1 - \gamma_5}{2} \right) \psi \quad (\text{F.2})$$

$$\psi_R = \left(\frac{1 + \gamma_5}{2} \right) \psi \quad (\text{F.3})$$

are relations distinguishing the left and right handed components.

As always, we must postulate a lagrangian. In the sections exploring $U(1)$ and $SU(2)$ symmetries, we used generalizations of the Klein-Gordon equation's lagrangian for scalar particles. Now we want to look at spin-1/2 fermions, so we must use the Dirac lagrangian in our gauge invariant form. This is why I want to explore the case of massless fermions before adding in mass generation from the Higgs mechanism.[33]

Recall the Dirac lagrangian

$$\mathcal{L} = i\bar{\psi}\gamma_\mu\partial^\mu\psi - m\bar{\psi}\psi \quad (\text{F.4})$$

Now we want a massless version for a fermion doublet:

$$\mathcal{L} = \bar{q} i \not{D} q \quad (\text{F.5})$$

$$\mathcal{L} = \bar{q}_L i \not{D}_L q_L + \bar{u}_R i \not{D}_R u_R + \bar{d}_R i \not{D}_R d_R \quad (\text{F.6})$$

where the covariant derivative for the doublet \not{D}_L is $SU(2) \times U(1)$ invariant, and \not{D}_R is only $U(1)$ invariant for the singlet:

$$D_L^\rho = \partial^\rho + \frac{ig}{2} \vec{\tau} \cdot \vec{W}^\rho + \frac{ig'Y}{2} B^\rho \quad (\text{F.7})$$

$$D_R^\rho = \partial^\rho + \frac{ig'Y}{2} B^\rho \quad (\text{F.8})$$

F.1 The \mathcal{L}_R terms

$$\mathcal{L}_R = \bar{u}_R i \not{D} u_R + \bar{d}_R i \not{D} d_R \quad (\text{F.9})$$

$$= \bar{u}_R i \gamma_\rho \left(\partial^\rho - \frac{ig'Y}{2} B^\rho \right) u_R + \bar{d}_R i \gamma_\rho \left(\partial^\rho - \frac{ig'Y}{2} B^\rho \right) d_R \quad (\text{F.10})$$

$$= i \bar{u}_R \gamma_\rho (\partial^\rho u_R) - \frac{g'Y}{2} \bar{u}_R \gamma_\rho B^\rho u_R + i \bar{d}_R \gamma_\rho (\partial^\rho d_R) - \frac{g'Y}{2} \bar{d}_R \gamma_\rho B^\rho d_R \quad (\text{F.11})$$

$$= i u_R^\dagger \gamma_0 \gamma_\rho (\partial^\rho u_R) - \frac{g'Y}{2} u_R^\dagger \gamma_0 \gamma_\rho B^\rho u_R + i d_R^\dagger \gamma_0 \gamma_\rho (\partial^\rho d_R) - \frac{g'Y}{2} d_R^\dagger \gamma_0 \gamma_\rho B^\rho d_R \quad (\text{F.12})$$

$$= i u^\dagger \left(\frac{1+\gamma_5}{2} \right) \gamma_0 \gamma_\rho \left(\frac{1+\gamma_5}{2} \right) (\partial^\rho u) - \frac{g'Y}{2} u^\dagger \left(\frac{1+\gamma_5}{2} \right) \gamma_0 \gamma_\rho B^\rho \left(\frac{1+\gamma_5}{2} \right) u \quad (\text{F.13})$$

$$+ i d^\dagger \left(\frac{1+\gamma_5}{2} \right) \gamma_0 \gamma_\rho \left(\frac{1+\gamma_5}{2} \right) (\partial^\rho d) - \frac{g'Y}{2} d^\dagger \left(\frac{1+\gamma_5}{2} \right) \gamma_0 \gamma_\rho B^\rho \left(\frac{1+\gamma_5}{2} \right) d \quad (\text{F.14})$$

$$(\text{F.15})$$

Use the fact that γ_5 anticommutes with the other γ_μ 's, so $\{\gamma_5, \gamma_\mu\} = 0 \Rightarrow \left(\frac{1+\gamma_5}{2} \right) \gamma_\mu = \left(\frac{\gamma_\mu + \gamma_5 \gamma_\mu}{2} \right) = \left(\frac{\gamma_\mu + (-\gamma_\mu \gamma_5)}{2} \right) = \gamma_\mu \left(\frac{1-\gamma_5}{2} \right)$. Also, note that after $\left(\frac{1+\gamma_5}{2} \right)$ commutes past $\gamma_0 \gamma_\rho$, $\left(\frac{1+\gamma_5}{2} \right) \left(\frac{1+\gamma_5}{2} \right) =$

$$\left(\frac{1+\gamma_5}{2}\right).$$

$$\Rightarrow \mathcal{L}_R = i\bar{u}\gamma_\rho \left(\frac{1+\gamma_5}{2}\right) (\partial^\rho u) - \frac{g'Y}{2}\bar{u}\gamma_\rho B^\rho \left(\frac{1+\gamma_5}{2}\right) u \quad (\text{F.16})$$

$$+ i\bar{d}\gamma_\rho \left(\frac{1+\gamma_5}{2}\right) (\partial^\rho d) - \frac{g'Y}{2}\bar{d}\gamma_\rho B^\rho \left(\frac{1+\gamma_5}{2}\right) d \quad (\text{F.17})$$

We will return to these terms later.

F.2 The \mathcal{L}_L terms

$$\mathcal{L}_L = \bar{q}_L i \not{D} q_L \quad (\text{F.18})$$

As before, note that $\bar{u}_L = u^\dagger \left(\frac{1-\gamma_5}{2}\right) \gamma_0$ and also that

$$\bar{q}_L = \overline{\begin{bmatrix} u_L \\ d_L \end{bmatrix}} = \begin{bmatrix} \bar{u}_L & \bar{d}_L \end{bmatrix} \quad (\text{F.19})$$

$$\mathcal{L}_L = \begin{bmatrix} \bar{u}_L & \bar{d}_L \end{bmatrix} i\gamma_\rho D^\rho \begin{bmatrix} u_L \\ d_L \end{bmatrix} \quad (\text{F.20})$$

$$= \begin{bmatrix} \bar{u}_L & \bar{d}_L \end{bmatrix} i\gamma_\rho \left(\partial^\rho + \frac{ig}{2} \vec{\tau} \cdot \vec{W}^\rho + \frac{ig'Y}{2} B^\rho \right) \begin{bmatrix} u_L \\ d_L \end{bmatrix} \quad (\text{F.21})$$

$$= i \underbrace{\begin{bmatrix} \bar{u}_L & \bar{d}_L \end{bmatrix} \gamma_\rho \partial^\rho \begin{bmatrix} u_L \\ d_L \end{bmatrix}}_{\text{II.A}} - \underbrace{\frac{g}{2} \begin{bmatrix} \bar{u}_L & \bar{d}_L \end{bmatrix} \gamma_\rho \vec{\tau} \cdot \vec{W}^\rho \begin{bmatrix} u_L \\ d_L \end{bmatrix}}_{\text{II.B}} - \underbrace{\begin{bmatrix} \bar{u}_L & \bar{d}_L \end{bmatrix} \frac{g'Y}{2} \gamma_\rho B^\rho \begin{bmatrix} u_L \\ d_L \end{bmatrix}}_{\text{II.C}} \quad (\text{F.22})$$

II.A The Derivative Terms

$$i \begin{bmatrix} \bar{u}_L & \bar{d}_L \end{bmatrix} \gamma_\rho \partial^\rho \begin{bmatrix} u_L \\ d_L \end{bmatrix} = i \begin{bmatrix} \bar{u}_L & \bar{d}_L \end{bmatrix} \begin{bmatrix} \not{\partial} u_L \\ \not{\partial} d_L \end{bmatrix} \quad (\text{F.23})$$

$$= i \bar{u}_L \not{\partial} u_L + i \bar{d}_L \not{\partial} d_L \quad (\text{F.24})$$

$$= i u^\dagger \left(\frac{1 - \gamma_5}{2} \right) \gamma_0 \gamma_\rho \left(\frac{1 - \gamma_5}{2} \right) (\partial^\rho u) \quad (\text{F.25})$$

$$+ i d^\dagger \left(\frac{1 - \gamma_5}{2} \right) \gamma_0 \gamma_\rho \left(\frac{1 - \gamma_5}{2} \right) (\partial^\rho d) \quad (\text{F.26})$$

$$= i u^\dagger \gamma_0 \left(\frac{1 + \gamma_5}{2} \right) \gamma_\rho \left(\frac{1 - \gamma_5}{2} \right) (\partial^\rho u) \quad (\text{F.27})$$

$$+ i d^\dagger \gamma_0 \left(\frac{1 + \gamma_5}{2} \right) \gamma_\rho \left(\frac{1 - \gamma_5}{2} \right) (\partial^\rho d) \quad (\text{F.28})$$

$$= i u^\dagger \gamma_0 \gamma_\rho \left(\frac{1 - \gamma_5}{2} \right)^2 (\partial^\rho u) + i d^\dagger \gamma_0 \gamma_\rho \left(\frac{1 - \gamma_5}{2} \right)^2 (\partial^\rho d) \quad (\text{F.29})$$

$$= i u^\dagger \gamma_0 \gamma_\rho \left(\frac{1 - \gamma_5}{2} \right) (\partial^\rho u) + i d^\dagger \gamma_0 \gamma_\rho \left(\frac{1 - \gamma_5}{2} \right) (\partial^\rho d) \quad (\text{F.30})$$

$$= i \bar{u} \gamma_\rho \left(\frac{1 - \gamma_5}{2} \right) (\partial^\rho u) + i \bar{d} \gamma_\rho \left(\frac{1 - \gamma_5}{2} \right) (\partial^\rho d) \quad (\text{F.31})$$

II.B The W, W^\dagger, W_3 Terms The key here is to express

$$\frac{1}{2} \vec{\tau} \cdot \vec{W}^\mu = \frac{1}{2} [\tau_1 W_1^\mu + \tau_2 W_2^\mu + \tau_3 W_3^\mu] \quad (\text{F.32})$$

$$= \frac{1}{\sqrt{2}} \left[\tau_+ \left(\frac{W_1^\mu - i W_2^\mu}{\sqrt{2}} \right) \tau_- \left(\frac{W_1^\mu + i W_2^\mu}{\sqrt{2}} \right) \right] + \frac{1}{2} \tau_3 W_3^\mu \quad (\text{F.33})$$

$$= \frac{1}{\sqrt{2}} [\tau_+ W^\mu + \tau_- W_\mu^\dagger] + \frac{1}{2} \tau_3 W_3^\mu \quad (\text{F.34})$$

Where we denote

$$\tau_+ \equiv \frac{1}{2}(\tau_1 + i\tau_2) = \frac{1}{2} \left[\begin{bmatrix} 0 & 1 \\ 1 & 0 \end{bmatrix} + i \begin{bmatrix} 0 & -i \\ i & 0 \end{bmatrix} \right] = \frac{1}{2} \begin{bmatrix} 0 & 2 \\ 0 & 0 \end{bmatrix} = \begin{bmatrix} 0 & 1 \\ 0 & 0 \end{bmatrix} \quad (\text{F.35})$$

$$\tau_- \equiv \frac{1}{2}(\tau_1 - i\tau_2) = \frac{1}{2} \left[\begin{bmatrix} 0 & 1 \\ 1 & 0 \end{bmatrix} - i \begin{bmatrix} 0 & -i \\ i & 0 \end{bmatrix} \right] = \frac{1}{2} \begin{bmatrix} 0 & 0 \\ 2 & 0 \end{bmatrix} = \begin{bmatrix} 0 & 0 \\ 1 & 0 \end{bmatrix} \quad (\text{F.36})$$

$$W^\mu \equiv \frac{W_1^\mu - iW_2^\mu}{\sqrt{2}} \quad (\text{F.37})$$

$$W^{\mu\dagger} \equiv \frac{W_1^\mu + iW_2^\mu}{\sqrt{2}} \quad (\text{F.38})$$

The reason we want to do this is for the following:

$$\frac{1}{\sqrt{2}}\tau_+W^\mu \begin{bmatrix} u_L \\ d_L \end{bmatrix} = \frac{1}{\sqrt{2}} \begin{bmatrix} 0 & W^\mu \\ 0 & 0 \end{bmatrix} \begin{bmatrix} u_L \\ d_L \end{bmatrix} = \frac{1}{\sqrt{2}} \begin{bmatrix} W^\mu d_L \\ 0 \end{bmatrix} = \frac{W^\mu}{\sqrt{2}} \begin{bmatrix} d_L \\ 0 \end{bmatrix} \quad (\text{F.39})$$

$$\frac{1}{\sqrt{2}}\tau_+W^{\mu\dagger} \begin{bmatrix} u_L \\ d_L \end{bmatrix} = \frac{1}{\sqrt{2}} \begin{bmatrix} 0 & 0 \\ W^{\mu\dagger} & 0 \end{bmatrix} \begin{bmatrix} u_L \\ d_L \end{bmatrix} = \frac{1}{\sqrt{2}} \begin{bmatrix} 0 \\ W^{\mu\dagger} u_L \end{bmatrix} = \frac{W^\mu}{\sqrt{2}} \begin{bmatrix} 0 \\ u_L \end{bmatrix} \quad (\text{F.40})$$

Notice how the u_L and d_L fields switch positions in the vector. This is what will subsequently allow interactions between these fields via the gauge bosons W^μ .

Lastly,

$$\frac{1}{2}\tau_3W_3^\mu \begin{bmatrix} u_L \\ d_L \end{bmatrix} = \frac{1}{2} \begin{bmatrix} 1 & 0 \\ 0 & -1 \end{bmatrix} \begin{bmatrix} W_3^\mu u_L \\ W_3^\mu d_L \end{bmatrix} = \frac{1}{2} \begin{bmatrix} W_3^\mu u_L \\ -W_3^\mu d_L \end{bmatrix} = \frac{W_3^\mu}{2} \begin{bmatrix} u_L \\ -d_L \end{bmatrix} \quad (\text{F.41})$$

Now we are ready to return to the term II.B from the lagrangian.

$$\frac{g}{2} \begin{bmatrix} \bar{u}_L & \bar{d}_L \end{bmatrix} \gamma_\rho \vec{\tau} \cdot \vec{W}^\rho \begin{bmatrix} u_L \\ d_L \end{bmatrix} \quad (\text{F.42})$$

$$= g \begin{bmatrix} \bar{u}_L & \bar{d}_L \end{bmatrix} \gamma_\rho \left(\frac{1}{2} \tau_+ (W_1^\rho - iW_2^\rho) + \frac{1}{2} \tau_- (W_1^\rho + iW_2^\rho) + \frac{1}{2} \tau_3 W_3^\rho \right) \begin{bmatrix} u_L \\ d_L \end{bmatrix} \quad (\text{F.43})$$

$$= g \begin{bmatrix} \bar{u}_L & \bar{d}_L \end{bmatrix} \gamma_\rho \left(\frac{1}{\sqrt{2}} \tau_+ W^\rho + \frac{1}{\sqrt{2}} \tau_- W^{\rho\dagger} + \frac{1}{2} \tau_3 W_3^\rho \right) \begin{bmatrix} u_L \\ d_L \end{bmatrix} \quad (\text{F.44})$$

$$= g \begin{bmatrix} \bar{u}_L & \bar{d}_L \end{bmatrix} \gamma_\rho \left(\frac{1}{\sqrt{2}} W^\rho \begin{bmatrix} d_L \\ 0 \end{bmatrix} + \frac{1}{\sqrt{2}} W^{\rho\dagger} \begin{bmatrix} 0 \\ u_L \end{bmatrix} + \frac{1}{2} W_3^\rho \begin{bmatrix} u_L \\ -d_L \end{bmatrix} \right) \quad (\text{F.45})$$

$$= \frac{1}{\sqrt{2}} g \begin{bmatrix} \bar{u}_L & \bar{d}_L \end{bmatrix} \begin{bmatrix} W^\rho d_L \\ 0 \end{bmatrix} \frac{1}{\sqrt{2}} g \begin{bmatrix} \bar{u}_L & \bar{d}_L \end{bmatrix} \begin{bmatrix} 0 \\ W^{\dagger\rho} u_L \end{bmatrix} \frac{1}{2} g \begin{bmatrix} \bar{u}_L & \bar{d}_L \end{bmatrix} \begin{bmatrix} W_3^\rho u_L \\ -W_3^\rho d_L \end{bmatrix} \quad (\text{F.46})$$

$$= \frac{1}{\sqrt{2}} g \bar{u}_L W^\rho d_L + \frac{1}{\sqrt{2}} g \bar{d}_L W^{\dagger\rho} u_L + \frac{1}{2} g \bar{u}_L W_3^\rho u_L + \frac{1}{2} g \bar{d}_L (-W_3^\rho d_L) \quad (\text{F.47})$$

$$(\text{F.48})$$

$$\frac{g}{2} \begin{bmatrix} \bar{u}_L & \bar{d}_L \end{bmatrix} \gamma_\rho \vec{\tau} \cdot \vec{W}^\rho \begin{bmatrix} u_L \\ d_L \end{bmatrix} \quad (\text{F.49})$$

$$= \frac{1}{\sqrt{2}} g u_L^\dagger \gamma_0 \gamma_\rho W^\rho d_L + \frac{1}{\sqrt{2}} g d_L^\dagger \gamma_0 \gamma_\rho W^{\rho\dagger} u_L \quad (\text{F.50})$$

$$+ \frac{1}{2} g u_L^\dagger \gamma_0 \gamma_\rho W_3^\rho u_L - \frac{1}{2} g d_L^\dagger \gamma_0 \gamma_\rho W_3^\rho d_L \quad (\text{F.51})$$

$$= \frac{1}{\sqrt{2}} g u^\dagger \left(\frac{1 - \gamma_5}{2} \right) \gamma_0 \gamma_\rho W^\rho \left(\frac{1 - \gamma_5}{2} \right) d \quad (\text{F.52})$$

$$+ \frac{1}{\sqrt{2}} g d^\dagger \left(\frac{1 - \gamma_5}{2} \right) \gamma_0 \gamma_\rho W^{\rho\dagger} \left(\frac{1 - \gamma_5}{2} \right) u \quad (\text{F.53})$$

$$+ \frac{1}{2} g u^\dagger \left(\frac{1 - \gamma_5}{2} \right) \gamma_0 \gamma_\rho W_3^\rho \left(\frac{1 - \gamma_5}{2} \right) u \quad (\text{F.54})$$

$$- \frac{1}{2} g d^\dagger \left(\frac{1 - \gamma_5}{2} \right) \gamma_0 \gamma_\rho W_3^\rho \left(\frac{1 - \gamma_5}{2} \right) d \quad (\text{F.55})$$

$$= \frac{1}{\sqrt{2}} g \bar{u} \gamma_\rho W^\rho \left(\frac{1 - \gamma_5}{2} \right) d + \frac{1}{\sqrt{2}} g \bar{d} \gamma_\rho W^{\rho\dagger} \left(\frac{1 - \gamma_5}{2} \right) u \quad (\text{F.56})$$

$$+ \frac{1}{2} g \bar{u} \gamma_\rho W_3^\rho \left(\frac{1 - \gamma_5}{2} \right) u - \frac{1}{2} g \bar{d} \gamma_\rho W_3^\rho \left(\frac{1 - \gamma_5}{2} \right) d \quad (\text{F.57})$$

It is important to note that while these terms do describe quark interactions, the vertex factors here are not in their final Standard Model form. There are still the CKM matrix elements that govern the strength of the interactions to deal with. The proper form with the CKM matrix elements follows directly from the presence of the Higgs field and is therefore excluded from this section. That problem requires separate treatment.

II.C The B^ρ Field Terms

$$\begin{bmatrix} \bar{u}_L & \bar{d}_L \end{bmatrix} \frac{g'Y}{2} \gamma_\rho B^\rho \begin{bmatrix} u_L \\ d_L \end{bmatrix} \quad (\text{F.58})$$

$$= \frac{g'Y}{2} \begin{bmatrix} \bar{u}_L & \bar{d}_L \end{bmatrix} \begin{bmatrix} \not{B} u_L \\ \not{B} d_L \end{bmatrix} \quad (\text{F.59})$$

$$= \frac{g'Y}{2} [\bar{u}_L \not{B} u_L + \bar{d}_L \not{B} d_L] \quad (\text{F.60})$$

$$= \frac{g'Y}{2} [u_L^\dagger \gamma_0 \gamma_\rho B^\rho u_L + d_L^\dagger \gamma_0 \gamma_\rho B^\rho d_L] \quad (\text{F.61})$$

$$= \frac{g'Y}{2} \left[u^\dagger \left(\frac{1-\gamma_5}{2} \right) \gamma_0 \gamma_\rho B^\rho \left(\frac{1-\gamma_5}{2} \right) u + d^\dagger \left(\frac{1-\gamma_5}{2} \right) \gamma_0 \gamma_\rho B^\rho \left(\frac{1-\gamma_5}{2} \right) d \right] \quad (\text{F.62})$$

$$= \frac{g'Y}{2} \left[\bar{u} \gamma_\rho \left(\frac{1-\gamma_5}{2} \right) B^\rho u + \bar{d} \gamma_\rho \left(\frac{1-\gamma_5}{2} \right) B^\rho d \right] \quad (\text{F.63})$$

F.3 Find the Z -boson and Photon Interactions

The next task is to mix these terms with the W_3^μ terms from before to yield the photon and Z -boson interactions with the quarks. Note that the work of mixing these fields into A^μ and Z^μ was done in E. So we are going to collect the B^ρ and W_3^ρ terms from II.A, II.B, and II.C, then switch to expressing those terms with A^μ and Z^μ instead. This will yield quark interactions with the photon and Z -boson. Afterward, we will collect all the terms of the lagrangian and express it in a manner that elucidates the electroweak physics of quarks.

$$-\frac{g'Y}{2}\bar{u}\gamma_\rho B^\rho \left(\frac{1+\gamma_5}{2}\right)u - \frac{g'Y}{2}\bar{d}\gamma_\rho B^\rho \left(\frac{1+\gamma_5}{2}\right)d \quad (\text{F.64})$$

$$-\frac{1}{2}g\bar{u}\gamma_\rho W_3^\rho \left(\frac{1-\gamma_5}{2}\right)u + \frac{1}{2}g\bar{d}\gamma_\rho W_3^\rho \left(\frac{1-\gamma_5}{2}\right)d \quad (\text{F.65})$$

$$-\frac{g'Y}{2}\bar{u}\gamma_\rho \left(\frac{1-\gamma_5}{2}\right)B^\rho u - \frac{g'Y}{2}\bar{d}\gamma_\rho \left(\frac{1-\gamma_5}{2}\right)B^\rho d \quad (\text{F.66})$$

$$= -\frac{g'Y}{2}\bar{u}\gamma_\rho \left(\frac{1+\gamma_5}{2}\right)u(-Z^\rho \sin \theta_W + A^\rho \cos \theta_W) \quad (\text{F.67})$$

$$-\frac{g'Y}{2}\bar{d}\gamma_\rho \left(\frac{1+\gamma_5}{2}\right)d(-Z^\rho \sin \theta_W + A^\rho \cos \theta_W) \quad (\text{F.68})$$

$$-\frac{g}{2}\bar{u}\gamma_\rho \left(\frac{1-\gamma_5}{2}\right)u(Z^\rho \cos \theta_W + A^\rho \sin \theta_W) \quad (\text{F.69})$$

$$+\frac{g}{2}\bar{d}\gamma_\rho \left(\frac{1-\gamma_5}{2}\right)d(Z^\rho \cos \theta_W + A^\rho \sin \theta_W) \quad (\text{F.70})$$

$$-\frac{g'Y}{2}\bar{u}\gamma_\rho \left(\frac{1-\gamma_5}{2}\right)u(-Z^\rho \sin \theta_W + A^\rho \cos \theta_W) \quad (\text{F.71})$$

$$-\frac{g'Y}{2}\bar{d}\gamma_\rho \left(\frac{1-\gamma_5}{2}\right)d(-Z^\rho \sin \theta_W + A^\rho \cos \theta_W) \quad (\text{F.72})$$

Use $Y = 1/3$ for u_L ; $Y = 4/3$ for u_R ; $Y = 1/3$ for d_L ; and $Y = -2/3$ for d_R [15].

$$= -\frac{2g'}{3}\bar{u}\gamma_\rho\left(\frac{1+\gamma_5}{2}\right)u(-Z^\rho\sin\theta_W + A^\rho\cos\theta_W) \quad (\text{F.73})$$

$$+ \frac{g'}{3}\bar{d}\gamma_\rho\left(\frac{1+\gamma_5}{2}\right)d(-Z^\rho\sin\theta_W + A^\rho\cos\theta_W) \quad (\text{F.74})$$

$$- \frac{g}{2}\bar{u}\gamma_\rho\left(\frac{1-\gamma_5}{2}\right)u(Z^\rho\cos\theta_W + A^\rho\sin\theta_W) \quad (\text{F.75})$$

$$+ \frac{g}{2}\bar{d}\gamma_\rho\left(\frac{1-\gamma_5}{2}\right)d(Z^\rho\cos\theta_W + A^\rho\sin\theta_W) \quad (\text{F.76})$$

$$- \frac{g'}{6}\bar{u}\gamma_\rho\left(\frac{1-\gamma_5}{2}\right)u(-Z^\rho\sin\theta_W + A^\rho\cos\theta_W) \quad (\text{F.77})$$

$$- \frac{g'}{6}\bar{d}\gamma_\rho\left(\frac{1-\gamma_5}{2}\right)d(-Z^\rho\sin\theta_W + A^\rho\cos\theta_W) \quad (\text{F.78})$$

$$= \frac{2g'}{3}\bar{u}\gamma_\rho\left(\frac{1+\gamma_5}{2}\right)u(Z^\rho\sin\theta_W) - \frac{2g'}{3}\bar{u}\gamma_\rho\left(\frac{1+\gamma_5}{2}\right)u(A^\rho\cos\theta_W) \quad (\text{F.79})$$

$$- \frac{g'}{3}\bar{d}\gamma_\rho\left(\frac{1+\gamma_5}{2}\right)d(Z^\rho\sin\theta_W) + \frac{g'}{3}\bar{d}\gamma_\rho\left(\frac{1+\gamma_5}{2}\right)d(A^\rho\cos\theta_W) \quad (\text{F.80})$$

$$+ \bar{u}\gamma_\rho\left(\frac{1-\gamma_5}{2}\right)uZ^\rho\left(-\frac{1}{2}g\cos\theta_W + \frac{1}{6}g'\sin\theta_W\right) \quad (\text{F.81})$$

$$+ \bar{u}\gamma_\rho\left(\frac{1-\gamma_5}{2}\right)uA^\rho\left(-\frac{1}{2}g\sin\theta_W - \frac{1}{6}g'\cos\theta_W\right) \quad (\text{F.82})$$

$$+ \bar{d}\gamma_\rho\left(\frac{1-\gamma_5}{2}\right)dZ^\rho\left(\frac{1}{2}g\cos\theta_W + \frac{1}{6}g'\sin\theta_W\right) \quad (\text{F.83})$$

$$+ \bar{d}\gamma_\rho\left(\frac{1-\gamma_5}{2}\right)dA^\rho\left(\frac{1}{2}g\sin\theta_W - \frac{1}{6}g'\cos\theta_W\right) \quad (\text{F.84})$$

$$(\text{F.85})$$

Now use $g' = g \frac{\sin \theta_W}{\cos \theta_W}$ in all terms.

$$= \frac{2}{3} \bar{u} \gamma_\rho \left(\frac{1 + \gamma_5}{2} \right) u Z^\rho \left(g \frac{\sin \theta_W}{\cos \theta_W} \sin \theta_W \right) \quad (\text{F.86})$$

$$- \frac{2}{3} \bar{u} \gamma_\rho \left(\frac{1 + \gamma_5}{2} \right) u A^\rho (g \sin \theta_W) \quad (\text{F.87})$$

$$- \frac{1}{3} \bar{d} \gamma_\rho \left(\frac{1 + \gamma_5}{2} \right) d Z^\rho \left(g \frac{\sin \theta_W}{\cos \theta_W} \sin \theta_W \right) \quad (\text{F.88})$$

$$+ \frac{1}{3} \bar{d} \gamma_\rho \left(\frac{1 + \gamma_5}{2} \right) d A^\rho g \sin \theta_W \quad (\text{F.89})$$

$$\bar{u} \gamma_\rho \left(\frac{1 - \gamma_5}{2} \right) u Z^\rho \left(-\frac{1}{2} g \cos \theta_W + \frac{1}{6} g \frac{\sin \theta_W}{\cos \theta_W} \sin \theta_W \right) \quad (\text{F.90})$$

$$\bar{u} \gamma_\rho \left(\frac{1 - \gamma_5}{2} \right) u A^\rho \left(-\frac{1}{2} g \sin \theta_W - \frac{1}{6} g \sin \theta_W \right) \quad (\text{F.91})$$

$$\bar{d} \gamma_\rho \left(\frac{1 - \gamma_5}{2} \right) u Z^\rho \left(\frac{1}{2} g \cos \theta_W + \frac{1}{6} g \frac{\sin \theta_W}{\cos \theta_W} \sin \theta_W \right) \quad (\text{F.92})$$

$$\bar{d} \gamma_\rho \left(\frac{1 - \gamma_5}{2} \right) d A^\rho \left(\frac{1}{2} g \sin \theta_W - \frac{1}{6} g \sin \theta_W \right) \quad (\text{F.93})$$

$$(\text{F.94})$$

$$= \frac{2g}{3} \bar{u} \gamma_\rho \left(\frac{1 + \gamma_5}{2} \right) u Z^\rho \left(\frac{\sin^2 \theta_W}{\cos \theta_W} \right) - \frac{2g}{3} \bar{u} \gamma_\rho \left(\frac{1 + \gamma_5}{2} \right) u A^\rho \sin \theta_W \quad (\text{F.95})$$

$$- \frac{g}{3} \bar{d} \gamma_\rho \left(\frac{1 + \gamma_5}{2} \right) d Z^\rho \left(\frac{\sin^2 \theta_W}{\cos \theta_W} \right) + \frac{g}{3} \bar{d} \gamma_\rho \left(\frac{1 + \gamma_5}{2} \right) d A^\rho \sin \theta_W \quad (\text{F.96})$$

$$+ \frac{g}{2 \cos \theta_W} \bar{u} \gamma_\rho \left(\frac{1 - \gamma_5}{2} \right) u Z^\rho \left(-\cos^2 \theta_W + \frac{1}{3} \sin^2 \theta_W \right) \quad (\text{F.97})$$

$$- \frac{2g}{3} \bar{u} \gamma_\rho \left(\frac{1 - \gamma_5}{2} \right) u A^\rho \sin \theta_W \quad (\text{F.98})$$

$$+ \frac{g}{2 \cos \theta_W} \bar{d} \gamma_\rho \left(\frac{1 - \gamma_5}{2} \right) d Z^\rho \left(\cos^2 \theta_W + \frac{1}{3} \sin^2 \theta_W \right) \quad (\text{F.99})$$

$$+ \frac{g}{3} \bar{d} \gamma_\rho \left(\frac{1 - \gamma_5}{2} \right) d A^\rho \sin \theta_W \quad (\text{F.100})$$

Use these trigonometric relations,

$$-\cos^2 \theta_W + \frac{1}{3} \sin^2 \theta_W = -1 + \frac{4}{3} \sin^2 \theta_W \quad (\text{F.101})$$

$$\cos^2 \theta_W + \frac{1}{3} \sin^2 \theta_W = 1 - \frac{2}{3} \sin^2 \theta_W \quad (\text{F.102})$$

$$\left(\frac{1 - \gamma_5}{2} \right) + \left(\frac{1 + \gamma_5}{2} \right) = 1 \quad (\text{F.103})$$

and the electric charge defined as $e_0 = g \sin \theta_W$ in recollecting all the terms of the lagrangian, which now has the form:

$$\mathcal{L} = i\bar{u}\gamma_\rho \left(\frac{1 + \gamma_5}{2} \right) (\partial^\rho u) + i\bar{d}\gamma_\rho \left(\frac{1 + \gamma_5}{2} \right) (\partial^\rho d) \quad (\text{F.104})$$

$$+ i\bar{u}\gamma_\rho \left(\frac{1 - \gamma_5}{2} \right) (\partial^\rho u) + i\bar{d}\gamma_\rho \left(\frac{1 - \gamma_5}{2} \right) (\partial^\rho d) \quad (\text{F.105})$$

$$+ \frac{1}{\sqrt{2}} g \bar{u}\gamma_\rho W^\rho \left(\frac{1 - \gamma_5}{2} \right) d + \frac{1}{\sqrt{2}} g \bar{d}\gamma_\rho W^{\rho\dagger} \left(\frac{1 - \gamma_5}{2} \right) u \quad (\text{F.106})$$

$$+ \frac{g}{2 \cos \theta_W} Z^\rho \left[\bar{u}\gamma_\rho \left(\frac{1 + \gamma_5}{2} \right) u \left(\frac{4}{3} \sin^2 \theta_W \right) - \bar{d}\gamma_\rho \left(\frac{1 + \gamma_5}{2} \right) d \left(\frac{2}{3} \sin^2 \theta_W \right) \right] \quad (\text{F.107})$$

$$+ \bar{u}\gamma_\rho \left(\frac{1 - \gamma_5}{2} \right) u \left(-1 + \frac{4}{3} \sin^2 \theta_W \right) - \bar{d}\gamma_\rho \left(\frac{1 - \gamma_5}{2} \right) d \left(-1 + \frac{2}{3} \sin^2 \theta_W \right) \quad (\text{F.108})$$

$$- \frac{2e_0}{3} \bar{u}\gamma_\rho u A^\rho + \frac{e_0}{3} \bar{d}\gamma_\rho d A^\rho \quad (\text{F.109})$$

Appendix G: The Higgs Mechanism and Fermion Mass Generation

Recall from section F that the kinetic part of a free Dirac fermion does not mix the left and right components of the field:

$$\bar{\psi}\gamma_\mu\partial^\mu\psi = \bar{\psi}_R\gamma_\mu\partial^\mu\psi_R + \bar{\psi}_L\gamma_\mu\partial^\mu\psi_L \quad (\text{G.1})$$

Because of this, we can gauge the left and right handed components differently. Weak interactions are parity violating in the Standard Model and the $SU(2)_L$ covariant derivative acts only on the left-handed term. However, a Dirac mass term has the form

$$-m(\bar{\psi}_L\psi_R + \bar{\psi}_R\psi_L) \quad (\text{G.2})$$

when we write the left and right handed components separately. So the components are coupled, meaning any such mass term breaks $SU(2)_L$ gauge invariance.

In a theory with spontaneous symmetry breaking, there is a way of giving mass to fermions without explicitly introducing gauge invariance breaking mass terms in the lagrangian. Consider the electron $SU(2)_L$ doublet

$$l = \begin{bmatrix} \nu \\ e \end{bmatrix}_L \quad (\text{G.3})$$

the Higgs doublet

$$\phi = \begin{bmatrix} \phi^+ \\ \phi^0 \end{bmatrix} \quad (\text{G.4})$$

$$\phi^+ = \frac{1}{\sqrt{2}}(\phi_1 - i\phi_2) \quad (\text{G.5})$$

$$\phi^0 = \frac{1}{\sqrt{2}}(\phi_3 - i\phi_4) \quad (\text{G.6})$$

and the right handed electron singlet in a Yukawa model.

$$\mathcal{L}_e = -g_e\bar{l}_L\phi e_R - g_e\bar{e}_R\phi^\dagger l_L \quad (\text{G.7})$$

It is important to notice that the structure of these terms has two $SU(2)_L$ doublets multiplied to form an $SU(2)_L$ scalar ($\bar{l}_L \phi, \phi^\dagger l$), and that scalar multiplies the $SU(2)_L$ scalar R-component. So this lagrangian is $SU(2)_L$ invariant and the symmetry is preserved.[15]

Recall from section E that the vacuum expectation value of the Higgs doublet assumes the value

$$\langle 0 | \phi | 0 \rangle = \begin{bmatrix} 0 \\ \frac{v}{\sqrt{2}} \end{bmatrix} \quad (\text{G.8})$$

but that section dealt with a scalar Klein-Gordon particle. The consequence for a fermion doublet in this lagrangian is

$$\mathcal{L}_e = -g_e \bar{l}_L \phi e_R - g_e \bar{e}_R \phi^\dagger l_L \quad (\text{G.9})$$

$$= -g_e \begin{bmatrix} \nu_L \\ e_L \end{bmatrix} \phi e_R - g_e \bar{e}_R \phi^\dagger \begin{bmatrix} \nu_L \\ e_L \end{bmatrix} \quad (\text{G.10})$$

$$= -g_e \begin{bmatrix} \bar{\nu}_L & \bar{e}_L \end{bmatrix} \begin{bmatrix} \phi^+ \\ \phi^0 \end{bmatrix} e_R - g_e \bar{e}_R \begin{bmatrix} \phi^+ & \phi^0 \end{bmatrix} \begin{bmatrix} \nu_L \\ e_L \end{bmatrix} \quad (\text{G.11})$$

$$= -g_e (\bar{\nu}_L \phi^+ + \bar{e}_L \phi^0) e_R - g_e \bar{e}_R (\phi^+ \nu_L + \phi^0 e_L) \quad (\text{G.12})$$

$$= -g_e [\bar{\nu}_L \phi^+ e_R + \bar{e}_L \phi^0 e_R + \bar{e}_R \phi^+ \nu_L + \bar{e}_R \phi^0 e_L] \quad (\text{G.13})$$

Take on the vacuum expectation values.

$$\langle 0 | \mathcal{L}_e | 0 \rangle = -g_e \left[\bar{\nu}_L \underbrace{\langle 0 | \phi^+ | 0 \rangle}_{=0} e_R + \bar{e}_L \underbrace{\langle 0 | \phi^0 | 0 \rangle}_{\frac{v}{\sqrt{2}}} e_R \right] \quad (\text{G.14})$$

$$+ \bar{e}_R \underbrace{\langle 0 | \phi^+ | 0 \rangle}_{=0} \nu_L + \bar{e}_R \underbrace{\langle 0 | \phi^0 | 0 \rangle}_{\frac{v}{\sqrt{2}}} e_L \quad (\text{G.15})$$

$$= -\frac{g_e v}{\sqrt{2}} [\bar{e}_L e_R + \bar{e}_R e_L] \quad (\text{G.16})$$

This is exactly a Dirac mass with $m_e = \frac{g_e v}{\sqrt{2}}$. That was precisely the vacuum. Now let's see that if we consider also oscillations about the vacuum we generate a coupling between the electron and the Higgs field. In the last line, use $v + H$ instead of just v .

$$\langle 0 | \mathcal{L}_e | 0 \rangle = -\frac{g_e v}{\sqrt{2}} [\bar{e}_L(v+H)e_R + \bar{e}_R(v+H)e_L] \quad (\text{G.17})$$

$$= -\frac{g_e v}{\sqrt{2}} [v\bar{e}_L e_R + \bar{e}_L H e_R + v\bar{e}_R e_L + \bar{e}_R H e_L] \quad (\text{G.18})$$

$$= -\frac{g_e v}{\sqrt{2}} \left[v e^\dagger \left(\frac{1-\gamma_5}{2} \right) \gamma_0 \left(\frac{1+\gamma_5}{2} \right) e + e^\dagger \left(\frac{1-\gamma_5}{2} \right) \gamma_0 H \left(\frac{1+\gamma_5}{2} \right) e \right. \quad (\text{G.19})$$

$$\left. + v e^\dagger \left(\frac{1+\gamma_5}{2} \right) \gamma_0 \left(\frac{1-\gamma_5}{2} \right) e + e^\dagger \left(\frac{1+\gamma_5}{2} \right) \gamma_0 H \left(\frac{1-\gamma_5}{2} \right) e \right] \quad (\text{G.20})$$

$$= -\frac{g_e v}{\sqrt{2}} \left[v \bar{e} \left(\frac{1+\gamma_5}{2} \right) e + \bar{e} H e \left(\frac{1+\gamma_5}{2} \right) \right. \quad (\text{G.21})$$

$$\left. + v \bar{e} \left(\frac{1-\gamma_5}{2} \right) e + \bar{e} H e \left(\frac{1-\gamma_5}{2} \right) \right] \quad (\text{G.22})$$

$$= -\frac{g_e v}{\sqrt{2}} \left[\underbrace{v \bar{e} e}_{\text{Dirac electron mass}} + \underbrace{\bar{e} H e}_{\text{electron-Higgs coupling}} \right] \quad (\text{G.23})$$

Notice for the coupling term

$$\left(\frac{-g_e}{\sqrt{2}} \right) \bar{e} H e = \left(-\frac{m_e}{v} \right) \bar{e} H e = \left(-\frac{g m_e}{2m_W} \right) \bar{e} H e \quad (\text{G.24})$$

So in addition to interactions of the form $f\bar{f} \rightarrow (\gamma \text{ or } Z^0) \rightarrow W^+W^-$ we also have the possibility $f\bar{f} \rightarrow H \rightarrow W^+W^-$. The presence of the fermion mass in the coupling to the Higgs is significant.

We must now recall that if an $SU(2)$ doublet transforms as

$$l' = e^{\frac{i}{2}\vec{\alpha} \cdot \vec{\tau}} l \quad (\text{G.25})$$

then the charge conjugate states

$$i\tau_2 \begin{bmatrix} u^* \\ d^* \end{bmatrix} \quad (\text{G.26})$$

transform the same way. So then the charge conjugate of the Higgs field is

$$\phi_c = i\tau_2\phi^* \quad (\text{G.27})$$

$$= i \begin{bmatrix} 0 & -i \\ i & 0 \end{bmatrix} \begin{bmatrix} \phi^+ \\ \phi^0 \end{bmatrix}^* \quad (\text{G.28})$$

$$= \begin{bmatrix} 0 & 1 \\ -1 & 0 \end{bmatrix} \begin{bmatrix} \frac{1}{\sqrt{2}}(\phi_1 - i\phi_2)^* \\ \frac{1}{\sqrt{2}}(\phi_3 - i\phi_4)^* \end{bmatrix} \quad (\text{G.29})$$

$$= \begin{bmatrix} 0 & 1 \\ -1 & 0 \end{bmatrix} \begin{bmatrix} \frac{1}{\sqrt{2}}(\phi_1 + i\phi_2) \\ \frac{1}{\sqrt{2}}(\phi_3 + i\phi_4) \end{bmatrix} \quad (\text{G.30})$$

$$= \begin{bmatrix} \frac{1}{\sqrt{2}}(\phi_3 + i\phi_4) \\ -\frac{1}{\sqrt{2}}(\phi_1 + i\phi_2) \end{bmatrix} \quad (\text{G.31})$$

$$\equiv \begin{bmatrix} \phi^{0\dagger} \\ -\phi^- \end{bmatrix} \quad (\text{G.32})$$

ϕ_c is also an $SU(2)$ doublet which transforms the same way ϕ does.

Note that in the use of the ϕ Higgs doublet we could not use the terms $\bar{l}_L\phi\nu_R$ or $\bar{\nu}_R\phi^\dagger l_L$ in the lagrangian (ν_R has replaced e_R) because it leads to unphysical terms $\bar{e}_L\nu_R$ and $\bar{\nu}_Re_L$. With the Higgs conjugate field doublet ϕ_c we may include $\bar{l}_L\phi_c\nu_R$ and $\bar{\nu}_R\phi_c^\dagger l_L$ terms (but not $\bar{l}_L\phi_ce_R$ and $\bar{e}_R\phi_c^\dagger l_L$ terms for the same reasons just discussed) which yield Dirac masses for the neutrinos as well as Higgs interactions. Observe,

$$\mathcal{L}_\nu = -g_\nu \left[\bar{l}_L\phi\nu_R + \bar{\nu}_R\phi^\dagger l_L \right] \quad (\text{G.33})$$

$$= -g_\nu \left[\begin{bmatrix} \bar{\nu}_L & \bar{e}_L \end{bmatrix} \begin{bmatrix} \phi^{0\dagger} \\ -\phi^- \end{bmatrix} \nu_R + \begin{bmatrix} \phi^0 & -\phi^{-\dagger} \end{bmatrix} \begin{bmatrix} \nu_L \\ e_L \end{bmatrix} \right] \quad (\text{G.34})$$

$$= -g_\nu \left[\left(\bar{\nu}_L\phi^{0\dagger} - \bar{e}_L\phi^- \right) \nu_R + \bar{\nu}_R \left(\phi^0\nu_L - \phi^{-\dagger}e_L \right) \right] \quad (\text{G.35})$$

$$= -g_\nu \left[\bar{\nu}_L\phi^{0\dagger}\nu_R - \bar{e}_L\phi^-\nu_R + \bar{\nu}_R\phi^0\nu_L - \bar{\nu}_R\phi^{-\dagger}e_L \right] \quad (\text{G.36})$$

Take the vacuum expectation value and all ϕ^- terms vanish. The ϕ^0 factors become $\frac{1}{\sqrt{2}}(v + H)$ again.

$$\langle 0 | \mathcal{L}_\nu | 0 \rangle = -\frac{g_\nu}{\sqrt{2}} \left[\bar{\nu}_L(v + H)\nu_R + \bar{\nu}_R(v + H)\nu_L \right] \quad (\text{G.37})$$

$$= -\frac{g_\nu}{\sqrt{2}} \left[\underbrace{v\bar{\nu}_L\nu_R + v\bar{\nu}_R\nu_L}_{\text{Dirac Mass}} + \underbrace{\bar{\nu}_L H\nu_R + \bar{\nu}_R H\nu_L}_{\nu\text{-Higgs Interaction}} \right] \quad (\text{G.38})$$

$$= -\frac{g_\nu}{\sqrt{2}} \left[v\bar{\nu}\nu + \bar{\nu}H\nu \right] \quad (\text{G.39})$$

Summarily, to give the electron-neutrino $SU(2)$ doublet mass (as well as the other lepton and quark doublets), we are adding more terms to the lagrangian derived at the end of section F of the form:

$$\mathcal{L}_{f,\text{Higgs}} = \sum_{l=e,\mu,\tau} \left[-\frac{g_l}{\sqrt{2}} \left[v\bar{l}l + \bar{l}Hl \right] - \frac{g_{\nu_l}}{\sqrt{2}} \left[v\bar{\nu}_l\nu_l + \bar{\nu}_l H\nu_l \right] \right] \quad (\text{G.40})$$

for the three lepton generations and similar terms for the three quark doublets. Because of the Higgs mechanism, we now have sensible masses for Standard Model particles.

Appendix H: The Higgs Sector in Standard Model Electroweak Physics

Let's refer back to section E, line E.15. We shall now see the details of how we go from the postulated $SU(2) \times U(1)$ invariant lagrangian for a scalar particle to a form that determines the physics it implies.

Recall the lagrangian for the (scalar) Higgs sector is

$$\mathcal{L} = (D_\mu \phi)^\dagger (D^\mu \phi) + m_0^2 \phi^\dagger \phi - \frac{\lambda}{4} (\phi^\dagger \phi)^2 - \frac{1}{4} \vec{F}_{\mu\nu} \cdot \vec{F}^{\mu\nu} - \frac{1}{4} G_{\mu\nu} G^{\mu\nu} \quad (\text{H.1})$$

$$(\text{H.2})$$

for

$$\vec{F}^{\mu\nu} = \partial^\mu \vec{W}^\nu - \partial^\nu \vec{W}^\mu - g \vec{W}^\mu \times \vec{W}^\nu \quad (\text{H.3})$$

$$G^{\mu\nu} = \partial^\mu B^\nu - \partial^\nu B^\mu \quad (\text{H.4})$$

$$D^\mu \phi = \left(\partial^\mu + \underbrace{\frac{ig}{2} \vec{\tau} \cdot \vec{W}^\mu}_{SU(2)\text{piece}} + \underbrace{\frac{ig'Y}{2} B^\mu}_{U(1)\text{piece}} \right) \phi \quad (\text{H.5})$$

Consider only the first term for now.

$$(D^\mu \phi)^\dagger (D^\mu \phi) = \left(\partial_\mu \phi + \frac{ig}{2} \vec{\tau} \cdot \vec{W}_\mu \phi + \frac{ig'Y}{2} B_\mu \phi \right)^\dagger \left(\partial^\mu \phi + \frac{ig}{2} \vec{\tau} \cdot \vec{W}^\mu \phi + \frac{ig'Y}{2} B^\mu \phi \right) \quad (\text{H.6})$$

$$= (\partial_\mu \phi)^\dagger (\partial^\mu \phi) \quad (\text{H.7})$$

$$+ (\partial_\mu \phi)^\dagger \left(\frac{ig}{2} \vec{\tau} \cdot \vec{W}^\mu \phi + \frac{ig'Y}{2} B^\mu \phi \right) + \left(\frac{ig}{2} \vec{\tau} \cdot \vec{W}_\mu \phi + \frac{ig'Y}{2} B_\mu \phi \right)^\dagger (\partial^\mu \phi) \quad (\text{H.8})$$

$$+ \left[\frac{ig}{2} \vec{\tau} \cdot \vec{W}_\mu \phi + \frac{ig'Y}{2} B_\mu \phi \right]^\dagger \left[\frac{ig}{2} \vec{\tau} \cdot \vec{W}^\mu \phi + \frac{ig'Y}{2} B^\mu \phi \right] \quad (\text{H.9})$$

Now let's work on the last line of this. Note that in my expression of the Higgs doublet I'll be skipping straight to vacuum expectation values.

$$\frac{ig}{2}\vec{\tau} \cdot \vec{W}_\mu \phi + \frac{ig'Y}{2}B_\mu \phi = \frac{ig}{2} \left[\begin{bmatrix} 0 & 1 \\ 1 & 0 \end{bmatrix} W_{1\mu} + \begin{bmatrix} 0 & -i \\ i & 0 \end{bmatrix} W_{2\mu} + \begin{bmatrix} 1 & 0 \\ 0 & -1 \end{bmatrix} W_{3\mu} \right] \quad (\text{H.10})$$

$$\cdot \begin{bmatrix} 0 \\ \frac{1}{\sqrt{2}}(v+H) \end{bmatrix} + \frac{ig'Y}{2}B_\mu \begin{bmatrix} 0 \\ \frac{1}{\sqrt{2}}(v+H) \end{bmatrix} \quad (\text{H.11})$$

$$(\text{H.12})$$

$$= \frac{ig}{2} \left[\begin{bmatrix} \frac{1}{\sqrt{2}}W_{1\mu}(v+H) \\ 0 \end{bmatrix} + \begin{bmatrix} \frac{-i}{\sqrt{2}}W_{2\mu}(v+H) \\ 0 \end{bmatrix} + \begin{bmatrix} 0 \\ \frac{-1}{\sqrt{2}}W_{3\mu}(v+H) \end{bmatrix} \right] \quad (\text{H.13})$$

$$+ \begin{bmatrix} 0 \\ \frac{ig'Y}{2\sqrt{2}}B_\mu(v+H) \end{bmatrix} \quad (\text{H.14})$$

$$= \begin{bmatrix} \frac{ig}{2\sqrt{2}}W_{1\mu}(v+H) + \frac{g}{2\sqrt{2}}W_{2\mu}(v+H) \\ \frac{-ig}{2\sqrt{2}}W_{3\mu}(v+H) + \frac{ig'Y}{2\sqrt{2}}B_\mu(v+H) \end{bmatrix} \quad (\text{H.15})$$

$$= \begin{bmatrix} \frac{ig}{2}(W_{1\mu} - iW_{2\mu})\frac{1}{\sqrt{2}}(v+H) \\ -\frac{ig}{2}W_{3\mu}\frac{1}{\sqrt{2}}(v+H) + \frac{ig'Y}{2}B_\mu\frac{1}{\sqrt{2}}(v+H) \end{bmatrix} \quad (\text{H.16})$$

Next, multiply this by it's Hermitian conjugate from the left:

$$\left[-\frac{ig}{2}(W_{1\mu} + iW_{2\mu})\frac{1}{\sqrt{2}}(v + H) \quad \frac{ig}{2}W_{3\mu}\frac{1}{\sqrt{2}}(v + H) - \frac{ig'Y}{2}B_\mu\frac{1}{\sqrt{2}}(v + H) \right] \quad (\text{H.17})$$

$$\left[\begin{array}{c} \frac{ig}{2}(W_1^\mu - iW_2^\mu)\frac{1}{\sqrt{2}}(v + H) \\ -\frac{ig}{2}W_3^\mu\frac{1}{\sqrt{2}}(v + H) + \frac{ig'Y}{2}B^\mu\frac{1}{\sqrt{2}}(v + H) \end{array} \right] \quad (\text{H.18})$$

$$= \frac{g^2}{4}|W_1 - iW_2|^2\frac{1}{2}(v + H)^2 + \frac{g^2}{4}|W_3|^2\frac{1}{2}(v + H)^2 - \frac{gg'Y}{4}W_{3\mu}B^\mu\frac{1}{2}(v + H)^2 \quad (\text{H.19})$$

$$- \frac{gg'Y}{4}W_3^\mu B_\mu\frac{1}{2}(v + H)^2 + \frac{g'^2Y^2}{4}|B|^2\frac{1}{2}(v + H)^2 \quad (\text{H.20})$$

$$= \frac{g^2}{4}W_\mu^\dagger W^\mu v^2 + \frac{g^2}{2}W_\mu^\dagger W_\mu vH + \frac{g^2}{4}W_\mu^\dagger W^\mu H + \frac{g^2}{8}|W_3|^2v^2 + \frac{g^2}{4}|W_3|^2vH + \frac{g^2}{8}|W_3|^2H^2 \quad (\text{H.21})$$

$$- \frac{gg'Y}{4}W_{3\mu}B^\mu v^2 - \frac{gg'Y}{2}W_{3\mu}B^\mu vH - \frac{gg'Y}{2}W_{3\mu}B^\mu H^2 \quad (\text{H.22})$$

$$+ \frac{g'^2Y^2}{8}|B|^2v^2 + \frac{g'^2Y^2}{4}|B|^2vH + \frac{g'^2Y^2}{8}|B|^2H^2 \quad (\text{H.23})$$

Now we have mass terms for the gauge boson fields and interaction terms among the gauge and Higgs bosons. With that done, let's go back and deal with the terms from lines H.7 and H.8.

$$(\partial_\mu\phi)^\dagger(\partial^\mu\phi) = \left[0 \quad \frac{1}{\sqrt{2}}(\partial_\mu v + \partial_\mu H) \right] \left[\begin{array}{c} 0 \\ \frac{1}{\sqrt{2}}(\partial_\mu v + \partial_\mu H) \end{array} \right] = \frac{1}{2}(\partial_\mu H)(\partial^\mu H) \quad (\text{H.24})$$

$$(\partial_\mu\phi)^\dagger \left(\frac{ig}{2}\vec{\tau} \cdot \vec{W}^\mu\phi + \frac{ig'Y}{2}B^\mu\phi \right) = -\frac{ig}{4}(\partial_\mu H)W_3^\mu(v + H) + \frac{ig'Y}{2}(\partial_\mu H)B^\mu(v + H) \quad (\text{H.25})$$

$$\left(\frac{ig}{2}\vec{\tau} \cdot \vec{W}^\mu\phi + \frac{ig'Y}{2}B^\mu\phi \right)^\dagger (\partial^\mu\phi) = \frac{ig}{4}W_{3\mu}(v + H)(\partial^\mu H) - \frac{ig'Y}{4}B_\mu(v + H)(\partial^\mu H) \quad (\text{H.26})$$

We are now ready to put the first term of the lagrangian back together.

$$(D_\mu \phi)^\dagger (D^\mu \phi) = \frac{1}{2}(\partial_\mu H)(\partial^\mu H) - \frac{ig}{4}(\partial_\mu H)W_3^\mu(v+H) + \frac{ig'Y}{4}(\partial_\mu H)B^\mu(v+H) \quad (\text{H.27})$$

$$+ \frac{ig}{4}W_{3\mu}(v+H)(\partial^\mu H) - \frac{ig'Y}{4}B_\mu(v+H)(\partial^\mu H) \quad (\text{H.28})$$

$$+ \frac{g^2}{4}W_\mu^\dagger W^\mu v^2 + \frac{g^2}{2}W_\mu^\dagger W^\mu vH + \frac{g^2}{4}W_\mu^\dagger W^\mu H^2 \quad (\text{H.29})$$

$$+ \frac{g^2}{8}|W_3|^2 v^2 + \frac{g^2}{4}|W_3|^2 vH + \frac{g^2}{8}|W_3|^2 H^2 \quad (\text{H.30})$$

$$- \frac{gg'Y}{4}W_{3\mu}B^\mu v^2 - \frac{gg'Y}{4}W_{3\mu}B^\mu vH - \frac{gg'Y}{4}W_{3\mu}B^\mu H^2 \quad (\text{H.31})$$

$$+ \frac{g'^2Y}{8}|B|^2 v^2 + \frac{g'^2Y}{4}|B|^2 vH + \frac{g'^2Y}{8}|B|^2 H^2 \quad (\text{H.32})$$

And the $SU(2)$ gauge fields kinetic terms:

$$\vec{F}_{\mu\nu} \cdot \vec{F}^{\mu\nu} = (\partial_\mu \vec{W}_\nu - \partial_\nu \vec{W}_\mu - g\vec{W}_\mu \times \vec{W}_\nu) \cdot (\partial^\mu \vec{W}^\nu - \partial^\nu \vec{W}^\mu - g\vec{W}^\mu \times \vec{W}^\nu) \quad (\text{H.33})$$

$$= (\partial_\mu \vec{W}_\nu - \partial_\nu \vec{W}_\mu) \cdot (\partial^\mu \vec{W}^\nu - \partial^\nu \vec{W}^\mu) - g(\partial_\mu \vec{W}_\nu - \partial_\nu \vec{W}_\mu) \cdot (\vec{W}^\mu \times \vec{W}^\nu) \quad (\text{H.34})$$

$$- g(\vec{W}_\mu \times \vec{W}_\nu) \cdot (\partial^\mu \vec{W}^\nu - \partial^\nu \vec{W}^\mu) + g^2(\vec{W}_\mu \times \vec{W}_\nu) \cdot (\vec{W}^\mu \times \vec{W}^\nu) \quad (\text{H.35})$$

$$= (\partial_\mu \vec{W}_\nu - \partial_\nu \vec{W}_\mu) \cdot (\partial^\mu \vec{W}^\nu - \partial^\nu \vec{W}^\mu) - 2g(\vec{W}_\mu \times \vec{W}_\nu) \cdot (\partial^\mu \vec{W}^\nu - \partial^\nu \vec{W}^\mu) \quad (\text{H.36})$$

$$+ g^2 \left[|W_\mu|^2 |W_\nu|^2 - |\vec{W}_\mu \cdot \vec{W}_\nu|^2 \right] \quad (\text{H.37})$$

$$(\text{H.38})$$

Now we're ready to put the lagrangian back together. After a little algebra:

$$\mathcal{L} = \underbrace{\frac{1}{2}(\partial_\mu H)(\partial^\mu H) + \frac{1}{2}m_0^2(v+H)^2 - \frac{\lambda}{16}(v+H)^4}_{\text{Higgs kinetic, mass, and self-interaction terms}} \quad (\text{H.39})$$

$$- \underbrace{\frac{1}{4}(\partial_\mu W_{1\nu} - \partial_\nu W_{1\mu})(\partial^\mu W_1^\nu - \partial^\nu W_1^\mu) - \frac{1}{4}(\partial_\mu W_{2\nu} - \partial_\nu W_{2\mu})(\partial^\mu W_2^\nu - \partial^\nu W_2^\mu)}_{W^\pm \text{ kinetic terms}} \quad (\text{H.40})$$

$$- \frac{1}{4}(\partial_\mu W_{3\nu} - \partial_\nu W_{3\mu})(\partial^\mu W_3^\nu - \partial^\nu W_3^\mu) - \frac{1}{4}G_{\mu\nu}G^{\mu\nu} \quad (\text{H.41})$$

$$+ \underbrace{\frac{1}{8}v^2(gW_{3\mu} - g'YB_\mu)(gW_3^\mu - g'YB^\mu)}_{\text{Terms that become the } Z\text{-boson and photon}} \quad (\text{H.42})$$

$$+ \frac{g^2v^2}{4}W_\mu^\dagger W^\mu + \frac{g^2v}{2}W_\mu^\dagger W^\mu H + \frac{g^2}{4}W_\mu^\dagger W^\mu H^2 + \frac{g^2v}{4}|W_3|^2H + \frac{g^2}{8}|W_3|^2H^2 \quad (\text{H.43})$$

$$- \underbrace{\frac{gg'Yv}{2}W_{3\mu}B^\mu H - \frac{gg'Y}{2}W_{3\mu}B^\mu H^2 + \frac{g'^2Y^2v}{4}|B|^2H + \frac{g'^2Y^2}{8}|B|^2H^2}_{W^\pm \text{ mass, trilinear, quadrilinear couplings with the Higgs}} \quad (\text{H.44})$$

$$\underbrace{\frac{1}{2}g(\vec{W}_\mu \times \vec{W}_\nu) \cdot (\partial^\mu \vec{W}^\mu - \partial^\nu \vec{W}^\mu) - \frac{1}{4}g^2 \left[|W_\mu|^2 |W_\nu|^2 - |\vec{W}_\mu \cdot \vec{W}_\nu|^2 \right]}_{\text{Quadrilinear couplings among the gauge bosons}} \quad (\text{H.45})$$

Appendix I: WH Production Amplitude

The Tevatron consists of a proton beam colliding with an antiproton beam. So let's consider this interaction when an up quark interacts with an anti-down quark; the interaction of an anti-up quark with a down quark follows analogously. The full Lagrangian for the interaction is the sum of the Higgs Sector of the Standard Model Lagrangian with the Lagrangian for a quark doublet.

$$\mathcal{L} = \underbrace{\frac{1}{2} (\partial_\mu H) (\partial^\mu H) + \frac{1}{2} \mu^2 H^2 + \frac{g^2 v^2}{4} W_\mu^\dagger W^\mu + \frac{g^2 v}{2} W_\mu^\dagger W^\mu H}_{\text{Higgs Sector}} \quad (\text{I.1})$$

$$\underbrace{-\frac{1}{4} \sum_{i=1,2} (\partial_\mu W_{i\nu} - \partial_\nu W_{i\mu}) (\partial^\mu W_i^\nu - \partial^\nu W_i^\mu)}_{\text{W boson kinetic terms}} \quad (\text{I.2})$$

$$\underbrace{+ i \bar{u} \gamma_\rho \left(\frac{1 - \gamma_5}{2} \right) \partial^\rho u + i \bar{d} \gamma_\rho \left(\frac{1 - \gamma_5}{2} \right) \partial^\rho d + \frac{g V_{ud}}{\sqrt{2}} \bar{d} \gamma_\rho W^{\rho\dagger} \left(\frac{1 - \gamma_5}{2} \right) u}_{\text{Quark Doublet}} \quad (\text{I.3})$$

To calculate the cross section for this interaction, I want the interaction Lagrangian, which is found by just collecting the interaction terms in the above Lagrangian.

$$\mathcal{L}_I = \frac{g^2 v}{2} W_\mu^\dagger W^\mu H + \frac{g V_{ud}}{\sqrt{2}} \bar{d} \gamma_\rho W^{\rho\dagger} \left(\frac{1 - \gamma_5}{2} \right) u \quad (\text{I.4})$$

I would like to change the form of the coefficients to be expressed in terms of the W mass and electric charge. Using $m_W = \frac{gv}{2}$ and $e_0 = g \sin \theta_W$,

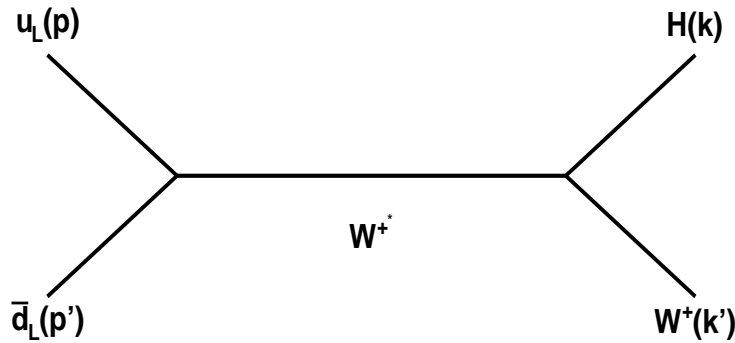


Figure I.1 Associated Production with a W boson

$$\mathcal{L}_I = \frac{2m_W^2}{v} W_\mu^\dagger W^\mu H + \frac{e_0 V_{ud}}{\sqrt{2} \sin \theta_W} \bar{d} \gamma_\rho W^{\rho\dagger} \left(\frac{1 - \gamma_5}{2} \right) u \quad (\text{I.5})$$

Later, I'll re-express the leftover v in terms of the Fermi Coupling Constant $G_F = \sqrt{2}/2v^2$. This way, I'll be able to express the cross section in terms of measured quantities.

From the interaction Lagrangian density I need the interaction Hamiltonian density.

$$\mathcal{H}_I(x) = \pi(x) \dot{\Phi}(x) - \mathcal{L}_I(x) \quad (\text{I.6})$$

where $\Phi(x)$ is a position-space field and $\pi(x)$ is its conjugate momentum field. However, in this case there are no time-derivatives of fields in the interaction Lagrangian density. So it is simply

$$\mathcal{H}_I(x) = -\mathcal{L}(x) \quad (\text{I.7})$$

$$= - \underbrace{\frac{2m_W^2}{v} W_\mu^\dagger W^\mu H}_{\mathcal{H}_{IH}(x)} - \underbrace{\frac{e_0 V_{ud}}{\sqrt{2} \sin \theta_W} \bar{d} \gamma_\rho W^{\rho\dagger} \left(\frac{1 - \gamma_5}{2} \right) u}_{\mathcal{H}_{Iq}(x)} \quad (\text{I.8})$$

$$\Rightarrow \mathcal{H}_I(x) = \mathcal{H}_{IH}(x) + \mathcal{H}_{Iq}(x) \quad (\text{I.9})$$

The scattering matrix for this interaction is [45]

$$\langle k'; k | S | p'; p \rangle = \langle k'; k | 1 | p'; p \rangle + i \langle k'; k | T | p'; p \rangle \quad (\text{I.10})$$

where we recall that the scattering matrix is defined as the time-evolution operator as $t \rightarrow \infty$.

$$\langle k'; k | S | p'; p \rangle = \lim_{t \rightarrow \infty} \langle k'; k | e^{iH(2t)} | p'; p \rangle \quad (\text{I.11})$$

The interaction component here is what I want to calculate. From (4.90) Peskin and Schroeder [45]

$$i \langle k'; k | T | p'; p \rangle = \lim_{t \rightarrow \infty (1-i\varepsilon)} \langle k'; k | T \exp \left[-i \int_{-t}^t dt' H_I(t') \right] | p'; p \rangle \quad (\text{I.12})$$

That exponential expands as (from (4.22) Peskin and Schroeder [45]):

$$T \exp \left[-i \int_{-t}^t dt' H_I(t') \right] = 1 + (-i) \int_{-t}^t dt_1 H_I(t_1) + \frac{(-i)^2}{2!} \int_{-t}^t \int_{-t}^t dt_1 dt_2 T [H_I(t_1) H_I(t_2)] + \dots \quad (\text{I.13})$$

As we are beginning and ending with two particle states, the second order term is the first that can contribute to this interaction, and any higher-order terms contain loops that we do not address here. The interaction part of the scattering matrix element becomes

$$i\langle k'; k | T | p'; p \rangle \cong \langle k'; k | \frac{(-i)^2}{2!} \int \int_{-t}^t dt_1 dt_2 T [H_I(x_1) H_I(x_2)] | p'; p \rangle \quad (\text{I.14})$$

where $H_I(x) = \int d^3\vec{x} \mathcal{H}_I(x) = \int d^3\vec{x} [\mathcal{H}_{IH}(x) + \mathcal{H}_{Iq}(x)]$, and in the Hamiltonian I replaced the variable t with full spacetime variable $x = (t, x_1, x_2, x_3)$ because all components now come into play.

$$= \langle k'; k | \frac{(-i)^2}{2} \int \int dt_1 dt_2 T \left[\int d^3\vec{x}_1 \mathcal{H}_I(x_1) \int d^3\vec{x}_2 \mathcal{H}_I(x_2) \right] | p'; p \rangle \quad (\text{I.15})$$

$$= \langle k'; k | \frac{(-i)^2}{2} T \left[\int d^4x_1 \mathcal{H}_I(x_1) \int d^4x_2 \mathcal{H}_I(x_2) \right] | p'; p \rangle \quad (\text{I.16})$$

$$= \frac{(-i)^2}{2} \int \int d^4x_1 d^4x_2 \langle k'; k | T [\mathcal{H}_I(x_1) \mathcal{H}_I(x_2)] | p'; p \rangle \quad (\text{I.17})$$

$$= \frac{(-i)^2}{2} \int \int d^4x_1 d^4x_2 \langle k'; k | T [\mathcal{H}_{IH}(x_1) \mathcal{H}_{IH}(x_2) + \mathcal{H}_{IH}(x_1) \mathcal{H}_{Iq}(x_2) + \mathcal{H}_{Iq}(x_1) \mathcal{H}_{IH}(x_2) + \mathcal{H}_{Iq}(x_1) \mathcal{H}_{Iq}(x_2)] | p'; p \rangle \quad (\text{I.18})$$

$$\quad \quad \quad \mathcal{H}_{Iq}(x_1) \mathcal{H}_{IH}(x_2) + \mathcal{H}_{Iq}(x_1) \mathcal{H}_{Iq}(x_2)] | p'; p \rangle \quad (\text{I.19})$$

Since I have an interaction that involves both the quark doublet and the Higgs, the $\mathcal{H}_{IH}(x_1) \mathcal{H}_{IH}(x_2)$ and $\mathcal{H}_{Iq}(x_1) \mathcal{H}_{Iq}(x_2)$ terms do not contribute.

$$= \frac{(-i)^2}{2} \int \int d^4x_1 d^4x_2 \langle k'; k | T [\mathcal{H}_{IH}(x_1) \mathcal{H}_{Iq}(x_2) + \mathcal{H}_{Iq}(x_1) \mathcal{H}_{IH}(x_2)] | p'; p \rangle \quad (\text{I.20})$$

Next, I have to calculate these two time-ordered products inside the brackets. Using terms from expression I.9 above,

$$T [\mathcal{H}_{Iq}(x_1) \mathcal{H}_{IH}(x_2)] = \frac{2e_0 m_W^2 V_{ud}}{v \sqrt{2} \sin \theta_W} T \left[W_\mu^\dagger(x_1) W^\mu(x_1) H(x_1) \bar{d}(x_2) W^\dagger(x_2) \left(\frac{1 - \gamma_5}{2} \right) u(x_2) \right] \quad (\text{I.21})$$

$$= \frac{2e_0 m_W^2 V_{ud}}{v \sqrt{2} \sin \theta_W} N [W_\mu^\dagger(x_1) W^\mu(x_1) H(x_1) \bar{d}(x_2) W^\dagger(x_2) \left(\frac{1 - \gamma_5}{2} \right) u(x_2)] \quad (\text{I.22})$$

$$+ \text{all contractions}] \quad (\text{I.23})$$

The N operator indicates we explore all possible combination of field contractions, most of which vanish as irrelevant. Field contractions will be expressed notationally as $\overline{A(x)B(x)C(x)}$ to contract

field A with field C .

$$= \frac{2e_0 m_W^2 V_{ud}}{v\sqrt{2} \sin \theta_W} N[W_\mu^\dagger(x_1) W^\mu(x_1) H(x_1) \bar{d}(x_2) W^\dagger(x_2) \left(\frac{1-\gamma_5}{2}\right) u(x_2)] \quad (\text{I.24})$$

$$+ \overline{W_\mu^\dagger(x_1) W^\mu(x_1)} H(x_1) \bar{d}(x_2) W^\dagger(x_2) \left(\frac{1-\gamma_5}{2}\right) u(x_2) \quad (\text{I.25})$$

$$+ \overline{W_\mu^\dagger(x_1) W^\mu(x_1) H(x_1)} \bar{d}(x_2) W^\dagger(x_2) \left(\frac{1-\gamma_5}{2}\right) u(x_2) \quad (\text{I.26})$$

$$+ \overline{W_\mu^\dagger(x_1) W^\mu(x_1) H(x_1) \bar{d}(x_2)} W^\dagger(x_2) \left(\frac{1-\gamma_5}{2}\right) u(x_2) \quad (\text{I.27})$$

$$+ \overline{W_\mu^\dagger(x_1) W^\mu(x_1) H(x_1) \bar{d}(x_2) W^\dagger(x_2)} \left(\frac{1-\gamma_5}{2}\right) u(x_2) \quad (\text{I.28})$$

$$+ \overline{W_\mu^\dagger(x_1) W^\mu(x_1) H(x_1) \bar{d}(x_2) W^\dagger(x_2) \left(\frac{1-\gamma_5}{2}\right) u(x_2)} \quad (\text{I.29})$$

$$+ W_\mu^\dagger(x_1) \overline{W^\mu(x_1) H(x_1)} \bar{d}(x_2) W^\dagger(x_2) \left(\frac{1-\gamma_5}{2}\right) u(x_2) \quad (\text{I.30})$$

$$+ W_\mu^\dagger(x_1) \overline{W^\mu(x_1) H(x_1) \bar{d}(x_2)} W^\dagger(x_2) \left(\frac{1-\gamma_5}{2}\right) u(x_2) \quad (\text{I.31})$$

$$+ W_\mu^\dagger(x_1) \overline{W^\mu(x_1) H(x_1) \bar{d}(x_2) W^\dagger(x_2)} \left(\frac{1-\gamma_5}{2}\right) u(x_2) \quad (\text{I.32})$$

$$+ W_\mu^\dagger(x_1) \overline{W^\mu(x_1) H(x_1) \bar{d}(x_2) W^\dagger(x_2) \left(\frac{1-\gamma_5}{2}\right) u(x_2)} \quad (\text{I.33})$$

$$+ W_\mu^\dagger(x_1) W^\mu(x_1) \overline{H(x_1) \bar{d}(x_2)} W^\dagger(x_2) \left(\frac{1-\gamma_5}{2}\right) u(x_2) \quad (\text{I.34})$$

$$+ W_\mu^\dagger(x_1) W^\mu(x_1) \overline{H(x_1) \bar{d}(x_2) W^\dagger(x_2)} \left(\frac{1-\gamma_5}{2}\right) u(x_2) \quad (\text{I.35})$$

$$+ W_\mu^\dagger(x_1) W^\mu(x_1) \overline{H(x_1) \bar{d}(x_2) W^\dagger(x_2) \left(\frac{1-\gamma_5}{2}\right) u(x_2)} \quad (\text{I.36})$$

$$+ W_\mu^\dagger(x_1) W^\mu(x_1) H(x_1) \overline{\bar{d}(x_2) W^\dagger(x_2)} \left(\frac{1-\gamma_5}{2}\right) u(x_2) \quad (\text{I.37})$$

$$+ W_\mu^\dagger(x_1) W^\mu(x_1) H(x_1) \overline{\bar{d}(x_2) W^\dagger(x_2) \left(\frac{1-\gamma_5}{2}\right) u(x_2)} \quad (\text{I.38})$$

$$+ W_\mu^\dagger(x_1) W^\mu(x_1) H(x_1) \bar{d}(x_2) \overline{W^\dagger(x_2) \left(\frac{1-\gamma_5}{2}\right) u(x_2)} \quad (\text{I.39})$$

$$+ \text{terms with more than one contraction}] \quad (\text{I.40})$$

There some important characteristics to note which will greatly simplify this mess:

- Since we are dealing only with the tree-level production process, terms with more than one contraction are automatically irrelevant.
- Contracted fields at the same spacetime coordinate constitute loops so they are not involved in tree-level interactions.
- Contractions between fields of different types vanish. Physically, the contracted fields are the propagator in the feynman diagram.
- If there are no contractions of a particular field at x_1 with a field at x_2 , then there is no interaction between the initial and final states.
- The initial and final particle fields must be uncontracted. They contract with the initial and final state vectors later.

Hence, the only term left is the one that contracts $W^\mu(x_1)$ to $W^{\nu\dagger}(x_2)$ in expression I.28– this establishes the physical propagation of a W -boson field from spacetime coordinate x_1 to x_2 . Notice that this is the only transition from initial to final states possible at tree-level.

Taking a step back to expression I.20, here's where we are:

$$i\langle k'; k | T | p'; p \rangle = \frac{(-i)^2 e_0 m_W^2 V_{ud}}{v\sqrt{2} \sin \theta_W} \iint d^4 x_1 d^4 x_2 \quad (\text{I.41})$$

$$\langle k'; k | [W_\mu^\dagger(x_1) \overline{W^\mu(x_1) H(x_1) \bar{d}(x_2) \gamma_\rho W^{\rho\dagger}(x_2)} \left(\frac{1 - \gamma_5}{2} \right) u(x_2) \quad (\text{I.42})$$

$$+ \overline{\bar{d}(x_1) \gamma_\rho W^{\rho\dagger}(x_1) \left(\frac{1 - \gamma_5}{2} \right) u(x_1) W_\mu^\dagger(x_2) W^\mu(x_2) H(x_2)} | p'; p \rangle \quad (\text{I.43})$$

$$i\langle k'; k | T | p'; p \rangle = \frac{(-i)^2 e_0 m_W^2 V_{ud}}{v\sqrt{2} \sin \theta_W} \times \iint d^4 x_1 d^4 x_2 \quad (\text{I.44})$$

$$\overline{\langle k'; k | W_\mu^\dagger(x_1) W^\mu(x_1) H(x_1) \bar{d}(x_2) \gamma_\rho W^{\rho\dagger}(x_2) \left(\frac{1 - \gamma_5}{2} \right) u(x_2) | p'; p \rangle} \quad (\text{I.45})$$

$$+ \frac{(-i)^2 e_0 m_W^2 V_{ud}}{v\sqrt{2} \sin \theta_W} \times \iint d^4 x_1 d^4 x_2 \quad (\text{I.46})$$

$$\overline{\langle k'; k | \bar{d}(x_1) \gamma_\rho W^{\rho\dagger}(x_1) \left(\frac{1 - \gamma_5}{2} \right) u(x_1) W_\mu^\dagger(x_2) W^\mu(x_2) H(x_2) | p'; p \rangle} \quad (\text{I.47})$$

The two terms cover two Feynman diagrams:

- u and \bar{d} quarks interact at spacetime coordinate x_1 to become a virtual W^+ , which then radiates a Higgs boson at spacetime coordinate x_2 .
- The same situation with spacetime coordinates x_1 and x_2 reversed.

The uncontracted terms now contract with the initial and final state vectors, corresponding physically to the incoming and outgoing particles of the Feynman diagram. They contract as follows:

$$\overline{\langle k' | W_\mu^\dagger(x)} = \langle 0 | \epsilon_\mu^{s*}(k') e^{ik' \cdot x} \quad (\text{I.48})$$

$$\overline{\langle k | H(x)} = \langle 0 | e^{ik \cdot x} \quad (\text{I.49})$$

$$\overline{\langle \bar{d}(x) | p' \rangle} = e^{-ip' \cdot x} \bar{d}^{r_1}(p') | 0 \rangle \quad (\text{I.50})$$

$$\overline{\langle u(x) | p \rangle} = e^{-ip \cdot x} u^{r_2}(p) | 0 \rangle \quad (\text{I.51})$$

where r_1, r_2 are the fermion spins.

In position-space, the W propagator includes an integral over the momentum q :

$$\overline{W^{\rho\dagger}(x_1) W^\mu(x_2)} = \int \frac{d^4 q}{(2\pi)^4} i \left[\frac{-g^{\mu\rho} + \frac{q^\mu q^\rho}{m_W^2}}{q^2 - m_W^2 + i\varepsilon} \right] e^{-iq \cdot (x_1 - x_2)} \quad (\text{I.52})$$

$$(\text{I.53})$$

Let's make the replacements in the scattering matrix.

$$i\langle k'; k | T | p'; p \rangle = \frac{(-i)^2 e_0 m_W^2 V_{ud}}{v\sqrt{2} \sin \theta_W} \times \quad (\text{I.54})$$

$$\iint d^4 x_1 d^4 x_2 \underbrace{[\langle 0 | \epsilon_\mu^{s*}(k') e^{ik' \cdot x_1} \rangle]_{W^\dagger}}_{W^\dagger} \underbrace{\langle 0 | e^{ik \cdot x_1} \rangle_H}_H \underbrace{\int \frac{d^4 q}{(2\pi)^4} i \left[\frac{-g^{\mu\rho} + \frac{q^\mu q^\rho}{m_W^2}}{q^2 - m_W^2 + i\varepsilon} \right] e^{-iq \cdot (x_2 - x_1)}}_{W\text{-propagator}} \quad (\text{I.55})$$

$$\underbrace{e^{-ip' \cdot x_2} \bar{d}^{r_1}(p') | 0 \rangle}_{\bar{d}} \gamma_\rho \left(\frac{1 - \gamma_5}{2} \right) \underbrace{e^{-ip \cdot x_2} u^{r_2}(p) | 0 \rangle}_u \quad (\text{I.56})$$

$$+ \frac{(-i)^2 e_0 m_W^2 V_{ud}}{v\sqrt{2} \sin \theta_W} \times \quad (\text{I.57})$$

$$\iint d^4 x_1 d^4 x_2 \underbrace{[e^{-ip' \cdot x_1} \bar{d}^{r_1}(p') | 0 \rangle]_{\bar{d}}}_{\bar{d}} \gamma_\rho \underbrace{\int \frac{d^4 q}{(2\pi)^4} i \left[\frac{-g^{\mu\rho} + \frac{q^\mu q^\rho}{m_W^2}}{q^2 - m_W^2 + i\varepsilon} \right] e^{-iq \cdot (x_1 - x_2)}}_{W\text{-propagator}} \left(\frac{1 - \gamma_5}{2} \right) \quad (\text{I.58})$$

$$\underbrace{e^{-ip \cdot x_1} u^{r_2}(p) | 0 \rangle}_u \underbrace{\langle 0 | \epsilon_\mu^{s*}(k') e^{ik' \cdot x_2} \rangle_{W^\dagger}}_{W^\dagger} \underbrace{\langle 0 | e^{ik \cdot x_2} \rangle_H}_H \quad (\text{I.59})$$

Integrating x_1 and x_2 over the exponentials is the very definition—or one of many—of a 4-dim Dirac delta function.

$$i\langle k'; k | T | p'; p \rangle = \left[\frac{i(-i)^2 e_0 m_W^2 V_{ud}}{v\sqrt{2} \sin \theta_W} \right] \int d^4 q \epsilon_\mu^{s*}(k') \left[\frac{-g^{\mu\rho} + \frac{q^\mu q^\rho}{m_W^2}}{q^2 - m_W^2 + i\varepsilon} \right] \bar{d}^{r_1}(p') \quad (\text{I.60})$$

$$\gamma_\rho \left(\frac{1 - \gamma_5}{2} \right) u^{r_2}(p) (2\pi)^4 \delta^4(-k' - k - q) \delta^4(p' + p + q) \quad (\text{I.61})$$

$$+ \left[\frac{i(-i)^2 e_0 m_W^2 V_{ud}}{v\sqrt{2} \sin \theta_W} \right] \int d^4 q \bar{d}^{r_1}(p') \gamma_\rho \left(\frac{1 - \gamma_5}{2} \right) u^{r_2}(p) \quad (\text{I.62})$$

$$\left[\frac{-g^{\mu\rho} + \frac{q^\mu q^\rho}{m_W^2}}{q^2 - m_W^2 + i\varepsilon} \right] \epsilon_\mu^{s*}(k') (2\pi)^4 \delta^4(-k' - k - q) \delta^4(p' + p + q) \quad (\text{I.63})$$

$$i\langle k'; k | T | p'; p \rangle = \left[\frac{i(-i)^2 e_0 m_W^2 V_{ud}}{v\sqrt{2} \sin \theta_W} \right] (2\pi)^4 \epsilon_\mu^{s*}(k') \left[\frac{-g^{\mu\rho} + \frac{q^\mu q^\rho}{m_W^2}}{q^2 - m_W^2 + i\varepsilon} \right] \bar{d}^{r_1}(p') \gamma_\rho \quad (\text{I.64})$$

$$\left(\frac{1 - \gamma_5}{2} \right) u^{r_2}(p) \delta^4(p' + p - k' - k) \quad (\text{I.65})$$

$$+ \left[\frac{i(-i)^2 e_0 m_W^2 V_{ud}}{v\sqrt{2} \sin \theta_W} \right] (2\pi)^4 \bar{d}^{r_1}(p') \gamma_\rho \left(\frac{1 - \gamma_5}{2} \right) u^{r_2}(p) \quad (\text{I.66})$$

$$\left[\frac{-g^{\mu\rho} + \frac{q^\mu q^\rho}{m_W^2}}{q^2 - m_W^2 + i\varepsilon} \right] \epsilon_\mu^{s*}(k') \delta^4(p' + p - k' - k) \quad (\text{I.67})$$

Now that the integral over q has been carried out over the δ -functions, it is understood that $q = k' + k = p' + p$ explicitly now.

$$i\langle k'; k | T | p'; p \rangle = \left[\frac{-2ie_0 m_W^2 V_{ud}}{v\sqrt{2} \sin \theta_W} \right] (2\pi)^4 \epsilon_\mu^{s*}(k') \left[\frac{-g^{\mu\rho} + \frac{q^\mu q^\rho}{m_W^2}}{q^2 - m_W^2 + i\varepsilon} \right] \quad (\text{I.68})$$

$$\bar{d}^{r_1}(p') \gamma_\rho \left(\frac{1 - \gamma_5}{2} \right) u^{r_2}(p) \delta^4(p' + p - k' - k) \quad (\text{I.69})$$

Recall from Peskin and Schroeder (4.73)[45]

$$i\langle k'; k | T | p'; p \rangle = (2\pi)^4 \delta^4(p' + p - k' - k) \cdot i\mathcal{M}(p', p \rightarrow k', k) \quad (\text{I.70})$$

Finally, the invariant amplitude for Higgs associated production with a W^+ -boson is

$$\boxed{i\mathcal{M} = \left[\frac{-2ie_0 m_W^2 V_{ud}}{v\sqrt{2} \sin \theta_W} \right] \epsilon_\mu^{s*}(k') \left[\frac{-g^{\mu\rho} + \frac{q^\mu q^\rho}{m_W^2}}{q^2 - m_W^2 + i\varepsilon} \right] \bar{d}^{r_1}(p') \gamma_\rho \left(\frac{1 - \gamma_5}{2} \right) u^{r_2}(p)} \quad (\text{I.71})$$

Appendix J: $H \rightarrow WW$ Lagrangian Density To Invariant Amplitude

For a Higgs boson decay to two W bosons, the Lagrangian density comes from the Higgs sector of the standard model Lagrangian. The Z boson and photon terms can be excluded.

$$\mathcal{L} = \underbrace{\frac{1}{2} (\partial_\mu H) (\partial^\mu H) + \frac{1}{2} \mu^2 H^2 + \frac{g^2 v^2}{4} W_\mu^\dagger W^\mu + \frac{g^2 v}{2} W_\mu^\dagger W^\mu H}_{\text{Higgs Sector}} - \underbrace{\frac{1}{4} \sum_{i=1,2} (\partial_\mu W_{i\nu} - \partial_\nu W_{i\mu}) (\partial^\mu W_i^\mu - \partial^\nu W_i^\nu)}_{\text{W boson kinetic terms}}$$

To calculate the invariant amplitude for the decay, I want the interaction Lagrangian.

$$\mathcal{L} = \frac{g^2 v}{2} W_\mu^\dagger W^\mu H$$

From this I need the interaction Hamiltonian density.

$$\mathcal{H}_I = \sum_{\text{fields}} \pi(x) \dot{\Phi}(x) - \mathcal{L}_I(x)$$

where $\Phi(x)$ is a position-space field and $\pi(x)$ is its conjugate momentum field. However, in this case there are no time-derivatives of fields in the interaction Lagrangian density. So it is simply

$$\begin{aligned} \mathcal{H}_I(x) &= -\mathcal{L} \\ &= -\frac{g^2 v}{2} W_\mu^\dagger W^\mu H \end{aligned}$$

The scattering matrix for this interaction is

$$\langle k_1, k_2 | S | p \rangle = \langle k_1, k_2 | 1 | p \rangle + i \langle k_1, k_2 | T | p \rangle$$

where we recall that the scattering matrix is defined as the time-evolution operator as $t \rightarrow \infty$.

$$\langle k_1, k_2 | S | p \rangle = \lim_{t \rightarrow \infty} \langle k_1, k_2 | e^{iH(2t)} | p \rangle$$

The interaction component here is what I want to calculate. From (4.90) Peskin,

$$i\langle k_1, k_2 | T | p \rangle = \lim_{t \rightarrow \infty(1-i\epsilon)} \langle k_1, k_2 | T \exp \left[-i \int_{-t}^t dt' H_I(t') \right] | p \rangle$$

That exponential expands as (from (4.22) Peskin)

$$T \exp \left[-i \int_{-t}^t dt' H_I(t') \right] = 1 + (-i) \int_{-t}^t dt_1 H_I(t_1) + \frac{(-i)^2}{2!} \iint_{-t}^t dt_1 dt_2 T [H_I(t_1) H_I(t_2)] + \dots$$

This scenario is just a tree-level decay—there are no loops to consider or propagators between two spacetime coordinates x_1 and x_2 . Hence, let's consider only the contribution from the 1st order term. The interaction part of the scattering matrix becomes

$$i\langle k_1, k_2 | T | p \rangle \cong \langle k_1, k_2 | (-i) \int_{-t}^t dt_1 H_I(x_1) | p \rangle$$

where $H_I(x) = \int d^3x \mathcal{H}_I(x)$, and in the Hamiltonian I replaced the variable t with the full space-time variable x because all components now come into play.

$$\begin{aligned} i\langle k_1, k_2 | T | p \rangle &= (-i) \langle k_1, k_2 | \int_{-t}^t dt_1 \int d^3x \mathcal{H}_I(x) | p \rangle \\ &= -i \langle k_1, k_2 | \int d^4x \mathcal{H}_I(x) | p \rangle \\ &= -i \int d^4x \langle k_1, k_2 | \mathcal{H}_I(x) | p \rangle \\ &= -i \int d^4x \langle k_1, k_2 | \frac{-g^2 v}{2} W_\mu^\dagger W^\mu H | p \rangle \\ &= \frac{-ig^2 v}{2} \int d^4x \langle k_1, k_2 | W_\mu^\dagger W^\mu H | p \rangle \end{aligned}$$

Assume the fields are now contracted with their state vectors.

If we go to my contractions section:

$$\begin{aligned}\langle k|W_\mu(x) &= \langle 0|\varepsilon_\mu^*(k, \lambda)e^{ik \cdot x} \\ H|p\rangle &= e^{-ip \cdot x}|0\rangle\end{aligned}$$

Using these

$$\begin{aligned}i\langle k_1, k_2|T|p\rangle &= \frac{ig^2v}{2} \int d^4x \varepsilon_\mu^*(k_1, \lambda_1)e^{ik_1 \cdot x} \varepsilon^{*\mu}(k_2, \lambda_2)e^{ik_2 \cdot x} e^{-ip \cdot x} \\ &= \frac{ig^2v}{2} \int d^4x \varepsilon_\mu^*(k_1, \lambda_1) \varepsilon^{*\mu}(k_2, \lambda_2) e^{i(k_1+k_2-p) \cdot x} \\ &= \frac{ig^2v}{2} \varepsilon_\mu^*(k_1, \lambda_1) \varepsilon^{*\mu}(k_2, \lambda_2) \delta^4(k_1 + k_2 - p) (2\pi)^4\end{aligned}$$

Recall from (4.73) Peskin

$$\begin{aligned}i\langle k_1, k_2|T|p\rangle &= (2\pi)^4 \delta^4(k_1 + k_2 - p) \cdot i\mathcal{M}(p \rightarrow k_1, k_2) \\ \Rightarrow i\mathcal{M} &= \frac{ig^2v}{2} \varepsilon_\mu^*(k_1, \lambda_1) \varepsilon^{*\mu}(k_2, \lambda_2)\end{aligned}$$

Appendix K: $H \rightarrow WW$ Invariant Amplitude to Decay Rate (Γ)

The decay rate from (4.83) Peskin is

$$\Gamma = \frac{1}{2m_H} \left[\frac{d^3k_1}{2E_1(2\pi)^3} \frac{d^3k_2}{2E_2(2\pi)^3} \right] \sum_{\lambda_1, \lambda_2} |\mathcal{M}|^2 (2\pi)^4 \delta^4(k_1 + k_2 - p)$$

So let's square the amplitude

$$i\mathcal{M} = igm_W \epsilon_\mu^*(k_1, \lambda_1) \epsilon^{*\mu}(k_2, \lambda_2)$$

$$|\mathcal{M}|^2 = g^2 m_W^2 (\epsilon_\mu^*(k_1, \lambda_1) \epsilon_\nu(k_1, \lambda_1)) (\epsilon^{*\mu}(k_2, \lambda_2) \epsilon^\nu(k_2, \lambda_2))$$

Now deal with the spin sum

$$\begin{aligned} \sum_{\lambda_1, \lambda_2} |\mathcal{M}|^2 &= g^2 m_W^2 \sum_{\lambda_1, \lambda_2} (\epsilon_\mu^*(k_1, \lambda_1) \epsilon_\nu(k_1, \lambda_1)) (\epsilon^{*\mu}(k_2, \lambda_2) \epsilon^\nu(k_2, \lambda_2)) \\ &= g^2 m_W^2 \left(-g_{\mu\nu} + \frac{k_{1\mu} k_{1\nu}}{m_W^2} \right) \left(-g^{\mu\nu} + \frac{k_2^\mu k_2^\nu}{m_W^2} \right) \\ &= g^2 m_W^2 \left(g_{\mu\nu} g^{\mu\nu} - g_{\mu\nu} \frac{k_2^\mu k_2^\nu}{m_W^2} - g^{\mu\nu} \frac{k_{1\mu} k_{1\nu}}{m_W^2} + \frac{k_{1\mu} k_{1\nu} k_2^\mu k_2^\nu}{m_W^2} \right) \\ &= g^2 m_W^2 \left(4 - \frac{k_2^2}{m_W^2} - \frac{k_1^2}{m_W^2} + \frac{(k_1 \cdot k_2)^2}{m_W^4} \right) \end{aligned}$$

Recall that in a reaction the 4-momentum squared is a relativistic invariant. Using this invariant, we may alternate among before and after the decay, and viewing from the lab frame or CM frame (or any other frame). In this case, let's try before and after decay entirely in the CM frame. This means $\vec{p} = 0$, and for the W boson energy and momenta $E_1 = E_2 = E$, $\vec{k}_1 = -\vec{k}_2 \equiv \vec{k}$.

$$\Rightarrow \frac{k^2}{m_W^2} = \frac{E^2 - |\vec{k}|^2}{m_W^2} = \frac{(m_W^2 + |\vec{k}|^2) - |\vec{k}|^2}{m_W^2} = 1$$

Also,

$$\begin{aligned}
(m_H, 0)^2 &= (E_1 + E_2, \vec{k}_1 + \vec{k}_2 = 0)^2 \\
m_H^2 &= 4E_2^2 = 4(m_W^2 + |\vec{k}|^2) \\
m_H^2 &= 4m_W^2 + 4|\vec{k}|^2 \\
m_H^2 - 2m_W^2 &= 2(m_W^2 + 2|\vec{k}|^2) \\
\frac{m_H^2 - 2m_W^2}{2} &= k_1 \cdot k_2
\end{aligned}$$

where in the last line I used

$$\begin{aligned}
k_1 \cdot k_2 &= (E_1, \vec{k}_1) \cdot (E_2, \vec{k}_2) \\
&= (E, \vec{k}) \cdot (E_2, -\vec{k}) \\
&= E^2 + |\vec{k}|^2 \\
&= (m_W^2 + |\vec{k}|^2) + |\vec{k}|^2 \\
&= m_W^2 + 2|\vec{k}|^2
\end{aligned}$$

Now we may put these results back into the spin-summed invariant amplitude.

$$\begin{aligned}
\sum_{\lambda_1, \lambda_2} |\mathcal{M}|^2 &= g^2 m_W^2 \left(4 - 1 - 1 + \frac{(m_H^2 - 2m_W^2)^2}{4m_W^4} \right) \\
&= g^2 m_W^2 \left(2 + \frac{m_H^2 - 4m_W^2 m_H^2 + 4m_W^4}{4m_W^4} \right) \\
&= g^2 m_W^2 \left(2 + \frac{m_H^4}{4m_W^4} - \frac{m_H^2}{m_W^2} + 1 \right) \\
&= g^2 m_W^2 \left(\frac{3m_H^4}{4m_W^4} \cdot \frac{4m_W^4}{m_H^4} + \frac{m_H^4}{4m_W^4} - \frac{m_H^4}{4m_W^4} \cdot \frac{4m_W^4}{m_H^4} \cdot \frac{m_H^2}{m_W^2} \right) \\
&= g^2 m_W^2 \frac{m_H^4}{4m_W^4} \left(1 + \frac{12m_W^4}{m_H^4} - \frac{4m_W^2}{m_H^2} \right) \\
&= \frac{g^2 m_H^4}{4m_W^4} \left(1 - \frac{4m_W^2}{m_H^2} + \frac{12m_W^4}{m_H^4} \right)
\end{aligned}$$

Put this into the decay rate.

$$d\Gamma = \frac{1}{2m_H} \left[\frac{d^3k_1}{2E_1(2\pi)^3} \frac{d^3k_2}{2E_2(2\pi)^3} \right] \frac{g^2 m_H^4}{4m_W^4} \left(1 - \frac{4m_W^2}{m_H^2} + \frac{12m_W^4}{m_H^4} \right) (2\pi)^4 \delta^4(k_1 + k_2 - p)$$

$$\Gamma = \frac{g^2 m_H^3}{32(2\pi)^2 m_W^2} \left(1 - \frac{4m_W^2}{m_H^2} + \frac{12m_W^4}{m_H^4} \right) \int \frac{d^3\vec{k}_1}{E_1} \frac{d^3\vec{k}_2}{E_2} \delta(E_1 + E_2 - E_p) \delta^3(\vec{k}_1 + \vec{k}_2 - \vec{p})$$

In the CM frame, $E_p = m_H$ and $\vec{p} = 0$.

$$\Gamma = \frac{g^2 m_H^3}{32(2\pi)^2 m_W^2} \left(1 - \frac{4m_W^2}{m_H^2} + \frac{12m_W^4}{m_H^4} \right) \int \frac{d^3\vec{k}_1}{E_1} \frac{d^3\vec{k}_2}{E_2} \delta(E_1 + E_2 - m_H) \delta^3(\vec{k}_1 + \vec{k}_2)$$

$$\Gamma = \frac{g^2 m_H^3}{32(2\pi)^2 m_W^2} \left(1 - \frac{4m_W^2}{m_H^2} + \frac{12m_W^4}{m_H^4} \right) \int \frac{d^3\vec{k}}{\sqrt{m_W^2 + |\vec{k}_1|^2}} \frac{d^3\vec{k}}{\sqrt{m_W^2 + |\vec{k}_2|^2}} \delta(E_1 + E_2 - m_H) \delta^3(\vec{k}_1 + \vec{k}_2)$$

Perform the k_2 integration. Because of $\delta^3(\vec{k}_1 + \vec{k}_2)$, this will just enforce $\vec{k}_1 = -\vec{k}_2 \Rightarrow |\vec{k}_1|^2 = |\vec{k}_2|^2$. Since we are dealing only with these momenta squared now, let's drop the index and just use $|\vec{k}|$.

$$\Gamma = \frac{g^2 m_H^3}{32(2\pi)^2 m_W^2} \left(1 - \frac{4m_W^2}{m_H^2} + \frac{12m_W^4}{m_H^4} \right) \int \frac{d^3\vec{k}}{m_W^2 + |\vec{k}|^2} \delta(E_1 + E_2 - m_H)$$

Express the remaining differential in spherical coordinates $d^3\vec{k} = |\vec{k}|^2 d|\vec{k}| \sin\theta d\theta d\phi$, where $\int \sin\theta d\theta d\phi = 4\pi$.

$$\Gamma = \frac{g^2 m_H^3}{32(2\pi)^2 m_W^2} \left(1 - \frac{4m_W^2}{m_H^2} + \frac{12m_W^4}{m_H^4} \right) \int \frac{|\vec{k}|^2 d|\vec{k}| \sin\theta d\theta d\phi}{m_W^2 + |\vec{k}|^2} \delta(E_1 + E_2 - m_H)$$

In the CM frame, $E_1 = E_2 = \sqrt{m_W^2 + |\vec{k}|^2}$.

$$\Gamma = \frac{g^2 m_H^3}{8(4\pi) m_W^2} \left(1 - \frac{4m_W^2}{m_H^2} + \frac{12m_W^4}{m_H^4} \right) \int d|\vec{k}| \frac{|\vec{k}|^2}{m_W^2 + |\vec{k}|^2} \delta\left(2\sqrt{m_W^2 + |\vec{k}|^2} - m_H\right)$$

We must take care here. The integral is over $|\vec{k}|$ but the argument of the δ -function has more than one zero, so there is an ambiguity of which value $|\vec{k}|$ should take from the integration. Fortunately, it is possible to expand the δ -function as follows:

$$\delta(f(x)) = \sum_j \frac{1}{f'(x_0^j)} \delta(x - x_0^j)$$

where j counts over the zeros of $f(x)$ and $f' = \frac{df}{dx}$. Let $f(k) = 2\sqrt{m_W^2 + |\vec{k}|^2} - m_H$ and find the zeros:

$$\begin{aligned} m_H &= 2\sqrt{m_W^2 + |\vec{k}|^2} \\ \frac{m_H^2}{4} &= m_W^2 + |\vec{k}|^2 \\ \frac{1}{4}(m_H^2 - 4m_W^2) &= k^2 \\ \pm \frac{1}{2}\sqrt{m_H^2 - 4m_W^2} &= k \end{aligned}$$

However, a negative momentum magnitude doesn't make sense so we only use the positive one.

$$\begin{aligned} f'(k) &= \frac{2k}{\sqrt{m_W^2 + k^2}} \\ f'(k_0) &= \frac{\sqrt{m_H^2 - 4m_W^2}}{\sqrt{m_W^2 + \frac{1}{4}m_H^2 - m_W^2}} \\ f'(k_0) &= \frac{\sqrt{m_H^2 - 4m_W^2}}{\frac{1}{2}m_H} \\ f'(k_0) &= \frac{2}{m_H} \sqrt{m_H^2 - 4m_W^2} \\ \Rightarrow \delta(f(k)) &= -\frac{m_H}{2\sqrt{m_H^2 - 4m_W^2}} \delta\left(|\vec{k}| - \frac{1}{2}\sqrt{m_H^2 - 4m_W^2}\right) \end{aligned}$$

Put this into the decay rate.

$$\begin{aligned}
\Gamma &= \frac{g^2 m_H^3}{32\pi m_W^2} \left(1 - \frac{4m_W^2}{m_H^2} + \frac{12m_W^4}{m_H^4} \right) \\
&\quad \int d|\vec{k}| \frac{|\vec{k}|^2}{m_W^2 + |\vec{k}|^2} \frac{m_H}{2\sqrt{m_H^2 - 4m_W^2}} \delta \left(|\vec{k}| - \frac{1}{2}\sqrt{m_H^2 - 4m_W^2} \right) \\
&= \frac{g^2 m_H^3}{32\pi m_W^2} \left(1 - \frac{4m_W^2}{m_H^2} + \frac{12m_W^4}{m_H^4} \right) \frac{\frac{1}{4}(m_H^2 - 4m_W^2)}{m_W^2 + \frac{1}{4}(m_H^2 - 4m_W^2)} \frac{m_H}{2\sqrt{m_H^2 - 4m_W^2}} \\
&= \frac{g^2 m_H^3}{32\pi m_W^2} \left(1 - \frac{4m_W^2}{m_H^2} + \frac{12m_W^4}{m_H^4} \right) \frac{\frac{1}{4}(m_H^2 - 4m_W^2)}{\frac{1}{4}m_H^2} \frac{m_H}{2\sqrt{m_H^2 - 4m_W^2}} \\
&= \frac{g^2 m_H^3}{32\pi m_W^2} \left(1 - \frac{4m_W^2}{m_H^2} + \frac{12m_W^4}{m_H^4} \right) \frac{\sqrt{m_H^2 - 4m_W^2}}{2m_H} \\
&= \frac{g^2 m_H^3}{64\pi m_W^2} \left(1 - \frac{4m_W^2}{m_H^2} + \frac{12m_W^4}{m_H^4} \right) \sqrt{1 - \frac{4m_W^2}{m_H^2}} \\
&= \boxed{\frac{G_F m_H^3}{8\sqrt{2}\pi} \left(1 - \frac{4m_W^2}{m_H^2} + \frac{12m_W^4}{m_H^4} \right) \sqrt{1 - \frac{4m_W^2}{m_H^2}}}
\end{aligned}$$

where $G_F = \frac{\sqrt{2}g^2}{8m_W^2} \Rightarrow \frac{G_F}{\sqrt{2}} = \frac{g^2}{8m_W^2}$.

Appendix L: WZ Cross Section Measurement in 5.9fb^{-1}

WZ production is a crucial background to the $H \rightarrow WW$ trilepton search. The WZ cross section is measured using the same lepton and event selection as the $H \rightarrow WW$ search. A NeuroBayes neural net is used to distinguish WZ signal from backgrounds in the final selection region. The WZ cross section is then extracted using a maximum likelihood method which best fits the neural net score signal and background shapes to the data. This analysis uses up to 5.9fb^{-1} of CDF Run II data. The measured WZ cross section is $3.7_{-0.8}^{+0.8}\text{pb}$, consistent with the $3.46 \pm 0.21\text{pb}$ predicted by theory. This is a significant improvement over the previously published result of $5.0_{-1.6}^{+1.8}\text{pb}$.

For the WZ cross section measurement, we use only events with

- three leptons (e or μ)
- any number of jets
- $E_T > 25.0\text{GeV}$
- Z -boson selection

In 5.9fb^{-1} of data, we find 53 events, ~ 40 of which are expected to be WZ events with the rest coming from other Standard Model processes.

The cross section measurement based on the event count alone can be estimated by

$$\begin{aligned}\sigma &= \frac{N_{\text{data}} - N_{\text{expected background}}}{\left[\int \mathcal{L} \cdot dt\right] \cdot \mathcal{BR}(W \rightarrow l\nu) \cdot \mathcal{BR}(Z \rightarrow l\bar{l}) \cdot a_{WZ}} \\ &= \boxed{3.76\text{ pb}}\end{aligned}$$

where

- $N_{\text{data}} = 53$
- $N_{\text{Back. exp.}} = 9$

CDF Run II				$\int \mathcal{L} = 5.9 \text{ fb}^{-1}$					
	Signal			low E_T			no- Z		
ZZ	4.97	\pm	0.66	6.97	\pm	0.92	1.70	\pm	0.23
Z +Jets	2.41	\pm	0.59	41.4	\pm	10.1	14.2	\pm	3.49
$Z\gamma$	0.77	\pm	0.27	71.4	\pm	25.0	80.3	\pm	28.2
$t\bar{t}$	0.15	\pm	0.04	0.02	\pm	0.005	0.32	\pm	0.10
Total Background	8.29	\pm	0.97	119.7	\pm	27.2	96.6	\pm	28.5
WZ	40.2	\pm	4.06	6.25	\pm	0.63	3.52	\pm	0.36
Sig.+Back.	48.5	\pm	4.20	126.0	\pm	27.4	100.1	\pm	28.6
Data	53			118			104		

High Mass

- $\mathcal{L} \cdot dt = 5900 \text{ pb}$
- $\mathcal{BR}(W \rightarrow l\nu) = 0.2528$
- $\mathcal{BR}(Z \rightarrow l\bar{l}) = 0.0713$
- $a_{WZ} = \frac{N_{WZ}^{MC}}{\sigma_{WZ}^{NLO} \mathcal{BR} \int \mathcal{L} \cdot dt} = 0.11$

For a more accurate computation with proper error included, a likelihood fit method is used. The likelihood function is formed from a product of Poisson probabilities for each bin in LR_{WZ} . Additionally, Gaussian constraints are applied corresponding to each systematic S_c . The likelihood is given by

$$\mathcal{L} = \left(\prod_i \frac{\mu_i^{n_i} e^{-\mu_i}}{n_i!} \right) \cdot \prod_c e^{-\frac{S_c^2}{2}} \quad (\text{L.1})$$

where μ_i is the total expectation in the i -th bin and n_i is the number of data events in the i -th bin. μ_i is given by

$$\mu_i = \sum_k \alpha_k \left[\prod_c (1 + f_k^c S_c) \right] (N_k^{Exp})_i \quad (\text{L.2})$$

Here f_k^c is the fractional uncertainty associated with the systematic S_c and process k . This is constructed such that the systematics are properly correlated (or uncorrelated) between the different contributions¹. $(N_k^{Exp})_i$ is the expected number of events from process k in the i -th bin. α_k is the parameter which is used to measure the WZ cross section. It is a freely floating parameter for α_{WZ} and fixed for all other processes. In this sense it allows one to measure an additional overall normalization factor for the WZ process. The measured value of this parameter (α_{WZ}) multiplied by the input WZ cross section gives the measured value of the WZ cross section, or if you like:

$$\sigma_{WZ}^{measured} = \alpha_{WZ} \cdot \sigma_{WZ}^{NLO}$$

In practice it is the negative log likelihood which is minimized, which is equivalent to maximizing the likelihood. The MINUIT program is used to minimize this function and MINOS is

¹Note that if a systematic is partially correlated it is possible to decompose that into its correlated and uncorrelated parts

used to extract the error on this minimization. The asymmetric errors from MINOS are the errors used in this analysis.

The fit gives a measured value for the WZ cross section of

$$\sigma(p\bar{p} \rightarrow WZ) = 3.7_{-0.8}^{+0.8}(\text{pb}) \quad (\text{L.3})$$

where the uncertainty includes statistical, systematic, and luminosity uncertainties. Separating out the statistical and systematic uncertainties gives

$$\sigma(p\bar{p} \rightarrow WZ) = 3.7 \pm 0.6|_{\text{stat}}^{+0.6}_{-0.4}|_{\text{syst}}(\text{pb}) \quad (\text{L.4})$$

where the systematic uncertainty quoted includes a 5.9% luminosity uncertainty. For more details, see CDF internal note 10138.

Appendix M: Monte Carlo Samples

mode	Period	Stntuple	$\sigma \times \mathcal{B}$ (pb)	K-factor ^a	Filter Eff
WZ	0-23	we0s6d,we0scd,we0shd we0sld,we0sod,we0sbf we0shf	3.46×0.101	1.0	0.754
ZZ	0-23	we0s7d,we0sdd,we0sid we0smd, we0spd,we0scf we0sif	1.511	1.0	0.233
$t\bar{t}$	0-11	te0s2z	7.9×0.1027	1.0	1.0
$Z\gamma$	0-11	re0s33, re0s34, re0s37	14.05	1.36^b	1.0

^a If cross section is NLO, then K-factor is one.

^b http://www-cdf.fnal.gov/tiki/tiki-index.php?page=EwkDatasets#_Drell_Yan_Z_gamma_Sample

Table M.1 Monte Carlo samples used in this analysis

$M_H (GeV^2)$	Period	Stntuple	σ (pb)	BR ($H \rightarrow WW$)	Filter Efficiency
110	0-23	fhgs4a,fhgs6a	0.2075	0.0441	0.6880
120	0-23	fhgs4b,fhgs6b	0.1529	0.1320	0.6978
130	0-23	fhgs4c,fhgs6c	0.1141	0.2869	0.7032
140	0-23	fhgs4d,fhgs6d	0.0860	0.4833	0.7065
150	0-23	fhgs4e,fhgs6e	0.0654	0.6817	0.7085
160	0-23	fhgs4f,fhgs6f	0.0510	0.9011	0.7108
170	0-23	fhgs4g,fhgs6g	0.0389	0.9653	0.7125
180	0-23	fhgs4h,fhgs6h	0.0306	0.9345	0.7141
190	0-23	fhgs4i,fhgs6i	0.0243	0.7761	0.7151
200	0-23	fhgs4j,fhgs6j	0.0193	0.7347	0.7165
145	0-23	fhgs4o,fhgs6o	0.0749	0.5731	0.7075
155	0-23	fhgs4p,fhgs6p	0.0572	0.8007	0.7098
165	0-23	fhgs4q,fhgs6q	0.0441	0.9566	0.7114
175	0-23	fhgs4r,fhgs6r	0.0344	0.9505	0.7130

Table M.2 Associated Higgs production with a W boson [20].

$M_H(GeV^2)$	Period	Stntuple	σ (pb)	BR ($H \rightarrow WW$)	Filter Efficiency
110	0-23	uhgs4a,uhgs6a	0.1236	0.0441	0.6930
120	0-23	uhgs4b,uhgs6b	0.0927	0.1320	0.7031
130	0-23	uhgs4c,uhgs6c	0.0705	0.2869	0.7087
140	0-23	uhgs4d,uhgs6d	0.0542	0.4833	0.7122
150	0-23	uhgs4e,uhgs6e	0.0421	0.6817	0.7151
160	0-23	uhgs4f,uhgs6f	0.0331	0.9011	0.7172
170	0-23	uhgs4g,uhgs6g	0.0261	0.9653	0.7184
180	0-23	uhgs4h,uhgs6h	0.0208	0.9345	0.7204
190	0-23	uhgs4i,uhgs6i	0.0166	0.7761	0.7220
200	0-23	uhgs4j,uhgs6j	0.0135	0.7347	0.7239
145	0-23	uhgs4o,uhgs6o	0.0477	0.5731	0.7135
155	0-23	uhgs4p,uhgs6p	0.0373	0.8007	0.7155
165	0-23	uhgs4q,uhgs6q	0.0294	0.9566	0.7183
175	0-23	uhgs4r,uhgs6r	0.0233	0.9505	0.7196

Table M.3 Associated Higgs production with a Z boson [20].

**Appendix N: Signal Summary for 19 Mass Points from $m_H = 110$
GeV to $m_H = 200$ GeV**

m_H GeV	<i>No-Z-Peak</i>			<i>In-Z-Peak</i>			1 jet	<i>InZPeak</i>	≥ 2 jets
	<i>WH</i>	<i>ZH</i>	Total	<i>WH</i>	<i>ZH</i>	Total	<i>WH</i>	<i>ZH</i>	Total
110	0.07	0.02	0.09	0.002	0.04	0.04	-	0.03	0.03
115	0.12	0.03	0.15	0.004	0.07	0.07	-	0.06	0.06
120	0.19	0.05	0.24	0.007	0.10	0.11	0.002	0.11	0.11
125	0.28	0.07	0.35	0.01	0.14	0.15	0.003	0.16	0.16
130	0.36	0.10	0.46	0.01	0.18	0.19	0.003	0.22	0.22
135	0.44	0.11	0.55	0.02	0.20	0.22	0.005	0.28	0.29
140	0.50	0.13	0.63	0.02	0.22	0.24	0.005	0.34	0.34
145	0.55	0.15	0.70	0.02	0.23	0.25	0.007	0.38	0.39
150	0.58	0.15	0.73	0.03	0.24	0.27	0.007	0.42	0.43
155	0.61	0.16	0.77	0.03	0.23	0.26	0.008	0.45	0.46
160	0.64	0.17	0.81	0.03	0.22	0.25	0.008	0.48	0.49
165	0.61	0.16	0.77	0.03	0.20	0.23	0.008	0.47	0.48
170	0.54	0.14	0.68	0.03	0.18	0.21	0.007	0.44	0.45
175	0.48	0.13	0.61	0.03	0.16	0.19	0.008	0.41	0.42
180	0.41	0.12	0.53	0.02	0.15	0.17	0.007	0.37	0.38
185	0.34	0.10	0.44	0.02	0.12	0.14	0.007	0.31	0.32
190	0.28	0.08	0.36	0.02	0.10	0.12	0.006	0.27	0.28
195	0.24	0.07	0.31	0.02	0.10	0.12	0.006	0.24	0.25
200	0.21	0.06	0.27	0.02	0.08	0.10	0.005	0.22	0.23

Table N.1 Signal Summary

Appendix O: Basic Event Information for the Signal and Control Regions

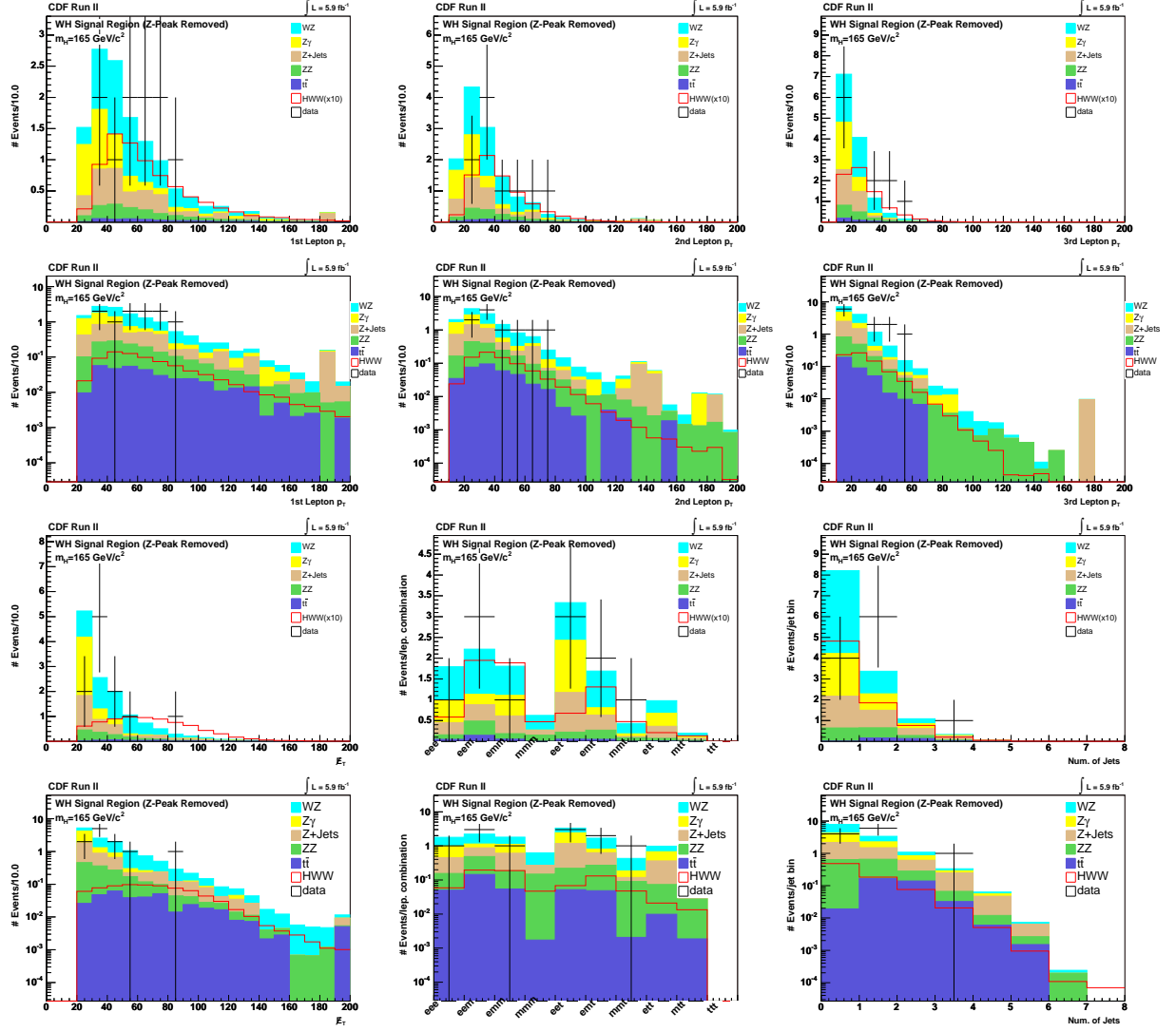


Figure O.1 Trilepton WH signal region lepton p_T (for muons) or E_T (for electrons)

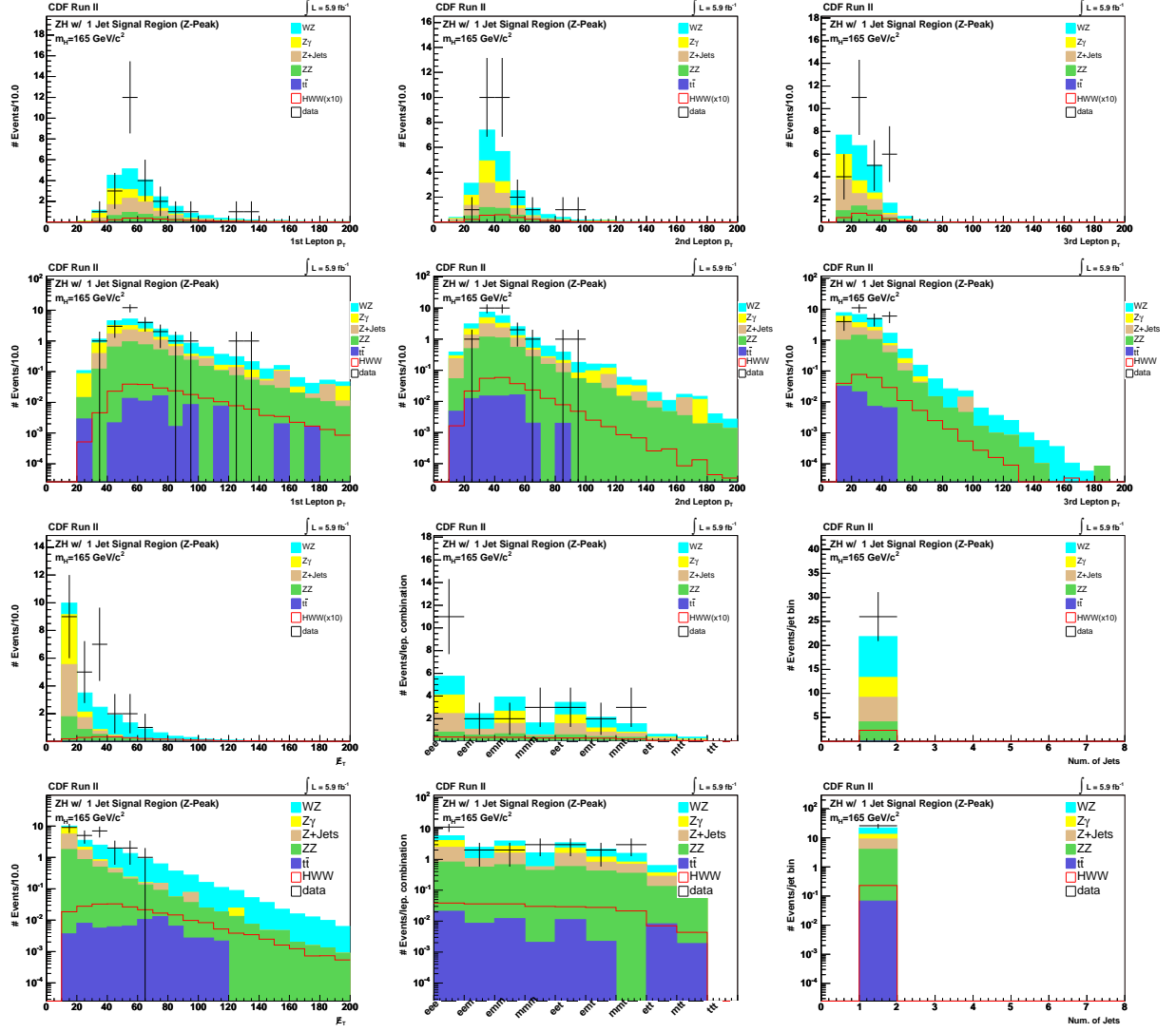


Figure O.2 Trilepton ZH (1 Jet) signal region lepton p_T (for muons) or E_T (for electrons)

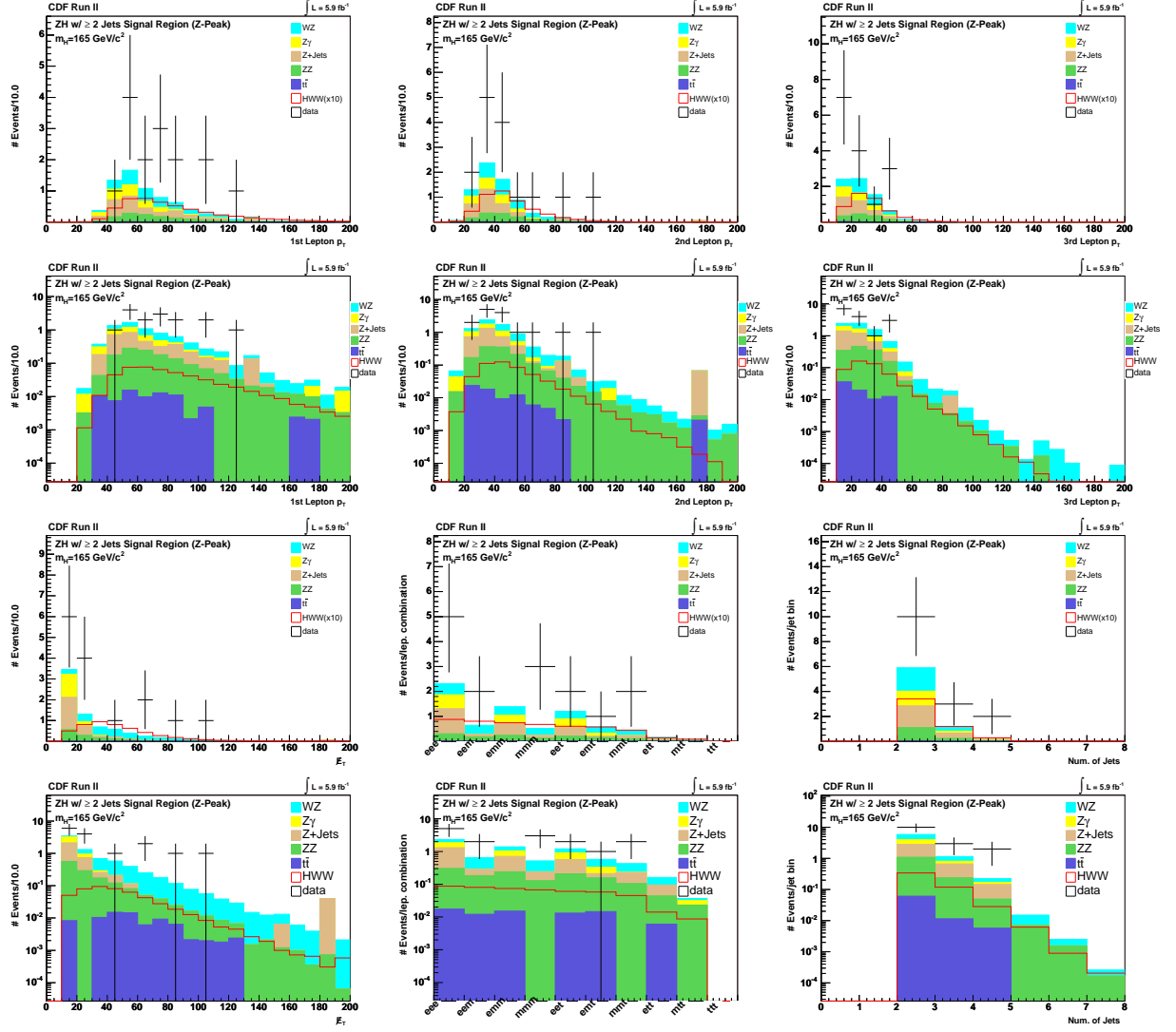


Figure O.3 Trilepton ZH (≥ 2 Jet) signal region lepton p_T (for muons) or E_T (for electrons)

Appendix P: Neural Net Input Variables for the Signal Regions

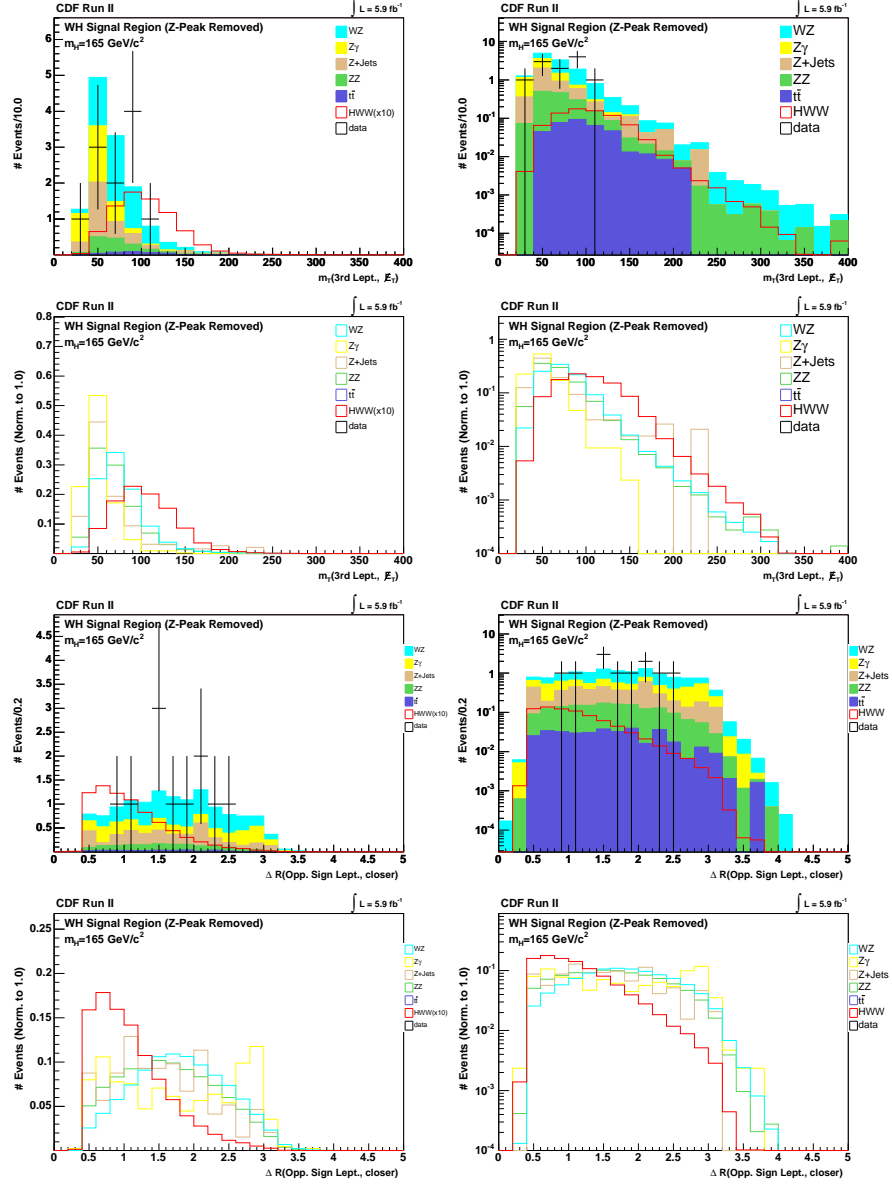


Figure P.1 WH Analysis: m_T (Lep3, E_T), ΔR b/w Opp. Sign Close Lept.

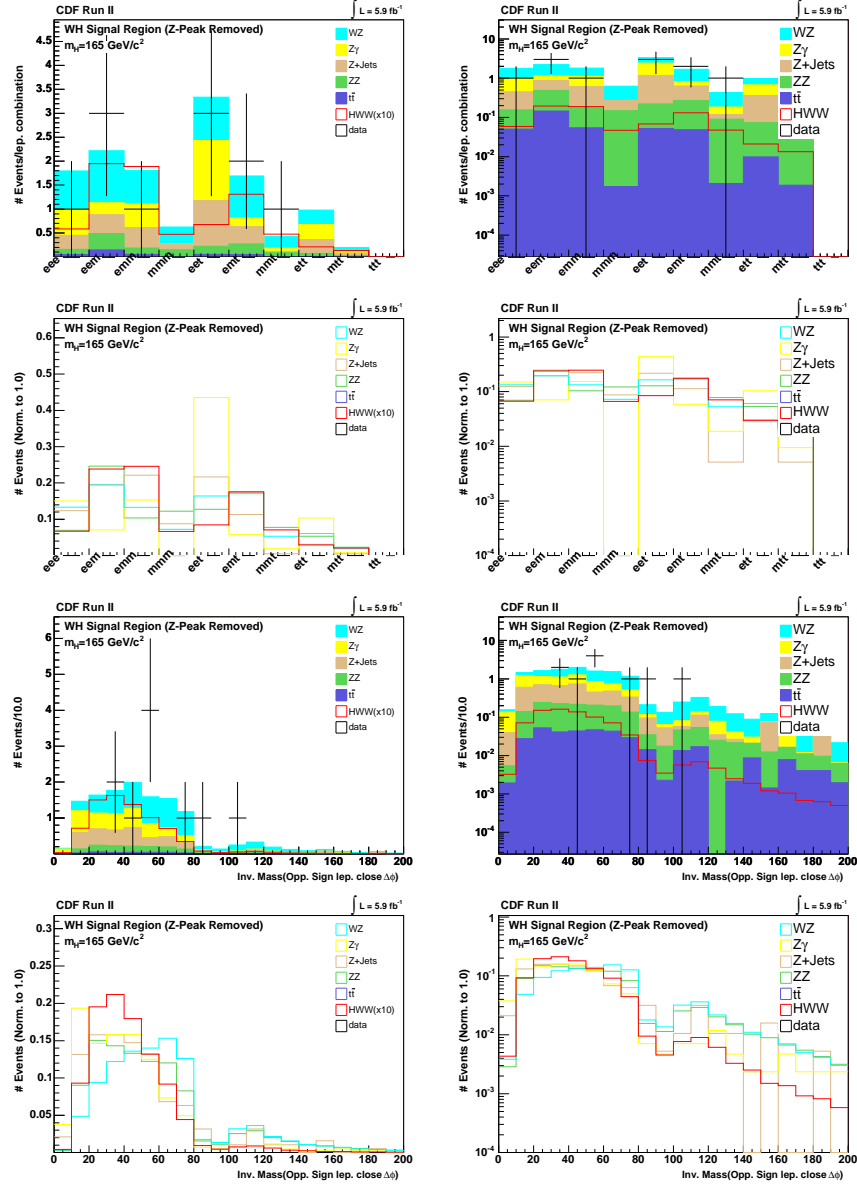
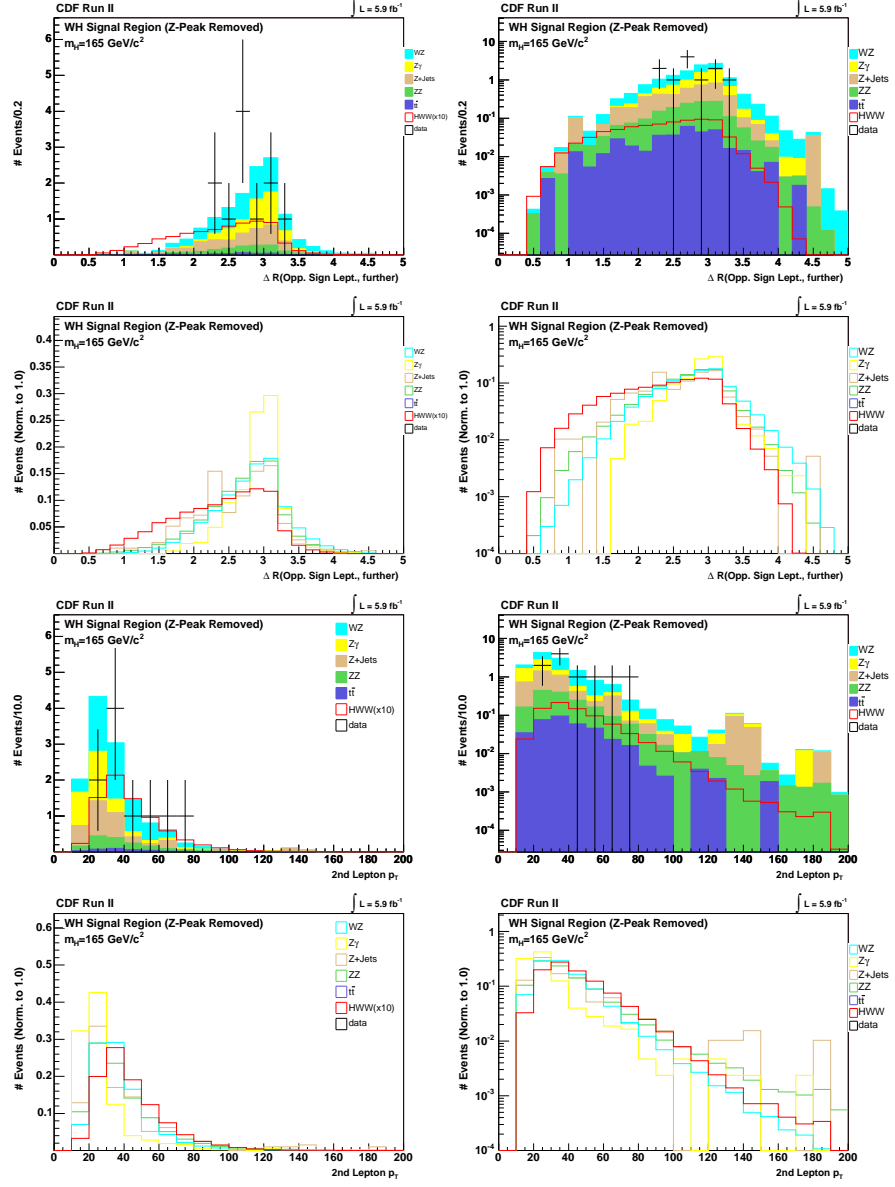
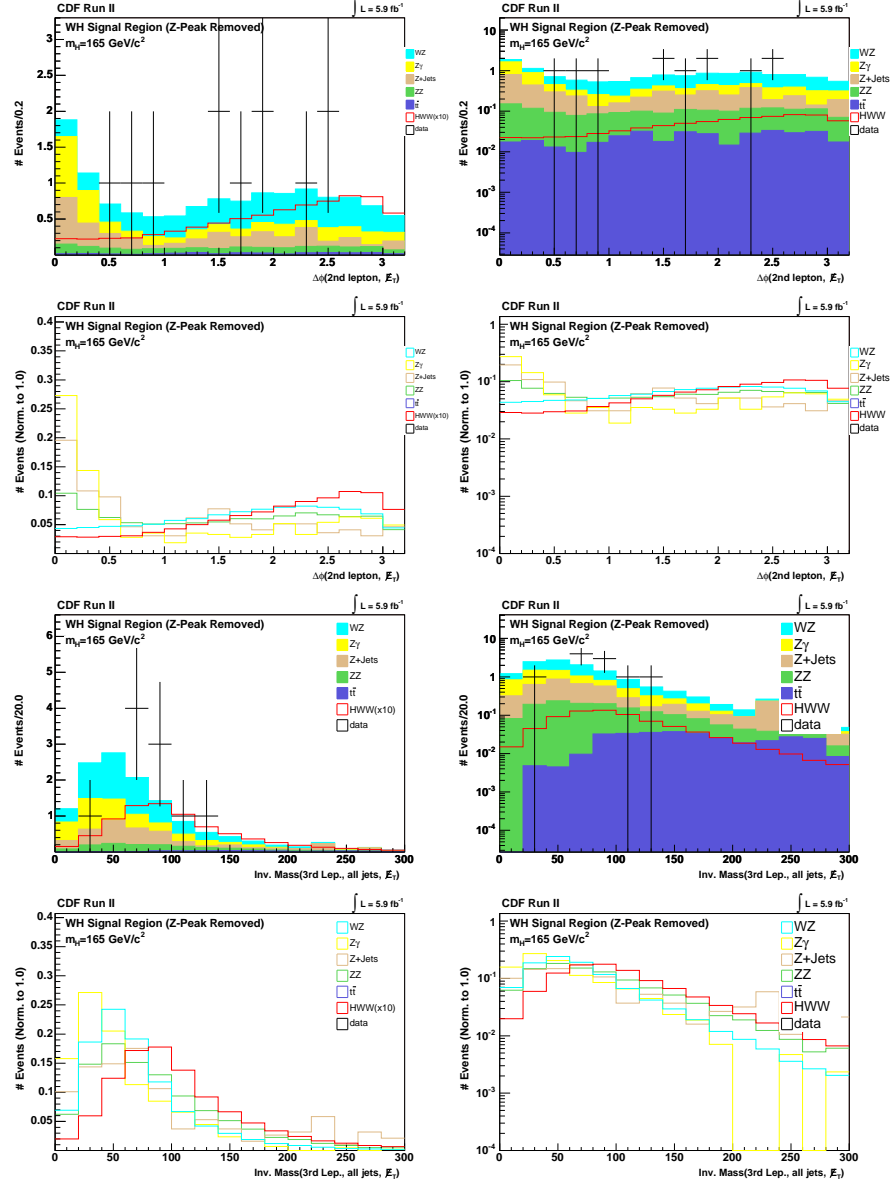
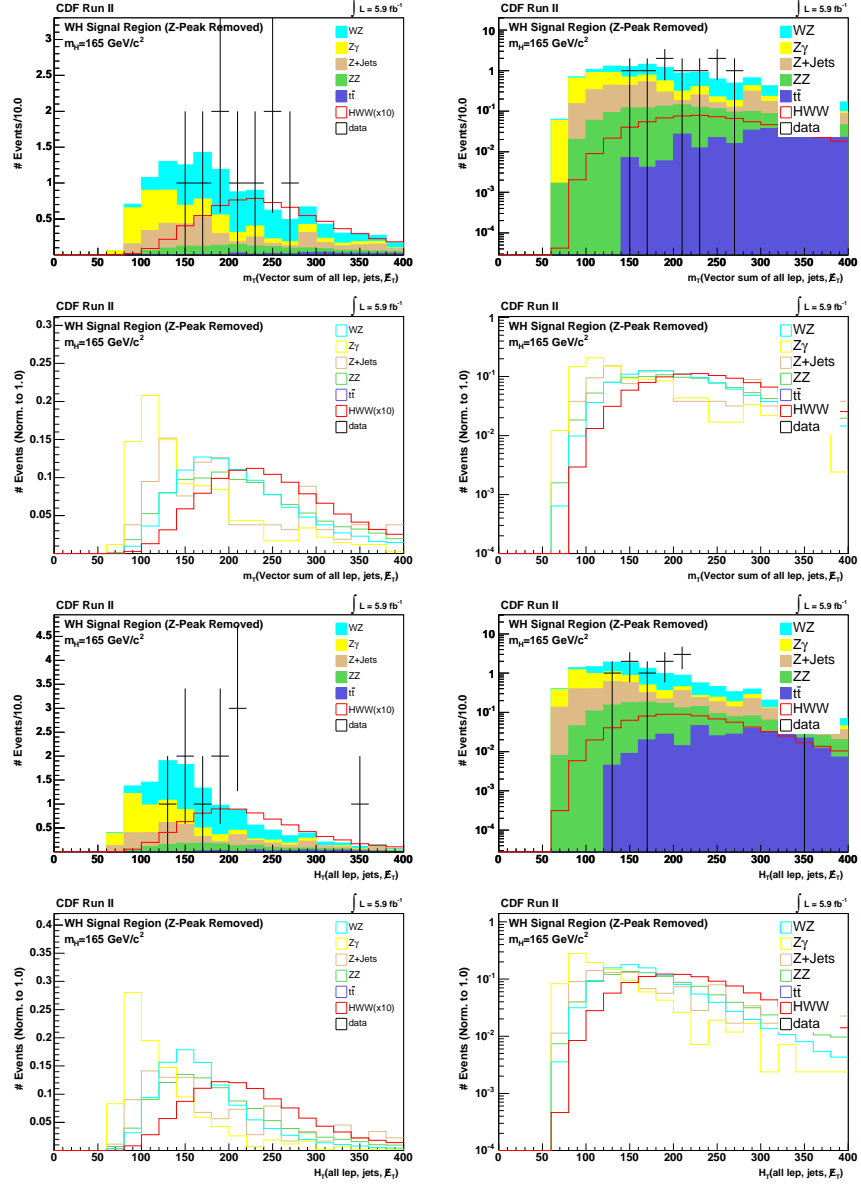
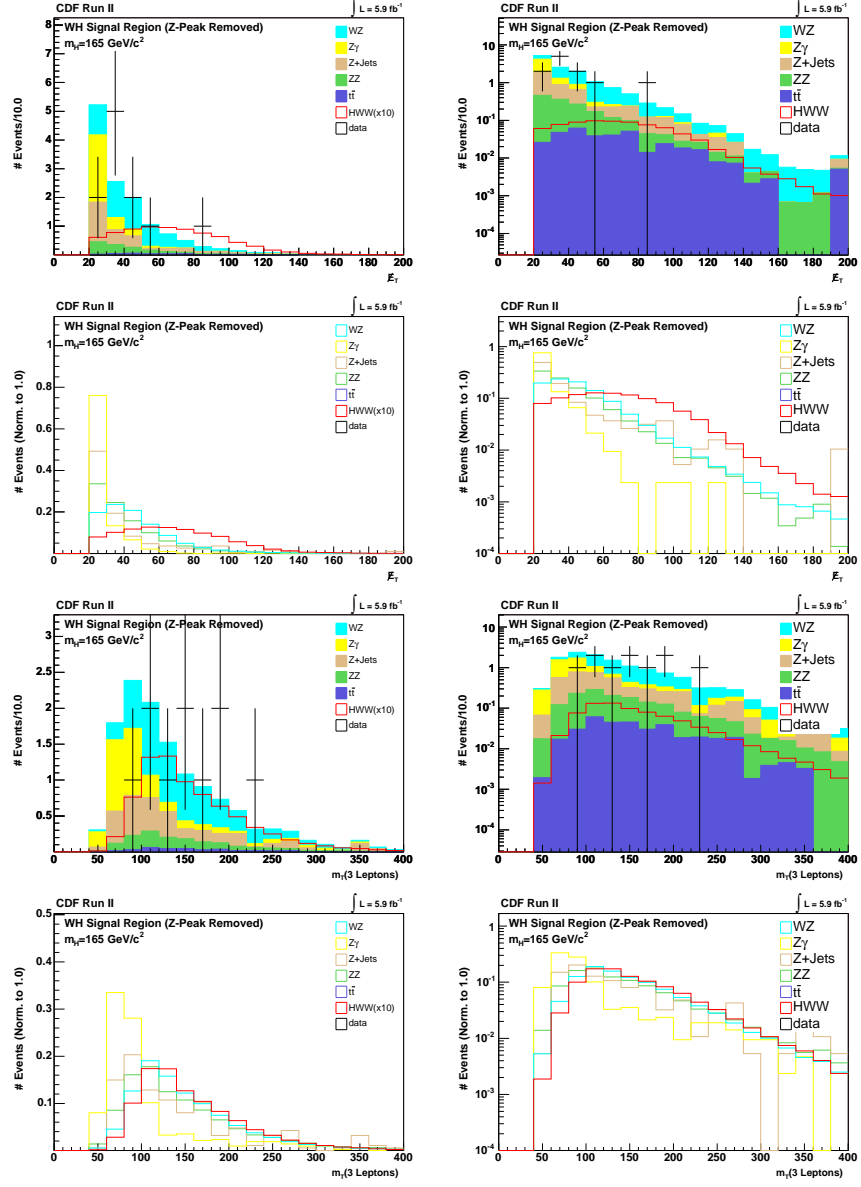


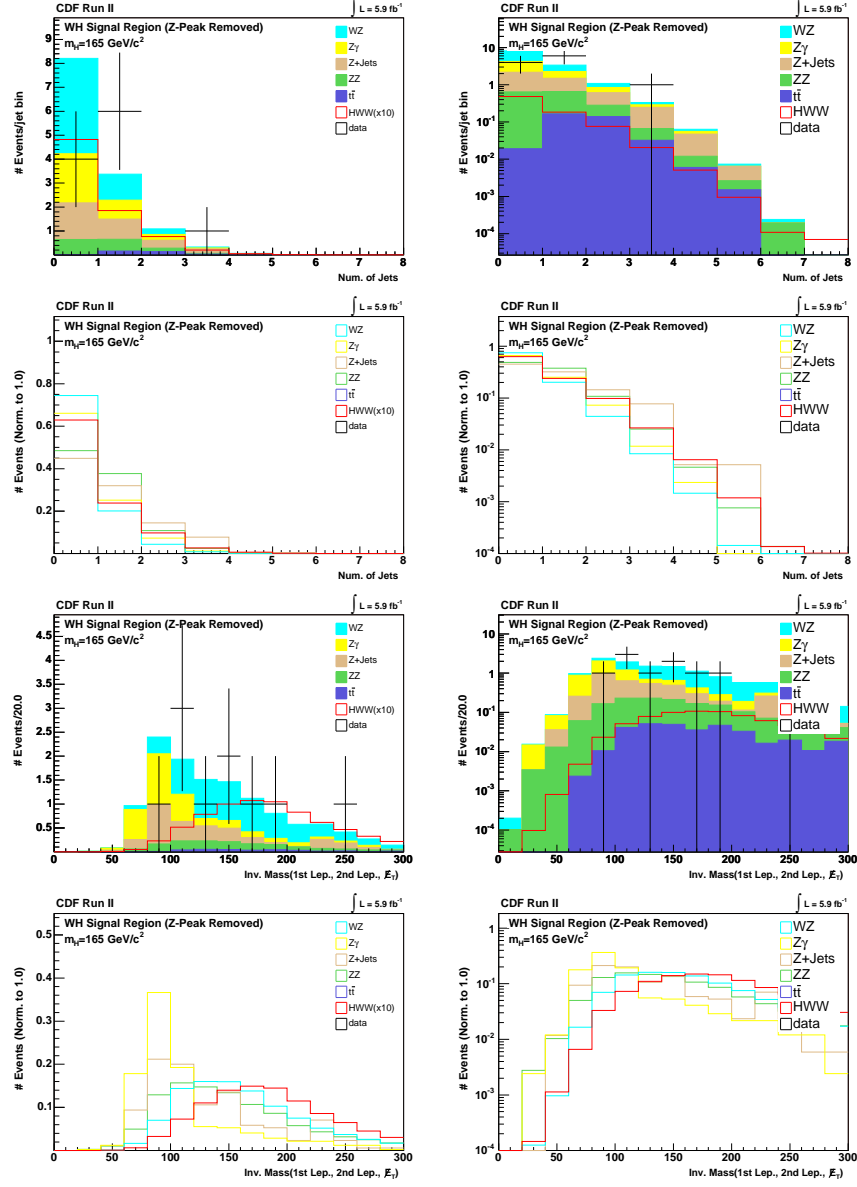
Figure P.2 WH Analysis: Lepton types, Dimass Opp. Sign Leptons (closer pair in ϕ).

Figure P.3 WH Analysis: ΔR Opp. Sign Far Lept., 2^{nd} Lepton p_T

Figure P.4 WH Analysis: $\Delta\phi(\text{Lep2}, \vec{E}_T)$, $\text{Inv. Mass}(\text{Lep3}, \vec{E}_T, \text{Jets})$

Figure P.5 WH Analysis: $m_T(\text{all lept.}, \vec{E}_T, \text{Jets})$, H_T

Figure P.6 WH Analysis: E_T , m_T Trilepton Mass

Figure P.7 WH Analysis: NJet, Inv. Mass(Lep1,Lep2, E_T)

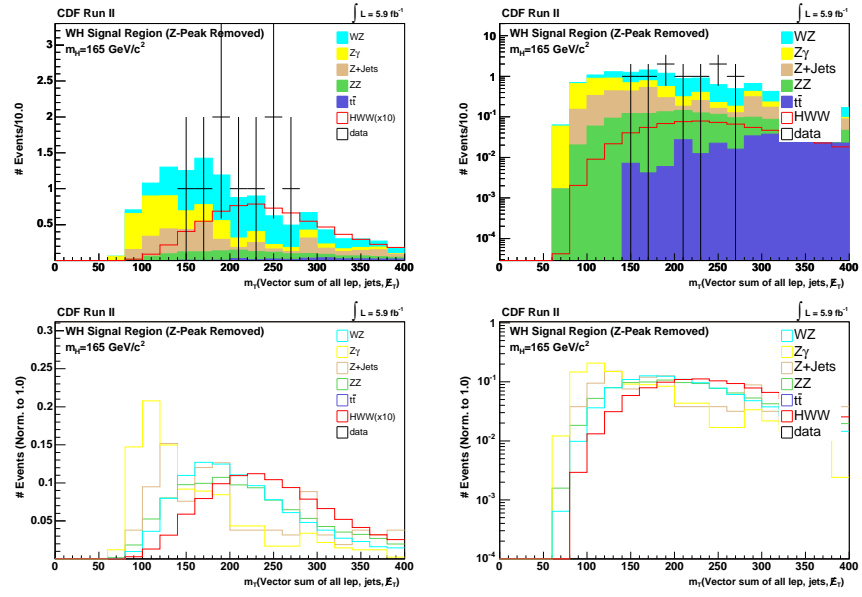
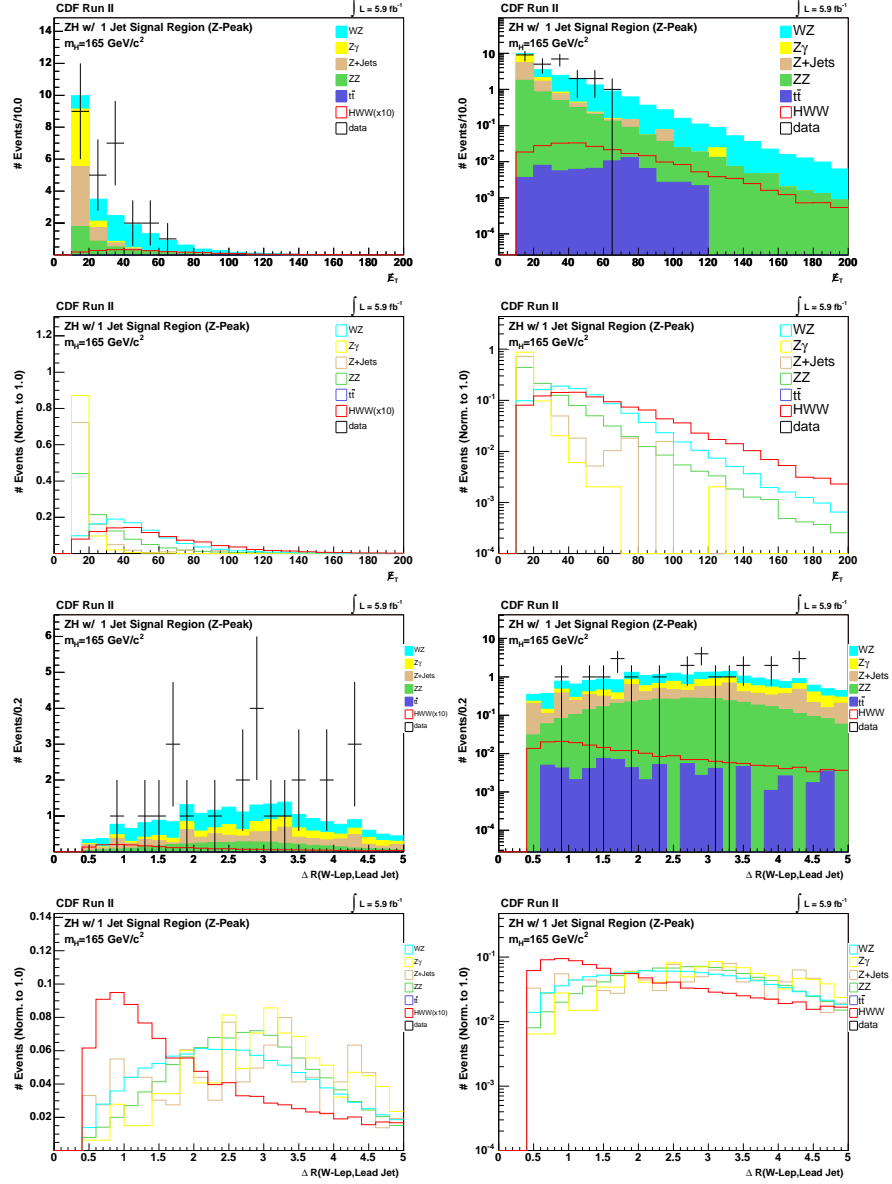


Figure P.8 WH Analysis: m_T (all lept., E_T , jets)

Figure P.9 ZH (1-jet) Analysis: E_T , $\Delta R(W\text{-lep, lead jet})$

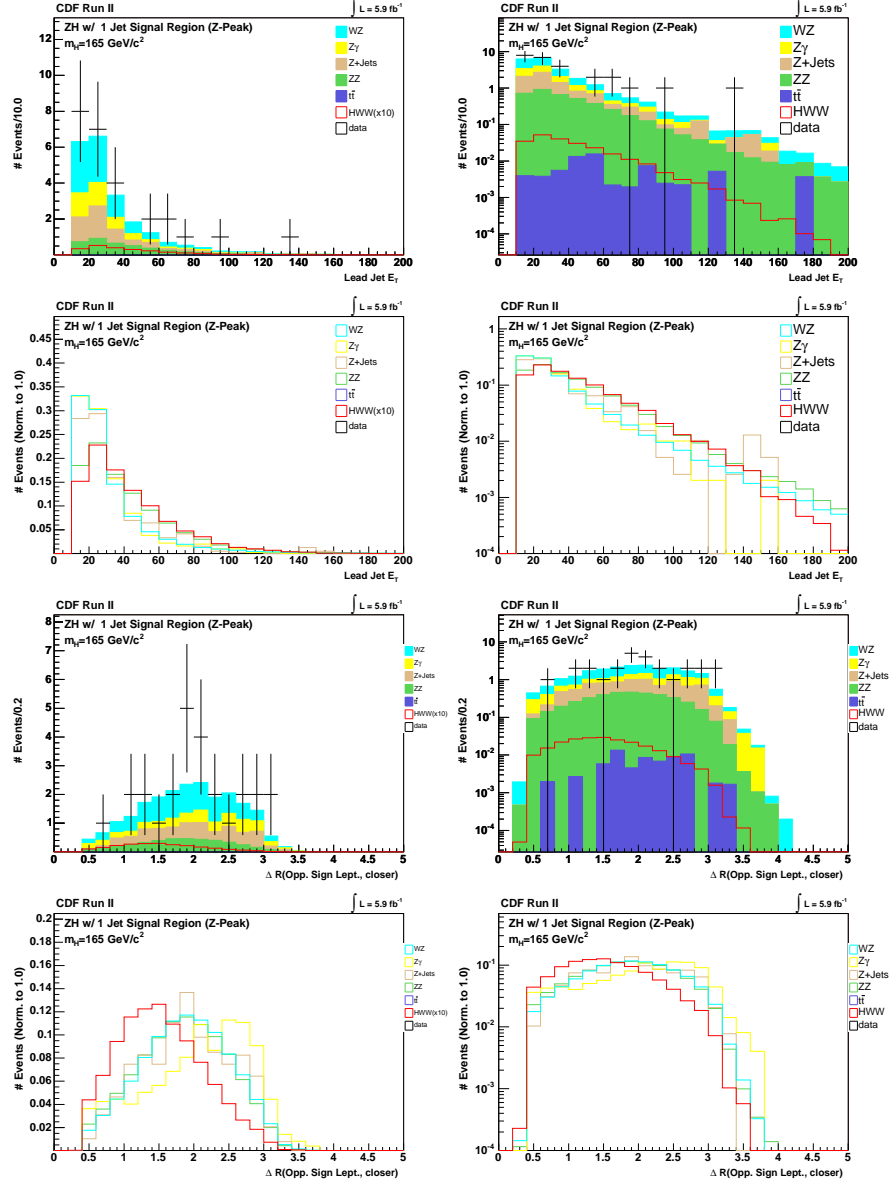


Figure P.10 ZH (1-jet) Analysis: Lead jet E_T , ΔR b/w Opp. Sign Close Lept.

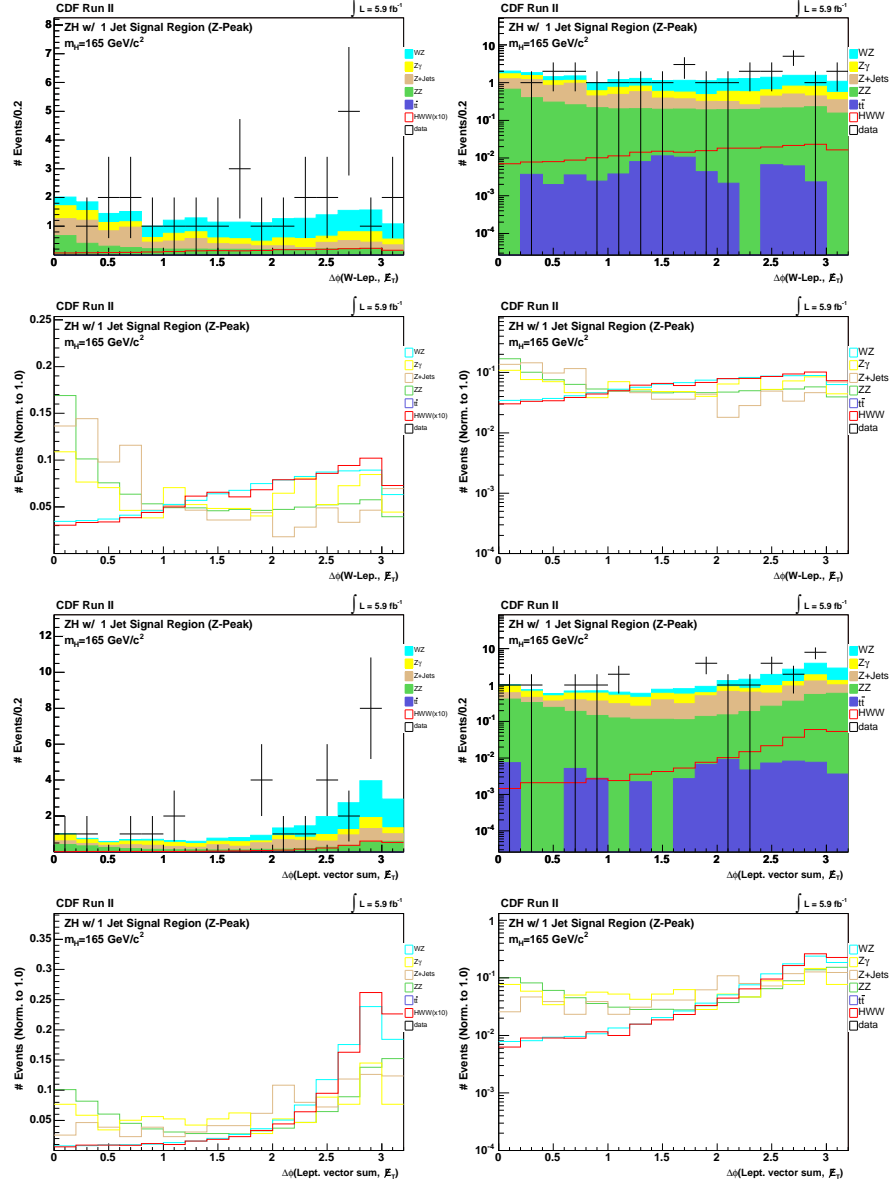
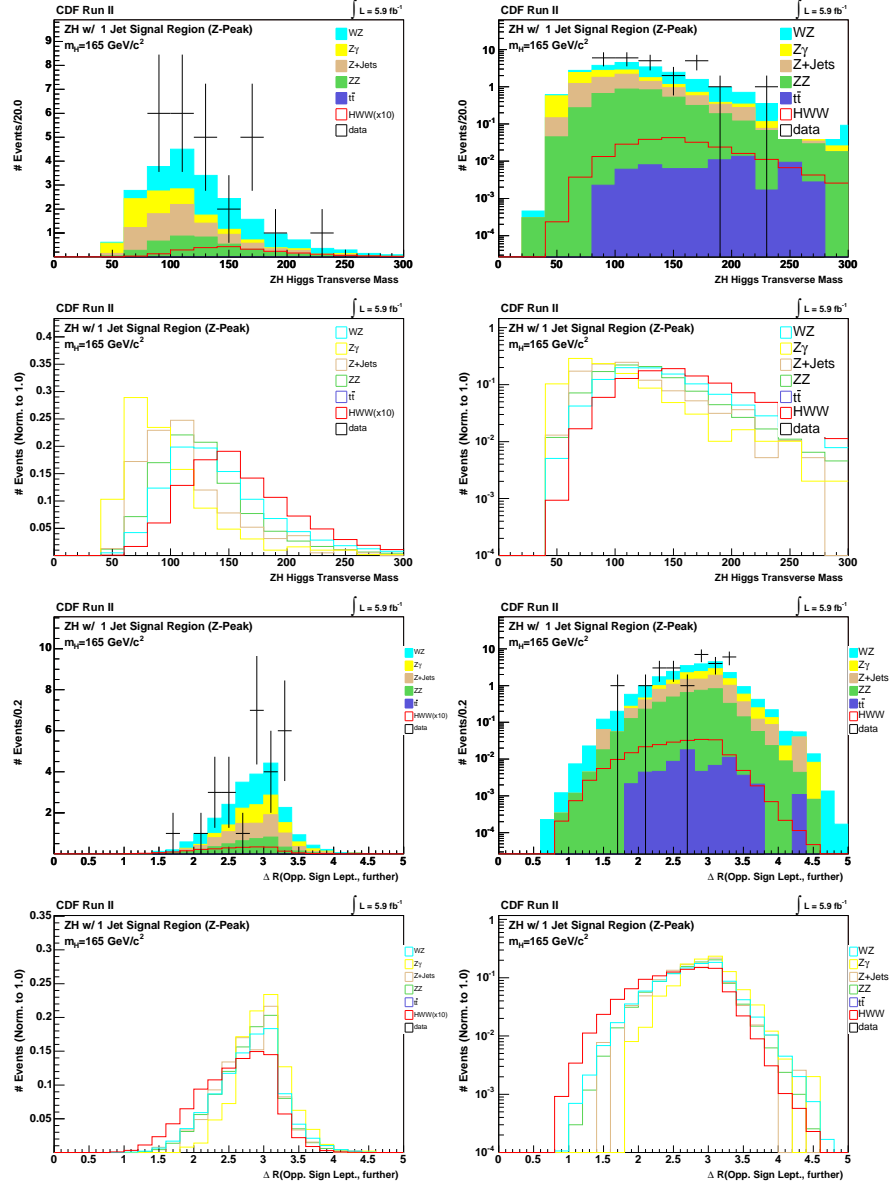


Figure P.11 ZH (1-jet) Analysis: $\Delta\phi(W\text{-lep}, E_T)$, $\Delta\phi(\text{lept. sum}, E_T)$

Figure P.12 ZH (1-jet) Analysis: ZH Higgs Mass, ΔR Opp. Sign Far Left

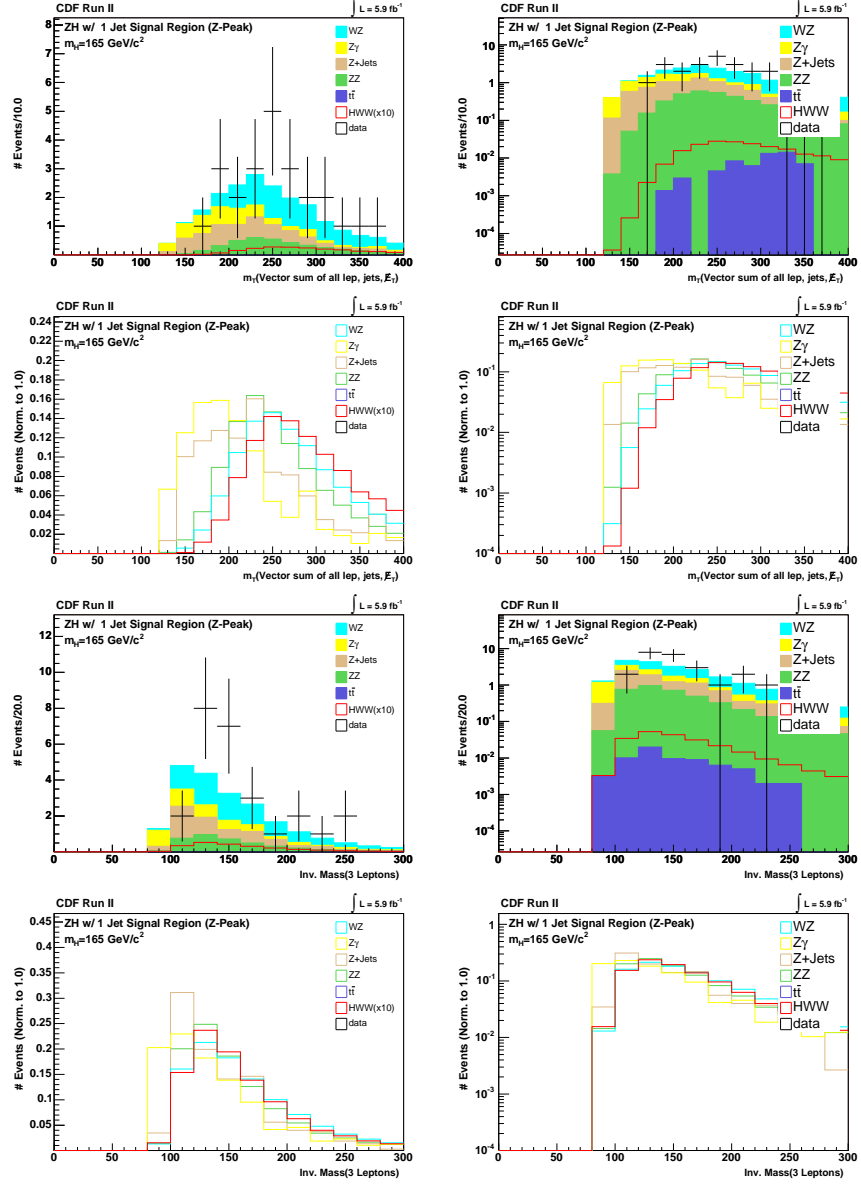
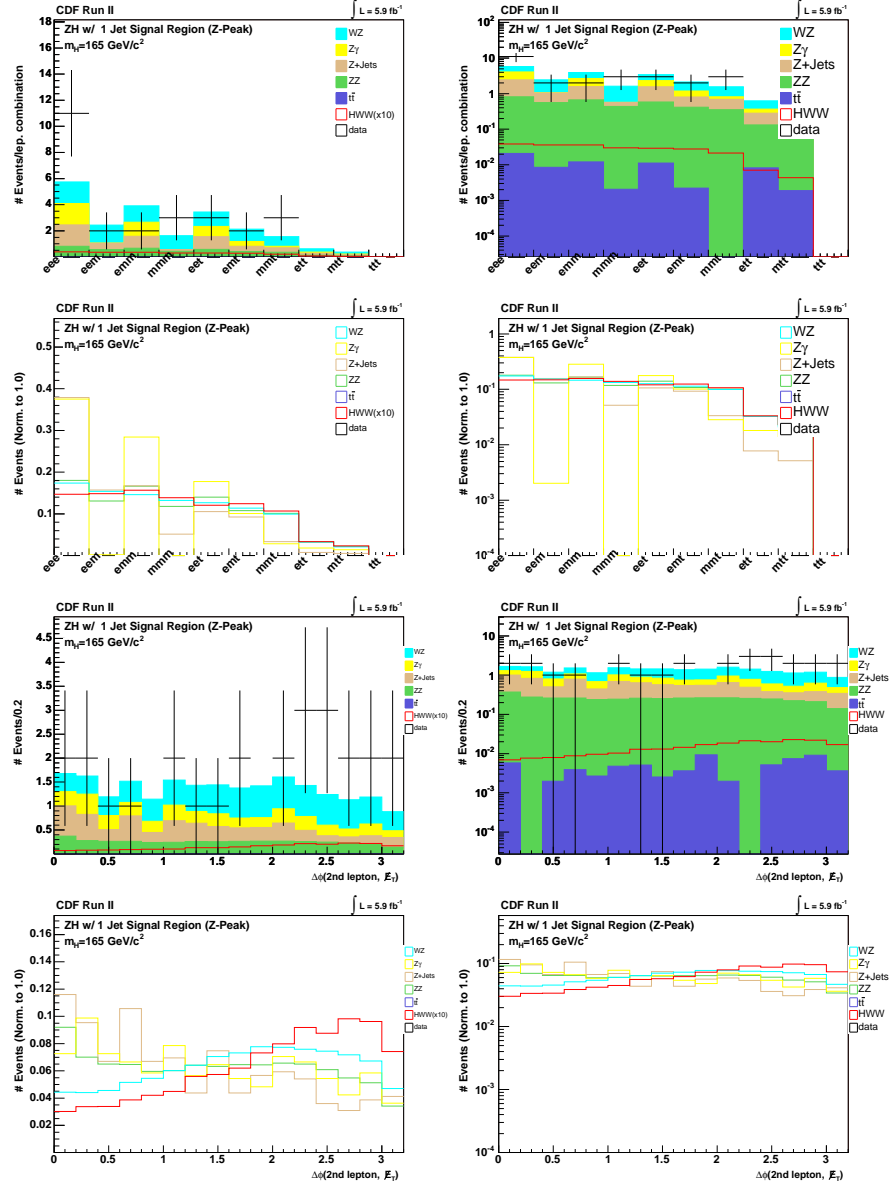
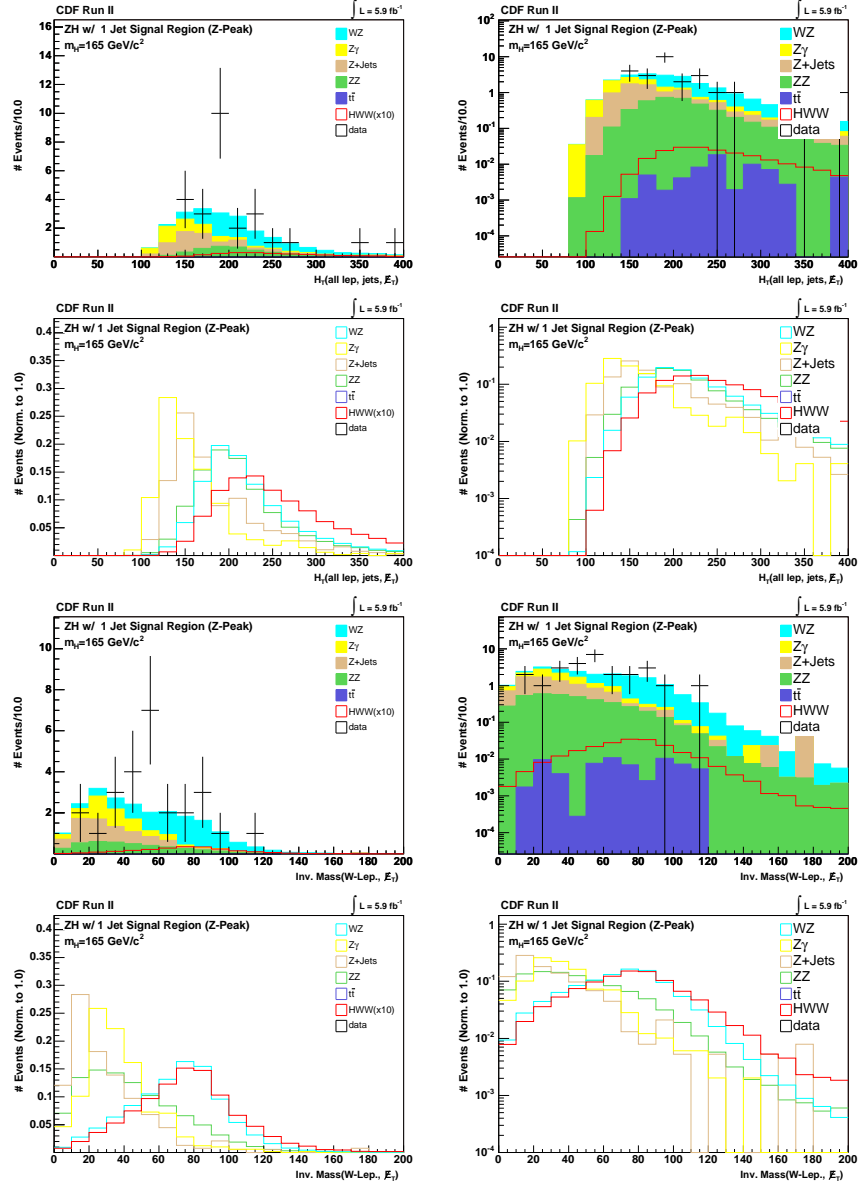
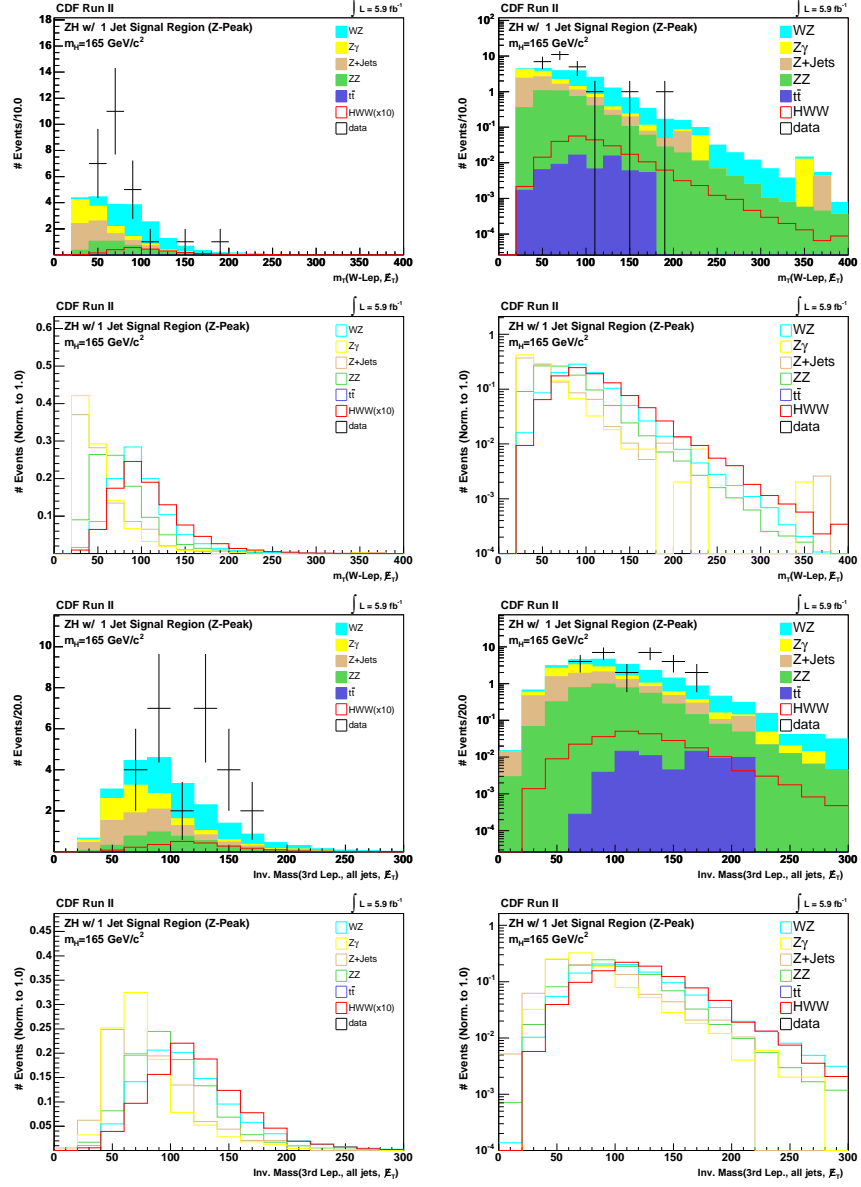
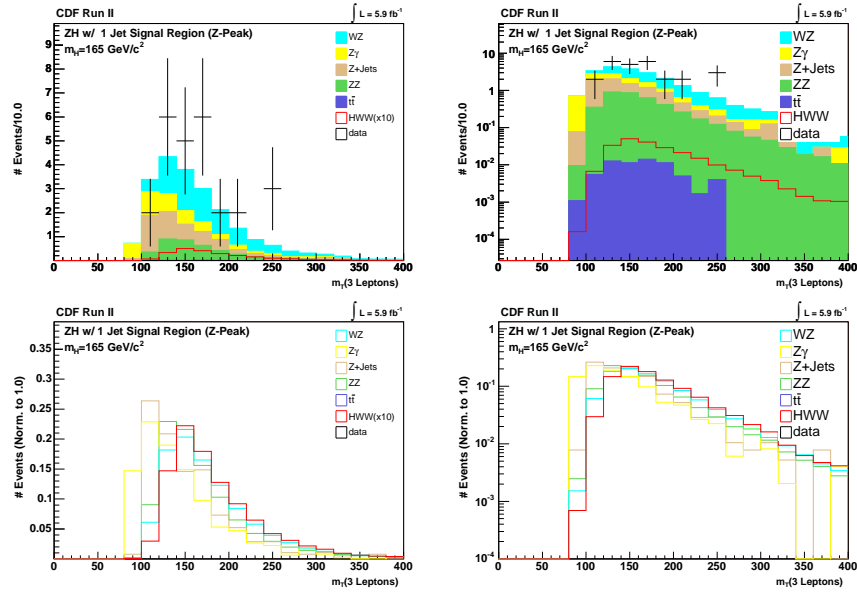


Figure P.13 ZH (1-jet) Analysis: m_T (all lept., \cancel{E}_T , Jets), Inv. Mass (all lept.)

Figure P.14 ZH (1-jet) Analysis: Lepton Types, $\Delta\phi(\text{Lep2}, E_T)$

Figure P.15 ZH (1-jet) Analysis: H_T , $\text{Inv. Mass (W-lep.)}$, E_T

Figure P.16 ZH (1-jet) Analysis: $m_T(W\text{-lep}, E_T)$, $\text{Inv. Mass}(\text{Lep3}, E_T, \text{Jets})$

Figure P.17 ZH (1-jet) Analysis: m_T Trilepton Mass

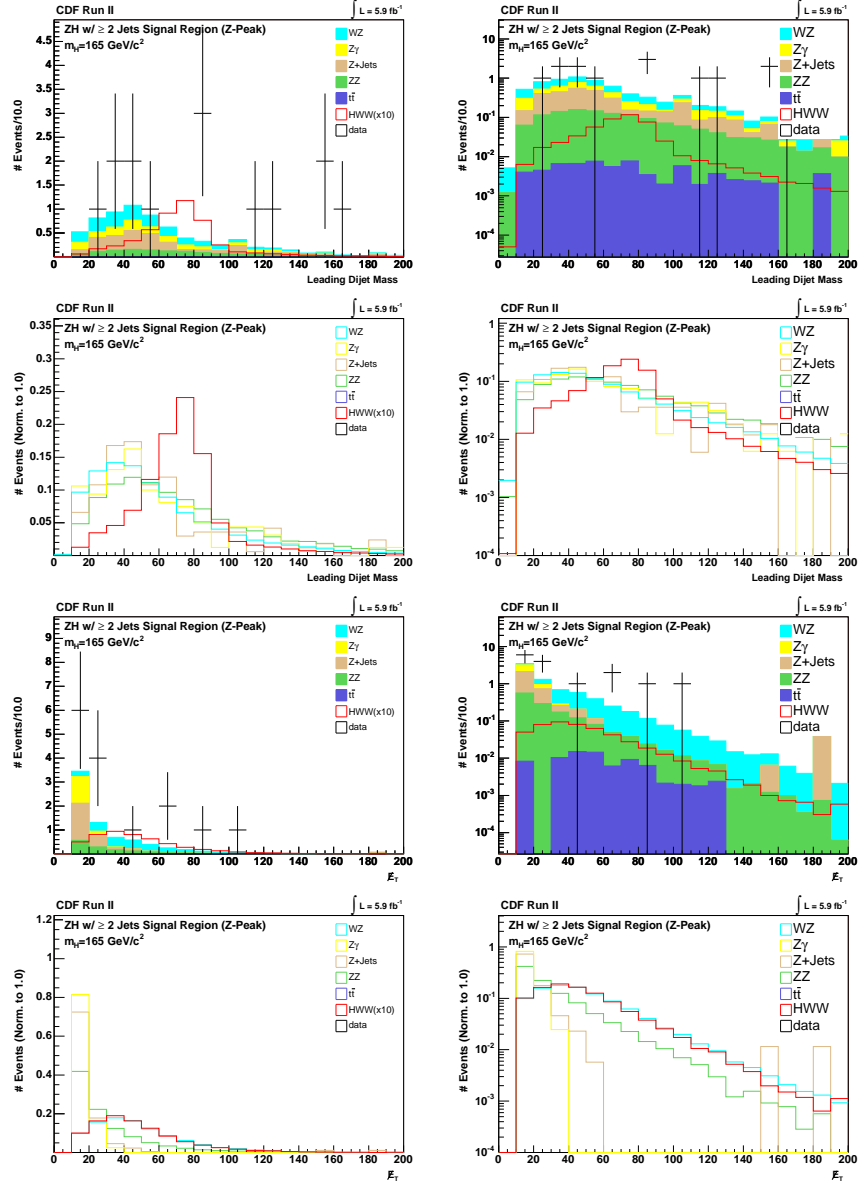


Figure P.18 ZH (≥ 2 -jet) Analysis: Inv. Mass ($1^{\text{st}} \& 2^{\text{nd}}$ jet), E_T

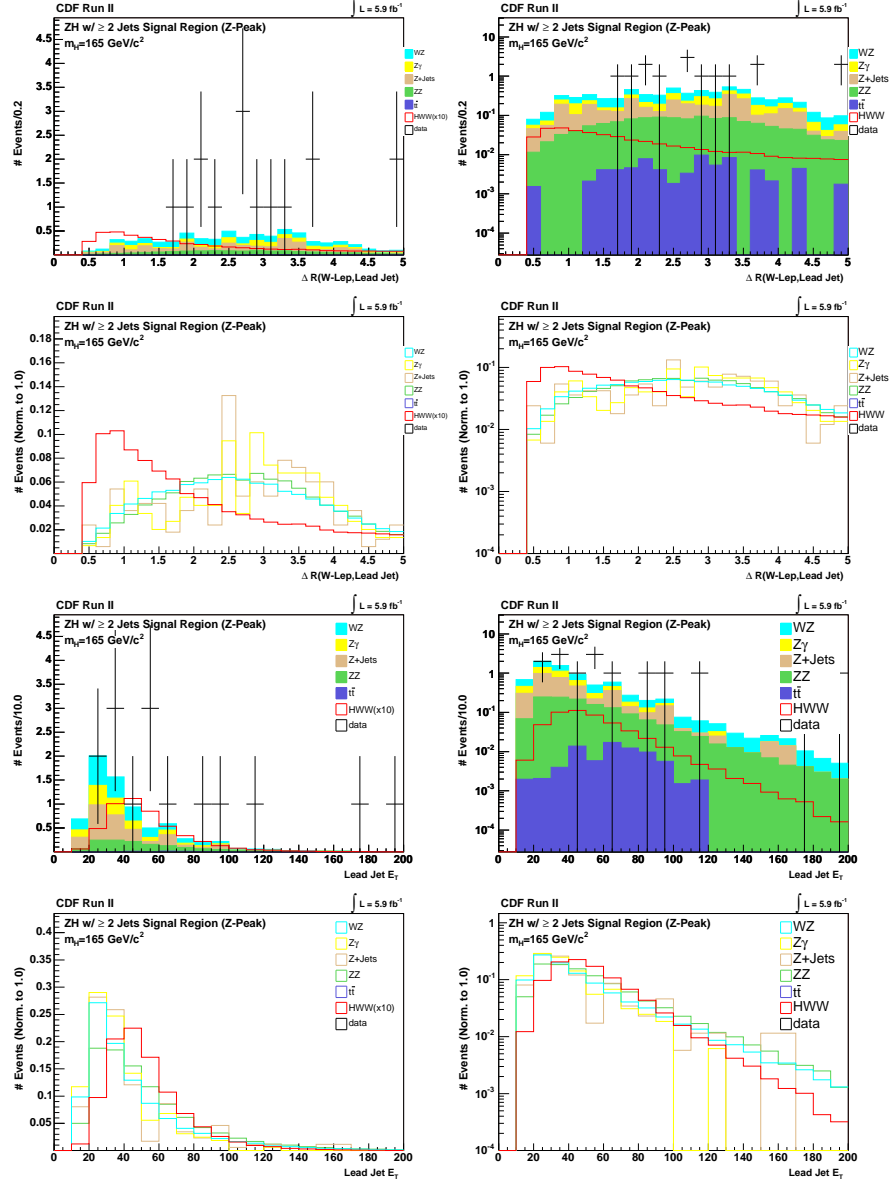


Figure P.19 ZH (≥ 2 -jet) Analysis: $\Delta R(W\text{-lep}, 1^{\text{st}} \text{ jet})$, $1^{\text{st}} \text{ jet } E_T$

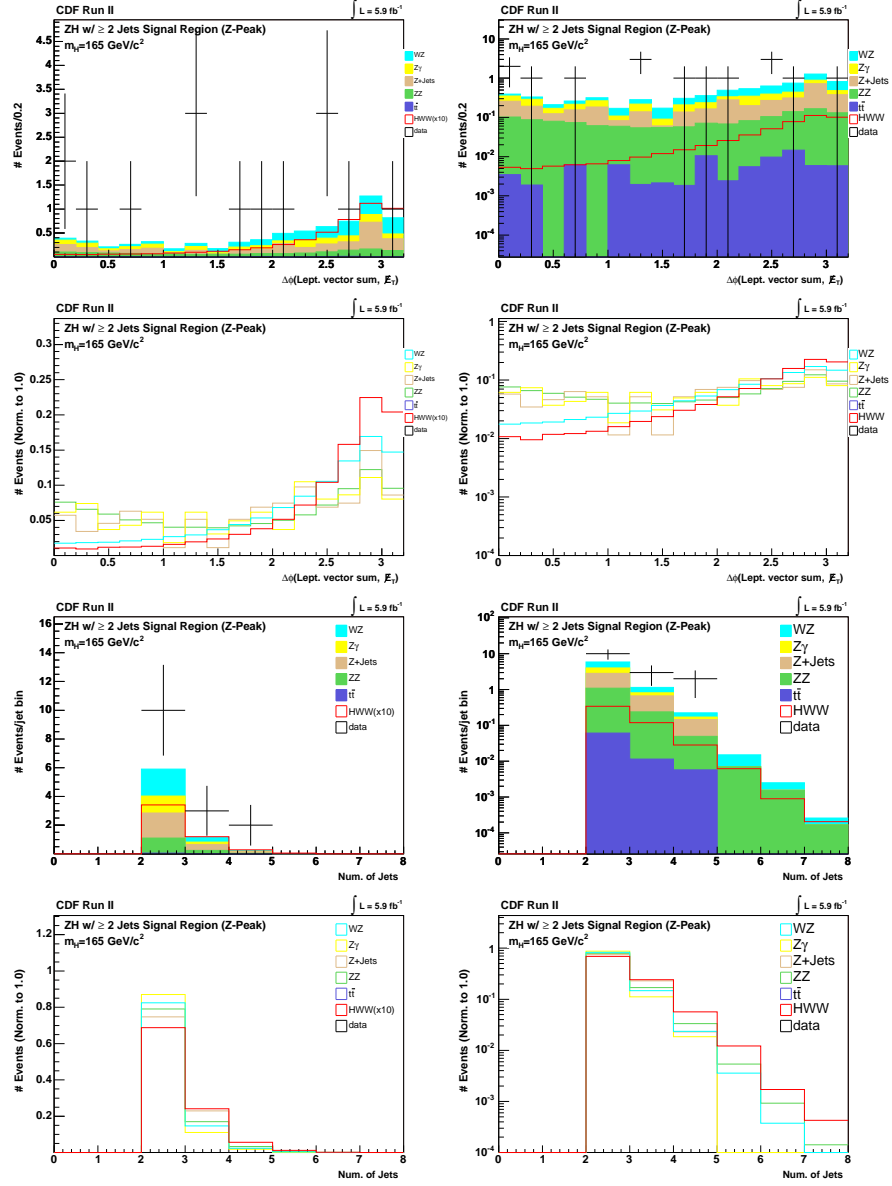


Figure P.20 ZH (≥ 2 -jet) Analysis: $\Delta\phi(\text{lept. sum}, E_T)$, N_{Jet}

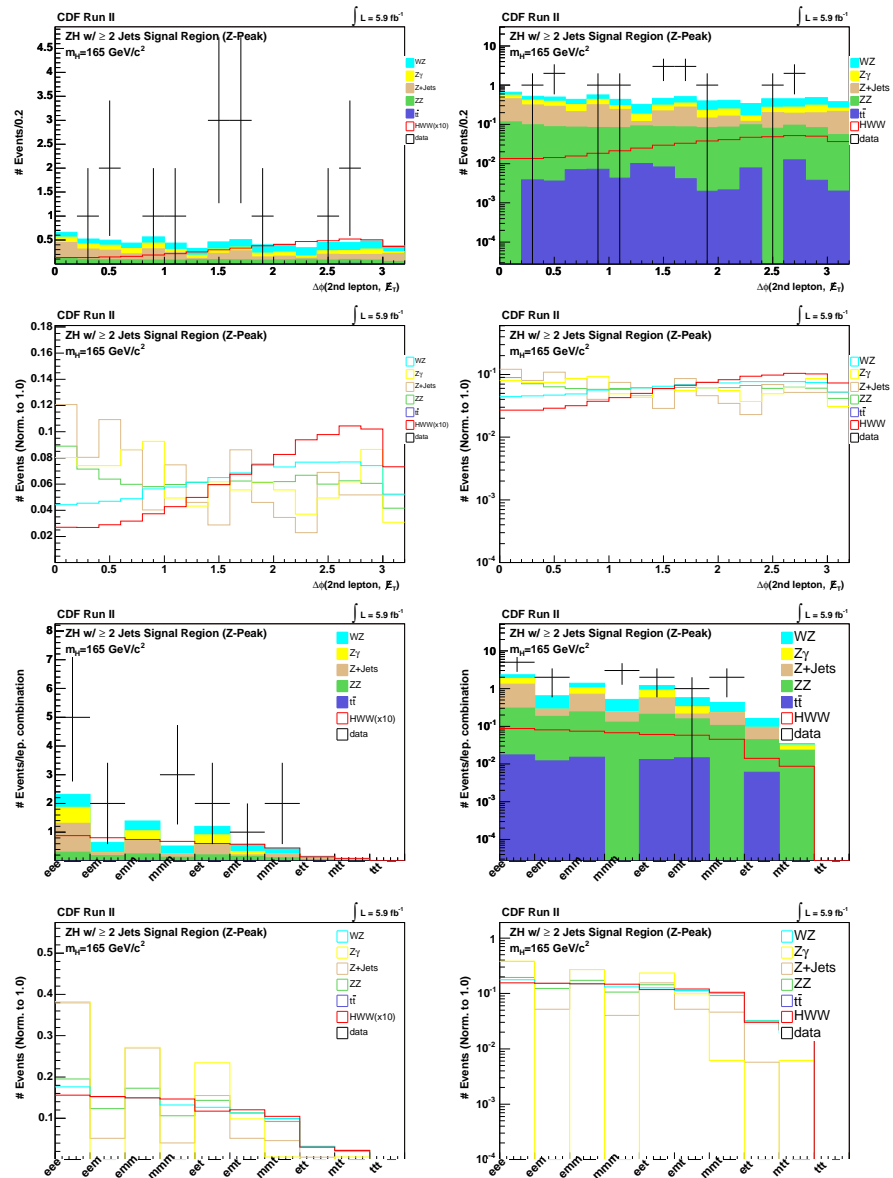


Figure P.21 ZH (≥ 2 -jet) Analysis: $\Delta\phi(\text{Lep2}, \vec{E}_T)$, Lepton Types

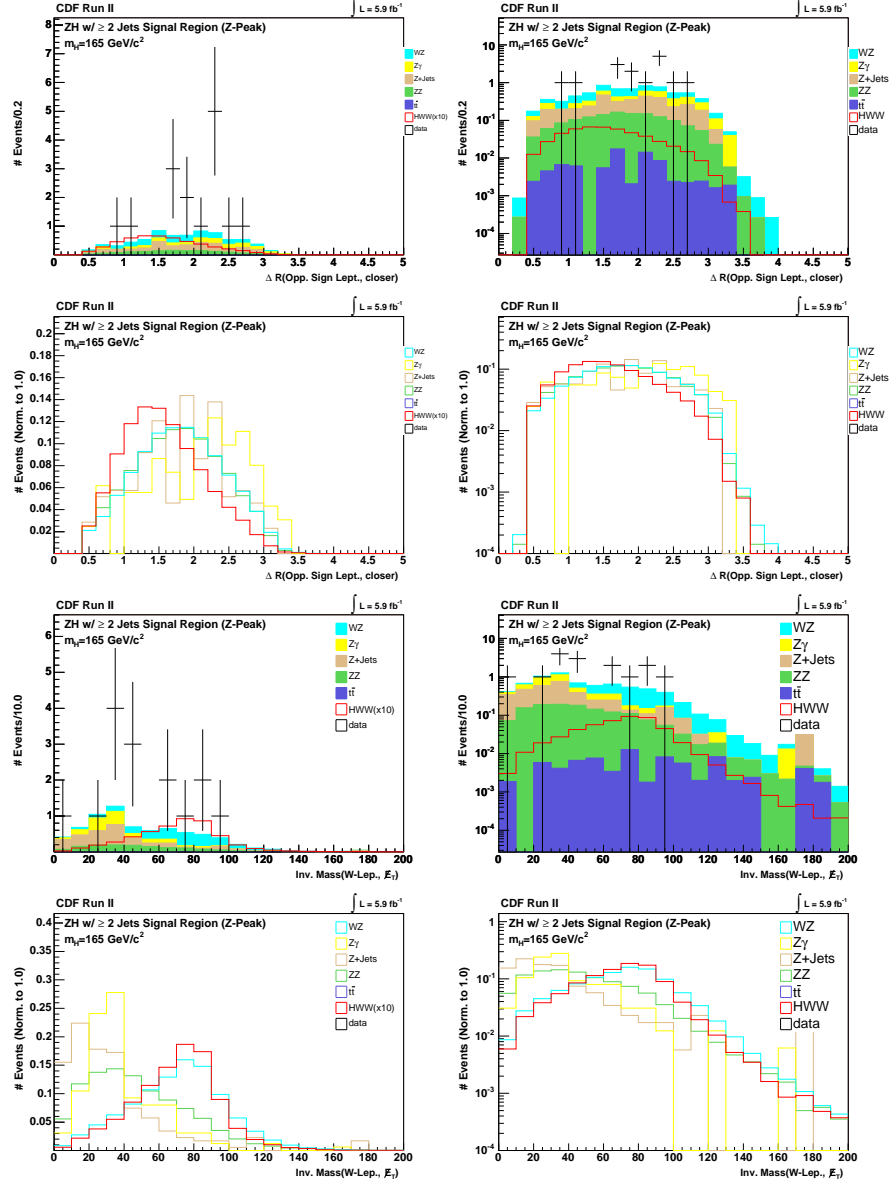
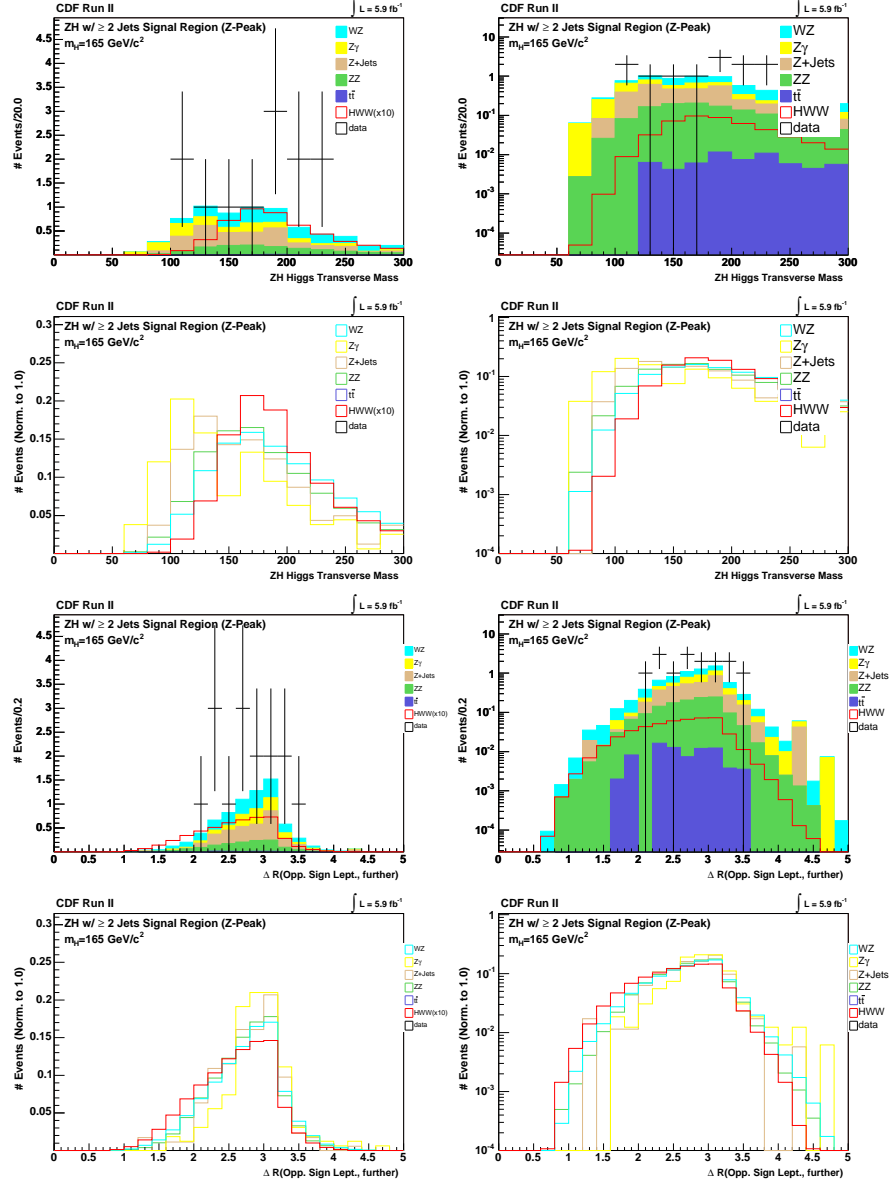


Figure P.22 ZH (≥ 2 -jet) Analysis: ΔR b/w Opp. Sign Close Lept., $\text{Inv. Mass}(W\text{-lep.}, E_T)$

Figure P.23 ZH (≥ 2 -jet) Analysis: ZH Higgs Mass, ΔR Opp. Sign Far Left.

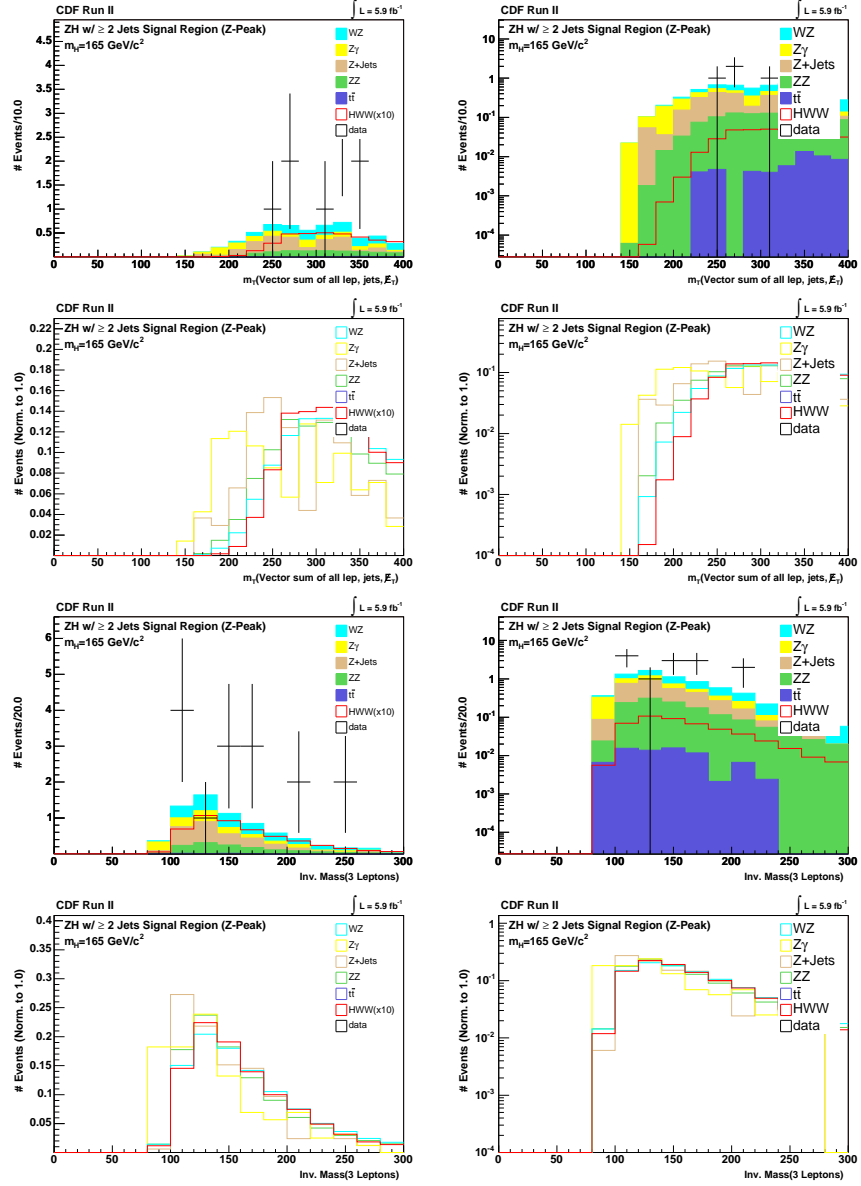


Figure P.24 ZH (≥ 2 -jet) Analysis: $m_T(\text{Leptons}, \vec{E}_T, \text{Jets})$, $\text{Inv. Mass}(\text{all lept.})$

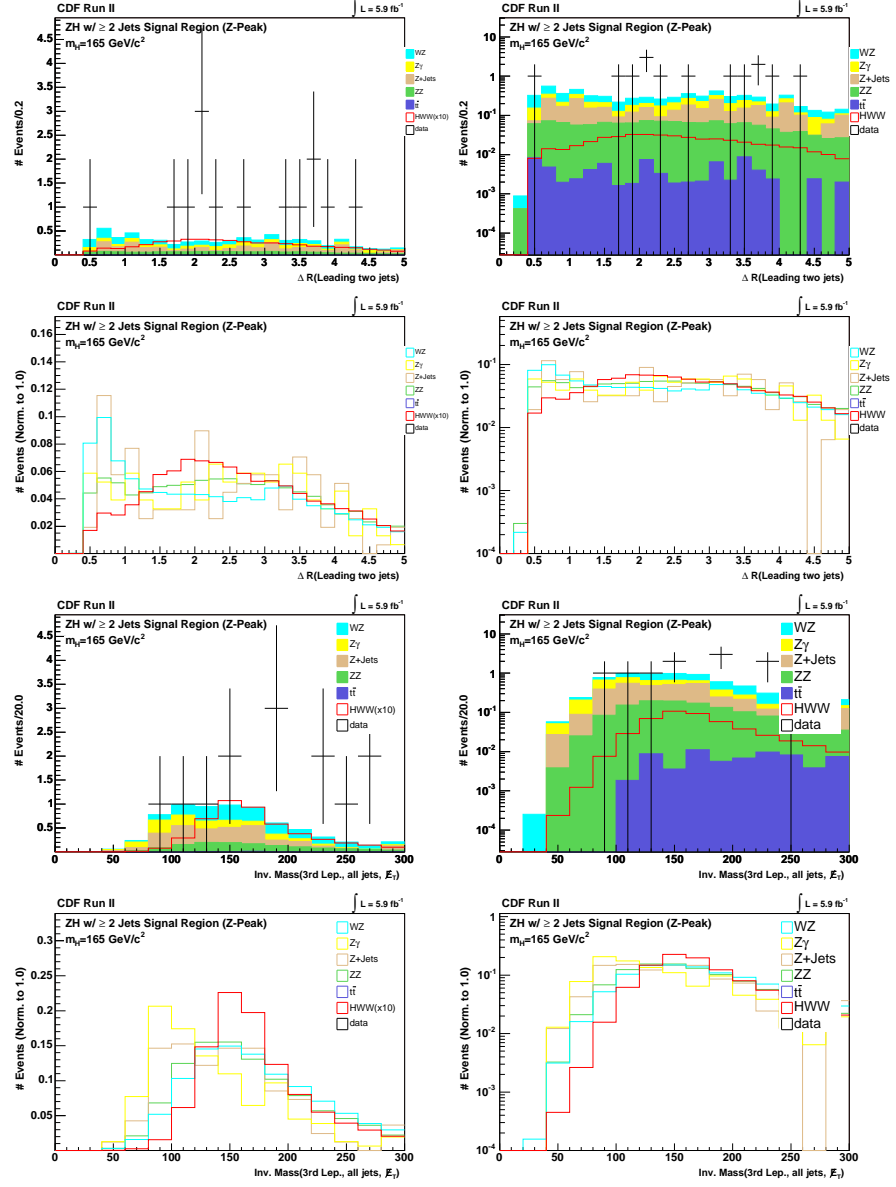
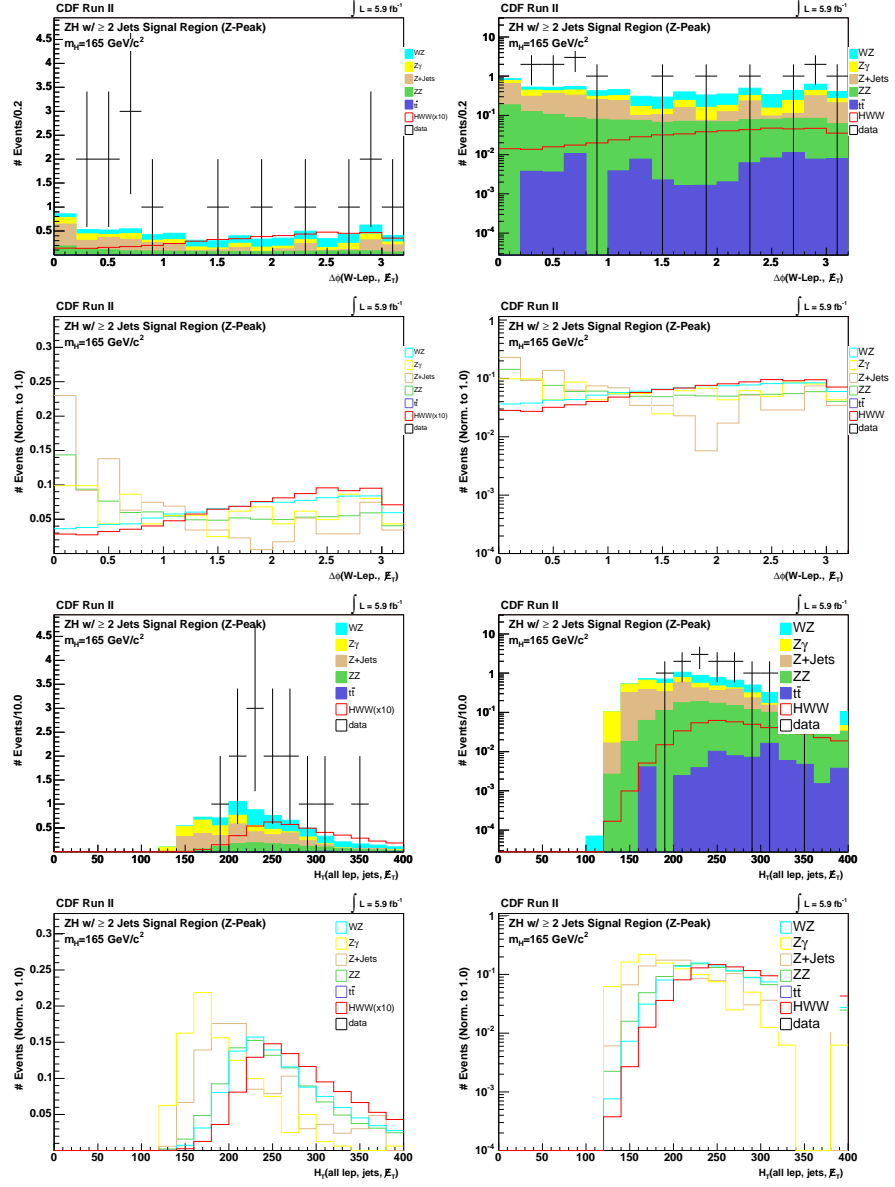


Figure P.25 ZH (≥ 2 -jet) Analysis: $\Delta R(1^{\text{st}} \& 2^{\text{nd}} \text{ jet})$, $\text{Inv. Mass}(\text{Lep3}, \mathcal{E}_T, \text{Jets})$

Figure P.26 ZH (≥ 2 -jet) Analysis: $\Delta\phi(W\text{-lep}, E_T)$, H_T

Appendix Q: Neural Net Input Variables for the Control Regions

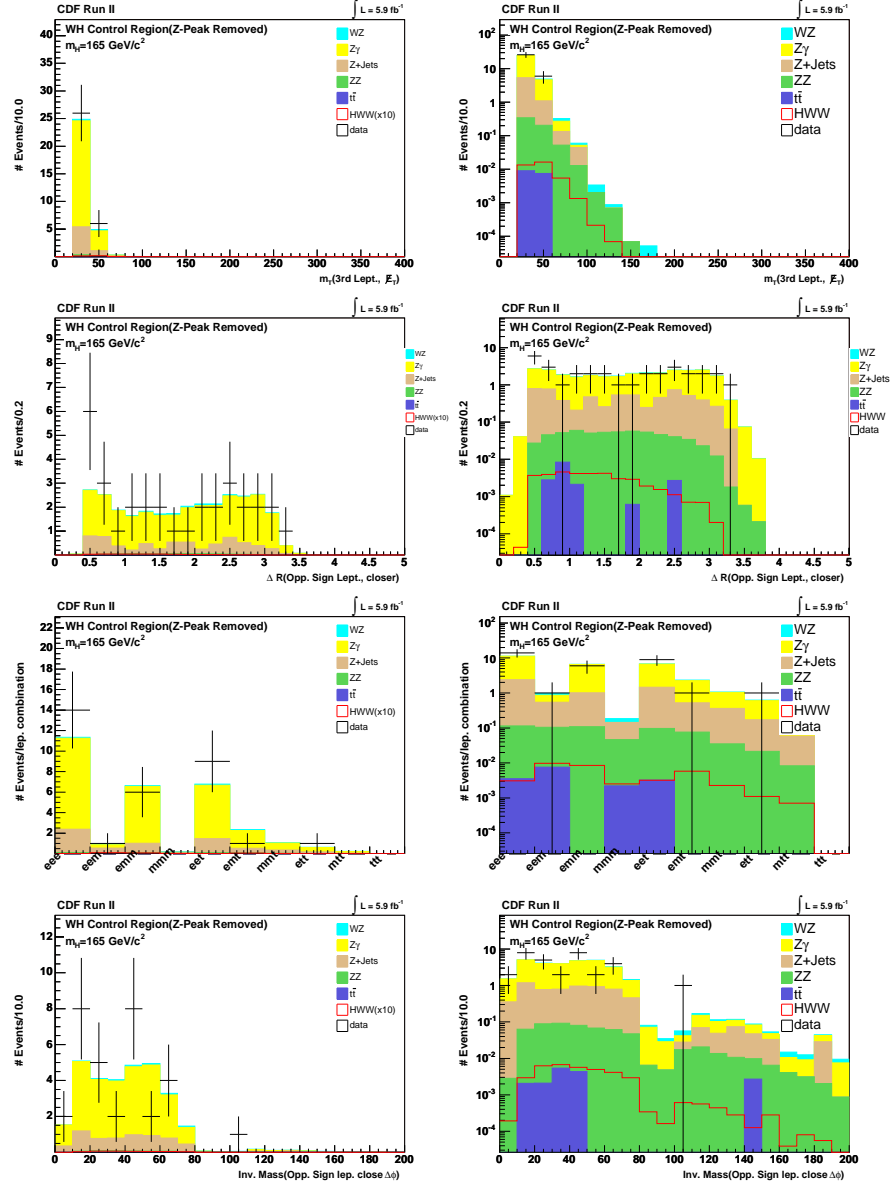


Figure Q.1 *WH* Analysis: m_T (Lep3, E_T), ΔR b/w Opp. Sign Close Lept., Lepton types, Dimass Opp. Sign Leptons (closer pair in ϕ)

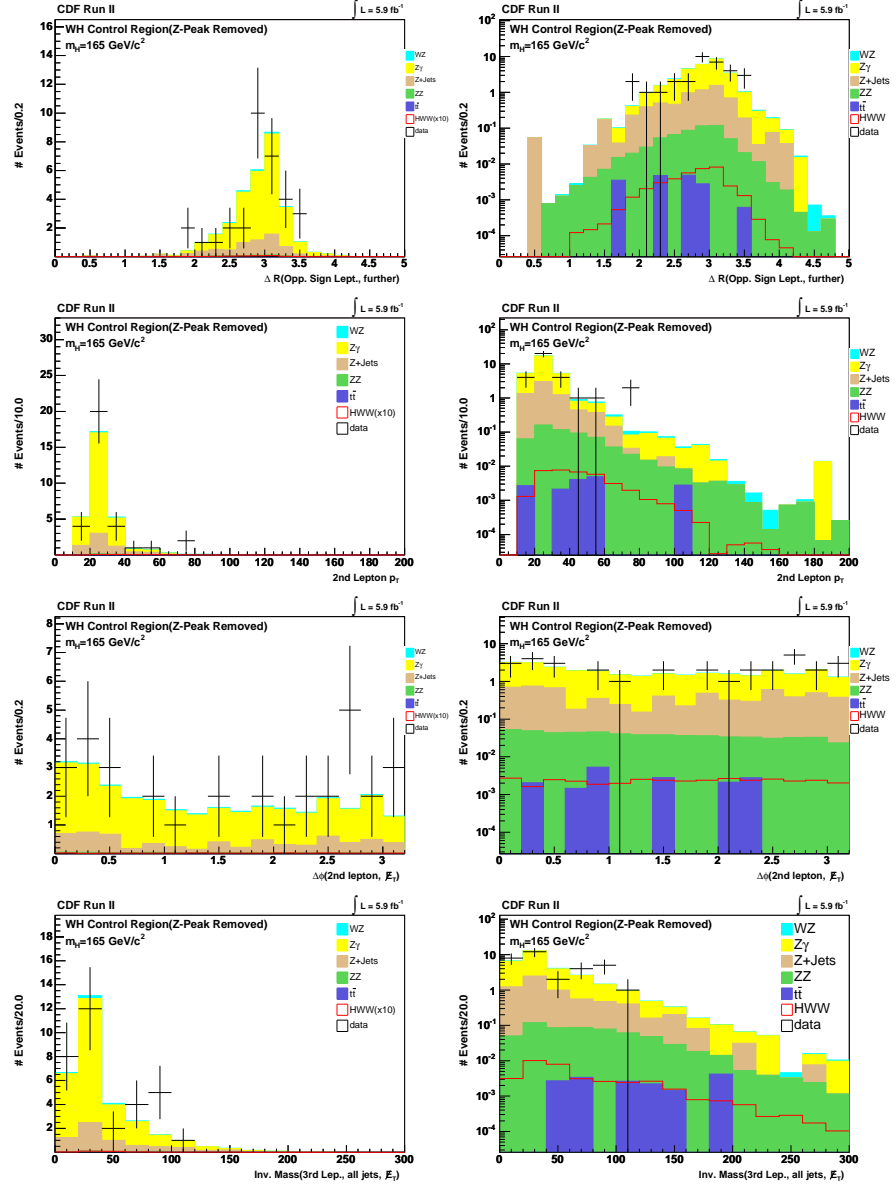


Figure Q.2 WH Analysis: ΔR Opp. Sign Far Lept., 2^{nd} Lepton p_T , $\Delta\phi(\text{Lep2}, \vec{E}_T)$, Inv. Mass(Lep3, \vec{E}_T , Jets)

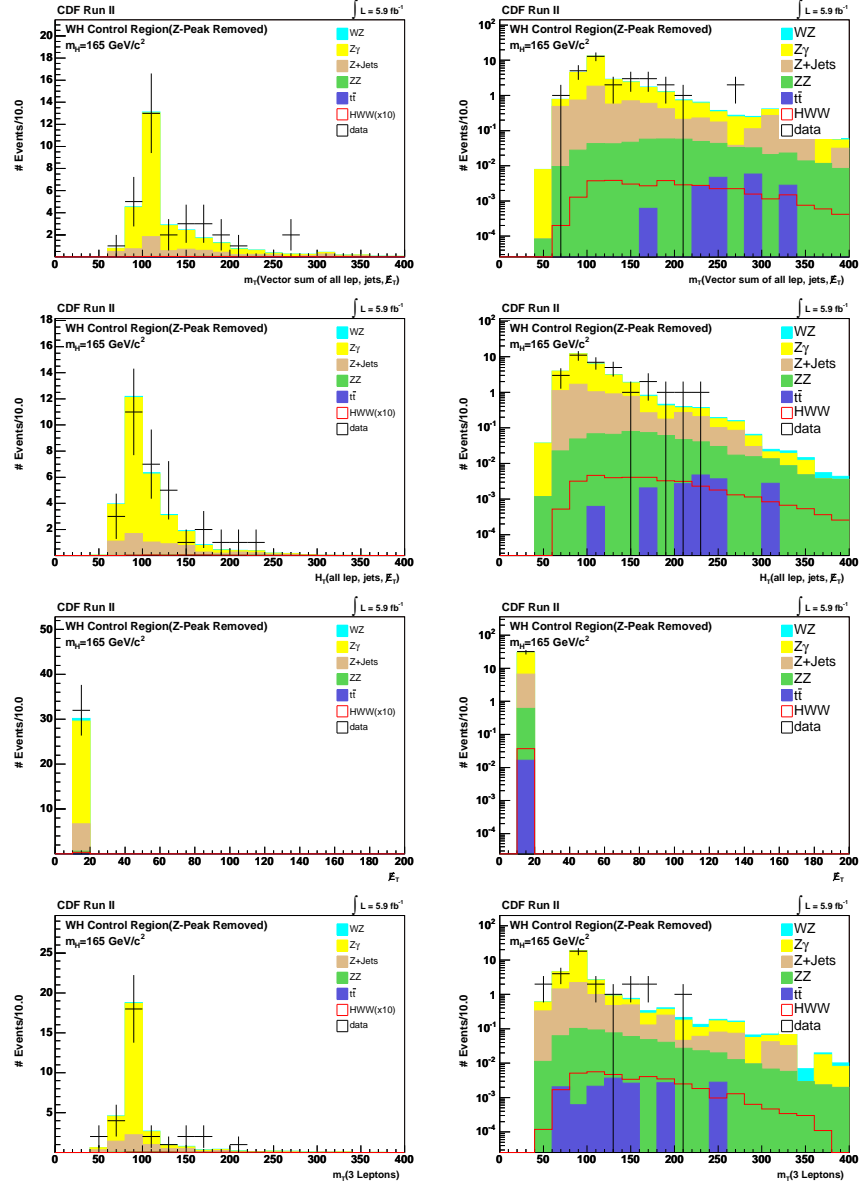


Figure Q.3 WH Analysis: m_T (all lept., E_T , Jets), H_T , E_T , m_T Tripleton Mass

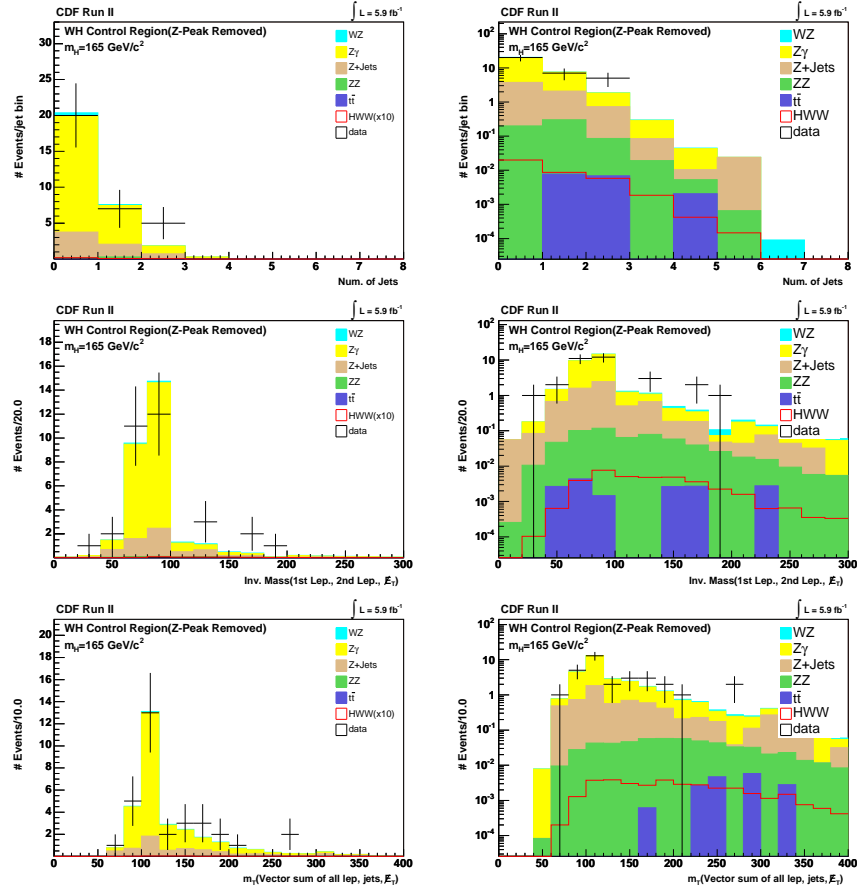


Figure Q.4 WH Analysis: NJet, Inv. Mass(Lep1,Lep2, E_T), m_T (all lept., E_T , jets)

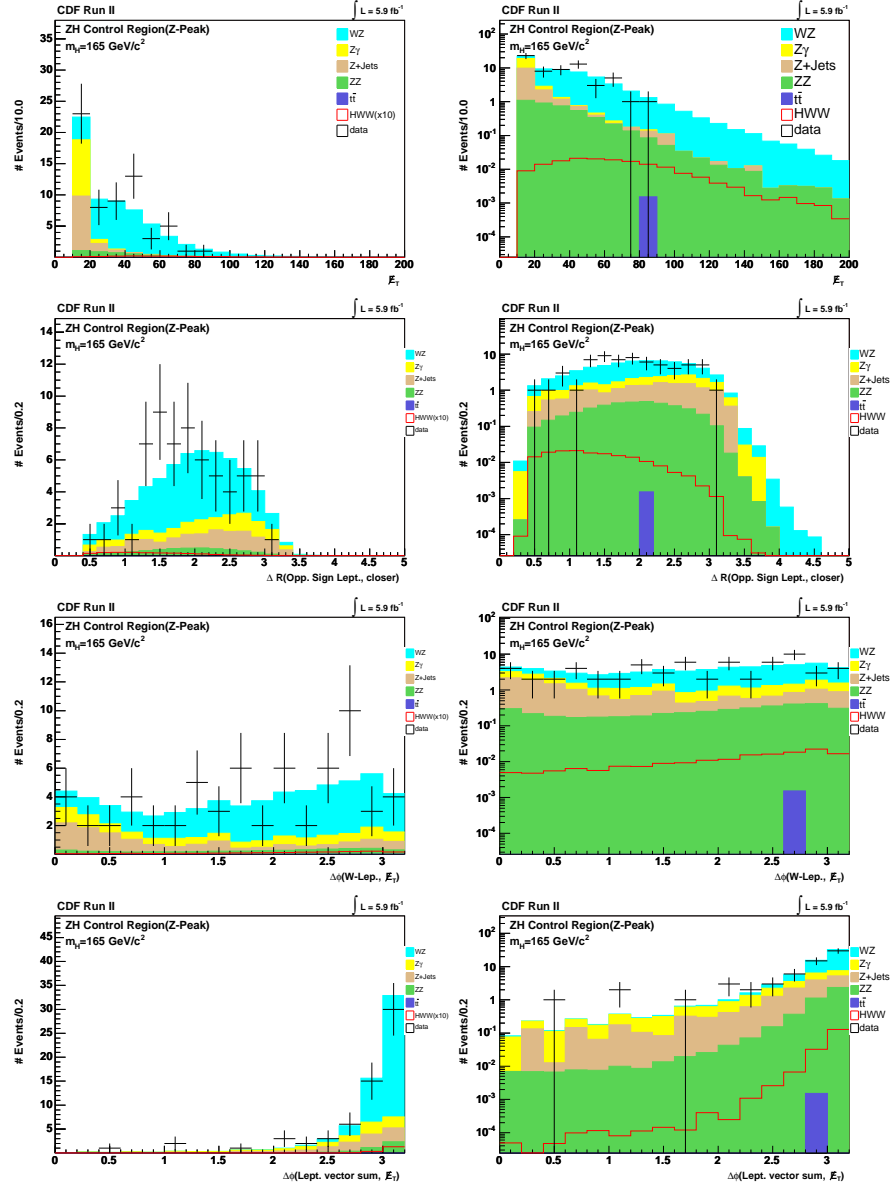


Figure Q.5 ZH Analysis: E_T , ΔR b/w Opp. Sign Close Lept., $\Delta\phi(W\text{-lep}, E_T)$, $\Delta\phi(\text{lept. sum}, E_T)$

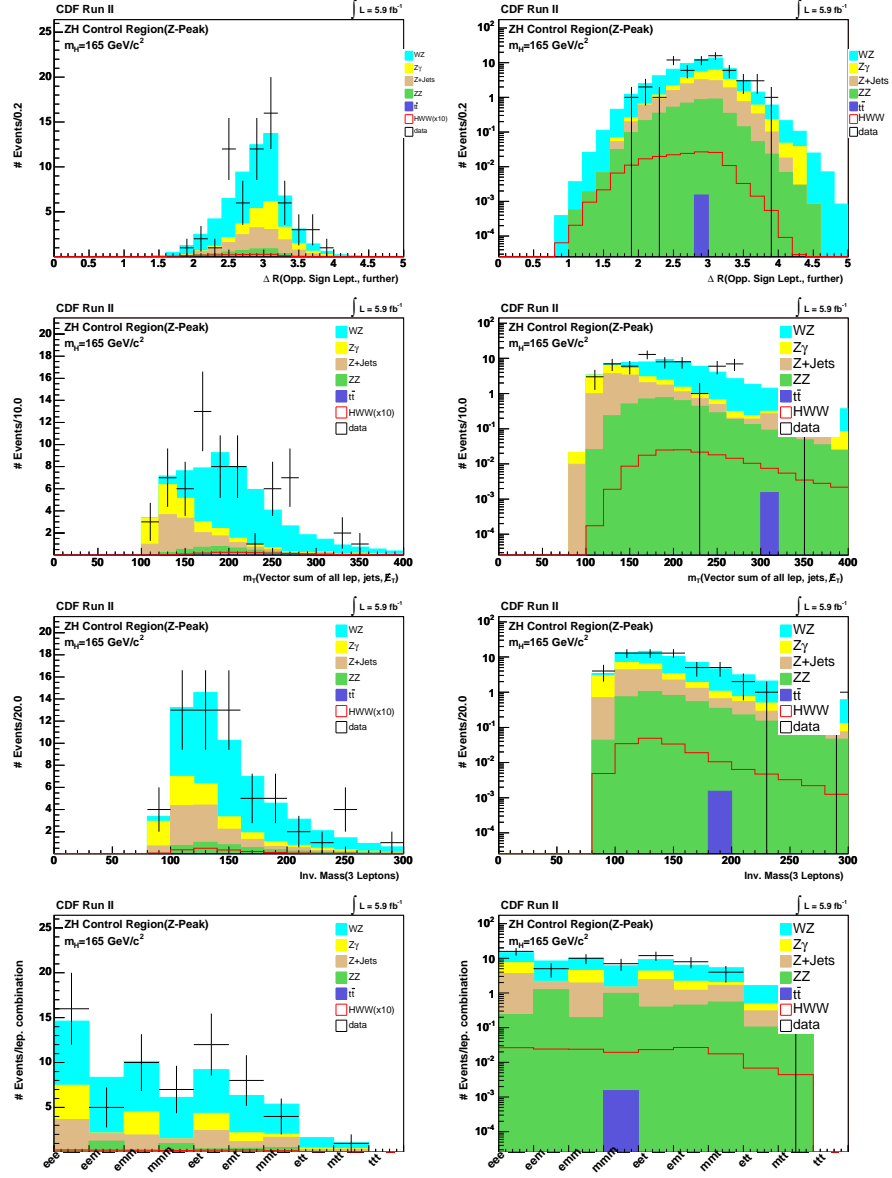


Figure Q.6 ZH Analysis: ΔR Opp. Sign Far Leptons, $m_T(\text{all lept.}, \vec{E}_T, \text{Jets})$, Inv. Mass (all lept.), Lepton Types

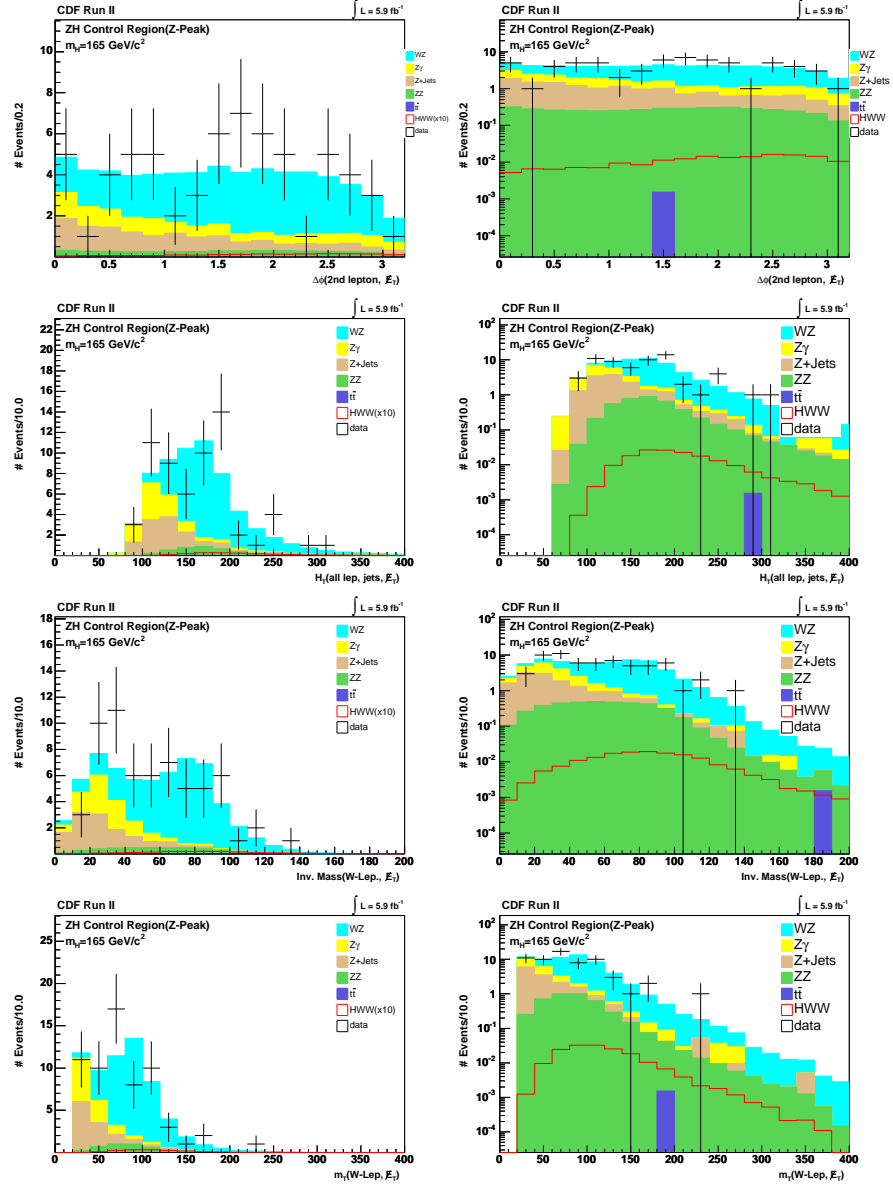


Figure Q.7 ZH Analysis: $\Delta\phi(\text{Lep}2, E_T)$, H_T , Inv. Mass ($W\text{-lep.}, E_T$), m_T ($W\text{-lep.}, E_T$)

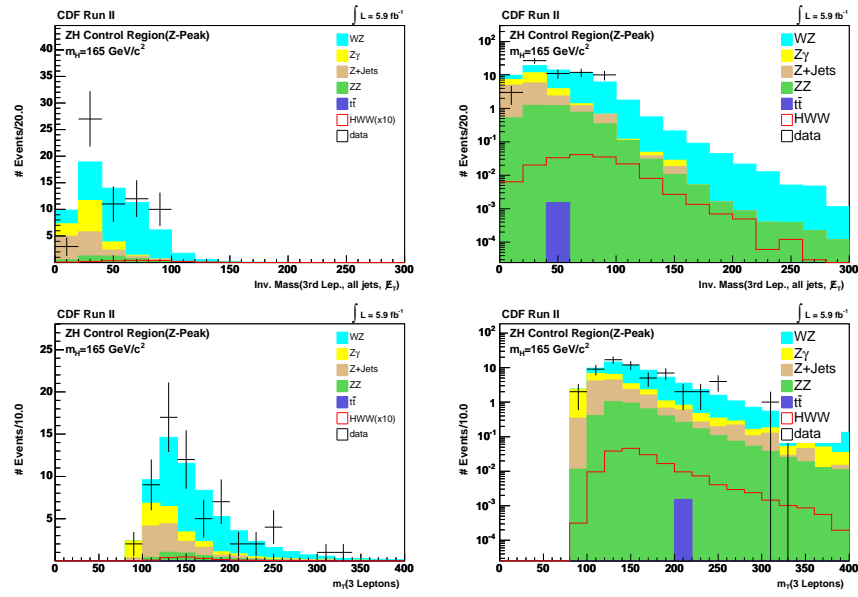
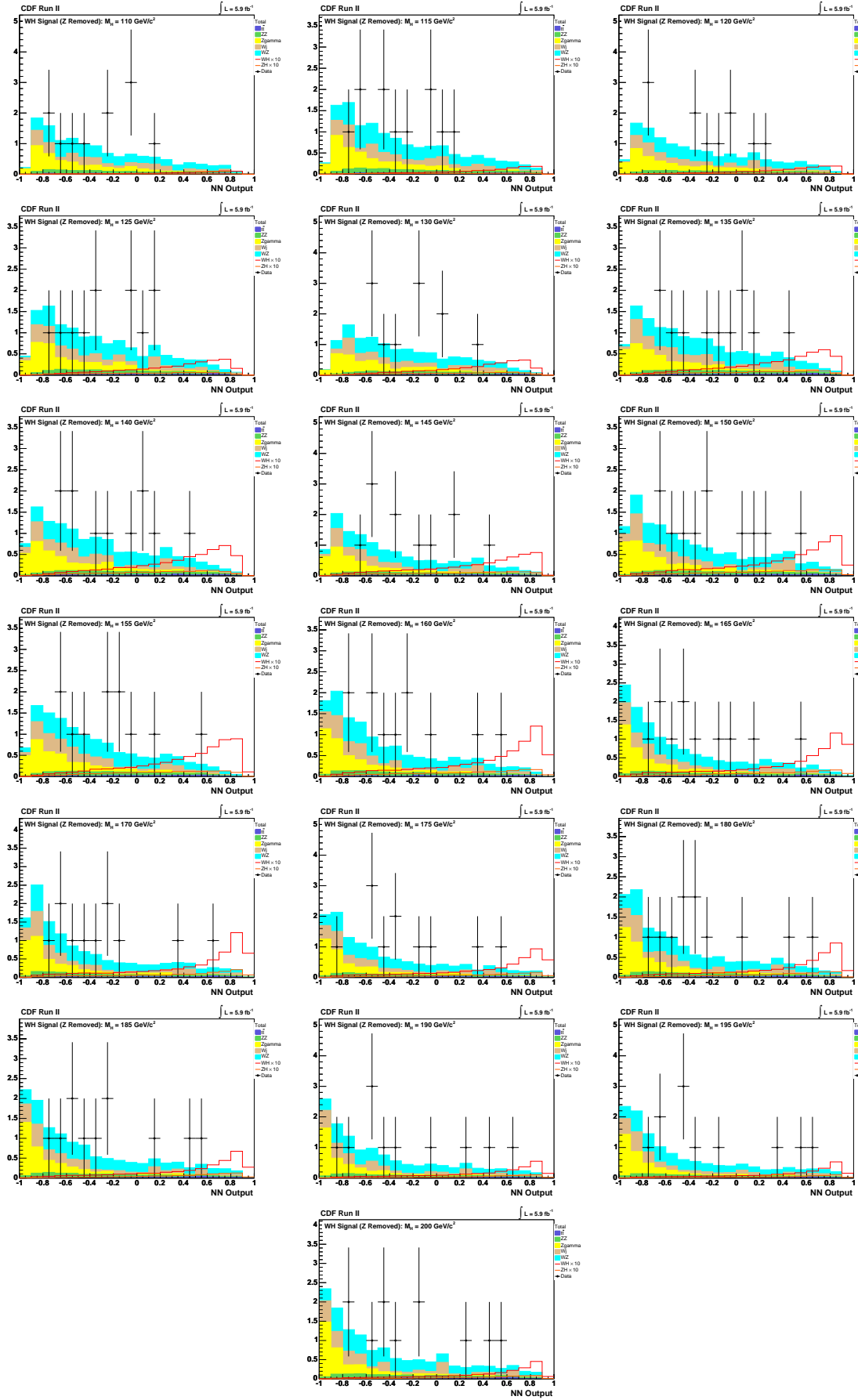
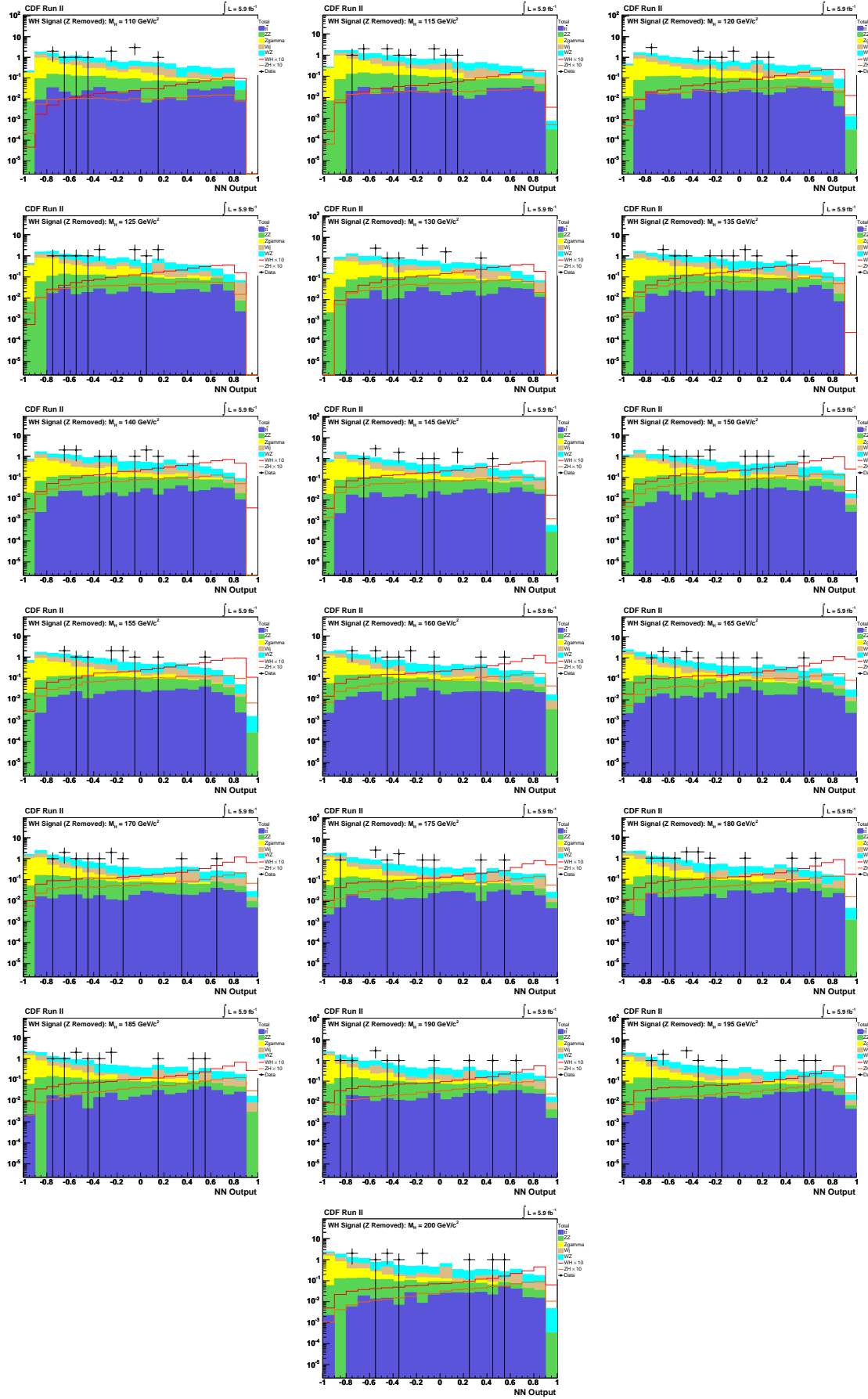


Figure Q.8 ZH Analysis: Inv. Mass(Lep3, \cancel{E}_T , Jets), m_T Trilepton Mass

Appendix R: Neural Net Scores

Figure R.1 Trilepton WH NeuroBayes Neural Network output (linear scale)

Figure R.2 Tripleton WH NeuroBayes Neural Network output (log scale)

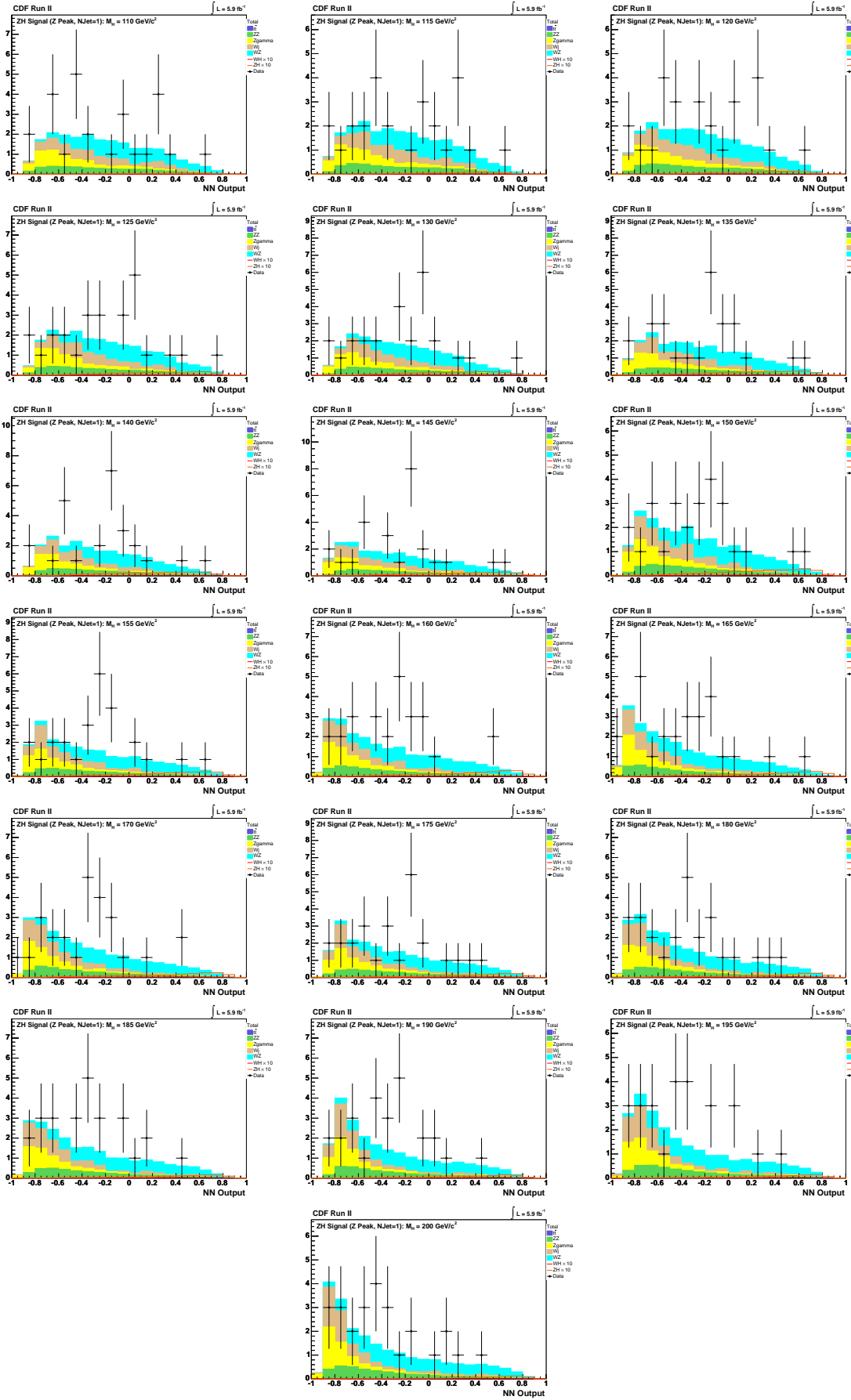


Figure R.3 Trilepton ZH (1 Jet) NeuroBayes Neural Network output (linear scale)

Figure R.4 Trilepton ZH (1 Jet) NeuroBayes Neural Network output (log scale)

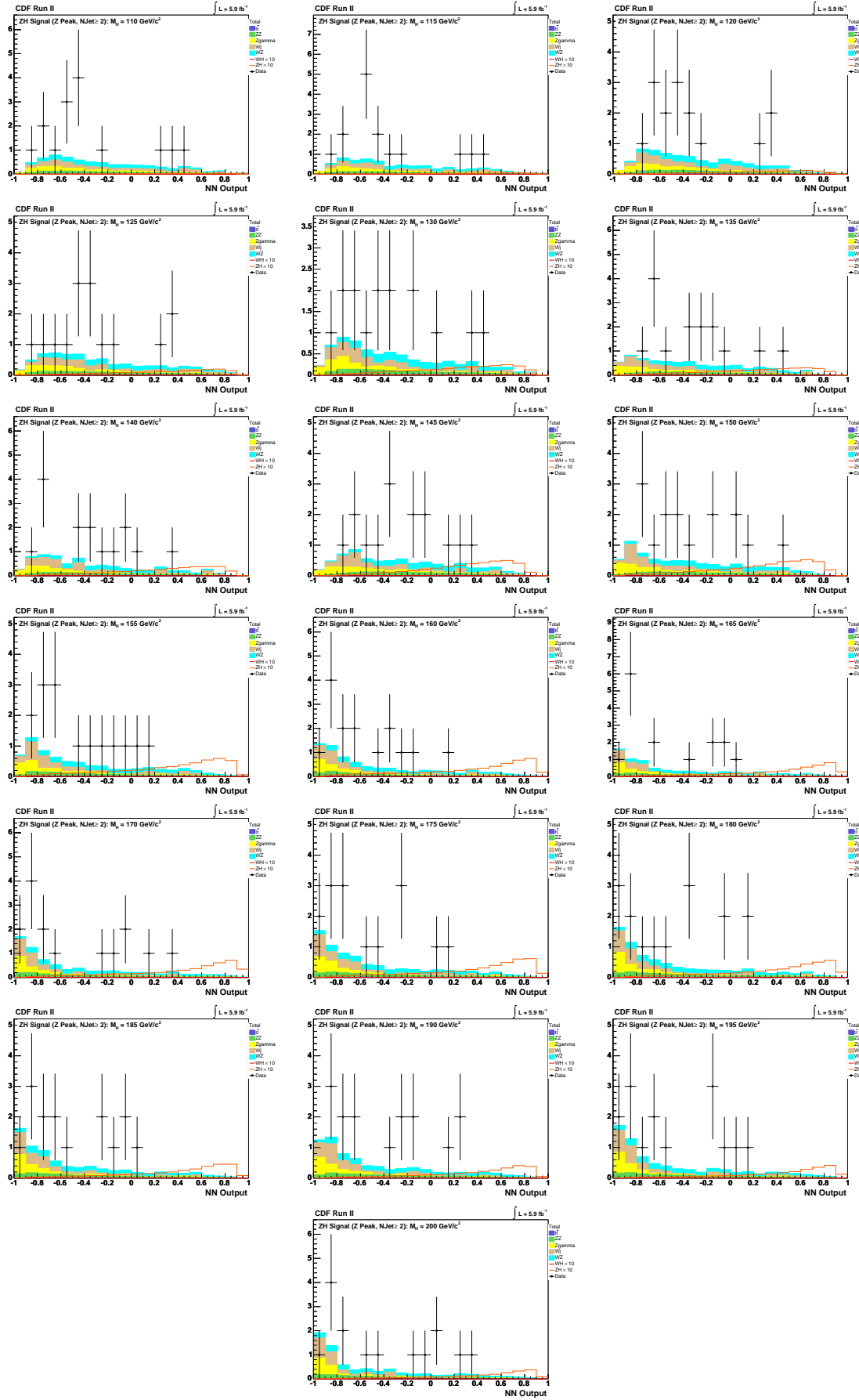
Figure R.5 Tripleton $ZH (\geq 2 \text{ Jets})$ NeuroBayes Neural Network output (linear scale)

Figure R.6 Trilepton ZH (≥ 2 Jets) NeuroBayes Neural Network output (log scale)

LIST OF REFERENCES

- [1] Pythia. Website. <http://home.thep.lu.se/torbjorn/Pythia.html>.
- [2] Fermilab's chain of accelerators, accelerator details: the antiproton source. Website, August 2000. <http://www-bd.fnal.gov/public/antiproton.html>.
- [3] Fermilab's chain of accelerators, accelerator details: the main injector. Website, August 2000. <http://www-bd.fnal.gov/public/maininj.html>.
- [4] Fermilab's chain of accelerators, accelerator details: the proton source. Website, August 2000. <http://www-bd.fnal.gov/public/tevatron.html>.
- [5] Layer 00. Website, November 2000. <http://www-cdf.fnal.gov/internal/upgrades/layer00/layer00.html>.
- [6] Svx ii homepage. Website, September 2000. http://www-cdf.fnal.gov/internal/upgrades/svxii/svxii_home.html.
- [7] Intermediate silicon layers. Website, February 2001. <http://www-cdf.fnal.gov/internal/upgrades/isl/isl.html>.
- [8] Fermilab: Tevatron luminosity. Website, March 2002. <http://www.fnal.gov/pub/now/tevlum.html>.
- [9] Cdf central outer tracker. Website, November 2004. <http://www-cdf.fnal.gov/internal/upgrades/cot/>.
- [10] Run ii luminosity. Website, August 2006. http://www-d0.fnal.gov/runcoor/RUN/run2_lumi.html.
- [11] Fermilab today. Website, June 2008. http://www.fnal.gov/pub/today/archive_2008/today08-06-18.html.
- [12] Combined cdf and d upper limits on standard-model higgs-boson production. Website, November 2009. http://tevnpnphwg.fnal.gov/results/SM.Higgs_Fall_09/.

- [13] Cdf run2 triggers and filters report group triggers and bits on cdf online production report – physics table physics_5_04_v-3. Website, March 2010. http://cdfdbb.fnal.gov:8520/cdfr2/databases?tdt=phy&tdv=PHYSICS_5_04_v-3.
- [14] The mc@nlo package. Website, 2010. <http://www.hep.phy.cam.ac.uk/theory/webber/MCatNLO/>.
- [15] I. J. R. Aitchison and A. J. G. Hey. *Gauge Theories in Particle Physics. Vol. 2: QCD and the Electroweak Theory*. Institute of Physics Publishing, Philadelphia, 2004.
- [16] I. J. R. Aitchison and A. J. G. Hey. *Gauge Theories in Particle Physics. Vol. 2: QCD and the Electroweak Theory*. Institute of Physics Publishing, Philadelphia, 2004.
- [17] A B Balantekin, editor. *Journal of Physics G Nuclear and Particle Physics*, volume 33. Institute of Physics, 2006.
- [18] R. Barate et al. Search for the standard model Higgs boson at LEP. *Phys. Lett.*, B565:61–75, 2003.
- [19] D. Benjamin, , M. Kruse, Seig Oh, Geumbong Yu, P. Bussey, E. James, D. Hidas, S. Jindariani, B. Rutherford, R. Lysak, M. Herndon, J. Nett, J. Pursley, M. d’Errico, S.P. Griso, D. Lucchesi, A. Robson, R. St.Denis, Maria d’Errico, Donatella Lucchesi, and Anadi Canepa. Search for $h \rightarrow ww$ production using 5.3 fb^{-1} . CDF/PHYS/EXOTIC/CDFR/10086, 2010.
- [20] D. Benjamin, M. Kruse, P. Bussey, E. James, D. Hidas, S. Jindariani, B. Rutherford, R. Lysak, M. Herndon, J. Nett, J. Pursley, M. d’Errico, S.P. Griso, D. Lucchesi, A. Robson, and R. St.Denis. Updated search for $h \rightarrow ww$ production using likelihood-based electron selection. CDF/PHYS/EXOTIC/CDFR/9863, 2009.
- [21] Florencia Canelli, Bruno Casal Larana, Craig Group, Eric James, Jonathon Lewis, and Tom. Wright. Muon trigger studies: Focusing on the gaps. CDF/DOC/JET/PUBLIC/9106, 2007.
- [22] CDF Collaboration. Cdf central outer tracker. CDF/PUB/TRACKING/PUBLIC/6267, 2001.
- [23] CDF Collaboration. *CDF Run II Technical Design Report*, 2003. CDF/DOC/CDF/PUBLIC/6261.
- [24] A. Djouadi, J. Kalinowski, and M. Spira. Hdecay: A program for higgs boson decays in the standard model and it’s supersymmetric extensions. *Phys. Rev. Lett.*, 1997. Comput.Phys.Commun.108:56-74,1998.
- [25] David Dummit and Richard Foote. *Abstract Algebra, 3rd. ed.* John Wiley & Sons, Inc., 2004.
- [26] F. Englert and Brout R. Broken Symmetry and the Mass of Gauge Vector Mesons. *Phys. Rev. Lett.*, 13:321, 1964.

- [27] Hans Erler. The Mass of the Higgs Boson in the Standard Electroweak Model. *Phys. Lett.*, B565, March 2010.
- [28] Michael Feindt. A neural bayesian estimator for conditional probability densities. *arXiv:physics/0402093v1 [physics.data-an]*, February 2004. IEKP-KA/04-05.
- [29] R. D. Field, Y. Kanev, M. Tayebnejad, and P. A. Griffin. Using neural networks to enhance the higgs boson signal at hadron colliders. *Physical Review D*, 53(5):2296–2308, March 1996. The American Physical Society.
- [30] S. L. Glashow. Partial symmetries of weak interactions. *Nucl. Phys.*, 22:579–588, 1961.
- [31] Joel Goldstein, Tim Nelson, and Rick. Snider. Silicon tracking for plug electrons. /CDF/DOC/TRACKING/CDFR/5970, 2002.
- [32] G.S. Guralnik, C.R. Hagen, and T.B.W. Kibble. Global Conservation Laws and Mass-less Particles. *Phys. Rev. Lett.*, 13:585, 1964.
- [33] Francis Halzen and Alan Martin. *Quarks and Leptons: An Introductory Course in Modern Particle Physics*. John Wiley & Sons, Inc., 1984.
- [34] Matthew Herndon. Tracking at cdf. Website, March 2003. www.slac.stanford.edu/econf/C0303241/proc/pres/360.PS.
- [35] Peter W. Higgs. Broken Symmetries and the Masses of Gauge Bosons. *Phys. Rev. Lett.*, 13:508, 1964.
- [36] Peter W. Higgs. Broken Symmetries, Massless Particles and Gauge Fields. *Phys. Lett.*, 12:132, 1964.
- [37] Thomas Junk. Confidence level computation for combining searches with small statistics. *arXiv:hep-ex/9902006v1*, February 1999. CARLETON/OPAL PHYS 99-01.
- [38] Thomas Junk. Sensitivity, exclusion, and discovery with small signals, large backgrounds, and large systematic uncertainties. CDF/DOC/STATISTICS/PUBLIC/8128, 2007.
- [39] Richard J. Larsen and Morris L. Marx. *An Introduction to Mathematical Statistics and Its Applications (3rd ed.)*. Prentice Hall, 2001.
- [40] Richard J. Larsen and Morris L. Marx. *An Introduction to Mathematical Statistics and Its Applications (3rd ed.)*. Prentice Hall, 2001.
- [41] Richard J. Larsen and Morris L. Marx. *An Introduction to Mathematical Statistics and Its Applications (3rd ed.)*. Prentice Hall, 2001.
- [42] M. McFarlane, H. Bachacou, J. Nielson, and W. Yao. Study of high p_T lepton identification efficiency factor and related cuts and parameters in 5.3.3. CDF/ANAL/TOP/CDFR/7682, 2005.

- [43] Donald H. Perkins. *Introduction to High Energy Physics, 3rd ed.* Addison-Wesley Publishing Company, Inc., 1987.
- [44] Michael E. Peskin and Daniel V. Schroeder. *An Introduction to Quantum Field Theory.* Addison-Wesley Publishing Company, Inc., 1995.
- [45] Michael E. Peskin and Daniel V. Schroeder. *An Introduction to Quantum Field Theory.* Addison-Wesley Publishing Company, Inc., 1995.
- [46] J. J. Sakurai. *Modern Quantum Mechanics (Revised Edition).* Addison-Wesley Publishing Company, 1994.
- [47] A. Salam. Weak and electromagnetic interactions. *Proc. of the 8th Nobel Symposium*, page 367, 1969.
- [48] Phil Schlabach. The cdf muon detectors. Website, July 2004. http://www.phy.duke.edu/kotwal/detectorLectures/detector_lectures_Phil_Schlabach_1_muondetectors.pdf.
- [49] R.G. Wagner. Electron identification for run ii: Understanding and using lshr. CDF/DOC/ELECTRON/CDFR/6249, 2003.
- [50] S. Weinberg. A model of leptons. *Phys. Rev. Lett.*, 19:1264–1266, 1967.
- [51] W.M. Yao and K. Bloom. “outside-in” silicon tracking at cdf. CDF/TRACKING/DOC/CDFR/5991, 2002.